Lecture Notes In Chemistry 78

Paola Ceroni *Editor*

The Exploration of Supramolecular Systems and Nanostructures by Photochemical Techniques

Springer

Lecture Notes in Chemistry

Volume 78

For further volumes:
http://www.springer.com/series/632

The Lecture Notes in Chemistry

The series Lecture Notes in Chemistry (LNC) reports new developments in chemistry and molecular science-quickly and informally, but with a high quality and the explicit aim to summarize and communicate current knowledge for teaching and training purposes. Books published in this series are conceived as bridging material between advanced graduate textbooks and the forefront of research. They will serve the following purposes:

- provide an accessible introduction to the field to postgraduate students and nonspecialist researchers from related areas,
- provide a source of advanced teaching material for specialized seminars, courses and schools, and
- be readily accessible in print and online.

The series covers all established fields of chemistry such as analytical chemistry, organic chemistry, inorganic chemistry, physical chemistry including electrochemistry, theoretical and computational chemistry, industrial chemistry, and catalysis. It is also a particularly suitable forum for volumes addressing the interfaces of chemistry with other disciplines, such as biology, medicine, physics, engineering, materials science including polymer and nanoscience, or earth and environmental science.
Both authored and edited volumes will be considered for publication. Edited volumes should however consist of a very limited number of contributions only. Proceedings will not be considered for LNC.
The year 2010 marks the relaunch of LNC.

Paola Ceroni
Editor

The Exploration of Supramolecular Systems and Nanostructures by Photochemical Techniques

Springer

Prof. Dr. Paola Ceroni
Dipartimento di Chimica Ciamician
Università di Bologna
Via Selmi 2
40126 Bologna
Italy
e-mail: paola.ceroni@unibo.it

ISSN 0342-4901
ISBN 978-94-007-2041-1 e-ISBN 978-94-007-2042-8
DOI 10.1007/978-94-007-2042-8
Springer Dordrecht Heidelberg London New York

Library of Congress Control Number: 2011940034

Cover design: eStudio Calamar, Berlin/Figueres

Printed on acid-free paper

Springer is part of Springer Science+Business Media (www.springer.com)

Preface

Photochemistry and photophysics, i.e. the study of the interaction between light and matter, is an everyday experience in our life both as a natural phenomenon and as a technology developed by humans. For example, vision is based on a photochemical reaction and gives us information on the world around us, while photovoltaic panels convert solar energy into electricity and are expected to provide solutions to mankind's energy thirst.

Within the scientific community, photochemistry is applied to a wide range of disciplines, from physical chemistry, to supramolecular chemistry, chemical biology, materials science and nanoscience. It is thus very important to understand the fundamental concepts at the basis of the interaction of light with molecules and to know what information can be gained by photophysical and photochemical techniques, as well as practical aspects for the application of these techniques.

In the last few decades, substrates of photochemical studies have changed from simple organic molecules and metal complexes to supramolecular systems and nanostructures. Supramolecular chemistry, according to its most popular definition, is "the chemistry beyond the molecule, bearing on organized entities of higher complexity that result from the association of two or more chemical species held together by intermolecular forces". More generally, supramolecular systems can be defined as multicomponent structures assembled by weak interactions and characterized by the emergence of new functions compared to their component units. Photochemical techniques are extremely useful to study such supramolecular systems and nanostructures since optical inputs can be used not only to "read" the state of the system, but also to provide energy for the system to function.

The essentials of a quantum mechanical treatment of the interaction of electromagnetic radiation with molecules is described in the first chapter, and the second one deals with supramolecular photochemistry, with particular emphasis on energy and electron transfer with a description of the Marcus theory. The following chapters are devoted to the different photochemical and photophysical techniques: spectrophotometry and spectrofluorimetry, actinometry, absorption and luminescence techniques with polarized light excitation, time-resolved absorption and luminescence spectroscopy, down to femtosecond resolution. Each

chapter comprises both the theoretical basis and the practical aspects and describes an example of the application of these techniques to the study of a supramolecular system.

This book is aimed at providing the newcomers of the field with an overview of the potential offered by the photophysical and photochemical techniques applied to supramolecular systems and nanoobjects. Indeed, it provides the basic concepts, without introducing too many technical and mathematical details, with the aid of self-explicative figures and schemes, and discusses the methodology to correctly perform a photochemical experiment, as well as the most critical aspects of the laboratory application. It is of interest also to scientists already involved in the field because it offers technical and operative details useful in the laboratory, as well as references to current research, pioneering contributions, and review articles on specific aspects.

I would like to express my gratitude to the authors of the chapters, most of them working together with me in the Photochemical Nanosciences Laboratory—Department of Chemistry "G. Ciamician" of the University of Bologna. This volume is the fruit of their long practical and teaching experience in the field of photochemistry and photochemical techniques.

Bologna, May 2011 Paola Ceroni

Contents

Contributors

Vincenzo Balzani Department of Chemistry "G. Ciamician", University of Bologna, Via Selmi 2, 40126 Bologna, Italy, e-mail: vinicenzo.balzani@unibo.it

Paola Ceroni Department of Chemistry "G. Ciamician", University of Bologna, Via Selmi 2, 40126 Bologna, Italy, e-mail: paola.ceroni@unibo.it

Claudio Chiorboli Istituto per la Sintesi Organica e la Fotoreattività (ISOF), Consiglio Nazionale delle Ricerche (CNR), Area della Ricerca, Via Piero Gobetti 101, 40129, Bologna, Italy; Sezione di Ferrara, Via Borsari 46, 44121 Ferrara, Italy, e-mail: chc@unife.it

Alberto Credi Department of Chemistry "G. Ciamician", University of Bologna, Via Selmi 2, 40126 Bologna, Italy, e-mail: alberto.credi@unibo.it

Maria Teresa Gandolfi Department of Chemistry "G. Ciamician", University of Bologna, Via Selmi 2, 40126 Bologna, Italy, e-mail: mariateresa.gandolfi@unibo.it

Alberto Juris Department of Chemistry "G. Ciamician", University of Bologna, Via Selmi 2, 40126 Bologna, Italy, e-mail: alberto.juris@unibo.it

Mauro Maestri Department of Chemistry "G. Ciamician", University of Bologna, Via Selmi 2, 40126 Bologna, Italy, e-mail: mauro.maestri@unibo.it

Luca Moggi Department of Chemistry "G. Ciamician", University of Bologna, Via Selmi 2, 40126 Bologna, Italy, e-mail: luca.moggi@unibo.it

Marco Montalti Department of Chemistry "G. Ciamician", University of Bologna, Via Selmi 2, 40126 Bologna, Italy, e-mail: marco.montalti2@unibo.it

Sandra Monti Istituto per la Sintesi Organica e la Fotoreattività (ISOF), Consiglio Nazionale delle Ricerche (CNR), Area della Ricerca, Via Piero Gobetti 101, 40129, Bologna, Italy, e-mail: monti@isof.cnr.it

Luca Prodi Department of Chemistry "G. Ciamician", University of Bologna, Via Selmi 2, 40126 Bologna, Italy, e-mail: luca.prodi@unibo.it

Margherita Venturi Department of Chemistry "G. Ciamician", University of Bologna, Via Selmi 2, 40126 Bologna, Italy, e-mail: margherita.venturi@unibo.it

Nelsi Zaccheroni Department of Chemistry "G. Ciamician", University of Bologna, Via Selmi 2, 40126 Bologna, Italy, e-mail: nelsi.zaccheroni@unibo.it

Chapter 1
Excited-State Properties

Paola Ceroni and Vincenzo Balzani

Abstract This chapter provides a general overview of photochemistry and photophysics, starting with photochemical processes in everyday life and the nature of light. Then, a discussion about formation of electronic excited states by light absorption is presented together with their deactivation processes. Both kinetic aspects and the efficiency of a single process are discussed. The most important take-home message is that electronically excited states are new chemical species with properties different from those of the ground state.

1.1 Introduction

The interaction of light and matter as a natural phenomenon and/or as an artificial process permeates most branches of science, from medicine to material science. [1, 2] Our life depends on photosynthesis, a photochemical process taking place in nature. We get information about the surrounding space by another natural photochemical process occuring in our eyes. We are encircled by substances that are produced by natural or artificial photochemical reactions. Many of the most common functions exploited in our technological environment, from signal processing, storage and display to the use of pigments, sensors and sensitizers are based on the interaction of light with matter. Solar energy, the most important resource on which humanity can rely, is artificially converted into useful energy forms by photophysical and photochemical processes [3, 4].

P. Ceroni (✉) · V. Balzani
Department of Chemistry G. Ciamician, University of Bologna, Via Selmi 2, 40126 Bologna, Italy
e-mail: paola.ceroni@unibo.it

P. Ceroni (ed.), *The Exploration of Supramolecular Systems and Nanostructures by Photochemical Techniques*, Lecture Notes in Chemistry 78,
DOI: 10.1007/978-94-007-2042-8_1, © Springer Science+Business Media B.V 2012

The first scientist to understand the importance of photochemistry for the future of mankind was Giacomo Ciamician, professor of Chemistry at the university of Bologna from 1889 to 1922. Inspired by the ability of plants to make use of solar energy, he decided to investigate photochemical reactions in a systematic way. Most of Ciamician's considerations and predictions on the development of photochemistry and the utilization of solar energy are contained in a famous address presented before the VIII International Congress of Applied Chemistry, held in New York in 1912. [5] After one century, it is still worthwhile reading at least the final part of this fascinating paper: "Where vegetation is rich, photochemistry may be left to the plants and, by rational cultivation, solar radiation may be used for industrial purposes. In the desert regions, unsuitable to any kind of cultivation, photochemistry will artificially put their solar energy to practical uses. On the arid lands there will spring up industrial colonies without smoke and without smoke-stacks; forests of glass tubes will extend over the plants and glass buildings will rise everywhere; inside of these will take place the photochemical processes that hitherto have been the guarded secret of the plants, but that will have been mastered by human industry which will know how to make them bear even more abundant fruit than nature, for nature is not in a hurry and mankind is. And if in a distant future the supply of coal becomes completely exhausted, civilization will not be checked by that, for life and civilization will continue as long as the sun shines! If our black and nervous civilization, based on coal, shall be followed by a quieter civilization based on the utilization of solar energy, that will not be harmful to progress and to human happiness."

As we will see below, any observable photochemical and photophysical event takes place by very fast processes that originate from short-lived excited states generated upon light absorption. Using the Sun as a light source for photochemical reactions does not allow, of course, to investigate the details of such primary processes. Continuous progress during the last 50 years, however, has made available instrumentations capable of spatial resolution at the molecular level and temporal resolution at the limit of the uncertainty principle ($\Delta E \times \Delta t \geq h$, where ΔE and Δt are the uncertainties on energy and time, respectively, and h is the Planck constant, so that if $\Delta t = 10^{-15}$ s $\Rightarrow \Delta E \geq 15$ kcal/mol, i.e., close to the energy of a chemical bond).

1.2 The Nature of Light

Usually "light" is taken to mean electromagnetic radiation in the visible, near ultraviolet, and near infrared spectral range (Fig. 1.1).

In the wave model, electromagnetic radiation is characterized by a wavelength, λ, a frequency, ν, and a velocity, c. The three quantities are related by the relationship $\lambda\nu = c$. The value of c is constant (2.998×10^8 m s^{-1} in vacuum), whereas λ (and ν) may cover a wide range of values. The SI units for λ and ν are the meter (m) and the hertz (Hz), respectively. In some cases, the wavenumber $\bar{\nu}$

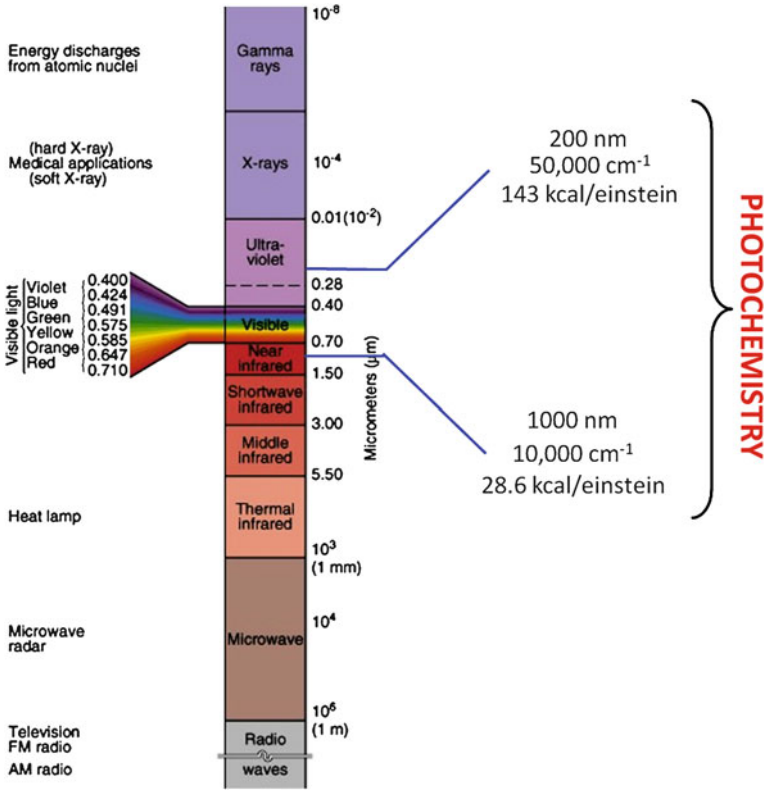

Fig. 1.1 Electromagnetic spectrum and the region of interest to photochemistry

(defined as the number of waves per centimeter) is also used to characterize electromagnetic radiation. The electromagnetic spectrum encompasses a variety of types of radiation from γ-rays to radiowaves, distinguished by their wavelengths (or frequencies, or wavenumbers). In photochemistry we are concerned with the region ranging from 200 to 1,000 nm (1.5×10^{15} to 3×10^{14} Hz, or 5×10^4 to 1×10^4 cm^{-1}).

In the quantum model a beam of radiation is regarded as a stream of *photons,* or *quanta.* A photon has a specific energy, E, related to the frequency of the radiation, v, by (1.1),

$$E = hv \tag{1.1}$$

where h is Planck's constant (6.63×10^{-34} J s). From the above relationships it follows that the photon energy is 9.95×10^{-19} and 1.99×10^{-19} J, respectively, for light of 200 and 1,000 nm. This picture of light as made up of individual photons is essential to photochemistry.

The interaction of light with molecular systems is generally an interaction between *one* molecule and *one* photon. It can be written in the very general form (1.2),

$$A + h\nu \rightarrow {}^{*}A \tag{1.2}$$

where A denotes the ground state molecule, hν the absorbed photon, and *A the molecule in an electronically excited state. As the equation implies, the excited molecule A is the molecule A with an extra energy hν.

To appreciate the size of the photon energy, we must compare it with the energies of the chemical bonds, which are normally expressed in kilojoules or kilocalories per mole. A mole is an Avogadro's number, 6.02×10^{23}, of objects. We may extend the concept of mole to photons, defining an *einstein* as one mole of photons. When *one mole* of molecules absorbs *one einstein* of photons, this is equivalent to one photon absorbed by one molecule, (1.2). The energy of one einstein of photons at 200 nm is 599 kJ (143 kcal), and that of one einstein of photons at 1,000 nm is 119.8 kJ (28.6 kcal). These energy values are of the same order of magnitude of those required to break chemical bonds (e.g., 190 kJ mol^{-1} for the Br–Br bond of Br_2; 416 kJ mol^{-1} for the C–H bond of CH_4). The energy that a molecule obtains when it absorbs a photon of light is therefore not at all negligible. Whether or not light absorption causes bond breaking will depend on the competition among various deactivating processes (Sect. 1.6). In any case, because of the availability of such an extra amount of energy, *an excited molecule has to be considered as a new chemical species* that has its own chemical and physical properties, often quite different from the properties of the ground state molecule.

1.3 Potential Energy Surfaces

Central to any understanding of photochemistry is the concept that molecular systems possess well-defined *electronic* states: ordinary (thermal) chemistry is the chemistry of the ground electronic state, while photochemistry is the chemistry of (or originating from) electronic excited states. It is important to keep in mind that this common notion relies on the Born–Oppenheimer (BO) approximation, a non-trivial conceptual separation between electronic and nuclear motions. [6] Such an approximation is justified by the huge difference in the masses of electrons and nuclei, so that the molecular system can be considered as made up of a fast subsystem (the electrons) and a slow one (the nuclei). Within such an approximation, the electronic wavefunctions can be solved at fixed values of the nuclear coordinates. For each geometry (Q), a set of electronic wavefunctions Ψ_k and energies E_k (k is an electronic quantum number) can be obtained. For each k, the set of energy values obtained at different geometries defines a surface called the "adiabatic potential energy surface" of the kth electronic state. Figure 1.2 shows

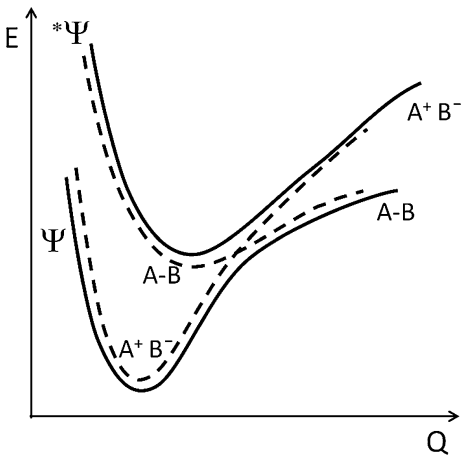

Fig. 1.2 Adiabatic potential energy curves (*full lines*) of the ground and the first excited state for a heteronuclear diatomic molecule. *Dashed lines* represent the energies of pure ionic and covalent structures

schematically the adiabatic potential energy curves of the ground and first singlet excited state of a heteronuclear diatomic molecule (e.g., HCl). The change in the electronic wavefunction brought about by changes in the nuclear geometry can be appreciated by looking at the curves (dashed lines) for pure ionic and covalent valence-bond wavefunctions: in going from equilibrium geometry to stretched geometry, the ground state changes from highly ionic to highly covalent, while the opposite change occurs for the first excited state.

The problem of the motion of the nuclei is next solved by letting the slow nuclear subsystem move in a potential field that is determined by the fast electronic subsystem: the electronic wavefunction is considered to respond instantaneously to the changes in the nuclear coordinates.

It is evident that the approximation is expected to work well in situations (such as that near to equilibrium distances in Fig. 1.2) in which the electronic wavefunctions are slowly changing functions of the nuclear coordinates, but to be much less valid when (as in the region of the crossing dashed lines of Fig. 1.2) the electronic wavefunctions change abruptly with nuclear motion. In the latter case, there may be some dynamic tendency for the states to preserve their electronic identity instead of following the changes predicted by the adiabatic BO approximation.

Since a nonlinear N-atomic molecule has 3N-6 internal nuclear degrees of freedom, each electronic state is described by a potential hypersurface in a 3N-5 dimensional space. The ground state hypersurface has usually a deep minimum corresponding to the stable geometry of the molecule (Fig. 1.3). Two or more minima separated by energy barriers may occur, however, in systems for which isomers are possible. It is useful to distinguish two types of nuclear motions along the ground-state potential energy hypersurface: (1) small-amplitude motions around the minima; (2) large-amplitude motions carrying the molecule to highly distorted geometries.

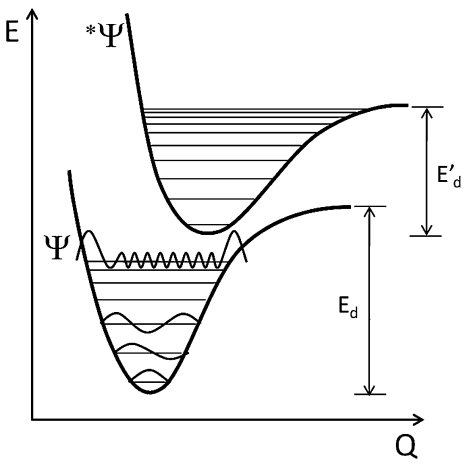

Fig. 1.3 Potential energy curves for the ground (ψ) and the first excited state ($^*\psi$). E_d and E'_d represent the corresponding dissociation energies. For more details, see text

It is customary to describe the small-amplitude nuclear motions around the minima as a superposition of normal modes of vibration, i.e., harmonic oscillations along suitable symmetry-adapted combinations of bond length and bond angle changes. Large-amplitude nuclear motions, that occur in relatively flat regions of the potential energy hypersurface, can be viewed as strongly anharmonic vibrations with very closely spaced levels. In this case, however, a simple description of the system as moving smoothly on the potential energy hypersurface along classical trajectories is also appropriate for most purposes. Large amplitude nuclear motions of this type are required to achieve chemical change, i.e., to break bonds or to go from one isomer to the other. Classical models of nuclear motions are thus widely used in the field of chemical kinetics. It should also be noted that a description of chemical reactions in terms of potential energy surfaces is not limited to unimolecular processes. For a bimolecular reaction, the potential energy hypersurface of a "supermolecule" including the nuclei of both reactants can be considered, with reactants and products corresponding to different minima of this surface [7].

For electronically excited states, nuclear motions can be described by the same arguments used for the ground-state. Generally speaking, electronic excitation of a molecule results in some kind of bond weakening (the energy minimum occurs at longer bond distance and the dissociation energy is lower, see Fig. 1.3). Two consequences of this fact should be stressed. First, excited-state minima tend to be less deep than the corresponding ground-state minima, so that small-amplitude vibrations in the excited state will generally have lower frequencies and smaller energy spacing than the corresponding vibrations in the ground state (Fig. 1.3). Second, large-amplitude motions along relatively flat pathways leading to highly distorted geometries will be found more frequently in excited states than in the ground state. These differences are expected to become more pronounced as one goes to higher and higher electronically excited states.

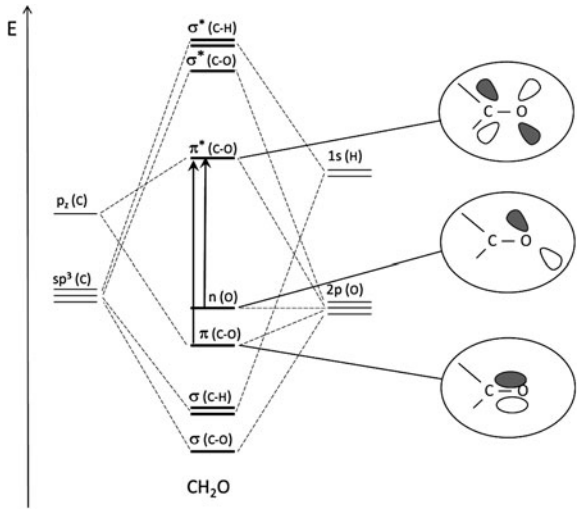

Fig. 1.4 Molecular orbital diagram for formaldehyde. The arrows indicate the n → π* and π → π* transitions

1.4 Electronic States and Electronic Configurations

Molecules are multielectron systems. Approximate electronic wavefunctions of a molecule can be written as products of one-electron wavefunctions, each consisting of an orbital and a spin part:

$$\Psi_e = \Phi S \ = \Pi_i \phi_i s_i \tag{1.3}$$

The Φ_i are appropriate molecular orbitals (MO) and s_i is one of the two possible spin eigenfunctions, α or β. The orbital part of this multielectron wavefunction defines the *electronic configuration*.

We illustrate now the procedure to construct energy level diagrams for organic molecules and metal complexes.

1.4.1 Organic Molecules

The molecular orbital diagram for formaldehyde, based on linear combination of the atomic orbitals (LCAO) of C, O and H atoms is shown in Fig. 1.4. [7] It consists of three low-lying σ-bonding orbitals, a π-bonding orbital of the CO group, a non-bonding orbital n of the oxygen atom (highest occupied molecular orbital, HOMO), a π-antibonding orbital of the CO group (lowest unoccupied molecular orbital, LUMO), and three high energy σ-antibonding orbitals. The lowest-energy electronic configuration (neglecting the filled low energy orbitals) is $\pi^2 n^2$. Excited configurations can be obtained from the ground configuration by promoting one electron from occupied to vacant MOs.

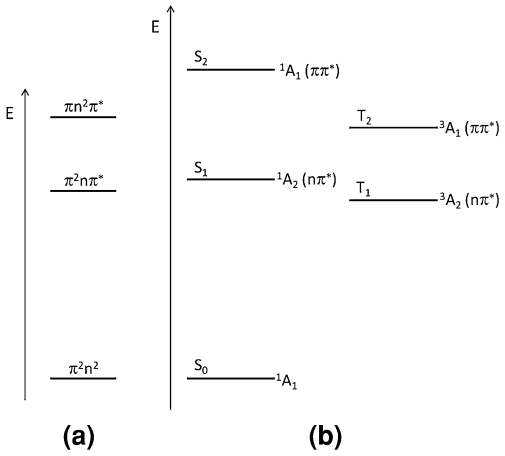

Fig. 1.5 Configurations **a** and states **b** diagrams for formaldehyde

At relatively low energies, one expects to find $n \rightarrow \pi^*$ and $\pi \rightarrow \pi^*$ electronic transitions (Fig. 1.4), leading to $\pi^2 n\pi^*$ and $\pi n^2\pi^*$ excited configurations (Fig. 1.5a).

In a very crude zero-order description, the energy associated with a particular electronic configuration would be given by the sum of the energies of the occupied MOs. In order to obtain a more realistic description of the energy states of the molecule, two features should be added to the simple configuration picture: (1) spin functions must be attached to the orbital functions describing the electronic configurations, and (2) interelectronic repulsion must be taken into account. These two closely interlocked points have important consequences since they may lead to the splitting of an electronic configuration into several state [7].

In the case of formaldehyde, the inclusion of spin and electronic repulsion leads to the schematic energy level diagram shown in Fig. 1.5: each excited electronic configuration is split into a pair of triplet and singlet states, with the latter at higher energy because electronic repulsion is higher for spin paired electrons. It can be noticed that the singlet–triplet splitting for the states arising from the $\pi \rightarrow \pi^*$ transition is larger than that of the states corresponding to the n $\rightarrow \pi^*$ transition. This result arises from the dependence of the interelectronic repulsions on the amount of spatial overlap between the MOs containing the two separated electrons, and this overlap is greater in the first than in the second case (see the MO shapes in Fig. 1.4). The electronic states can be designated by symbols that specify the symmetry of the wavefunction in the symmetry group of the molecule (e.g., A_1, A_2, etc. in the C_{2v} group of formaldehyde) and the spin multiplicity (number of unpaired electrons +1) as a left superscript. In organic photochemistry, it is customary to label the singlet and triplet states as S_n and T_n respectively, with $n = 0$ for the singlet ground state and $n = 1$, 2, etc. for states arising from the various excited configurations. Both notations are shown for formaldehyde in Fig. 1.5. The situation sketched above (i.e., singlet ground state, pairs of singlet and triplet excited states arising from each excited configuration, lowest excited state of

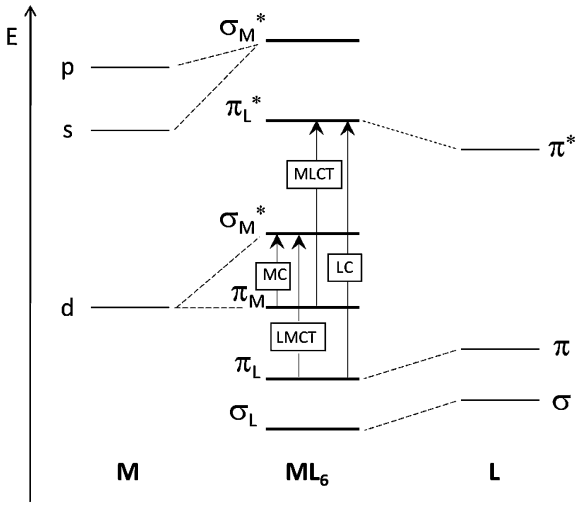

Fig. 1.6 Molecular orbital diagram for an octahedral complex of a transition metal. The *arrows* indicate the four types of transitions based on localized MO configurations. For more details, see text

multiplicity higher than the ground state) is quite general for organic molecules that usually exhibit a closed-shell ground-state configuration.

State energy diagrams of this type, called "Jablonski diagrams", are used for the description of light absorption and of the photophysical processes that follow light excitation (vide infra) [1].

1.4.2 Metal Complexes

Metal complexes, often called coordination compounds, are the most interesting species among inorganic molecules from a photochemical viewpoint. Usually metal complexes have high symmetry and contain a transition metal with open-shell *d* orbital configuration. The construction of Jablonski diagrams via electronic configurations from the MO description follows the same general lines described above for organic molecules [8, 9]. A schematic MO diagram for an octahedral transition metal complex is shown in Fig. 1.6. The various MOs can be conveniently classified according to their predominant atomic orbital contributions as: (1) strongly bonding, predominantly ligand centered σ_L orbitals; (2) bonding, predominantly ligand-centered π_L orbitals; (3) essentially non-bonding, metal-centered π_M orbitals of t_{2g} symmetry; (4) antibonding, predominantly metal-centered π_M* orbitals of e_g symmetry; (5) antibonding, predominantly ligand-centered π_L* orbitals; (6) strongly antibonding, predominantly metal-centered σ_M* orbitals. In the ground electronic configuration of an octahedral complex of a d^n metal ion, orbitals of types σ_L and π_L are completely filled, while n electrons reside in the orbitals of types π_M and σ_M*.

As for organic molecules, excited configurations can be obtained from the ground configuration by promoting one electron from occupied to vacant MOs. At relatively low energies, one expects to find electronic transitions of the following types (Fig. 1.6): *metal-centered* (MC) transitions from π_M orbitals to σ_M* orbitals (iv); *ligand-centered* (LC) transitions of type $\pi_L \rightarrow \pi_L$*; *ligand-to-metal charge-transfer* (LMCT) transitions e.g., of type $\pi_L \rightarrow \pi_M$*; *metal-to-ligand charge-transfer* (MLCT) transitions e.g., of type $\pi_M \rightarrow \pi_L$*. The relative energy ordering of the resulting excited electronic configurations depends on the nature of metal and ligands in more or less predictable ways. Low energy metal-centered transitions are expected for metals of the first transition row, low energy ligand-to-metal charge-transfer transitions are expected when at least one of the ligands is easy to oxidize and the metal is easy to reduce, low energy metal-to-ligand charge-transfer transitions are expected when the metal is easy to oxidize and a ligand is easy to reduce, and low energy ligand centered transitions are expected for aromatic ligands with extended π and π* orbitals.

The step from configurations to states is conceptually less simple than for organic molecules because, as mentioned above, coordination compounds may have high symmetry (i.e., degenerate MOs) and open-shell ground configurations (i.e., partially occupied HOMOs).

For octahedral complexes of Co(III), Ru(II), and the other d^6 metal ions, the σ_L and π_L orbitals are fully occupied and the ground state configuration is closed-shell since the HOMO, $\pi_M(t_{2g})^6$, is also completely occupied. The ground state is therefore a singlet, and the excited states are either singlets or triplets, as in the case of formaldehyde. In octahedral symmetry, the ground state configuration gives rise to the state $^1A_{1g}$. In the case of $[M(NH_3)_6]^{n+}$ complexes (e.g., M = Co or Ru), whose ligands do not possess π_L and π_L* orbitals, the lowest energy transition is metal centered and the resulting $\pi_M(t_{2g})^5\sigma_M^*(e_g)$ configuration gives rise to the singlet states $^1T_{1g}$ and $^1T_{2g}$ and to the corresponding triplets $^3T_{1g}$ and $^3T_{2g}$. The energy level diagram (at low energies) for $[Ru(NH_3)_6]^{2+}$ is shown in Fig. 1.7. In the case of $[M(bpy)_3]^{2+}$ (M = Ru or Os), however, since the M(II) metal is easy to oxidize and the 2,2′-bipyridine ligands are easy to reduce, the lowest triplet and singlet excited states are metal-to-ligand charge-transfer in character (Fig. 1.7). For the corresponding $[M(bpy)_3]^{3+}$ complexes, the lowest triplet and singlet excited states are ligand-to-metal charge-transfer in character since the M(III) metal can be easily reduced and the 2,2′-bipyridine ligands are not too difficult to oxidize (Fig. 1.7) [10].

In Cr(III) complexes (d^3 metal ion), there are three electrons in the HOMO $\pi_M(t_{2g})$ orbitals. Therefore, these complexes exhibit an open shell ground state configuration, $\pi_M(t_{2g})^3$, that splits into a quartet and doublet states (Fig. 1.8). For most Cr(III) complexes, e.g., for $[Cr(NH_3)_6]^{3+}$, the lowest energy excited state, ^2E_g, belongs to the ground state configuration, whereas the lowest energy transition is metal centered and the resulting $\pi_M(t_{2g})^2\sigma_M^*(e_g)$ configuration gives rise to $^4T_{2g}$ and $^4T_{1g}$ excited states (Fig. 1.8). Several other coordination compounds, including the complexes of lanthanide ions, have an open shell ground

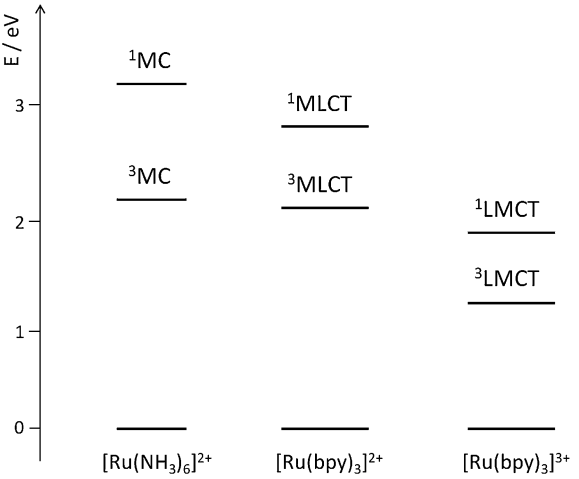

Fig. 1.7 Schematic energy level diagrams for $[Ru(NH_3)_6]^{2+}$, $[Ru(bpy)_3]^{2+}$ and $[Ru(bpy)_3]^{3+}$

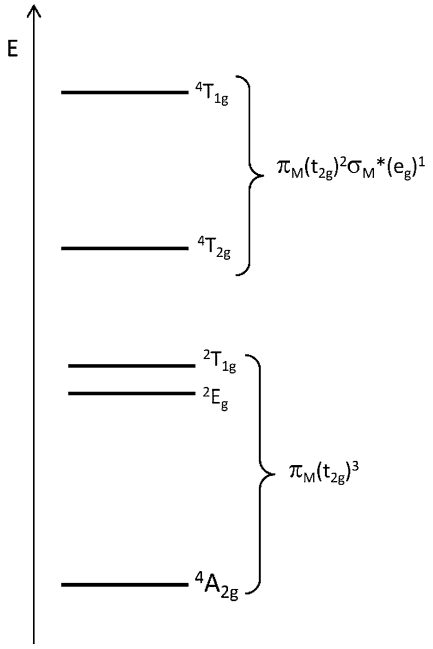

Fig. 1.8 State diagram for an octahedral Cr(III) complex; the corresponding configuration is reported on the right. Only the most relevant excited states of each configuration are shown

configuration and, as a consequence, a ground state with high multiplicity and low energy intraconfigurational metal-centered excited states.

In conclusion, metal complexes tend to have more complex and specific Jablonski diagrams than organic molecules. Points to be noticed are: (1) spin multiplicity other than singlet and triplet can occur, but for each electronic configuration the state with highest multiplicity remains the lowest one; (2) excited states can

exist that belong to the same configuration of the ground state (this implies that the ground state has the highest multiplicity); (3) more than one pair of states of different multiplicity can arise from a single electron configuration.

In the following, in order to discuss some general concept of molecular photochemistry we will make use of a generic Jablonski diagram based on singlet and triplet states.

1.5 Light Absorption

A molecule can be promoted from the ground electronic state to an electronically excited state by the absorption of a quantum of light. The necessary condition is that the photon energy, hν, matches the energy gap between the ground and the excited state. This energy gap, for low-energy states of common organic and inorganic molecules, corresponds to light in the visible and near ultraviolet regions (Sect. 1.1). When the above condition is satisfied, the probability of transition from the ground state Ψ to the excited state $^*\Psi$ is proportional to the square of the so-called transition moment M_{if} (1.4), where the subscripts i and f stand for initial and final:

$$M_{if} = \langle \Psi_i | \mu | \Psi_f \rangle \tag{1.4}$$

In (1.4), μ is the dipole moment operator defined as Σer_j, with e representing the electron charge and r_j representing the vector distance from the kth electron to the centre of positive charge of the molecule.

If the complete wavefunctions $\Psi = \Phi SX$ are substituted into (1.4), the transition moment splits into the product of three terms as shown in (1.5).

$$M_{if} = \langle \phi_i | \mu | \phi_f \rangle \langle S_i | S_f \rangle \Sigma_n \langle X_{i,0} | X_{f,n} \rangle \tag{1.5}$$

Notice that the dipole-moment operator is considered to be independent of nuclear coordinates (Condon approximation) and spin, and thus it only appears in the integral containing the orbital part of the electronic wavefunction. In (1.5), the summation in the third term is made over all the transitions between vibrational levels of the ground and excited states that contribute to the intensity of the electronic transition. For common molecular systems in the ground electronic state at room temperature, only transitions of the type $X_{i,0} \rightarrow X_{f,n}$ (thereafter referred to as $0 \rightarrow n$) need to be considered in most cases.

In practice, a very wide range of intensities is observed for electronic absorption bands of polyatomic molecules, with maximum molar absorption coefficients ranging from the lower limit of detection (0.1–0.01 $M^{-1}cm^{-1}$) up to values of the order of 5×10^5 $M^{-1}cm^{-1}$. Without carrying out any actual calculation of M_{if}, it is easy to identify typical cases in which the first or the second terms in (1.5) are expected to vanish, thus leading to a zero predicted intensity of the electronic

transition. The rules defining such cases are known as *selection rules* for light absorption.

It can be shown by the methods of group theory [11] that the first term in (1.5) vanishes if the symmetry properties of the initial and final orbital functions are not appropriate (that is, if the product $\Phi_i\Phi_f$ does not belong to the same irreducible representation of the point group of the molecule as μ). In these cases, the transition is said to be *symmetry-forbidden.* Examples of symmetry-forbidden transitions are the $n \rightarrow \pi^*$ transitions of organic molecules and the MC transitions in centrosymmetric coordination compounds. In practice, such transitions have low but sizeable intensity ($\varepsilon_{max} \sim 10^2\ M^{-1}\ cm^{-1}$) because of the poor separability of electronic and nuclear functions (breakdown of the Condon approximation). This again can be dealt with as a perturbation, called *vibronic coupling*. In this case, the transition acquires some intensity because vibrations of appropriate symmetry lead to admixture of the "forbidden" (zero-order) excited state by some "allowed" (zero-order) state.

Because of the orthogonality of spin wavefunctions, the second term in (1.5) is expected to vanish whenever the initial and final states have different spin multiplicity, and the corresponding electronic transitions are called *spin-forbidden.* This spin selection rule is valid to the extent to which spin and orbital functions can be rigorously separated. Departures from this approximation can be dealt with in terms of a perturbation called *spin–orbit coupling,* by which states of different spin multiplicity can be mixed. This perturbation increases as the fourth power of the atomic number of the atoms involved. Thus spin-forbidden transitions of typical organic molecules (for example, $S_0 \rightarrow T_1$) are actually almost unobservable ($\varepsilon_{max} < 1\ M^{-1}\ cm^{-1}$), whereas spin-forbidden transitions of metal complexes can reach quite sizeable intensities (for example, $10^2\ M^{-1}\ cm^{-1}$ for *5d* metal complexes).

The integrated band intensity only depends on the first two (electronic) terms of (1.5), since it can be shown that the summation in the third (nuclear) term always amounts to 1. This term, however, is important in determining the *shape* of the absorption band. It is often called the *Franck–Condon* term as it represents the quantum mechanical counterpart of the classical statement of the Franck–Condon principle (i.e., the nuclei cannot change either their position or their kinetic energy during the electronic transition). Let us consider the hypothetical situation sketched in Fig. 1.9a, in which the excited state has a potential energy surface identical in shape and equilibrium geometry to that of the ground state. In this case, the ground and excited-state nuclear wavefunctions are solutions of the same vibrational problem and constitute an orthonormal set. Thus $\langle X_{i,0}|X_{f,n}\rangle = 1$ and all other terms in the summation are zero. In other words, all the intensity of the electronic transition is concentrated in a sharp, line-shaped band corresponding to the 0–0 transition. The opposite case is shown in Fig. 1.9b, where the excited state is highly distorted (different equilibrium geometry and force constant) with respect to the ground state. In this case, the values of the vibrational overlap integrals for the various 0–n transitions should be evaluated to obtain the intensity distribution.

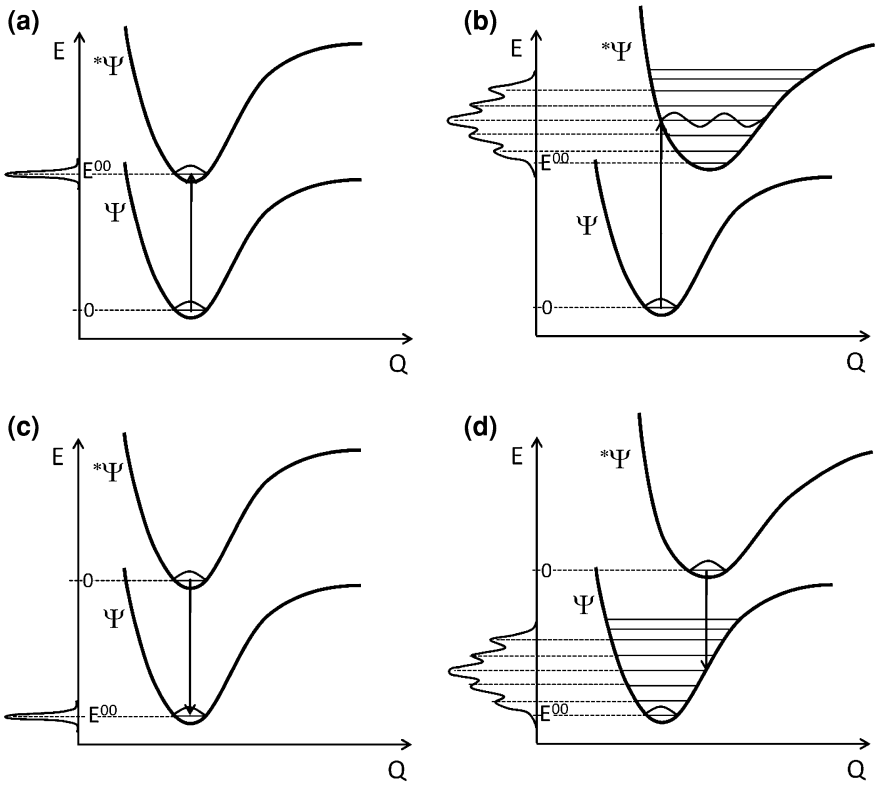

Fig. 1.9 Relationship between excited state distortion and width of the absorption (**a** and **b**) and emission (**c** and **d**) bands

It can be easily seen that the maximum vibrational overlap occurs with the excited-state vibrational level that intercepts the excited-state potential energy surface at the equilibrium geometry of the ground state (Fig. 1.9b). The overlap integrals for the other 0–n transitions decrease smoothly in going towards higher and lower n values. Thus, the intensity will be spread over a relatively broad, Gaussian-shaped band centered around the "vertical" transition. In the intermediate case of a small degree of excited-state distortion, more or less symmetric bandshapes (with lower slope on the high-energy side) are expected.

The schematic pictures used to discuss the effect of the Franck–Condon factors on absorption bandshape (Fig. 1.9) represent sections of the potential energy surfaces along a single coordinate. In an N-atomic molecule, the same type of arguments should be applied to *3N-6* sections along different nuclear coordinates, and the actual bandshape should be regarded as a convolution of the various single-mode profiles. In many cases, the superposition of different vibrational progressions may lead to complete loss of the vibrational structure in the absorption band.

1.6 Intramolecular Excited State Decay

1.6.1 Vibrational Relaxation

Light absorption often generates the excited state in a high vibrational level because of the Franck–Condon principle and of excited-state distortion (Fig. 1.9b). The newborn electronically excited molecules can thus be regarded as "hot" species with respect to the surrounding ground-state molecules that have a Boltzmann equilibrium distribution largely centered on the zero vibrational level. The vibrationally excited molecules will tend to dissipate their excess vibrational energy (thermalize) by interaction (collisions) with surrounding molecules. This process is usually called *vibrational relaxation.*

For most practical systems (solid, liquid, and atmospheric pressure gaseous phase) vibrational relaxation occurs in the picosecond time scale. Since most of the interesting chemistry and physics that takes place in electronically excited states occurs on a much longer timescale (see below), *thermally equilibrated excited states* should he considered as the only relevant intermediates in photochemistry, regardless of the initial amount of vibrational excitation with which they may have been created.

1.6.2 Radiative Deactivation

Electronically excited molecules can return to the ground state by emitting a quantum of light (1.6).

$$^{*}\mathrm{A} \rightarrow \mathrm{A} + \mathrm{h}\nu' \tag{1.6}$$

This radiative transition is the reverse process of light absorption (1.1) and is often indicated as *spontaneous emission* (in order to distinguish it from the process known as stimulated emission, that is relevant to lasers [1]). It can be shown that the probability of spontaneous emission depends on the third power of the frequency and is regulated by the same factors affecting that of light absorption. Therefore, a discussion parallel to that given in Sect. 1.5 could be made here. In particular, the same spin and symmetry selection rules as discussed for absorption hold for radiative deactivation, with the same arguments applying to the degree of validity of the rules. In the language of photochemistry, it is customary to call *fluorescence* a spin-allowed emission (e.g., $S_1 \rightarrow S_0$ in an organic molecule) and *phosphorescence a* spin forbidden emission (e.g., $T_1 \rightarrow S_0$ in an organic molecule). Typical values for the probability (per unit time) of strongly allowed radiative transitions is of the order of 10^9 s^{-1}. For strongly spin-forbidden emissions (e.g., phosphorescence of organic molecules), probabilities as small as 1 s^{-1} can be obtained.

The role of the Franck–Condon factor in radiative deactivation is again that of determining the band shape. As shown in Fig. 1.9c, emission from an undistorted excited state will result in a sharp, line-shaped emission band at the 0–0 energy, whereas in a highly distorted case the emission band will be broad, Gaussian-shaped, and centered at energies lower than the 0–0 energy (Fig. 1.9d). Since in a distorted case the absorption band maximum is at energies higher than the 0–0 energy, there must be a shift, called the *Stokes shift,* between the maxima in the absorption and emission spectra for the same transition. The magnitude of the Stokes shift is a simple, direct measure of the extent of distortion between the ground and the excited state. If the two states are considered as identical harmonic oscillators displaced in the nuclear space, the intensity distribution of the various 0–n transitions should be identical in absorption and emission, and a "mirror image" relationship (mirror at the 0–0 energy) should exist between absorption and emission spectra.

1.6.3 Radiationless Deactivation

In radiative deactivation, energy conservation is provided by the emission of light (1.6). If an excited state is to be converted into the ground state (or a lower excited state) *without* emission of radiation, a two-step mechanism must operate: (1) isoenergetic conversion of the electronic energy of an upper state into vibrational energy of the ground state (radiationless transition); (2) vibrational relaxation of the ground state. Since step (2) is known to be very fast, step (1) will be the rate determining process. The probability of the isoenergetic radiationless transition is given, according to perturbation theory, by Fermi's Golden Rule (1.7),

$$k_{nr} = (2\pi/h)\langle \phi_i S_i | H' | \phi_f S_f \rangle^2 \langle X_{i,0} | X_{f,n} \rangle^2 \tag{1.7}$$

where H′ is an appropriate perturbation (spin–orbit coupling or vibronic coupling) that promotes the transition. Radiationless transitions between states of different or equal spin multiplicity are called *intersystem crossing* and *internal conversion,* respectively.

Contrary to what happens with the related expression (1.5) for radiative transitions, the Franck–Condon term in (1.7) is made up of a single overlap integral for each vibrational mode, corresponding to the unique isoenergetic transition. In order to discuss the role of the Franck–Condon factor in radiationless transitions, it is worthwhile considering the two archetypal situations shown in Fig. 1.10.

The situation of Fig. 1.10a is that of "nested" surfaces. It is easy to see that the vibrational overlap tends to be poor because of the oscillatory behavior of the wavefunction of the high vibrational level of the ground state. In this situation, the probability of radiationless transition is small. For a given ground-state vibrational frequency, the probability decreases exponentially with the energy gap between the states *(energy gap law),* since the higher is the energy gap, the higher

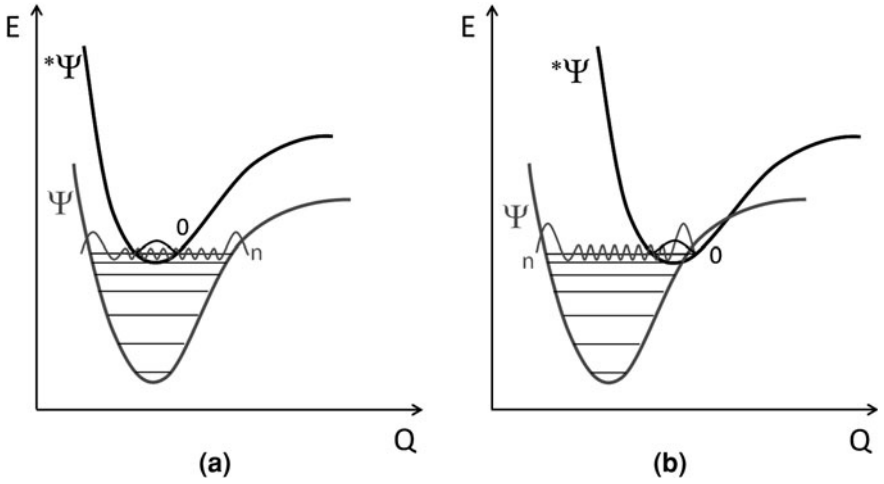

Fig. 1.10 Limiting cases for potential energy surfaces involved in radiationless deactivations

is the vibrational quantum number of the isoenergetic level of the ground state, and the smaller is the overlap. At a constant energy gap, the probability depends on the vibrational energy spacing of the ground state, since the smaller is the energy spacing, the higher is the vibrational quantum number of the isoenergetic level of the ground state, and the smaller is the overlap. Therefore, high-energy vibrations (e.g., C–H stretching in organic molecules) are more effective than low-frequency ones as energy-accepting modes. In fact, deuteration (lowering the frequency) is used as a tool for reducing the rate of radiationless transitions.

The situation sketched in Fig. 1.10b is that of potential energy surfaces crossing in the vicinity of the excited-state minimum. In this case there is always a relatively good vibrational overlap, independent of the vibrational quantum number of the ground-state level. In this situation, the probability of radiationless transition tends to be high, insensitive to the energy gap (as long as it does not alter the crossing situation), and independent of the vibrational frequency of the accepting mode.

In intermediate situations (minima nested but with crossing points not too far from the excited-state minimum) it may be more convenient for the molecule to go through the crossing point, because of a more favorable Franck–Condon factor, despite the substantial activation energy required. In these cases, the rates of radiationless transitions may become very sensitive to temperature.

In principle, radiationless transitions can occur between excited states as well as between an excited state and the ground state. Generally speaking, electronically excited states are relatively closely spaced with respect to the large energy separation occurring between the lowest excited state and the ground state. Moreover, high energy excited states are more likely to have distorted geometries than the lowest excited state. Both these facts favor radiationless transitions among excited states (small energy gaps and frequent crossing situations) with respect to those

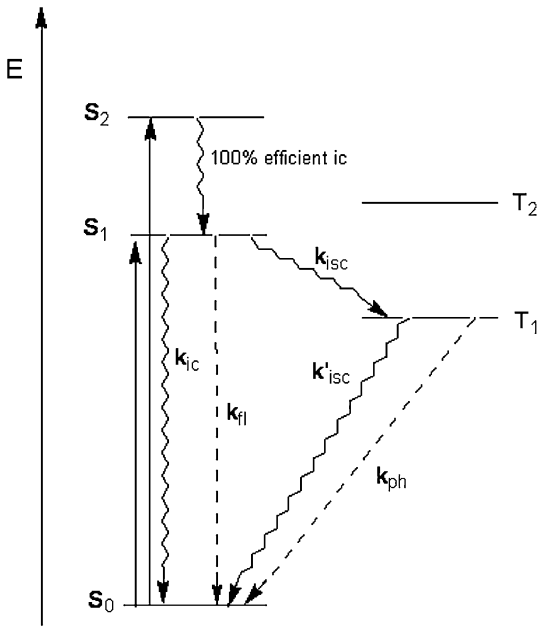

Fig. 1.11 Schematic energy level diagram for a generic organic molecule. For the sake of clarity, chemical reactions of excited states are not indicated

between the lowest state and the ground state (large energy gap and not distorted or even nested surfaces). Figure 1.11 illustrates the Jablonski diagram of a generic organic molecule. This schematic picture is at the basis of the experimental observation that (1) internal conversion within each excited state manifold of any given multiplicity (for example, $S_n \rightarrow \rightarrow S_1$ and $T_n \rightarrow \rightarrow T_1$) is exceedingly fast (usually in the picosecond region), (2) intersystem crossing between the lowest excited states of any multiplicity (for example, $S_1 \rightarrow T_1$) may be fast to moderately fast (sub-nanosecond to nanosecond region), and (3) radiationless deactivations from the lowest excited states of any multiplicity to the ground state are much slower (microseconds to nanoseconds for $S_1 \rightarrow S_0$ and seconds to milliseconds for $T_1 \rightarrow S_0$). This difference in rates is the basis of the famous Kasha rule (vide infra).

1.6.4 Chemical Reaction

The unimolecular excited-state processes described in Sects. 1.6.2 and 1.6.3 do not cause any chemical change in the light-absorbing molecule and can thus be classified as *photophysical* processes. Excited states can, however, achieve deactivation to ground-state species also by a variety of *chemical* processes. As energy-rich species, excited states are, as a whole, expected to be more reactive than the corresponding ground states. It would be misleading, however, to consider this enhanced reactivity from a quantitative viewpoint only. In fact, the excess

energy of electronically excited states is most often associated with an electronic structure quite different from that of the ground state. This may result in a reactivity that is qualitatively quite different. In this respect, it is worthwhile to think of electronically excited molecules as completely new chemical species, with their own specific reactivity.

A point which should be stressed is that excited-state reactions must be very fast on the conventional chemical time-scale, since they have to compete with the photophysical deactivation processes. In practice, excited-state reactions must be almost activationless processes. Therefore, the key to understanding excited-state reactivity is the identification of low-energy channels along the excited-state surface leading, perhaps via some surface crossing, to the potential energy minima of the ground-state products.

It is outside the scope of this introductory chapter to discuss in detail the types of reactions given by the various types of excited states. A number of textbooks [1, 8, 12] on organic and inorganic photochemistry cover this subject exhaustively.

1.6.5 Kinetic Aspects

Generally speaking, the three unimolecular processes (radiative deactivation, radiationless deactivation, and chemical reaction) described above compete for deactivation of any excited state of a molecule. Therefore their individual specific rates *and* the kinetics of their competition in each excited state are of utmost importance in determining the actual behavior of the excited molecule.

Thus, an excited state *A will decay according to an overall first-order kinetics, with *a lifetime,* $\tau(^*A)$, given by (1.8).

$$\tau(^*A) = 1/\left(k_r + k_{nr} + k_p\right) = 1/\Sigma_j k_j \tag{1.8}$$

For each process of the *A excited state, an *efficiency* $\eta_i(^*A)$ can be defined as in (1.9).

$$\eta_i(^*A) = k_i/\Sigma_j k_j = k_i \tau(^*A) \tag{1.9}$$

The *quantum yield* Φ_i of a given process originating from *A is defined as the ratio between the number of molecules undergoing the process per unit time and the number of photons absorbed per unit time. If an excited state *A (e.g., T_1 in Fig. 1.11) is populated following one or more nonradiative steps from other excited states, then the value of the quantum yield is given by Eq. (1.10),

$$\Phi_i = \Pi_n \eta_n \tag{1.10}$$

where the η_n terms represent the efficiencies of the various steps involved in the population of *A.

Since radiationless decay of upper excited states to the lowest one of the same multiplicity is very fast, generally it happens that the emitting level of a given

multiplicity is the lowest excited level of that multiplicity (Kasha rule [13]). For inorganic complexes, intersystem crossing has usually unitary efficiency because of the heavy atom (metal) induced spin–orbit coupling, so that emission (if any) occurs only from the lowest spin-forbidden excited state [14].

Though in principle the actual behavior of an excited molecule is the complex output of a complex system of consecutive/competitive processes, the exceedingly high rate of internal conversion between excited states is seen to simplify considerably the problem. In many instances, a careful evaluation of the factors affecting the kinetics of unimolecular processes of the lowest excited states gives the possibility of rationalizing and, to some extent, predicting the photochemical behavior.

References

1. Turro NJ, Ramamurthy V, Scaiano JC (2010) Modern molecular photochemistry of organic molecules, University Science Books, Sausalito
2. Klán P, Wirz J (2009) Photochemistry of organic compounds. Wiley, New York
3. Armaroli N, Balzani V (2011) Energy for a sustainable world from the oil age to a sun-powered future. Wiley-VCH, Weinheim ch. 11
4. Special issue on artificial photosynthesis (2009) Acc Chem Res 42(12)
5. Ciamician G (1912) Science 36:385–394
6. Atkins P, de Paula J (2009) Atkins physical chemistry, 9th edn. Oxford University Press, Oxford
7. Balzani V, Scandola F (1991) Supramolecular photochemistry. Horwood, Chichester
8. Balzani V, Carassiti V (1970) Photochemistry of coordination compounds. Academic Press, London
9. Jean Y (2005) Molecular orbitals of transition metal complexes. Oxford University Press, New York
10. Balzani V, Campagna S (2009) Photochemistry and photophysics of coordination compounds. Top Curr Chem, 280 and 281
11. Cotton FA (1990) Chemical applications of group theory, John Wiley & Sons, Chichester
12. Stochel G, Brindell M, Macyk W, Stasika Z, Szaciłowski K (2009) Bioinorganic photochemistry. Wiley, Chichester
13. Kasha M (1950) Faraday Soc Discuss 9:14
14. Crosby GA (1983) J Chem Ed 60:791

Chapter 2
Photoinduced Energy and Electron Transfer Processes

Paola Ceroni and Vincenzo Balzani

Abstract This chapter introduces the supramolecular photochemistry, i.e. photochemistry applied to supramolecular systems, and discusses the thermodynamic and kinetic aspects of photoinduced energy and electron transfer processes both between molecules and within supramolecular systems. In the case of electron transfer processes, Marcus theory is presented as well as quantum mechanical theory. For energy transfer processes, coulombic and exchange mechanisms are illustrated and the role of the bridge in supramolecular structures is discussed.

2.1 Bimolecular Processes

2.1.1 General Considerations

As we have seen in Sect. 1.6.5, each intramolecular decay step of an excited molecule is characterized by its own rate constant and each excited state is characterized by its *lifetime,* given by (1.8). In fluid solution, when the intramolecular deactivation processes are not too fast, i.e. when the lifetime of the excited state is sufficiently long, an excited molecule *A may have a chance to encounter a molecule of another solute, B. In such a case, some specific interaction can occur leading to the deactivation of the excited state by second order kinetic processes.

P. Ceroni · V. Balzani (✉)
Department of Chemistry "G. Ciamician", University of Bologna,
Via Selmi 2, 40126 Bologna, Italy
e-mail: vinicenzo.balzani@unibo.it

P. Ceroni (ed.), *The Exploration of Supramolecular Systems and Nanostructures by Photochemical Techniques*, Lecture Notes in Chemistry 78,
DOI: 10.1007/978-94-007-2042-8_2,

The two most important types of interactions in an encounter are those leading to electron or energy transfer:

$$^{*}\mathrm{A} + \mathrm{B} \rightarrow \mathrm{A}^{+} + \mathrm{B}^{-} \text{ oxidative electron transfer} \quad (2.1)$$

$$^{*}\mathrm{A} + \mathrm{B} \rightarrow \mathrm{A}^{-} + \mathrm{B}^{+} \text{ reductive electron transfer} \quad (2.2)$$

$$^{*}\mathrm{A} + \mathrm{B} \rightarrow \mathrm{A} + {}^{*}\mathrm{B} \text{ energy transfer} \quad (2.3)$$

Bimolecular electron and energy transfer processes are important because they can be used (i) to quench an electronically excited state, i.e. to prevent its luminescence and/or reactivity, and (ii) to sensitize other species, for example to cause chemical changes of, or luminescence from, species that do not absorb light.

Simple kinetic arguments (vide infra, Sect. 2.1.3) show that only the excited states that live longer than ca. 10^{-9} s may have a chance to be involved in encounters with other solute molecules. Usually, in the case of metal complexes only the lowest excited state satisfies this requirement.

A point that must be stressed is that an electronically excited state is a species with quite different properties compared with those of the ground state molecule. Therefore, both the thermodynamic and kinetic aspects of photoinduced energy and electron transfer reactions must be carefully examined.

2.1.2 Thermodynamic Aspects

In condensed phases, vibrational relaxation is a very fast process (10^{-12}–10^{-13} s) so that the electronically excited states involved in bimolecular processes are thermally equilibrated species (Sect. 1.6.1). This means that these reactions can be dealt with in the same way as any other chemical reaction, i.e. by using thermodynamic and kinetic arguments.

For a thermodynamic treatment of reactions involving excited states, we need to define the free energy difference between the excited and ground state of a molecule:

$$\Delta G(^{*}\mathrm{A}, \mathrm{A}) = \Delta H(^{*}\mathrm{A}, \mathrm{A}) - T\Delta S(^{*}\mathrm{A}, \mathrm{A}) \quad (2.4)$$

The readily available quantity for an excited state is its zero–zero energy E^{00}(*A, A), i.e. the energy difference between the ground and the excited state, both taken at their zero vibrational levels (Fig. 1.9). In the condensed phase at 1 atm, $\Delta H \approx \Delta E$, where ΔE is the internal (spectroscopic) energy. At 0 K, $\Delta E = \mathrm{NE}^{00}$(*A, A). This is also approximately true at room temperature if the vibrational partition functions of the two states are not very different. As far as the entropy term is concerned, it can receive three different contributions due to: (i) a change in dipole moment with consequent change in solvation; (ii) changes in the internal degrees of freedom; (iii) changes in orbital and spin degeneracy. This last

contribution is the only one which can be straightforwardly calculated, but unfortunately it is also the least important in most cases. For a change in multiplicity from singlet to triplet it amounts to 0.03 eV at 298 K, which means that it can usually be neglected if one considers the experimental uncertainties that affect the other quantities involved in these calculations. The entropy contribution due to changes in dipole moment can be calculated if the change in dipole moment in going from the ground to the excited state is known. Finally, the contribution of changes of internal degrees of freedom is difficult to evaluate.

Changes in size, shape and solvation of an excited state with respect to the ground state cause a shift (Stokes shift) between absorption and emission (Sect. 1.6.2). When the Stokes shift is small (often a necessary condition to have a sufficiently long lived excited state), the changes in shape, size, and solvation are also small and the entropy term in (2.4) may be neglected. In such a case, the standard free energy difference between the ground and the excited state can be approximated as

$$\Delta G^0(^*\mathrm{A}, \mathrm{A}) \approx \mathrm{NE}^{00}(^*\mathrm{A}, \mathrm{A}) \tag{2.5}$$

and the free energy changes of energy and electron transfer reactions can readily be obtained. An energy transfer process (2.3) will be thermodynamically allowed when E^{00}(*A, A)> E^{00}(*B, B). As far as the electron transfer processes (2.1) and (2.2) are concerned, within the approximation described above the redox potentials for the excited state couples may be calculated from the standard potentials of the ground state couples and the one-electron potential corresponding to the zero–zero spectroscopic energy (i.e. the E^{00} value in eV):

$$E^{\mathrm{o}}(\mathrm{A}^+/{}^*\mathrm{A}) = E^{\mathrm{o}}(\mathrm{A}^+/\mathrm{A}) - E^{00} \tag{2.6}$$

$$E^{\mathrm{o}}({}^*\mathrm{A}/\mathrm{A}^-) = E^{\mathrm{o}}(\mathrm{A}/\mathrm{A}^-) + E^{00} \tag{2.7}$$

The free energy change of a photoinduced redox process can then be readily calculated from the redox potentials, as is usually done for "normal" (i.e. ground state) redox reactions.

It should be noted that, as shown quantitatively by (2.6) and (2.7), an *excited state is both a stronger reductant and a stronger oxidant than the ground state* because of its extra energy content. Whether or not the excited state is a powerful oxidant and/or reductant depends, of course, on the redox potentials of the ground state.

2.1.3 Kinetic Aspects of Bimolecular Processes

Leaving aside for the moment a detailed treatment of the rate of photoinduced energy–and electron transfer (Sects. 2.3 and 2.5), we will briefly recall here some fundamental kinetic aspects of bimolecular processes involving excited states.

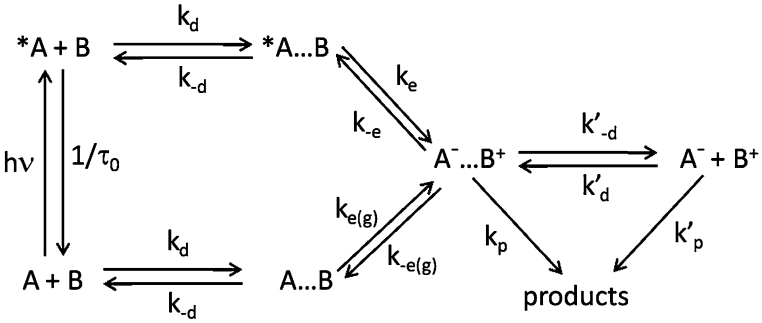

Fig. 2.1 Kinetic mechanism for photoinduced electron transfer reactions

For processes requiring diffusion and formation of encounters, we can use the Stern–Volmer model which assumes statistical mixing of *A and B. The simplest case is that of a species *A that decays via some intramolecular paths and, in fluid solution, can encounter a quencher B. The excited state lifetimes in the absence (τ_0) and in the presence (τ) of the quencher B are given by (2.8) and (2.9), where k_q is the bimolecular constant of the quenching process.

$$\tau_0 = 1/\left(k_r + k_{\mathrm{nr}} + k_p\right) \tag{2.8}$$

$$\tau = 1/\left(k_r + k_{\mathrm{nr}} + k_p + k_q[\mathrm{B}]\right) \tag{2.9}$$

Dividing (2.8) by (2.9), yields the well-known Stern–Volmer Eq. 2.10

$$\tau_0/\tau = 1 + k_q\tau_0[\mathrm{B}] \tag{2.10}$$

that can be used to obtain k_q when τ_0 is known. Since the maximum value of k_q is of the order of 10^{10} M^{-1} s^{-1} (diffusion limit) and [B] can hardly be $>10^{-2}$ M, it is clear that it is difficult to observe bimolecular processes in the case of excited states with lifetime $\leq 10^{-9}$ s.

The rate constant k_q of the bimolecular quenching process is, of course, controlled by several factors. In order to elucidate these factors, a detailed reaction mechanism must be considered. Since both electron transfer and exchange energy transfer are collisional processes, the same kinetic formalism may be used in both cases. Taking as an example a reductive excited state electron transfer process (2.2), the reaction rate can be discussed on the basis of the mechanism shown in the scheme of Fig. 2.1, where k_d, k_{-d}, k'_d, and k'_{-d} are rate constants for formation and dissociation of the outer-sphere encounter complex, k_e and k_{-e} are unimolecular rate constants for the electron transfer step involving the excited state, and $k_{e(g)}$ and $k_{-e(g)}$ are the corresponding rate constants for the ground state electron transfer step. A simple steady state treatment [1] shows that the experimental rate constant of (2.2) can be expressed as a function of the rate constants of the various steps by (2.11),

$$k_{\exp} = \frac{k_d}{1 + \frac{k_{-d}}{k_e} + \frac{k_{-d}k_{-e}}{k_x k_e}} \tag{2.11}$$

where k_x may often be replaced by k'_{-d} (for more details, see [2]). In a classical approach, k_{-e}/k_e is given by exp(- $\Delta G^0/RT$), where ΔG^0 is the standard free energy change of the electron transfer step. An analogous expression holds for bimolecular energy transfer.

The key step of the process is, of course, the unimolecular electron–(or energy-) transfer step (k_e). Before going into more details (Sect. 2.2.3), it is important to extend our discussion to photoinduced energy and electron transfer processes in supramolecular systems where *A does not need to diffuse to encounter B, but is already more or less close to B because A and B are linked together.

2.2 Supramolecular Photochemistry

2.2.1 Definition of a Supramolecular System

From a functional viewpoint the distinction between what is molecular and what is supramolecular can be based on the degree of inter-component electronic interactions [3]. This concept is illustrated, for example, in Fig. 2.2. In the case of a photon stimulation, a system A∼B, consisting of two units (∼indicates any type of "bond" that keeps the units together), can be defined a supramolecular species if light absorption leads to excited states that are substantially localized on either A or B, or causes an electron transfer from A to B (or viceversa). By contrast, when the excited states are substantially delocalized on the entire system, the species can be better considered as a large molecule. Similarly (Fig. 2.2), oxidation and reduction of a supramolecular species can substantially be described as oxidation and reduction of specific units, whereas oxidation and reduction of a large molecule leads to species where the hole or the electron are delocalized on the entire system. In more general terms, when the interaction energy between units is small compared to the other relevant energy parameters, a system can be considered a supramolecular species, regardless of the nature of the bonds that link the units. It should be noted that the properties of each component of a supramolecular species, i.e. of an assembly of weakly interacting molecular components, can be known from the study of the isolated components or of suitable model compounds.

A peculiar aspect of photoinduced energy and electron transfer in supramolecular systems is that the relative positions and distances between the excited state *A and the quencher B can be preorganized so as to control the rate of the process (vide infra).

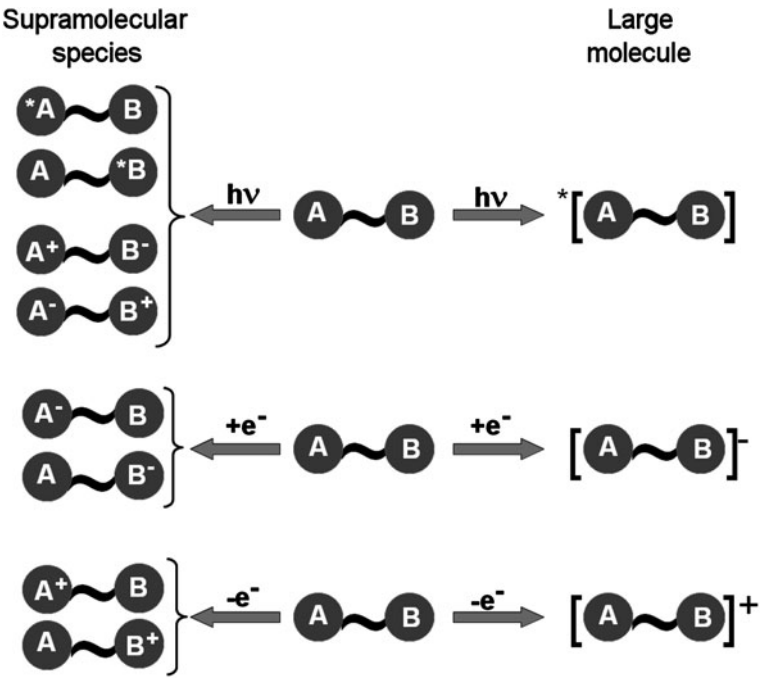

Fig. 2.2 Schematic representation of the difference between a supramolecular system and a large molecule based on the effects caused by a photon or an electron input. For more details, see text

2.2.2 Photoinduced Energy and Electron Transfer in Supramolecular Systems

For simplicity, we consider the case of an A–L–B supramolecular system, where A is the light-absorbing molecular unit (2.12), B is the other molecular unit involved with A in the light induced processes, and L is a connecting unit (often called bridge). In such a system, electron and energy transfer processes can be described as follows:

$$A - L - B \; + h\nu \rightarrow^{*} A - L - B \qquad \text{photoexcitation} \qquad (2.12)$$

$$^{*}A - L - B \rightarrow A^{+} - L - B^{-} \qquad \text{oxidative electron transfer} \qquad (2.13)$$

$$^{*}A - L - B \rightarrow A^{-} - L - B^{+} \qquad \text{reductive electron transfer} \qquad (2.14)$$

$$^{*}A - L - B \rightarrow A - L - ^{*}B \qquad \text{electronic energy transfer} \qquad (2.15)$$

In the absence of chemical complications (e.g. fast decomposition of the oxidized and/or reduced species), photoinduced electron transfer processes are followed by spontaneous back-electron transfer reactions that regenerate the

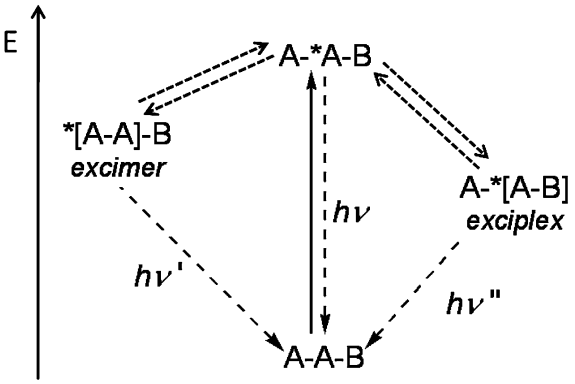

Fig. 2.3 Schematic representation of excimer and exciplex formation

starting ground state system (2.16 and 2.17), and photoinduced energy transfer is followed by radiative and/or non-radiative deactivation of the excited acceptor (2.18):

$$A^+ - L - B^- \rightarrow A - L - B \qquad \text{back oxidative electron transfer} \qquad (2.16)$$

$$A^- - L - B^+ \rightarrow A - L - B \qquad \text{back reductive electron transfer} \qquad (2.17)$$

$$A - L -^* B \rightarrow A - L - B \qquad \text{excited state decay} \qquad (2.18)$$

Since in supramolecular systems electron–and energy transfer processes are no longer limited by diffusion, they take place by first order kinetics and in suitably designed supramolecular systems they can involve even very short lived excited states. The reactions described by (2.13–2.15) correspond to the key step (first order rate constant k_e, Fig. 2.1) occurring in the analogous bimolecular reactions (2.1–2.3) taking place in the encounters formed by diffusion. The parameters affecting the rates of such unimolecular reactions will be discussed in Sects. 2.3 and 2.5.

2.2.3 Excimers and Exciplexes

In most cases, the interaction between excited and ground state components in a supramolecular system, and even more so in an encounter, is weak. When the interaction is strong, new chemical species, which are called excimers (from excited dimers) or exciplexes (from excited complexes), depending on whether the two interacting units have the same or different chemical nature. The scheme shown in Fig. 2.3 refers to a supramolecular system, but it holds true also for species in an encounter complex. It is important to notice that excimer and exciplex formation are reversible processes and that both excimers and exciplexes sometimes can give luminescence. Compared with the "monomer" emission, the

emission of an excimer or exciplex is always displaced to lower energy (longer wavelengths) and usually corresponds to a broad and rather weak band.

Excimers are usually obtained when an excited state of an aromatic molecule interacts with the ground state of a molecule of the same type. For example, between excited and ground state of anthracene units. Exciplexes are obtained when an electron donor (acceptor) excited state interacts with an electron acceptor (donor) ground state molecule, for example, between excited states of aromatic molecules (electron acceptors) and amines (electron donors).

It may also happen that in an encounter or a supramolecular structure there is a non negligible electronic interaction between adjacent chromophoric units already in the ground state. In such a case, the absorption spectrum of the species may substantially differ from the sum of the absorption spectra of the component units. When the units have the same chemical nature, the interaction leads to formation of dimers. When the two units are different, the interaction is usually charge-transfer in nature with formation of charge-transfer complexes. Excitation of a dimer leads to an excited state that is substantially the same as the corresponding excimer, and excitation of a charge-transfer ground state complex leads to an excited state that is substantially the same as that of the corresponding exciplex.

2.3 Electron Transfer Processes

From a kinetic viewpoint, electron transfer processes involving excited states, as well as those involving ground state molecules, can be dealt with in the frame of the Marcus theory [4] and of the successive, more sophisticated theoretical models [5].The only difference between electron transfer processes involving excited state instead of ground state molecules is that in the first case, in the calculation of the free energy change, the redox potential of the excited state couple has to be used (2.6 and 2.7).

2.3.1 Marcus Theory

In an absolute rate formalism (Marcus model [4]), potential energy curves of an electron transfer reaction for the initial (i) and final (f) states of the system are represented by parabolic functions (Fig. 2.4). The rate constant for an electron transfer process can be expressed as

$$k_{el} = \nu_N \kappa_{el} \exp\left(-\frac{\Delta G^{\neq}}{RT}\right) \tag{2.19}$$

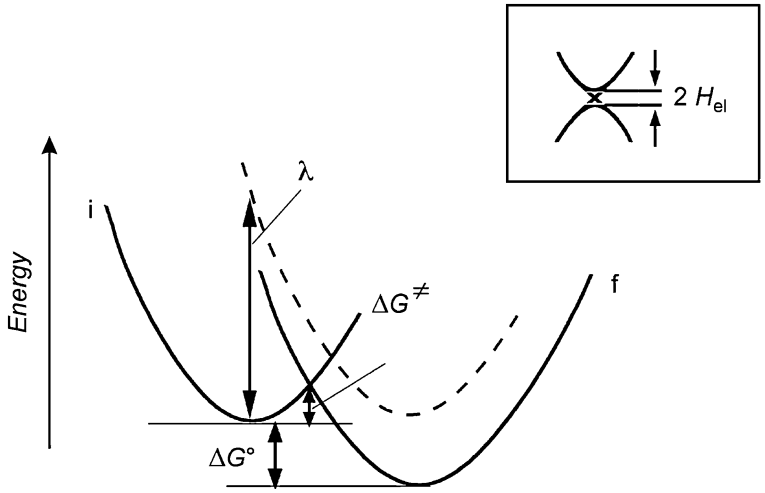

Fig. 2.4 Profile of the potential energy curves of an electron transfer reaction: *i* and *f* indicate the initial and final states of the system. The dashed curve indicates the final state for a self-exchange (isoergonic) process

where ν_N is the average nuclear frequency factor, κ_{el} is the electronic transmission coefficient, and $\Delta G^{\neq}$ is the free activation energy. This last term can be expressed by the Marcus quadratic relationship

$$\Delta G^{\neq} = \frac{1}{4\lambda}\left(\Delta G^0 + \lambda\right)^2 \tag{2.20}$$

where ΔG^0 is the standard free energy change of the reaction and λ is the nuclear reorganizational energy (Fig. 2.4).

Equations 2.19 and 2.20 predict that for a homogeneous series of reactions (i.e. for reactions having the same λ and k_{el} values) a ln k_{el} versus ΔG^0 plot is a bell-shaped curve (Fig. 2.5, solid line) involving:

- a normal regime for small driving forces ($-\lambda < \Delta G^0 < 0$) in which the process is thermally activated and ln k_{el} increases with increasing driving force;
- an activationless regime ($-\lambda \approx \Delta G^0$) in which a change in the driving force does not cause large changes in the reaction rate;
- an "inverted" regime for strongly exergonic processes ($-\lambda > \Delta G^0$) in which ln k_{el} *decreases* with increasing driving force [3].

The reorganizational energy λ can be expressed as the sum of two independent contributions corresponding to the reorganization of the "inner" (bond lengths and angles within the two reaction partners) and "outer" (solvent reorientation around the reacting pair) nuclear modes:

$$\lambda = \lambda_i + \lambda_o \tag{2.21}$$

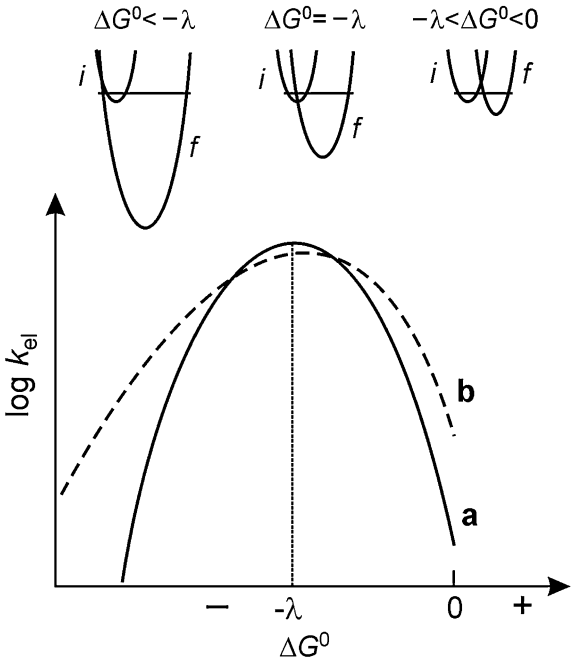

Fig. 2.5 Free energy dependence of electron transfer rate (*i*, initial state; *f*, final state) according to Marcus (a) and quantum mechanical (b) treatments. The three kinetic regimes (normal, activationless, and "inverted") are shown schematically in terms of Marcus parabolae

The outer reorganizational energy, which is often the predominant term in electron transfer processes, can be estimated, to a first approximation, by the expression

$$\lambda_o = e^2\left(\frac{1}{\varepsilon_{op}} - \frac{1}{\varepsilon_s}\right)\left(\frac{1}{2r_A} + \frac{1}{2r_B} - \frac{1}{r_{AB}}\right) \tag{2.22}$$

where e is the electronic charge, ε_{op} and ε_s are the optical and static dielectric constants of the solvent, r_A and r_B are the radii of the reactants, and r_{AB} is the inter reactant center-to-center distance. Equation 2.22 shows that λ_o is particularly large for reactions in polar solvents between reaction partners which are separated by a large distance.

The electronic transmission coefficient k_{el} is related to the probability of crossing at the intersection region (Fig. 2.4). It can be expressed by (2.23)

$$\kappa_{el} = \frac{2[1 - \exp(-v_{el}/2v_N)]}{2 - \exp(-v_{el}/2v_N)} \tag{2.23}$$

where

$$v_{el} = \frac{2\left(H^{el}\right)^2}{h}\left(\frac{\pi^3}{\lambda RT}\right)^{1/2} \tag{2.24}$$

and H^{el} is the matrix element for electronic interaction (Fig. 2.4, inset).

If H^{el} is large, $v_{el} \gg v_N$, $k_{el} = 1$ and

$$k_{el} = v_N \exp\left(\frac{-\Delta G^{\neq}}{RT}\right) \qquad \text{adiabatic limit} \tag{2.25}$$

If H^{el} is small, $v_{el} \ll v_N$, $k_{el} = v_{el}/v_N$ and

$$k_{el} = v_{el} \exp\left(\frac{-\Delta G^{\neq}}{RT}\right) \qquad \text{non - adiabatic limit} \tag{2.26}$$

Under the latter condition, k_{el} is proportional to $(H^{el})^2$. The value of H^{el} depends on the overlap between the electronic wavefunctions of the donor and acceptor groups, which decreases exponentially with donor–acceptor distance. It should be noticed that the amount of electronic interaction required to promote photoinduced electron transfer is very small in a common chemical sense. In fact, by substituting reasonable numbers for the parameters in (2.26), it can be easily verified that, for an activationless reaction, H^{el} values of a few wavenumbers are sufficient to give rates in the sub-nanosecond time scale, while a few hundred wavenumbers may be sufficient to reach the limiting adiabatic regime (2.25).

As discussed in Sect. 2.6, it can be expected that the connecting unit L (2.12–2.15) plays an important role in governing the electronic interaction between distant partners.

2.3.2 *Quantum Mechanical Theory*

From a quantum mechanical viewpoint, both the photoinduced and back-electron transfer processes can be viewed as radiationless transitions between different, weakly interacting electronic states of the A–L–B supermolecule (Fig. 2.6). The rate constant of such processes is given by an appropriate Fermi "golden rule" expression:

$$k_{el} = \frac{4\pi^2}{h}\left(H^{el}\right)^2 FC^{el} \tag{2.27}$$

where the electronic H^{el} and nuclear FC^{el} factors are obtained from the electronic coupling and the Franck–Condon density of states, respectively. In the absence of any intervening medium (through-space mechanism), the electronic factor decreases exponentially with increasing distance:

$$H^{el} = H^{el}(0) \exp\left[-\frac{\beta^{el}}{2}(r_{AB} - r_0)\right] \tag{2.28}$$

where r_{AB} is the donor–acceptor distance, $H^{el}(0)$ is the interaction at the "contact" distance r_0, and β^{el} is an appropriate attenuation parameter. The 1/2 factor arises

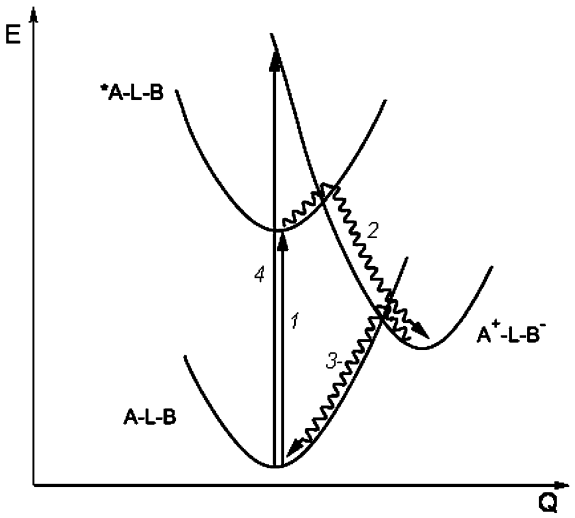

Fig. 2.6 Electron transfer processes in a supramolecular system: (1) photoexcitation; (2) photoinduced electron transfer; (3) thermal back-electron transfer; (4) optical electron transfer

because originally β^{el} was defined as the exponential attenuation parameter for rate constant rather than for electronic coupling, (2.29):

$$k_{el} \propto \exp\left(-\beta^{el} r_{AB}\right) \tag{2.29}$$

For donor–acceptor components separated by vacuum, β^{el} is estimated to be in the range 2–5 $Å^{-1}$.

When donor and acceptor are separated by "matter" (in our case, the bridge L) the electron transfer process can be mediated by the bridge. If the electron is temporarily localized on the bridge, an intermediate is produced and the process is said to take place by a sequential or "hopping" mechanism (Sect. 2.6). Alternatively, the electronic coupling can be mediated by mixing the initial and final states of the system with virtual, high energy electron transfer states involving the intervening medium (superexchange mechanism), as illustrated in Fig. 2.7.

The FC^{el} term of (2.27) is a thermally averaged Franck–Condon factor connecting the initial and final states. It contains a sum of overlap integrals between the nuclear wave functions of initial and final states of the same energy. Both inner and outer (solvent) vibrational modes are included. The general expression of FC^{el} is quite complicated. It can be shown that in the high temperature limit ($h\nu < k_B T$), an approximation sufficiently accurate for many room temperature processes, the nuclear factor takes the simple form:

$$FC^{el} = \left(\frac{1}{4\pi\lambda k_B T}\right)^{1/2} \exp\left[-\frac{(\Delta G^0 + \lambda)^2}{4\lambda k_B T}\right] \tag{2.30}$$

where λ is the sum of the inner (λ_i) and outer (λ_o) reorganizational energies. The exponential term of (2.30) is the same as that predicted by the classical Marcus model based on parabolic energy curves for initial and final states. Indeed, also the

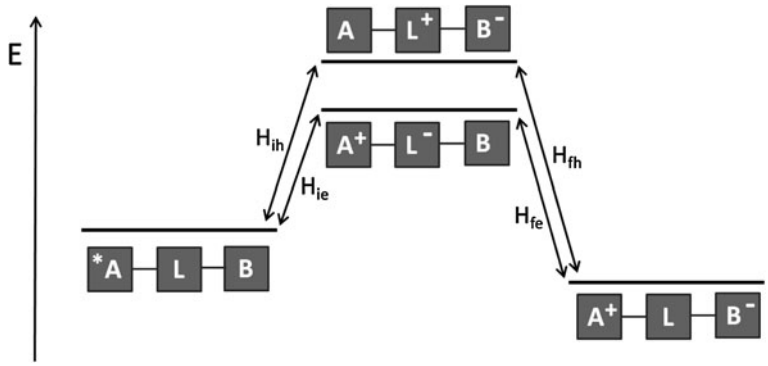

Fig. 2.7 State diagram illustrating superexchange interaction between an excited state electron donor (*A) and an electron acceptor (B) through a bridge (L)

quantum mechanical model contains the important prediction of three distinct kinetic regimes, depending on the driving force of the electron transfer process (Fig. 2.5). The quantum mechanical model, however, predicts a practically linear, rather then a parabolic, decrease of ln k_{el} with increasing driving force in the inverted region (Fig. 2.5, *dashed line*).

2.4 Optical Electron Transfer

The above discussion makes it clear that reactants and products of an electron transfer process are intertwined by a ground/excited state relationship. For example, for nuclear coordinates that correspond to the equilibrium geometry of the reactants, as shown in Fig. 2.6, A+–L–B− is an electronically excited state of A–L–B. Therefore, optical transitions connecting the two states are possible, as indicated by arrow 4 in Fig. 2.6.

The Hush theory [6] correlates the parameters that are involved in the corresponding thermal electron transfer process by means of (2.31–2.33)

$$E_{op} = \lambda + \Delta G^0 \tag{2.31}$$

$$\Delta\bar{\nu}_{1/2} = 48.06\left(E_{op} - \Delta G^0\right)^{1/2} \tag{2.32}$$

$$\varepsilon_{max}\Delta\bar{\nu}_{1/2} = \left(H^{el}\right)^2 \frac{r^2}{4.20 \times 10^{-4} E_{op}} \tag{2.33}$$

where E_{op}, $\Delta\bar{\nu}_{1/2}$ (both in cm^{-1}), and ε_{max} are the energy, halfwidth, and maximum intensity of the electron transfer band, and r (in Å) the center-to-center distance. As shown by (2.31–2.33), the energy depends on both reorganizational energy and thermodynamics, the halfwidth reflects the reorganizational energy, and the intensity

of the transition is mainly related to the magnitude of the electronic coupling between the two redox centers. In principle, therefore, important kinetic information on a thermal electron transfer process may be obtained from the study of the corresponding optical transition. In practice, due to the dependence of the intensity on H^{el}, optical electron transfer bands may only be observed in systems with relatively strong inter-component electronic coupling [e.g. for H^{el} values of 10, 100, and 1000 cm^{-1}, ε_{max} values of 0.2, 20, and 2000 M^{-1} cm^{-1}, respectively, $\Delta\bar{\nu}_{1/2} = 4000$ cm^{-1} and $r = 7$Å are obtained from (2.33) by using $E_{op} = 15000$ cm^{-1}]. By recalling what is said at the end of Sect. 2.3.1, it is clear that weakly coupled systems may undergo relatively fast electron transfer processes without exhibiting appreciably intense optical electron transfer transitions. More details on optical electron transfer and related topics (i.e. mixed valence metal complexes) can be found in the literature [7].

2.5 Energy Transfer Processes

The thermodynamic ability of an excited state to intervene in energy transfer processes is related to its zero–zero spectroscopic energy, E^{00}. From a kinetic viewpoint, bimolecular energy transfer processes involving encounters can formally be treated using a Marcus type approach, i.e. by equations like (2.19) and (2.20), with $\Delta G^0 = E_A{}^{00}–E_B{}^{00}$ and $\lambda \sim \lambda_i$ [8].

Energy transfer, particularly in supramolecular systems, can be viewed as a radiationless transition between two "localized", electronically excites states (2.15). Therefore, the rate constant can be again obtained by an appropriate "golden rule" expression:

$$k_{en} = \frac{4\pi^2}{h}(H^{en})^2 FC^{en} \tag{2.34}$$

where H^{en} is the electronic coupling between the two excited states inter-converted by the energy transfer process and FC^{en} is an appropriate Franck–Condon factor. As for electron transfer, the Franck–Condon factor can be cast either in classical or quantum mechanical terms. Classically, it accounts for the combined effects of energy gradient and nuclear reorganization on the rate constant. In quantum mechanical terms, the FC factor is a thermally averaged sum of vibrational overlap integrals. Experimental information on this term can be obtained from the overlap integral between the emission spectrum of the donor and the absorption spectrum of the acceptor.

The electronic factor H^{en} is a two-electron matrix element involving the HOMO and LUMO of the energy-donor and energy-acceptor components. By following standard arguments [5], this factor can be split into two additive terms, a *coulombic* term and an *exchange* term. The two terms depend differently on the parameters of the system (spin of ground and excited states, donor–acceptor

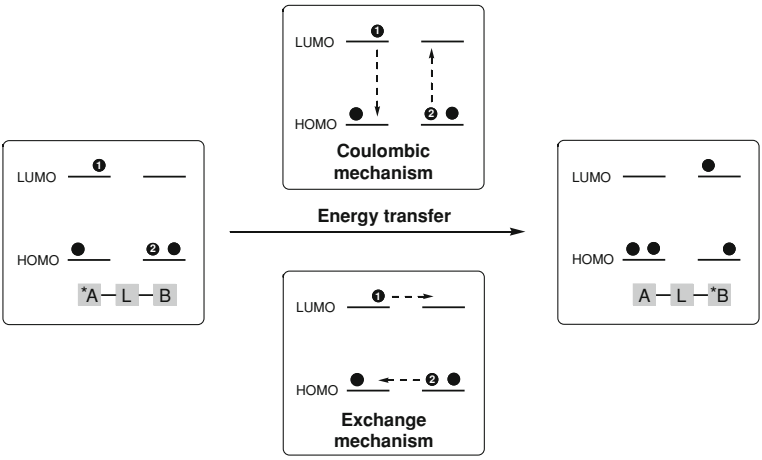

Fig. 2.8 Pictorial representation of the coulombic and exchange energy transfer mechanisms

distance, etc.). Because each of them can become predominant depending on the specific system and experimental conditions, two different mechanisms can occur, whose orbital aspects are schematically represented in Fig. 2.8.

2.5.1 Coulombic Mechanism

The coulombic (also called resonance, Förster-type [9, 10], or through-space) mechanism is a long-range mechanism that does not require physical contact between donor and acceptor. It can be shown that the most important term within the coulombic interaction is the dipole–dipole term [9, 10], that obeys the same selection rules as the corresponding electric dipole transitions of the two partners (*A → A and B → *B, Fig. 2.8). Coulombic energy transfer is therefore expected to be efficient in systems in which the radiative transitions connecting the ground and the excited state of each partner have high oscillator strength. The rate constant for the dipole–dipole coulombic energy transfer can be expressed as a function of the spectroscopic and photophysical properties of the two molecular components and their distance.

$$k_{\mathrm{en}}^{\mathrm{F}} = \frac{9000 \ln 10}{128\pi^5 N} \frac{K^2 \Phi}{n^4 r_{\mathrm{AB}}^6 \tau} J_{\mathrm{F}} = 8.8 \times 10^{-25} \frac{K^2 \Phi}{n^4 r_{\mathrm{AB}}^6 \tau} J_{\mathrm{F}} \tag{2.35}$$

$$J_F = \frac{\int \frac{F(\overline{\nu})\varepsilon(\overline{\nu})}{\overline{\nu}^4} \mathrm{d}\overline{\nu}}{\int F(\overline{\nu}) \mathrm{d}\overline{\nu}} \tag{2.36}$$

where K is an orientation factor which takes into account the directional nature of the dipole–dipole interaction ($K^2 = 2/3$ for random orientation), Φ and τ are, respectively, the luminescence quantum yield and lifetime of the donor, n is the solvent refractive index, r_{AB} is the distance (in Å) between donor and acceptor, and J_F is the Förster overlap integral between the luminescence spectrum of the donor, $F(\bar{\nu})$, and the absorption spectrum of the acceptor, $\varepsilon(\bar{\nu})$, on an energy scale (cm^{-1}). With good spectral overlap integral and appropriate photophysical properties, the $1/r_{AB}^6$ distance dependence enables energy transfer to occur efficiently over distances substantially exceeding the molecular diameters. The typical example of an efficient coulombic mechanism is that of singlet–singlet energy transfer between large aromatic molecules, a process used by Nature in the antenna systems of the photosynthetic apparatus [11].

2.5.2 Exchange Mechanism

The rate constant for the exchange (also called Dexter-type [12]) mechanism can be expressed by:

$$k_{en}^{D} = \frac{4\pi^2}{h}(H^{en})^2 J_D \tag{2.37}$$

where the electronic term H^{en} is obtained from the electronic coupling between donor and acceptor, exponentially dependent on distance:

$$H^{en} = H^{en}(0)\exp\left[-\frac{\beta^{en}}{2}(r_{AB} - r_0)\right] \tag{2.38}$$

The nuclear factor J_D is the Dexter overlap integral between the emission spectrum of the donor and the absorption spectrum of the acceptor:

$$J_D = \frac{\int F(\bar{\nu})\varepsilon(\bar{\nu})d\bar{\nu}}{\int F(\bar{\nu})d\bar{\nu}\int \varepsilon(\bar{\nu})d\bar{\nu}} \tag{2.39}$$

The exchange interaction can be regarded (Fig. 2.8) as a double electron transfer process, one-electron moving from the LUMO of the excited donor to the LUMO of the acceptor, and the other from the acceptor HOMO to the donor HOMO. This important insight is illustrated in Fig. 2.9, from which it is clear that the attenuation factor β^{en} for exchange energy transfer should be approximately equal to the sum of the attenuation factors for two separated electron transfer processes, i.e. β^{el} for electron transfer between the LUMO of the donor and acceptor (2.29), and β^{ht} for the electron transfer between the HOMO (superscript ht denotes for hole transfer from the donor to the acceptor).

The spin selection rules for this type of mechanism arise from the need to obey spin conservation in the reacting pair as a whole. This enables the exchange

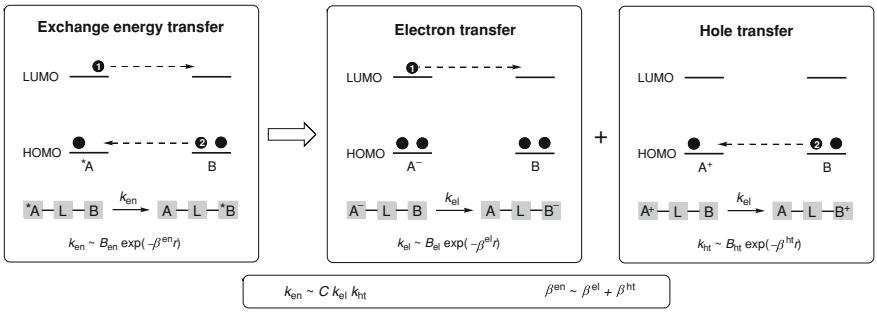

Fig. 2.9 Analysis of the exchange energy transfer mechanism in terms of electron–and hole transfer processes. The relationships between the rate constants and the attenuation factors of the three processes are also shown

mechanism to be operative in many instances in which the excited states involved are spin forbidden in the usual spectroscopic sense. Thus, the typical example of an efficient exchange mechanism is that of triplet–triplet energy transfer:

$$^{*}\mathrm{A}(\mathrm{T}_1) - \mathrm{L} - \mathrm{B}(\mathrm{S}_0) \rightarrow \mathrm{A}(\mathrm{S}_0) - \mathrm{L} - ^{*}\mathrm{B}(\mathrm{T}_1) \qquad (2.40)$$

Exchange energy transfer from the lowest spin forbidden excited state is expected to be the rule for metal complexes [13].

Although the exchange mechanism was originally formulated in terms of direct overlap between donor and acceptor orbitals, it is clear that it can be extended to coupling mediated by the intervening medium (i.e. the connecting bridge), as discussed above for electron transfer processes (hopping and super exchange mechanisms).

2.6 The Role of the Bridge in Supramolecular Systems

The discussion above underlines the important role played by the connecting units (bridges) in mediation of electron- and energy transfer processes between donor and acceptor components in supramolecular structures [3]. As a colloquial way of emphasizing this role, it has become customary to consider bridges as "molecular wires" and to talk of their "conducting" properties. It should be remarked, however, that in the super exchange mechanism the bridge levels are always much higher in energy than those of donor and acceptor (Fig. 2.7), so the electron tunnels in a single step from donor to acceptor. Electron–and energy transfer processes through such bridges are, therefore, not comparable with electron transfer in macroscopic systems where the electron really moves along the wire. In some cases, however, the energy level of the bridge is so low that it becomes intermediate between the initial and final states. As a consequence, electron or energy hopping occurs and the bridge is directly involved in the process.

When such a hopping-type mechanism is operative, very small distance dependence of the rate constants is expected [3].

Finally, when there is complete mixing among the donor/bridge/acceptor orbitals (large coupling limit) the bridge essentially acts as an incoherent molecular wire, as happens for conjugated conducting polymers, and the system is expected to behave according to an ohmic regime where the distance dependence of the rate varies inversely with bridge length.

References

1. Balzani V, Scandola F (1991) Supramolecular photochemistry. Horwood, Chichester
2. Balzani V, Bolletta F, Scandola F (1980) J Am Chem Soc 102:2152
3. Balzani V, Venturi M, Credi A (2008) Molecular devices and machines. Wiley-VCH, Weinheim
4. Marcus RA (1964) Annu Rev Phys Chem 15:155
5. Scandola F, Chiorboli C, Indelli MT, Rampi MA (2001) In: Balzani V (ed) Electron transfer in chemistry, Vol 3. Wiley-VCH, Weinheim, p 337
6. Hush NS (1967) Prog Inorg Chem 8:391
7. Launay J-P, Coudret C (2001) In: Balzani V (ed) Electron transfer in chemistry, Vol 5. Wiley-VCH, Weinheim, p 3
8. Balzani V, Indelli MT, Maestri M, Sandrini D, Scandola F (1980) J Phys Chem 84:852
9. Barigelletti F, Flamigni L (2000) Chem Soc Rev 29:1
10. Scholes GD (2003) Annu Rev Phys Chem 54:57
11. Pullerits T, Sundström V (1996) Acc Chem Res 29:381
12. Dexter DL (1953) J Chem Phys 21:836
13. Scandola F, Balzani V (1983) J Chem Ed 60:814

Chapter 3
Spectrophotometry, Measurements in Solution

Nelsi Zaccheroni

Abstract In this chapter the reader can find an overview on the UV–vis absorption spectroscopy technique. A very brief introduction on the nature and formation of the electronically excited states is functional to the following discussion on the characteristics, and interpretation of UV–vis absorption spectra. The typical instrumentation is also schematically described, and a particular emphasis is devoted to the possible qualitative and quantitative information that can be obtained with this kind of measurements. Practical indications to obtain accurate and reliable experimental results were introduced with the aim to help the readers that will approach for the first time this fundamental experimental technique. The chapter ends with the discussion of a few examples, taken from the literature, with the aim to make clear the investigative great potentialities of this spectroscopy in different fields.

3.1 Introduction

Molecules can be promoted to their excited states if exposed to suitable 'perturbations', in particular when appropriate energy to be absorbed is provided, as discussed in Chap. 1. The light-matter interaction is the easiest way to obtain an excited state. The energy gained by a molecule when it absorbs a photon (or better, the energy transported by photons) causes an electron to be promoted to a higher

N. Zaccheroni (✉)
Department of Chemistry "G. Ciamician", University of Bologna, Via Selmi 2, 40126 Bologna, Italy
e-mail: nelsi.zaccheroni@unibo.it

P. Ceroni (ed.), *The Exploration of Supramolecular Systems and Nanostructures by Photochemical Techniques*, Lecture Notes in Chemistry 78,
DOI: 10.1007/978-94-007-2042-8_3,

electronic energy level. This is possible only if the energy of the radiation is at least equal to the energy gap between the ground and the excited state.

Electronic transitions in molecules need energies correlated to wavelengths that are in the range of the ultraviolet (UV) and visible spectral regions. The absorption of a UV or visible photon by a molecule induces changes in the distribution of the electrons surrounding the nuclei, and in the forces between the atomic nuclei of a molecule. As a result, molecules in electronically excited states often have very different chemical and physical properties than their electronic ground states.

These transitions give rise to electronic absorption spectra typical of each species. *Spectrophotometry* studies in a qualitative and quantitative way the absorption spectra and, more in detail, can be seen as the collection of the techniques, methodologies, and analytical and theoretical concepts that enables the characterization of the electronic absorption spectra.

This chapter aims to give an easy-reading overview on this theme with particular attention for the more technical aspects of the field. For a deeper and exhaustive treatment of electronic absorption spectroscopy more specific texts are recommended [1, 3].

3.2 The Absorption Spectrum

The interaction of a photon with a molecule can be schematized in a very general form:

$$A + h\nu \rightarrow A^* \tag{3.1}$$

where A is the molecule in its ground state, $h\nu$ is the absorbed photon and A* the molecule in its excited state. A* has an extra energy of hν with respect to A.

As already mentioned, the regions of interest for photochemistry are the UV–vis ones, and this means light radiations in the range 200 nm–1,000 nm. The energy that one molecule can gain with the absorption of a photon is therefore significant and it could take to bond breaking, but there are many different possible deactivation processes and the fate of the molecule depends on their competition, as discussed in detail in Chap.1.

Very importantly, *an excited state must be considered as a new chemical species in comparison with the molecule in its ground state* and can present different chemical and physical properties. The excited states and the ground one differ, in fact, for the distribution of the external electrons that are the ones interacting with the environment, and, therefore, the ones determining the chemical reactivity of a substance. An example is reported in Fig. 3.1 that compares some characteristics of formaldehyde in the ground state and in its lower excited state.

The extra-energy of an excited state that comes from the photon absorbance induces the promotion of an electron from an orbital at lower energy to an orbital at a higher energy level. This means that *the absorption of radiant energy*

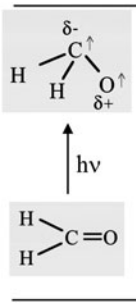

	+ 76 Kcal/mol	pyramidal	paramagnetic	1.3 D	1.31 Å	$<10^{-3}$ sec
	energy	**geometry**	**magnetism**	**Dipolar moment**	**r_{CO}**	**lifetime**
	0	planar	diamagnetic	2.3 D	1.22 Å	∞

Fig. 3.1 Comparison between some of the properties of formaldehyde in its ground state and in its lower excited state

is associated to an electronic transition. Being the energetic order and separation of the orbitals an own characteristic of each molecular species, as a consequence, *each molecule presents its own characteristic absorption spectrum*.

Since each transition corresponds to the absorption of light with the energy corresponding to the energetic separation between the initial and final levels of the electronic transition, one could expect absorption spectra to appear as series of separated lines, each typical of a specific transition. This is exactly true only for atoms but not for molecules that possess also vibrational and rotational energy levels for each electronic state. For each single electronic energy level, in fact, many transitions are possible to different vibrational and/or rotational energy levels, with the evident consequence that the absorption spectra are not constituted by lines but by bands of different width (Fig. 3.2). If the sample is in the gas phase it is possible to have vibrational resolution and the absorption spectrum is constituted by a series of joint sharp peaks. This is not the case for species in solution, where the additional interactions with the solvent make the vibrational multiplicity so high that the sharp peaks are so close together to coalesce forming non structured large bands.

The two fundamental characteristics of these bands are their position and their intensity. The position of a band is defined by the wavelength of its maximum intensity that is called λ maximum (λmax), and therefore the energy connected to that electronic transition can be calculated with the Plank equation:

$$\mathrm{E} = h\nu$$

The intensity of the band depends on the probability of the absorption, that is to say of the interaction between the incident radiation and the electrons of the system. The excitation of a molecule changes its electronic distribution and this gives rise to a dipole moment connected with the transition itself, that is proportional to its probability. A high absorption of light is possible for transitions with an high probability, that is to say with transitions that induce high variations in the dipole moment. These transitions are called *allowed* while low probability transitions are called *forbidden* and they present low absorptions values.

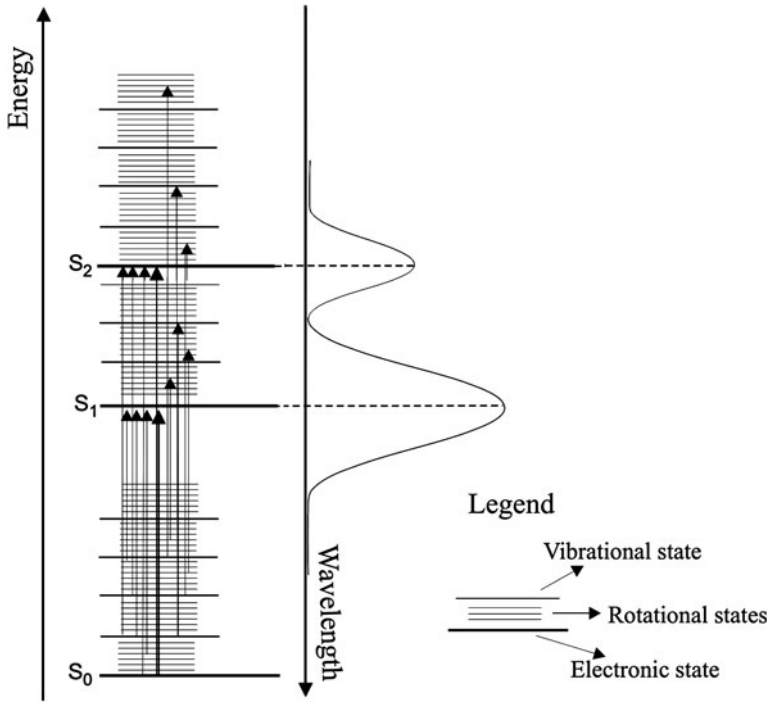

Fig. 3.2 Correlation between electronic transitions and absorption spectra in molecules

Some mathematical rules deriving by quantum mechanics and called *selection rules* (see Sect.1.5) allow to determine if a certain transition is possible and intense or not. This topic is very complex and a deeper discussion is beyond the scope of this chapter, the interested readers can find exhaustive treatments in specialized texts [1–3].

In the following section, anyway, the reader can find a qualitative and brief overview of the groups that give rise to absorption bands in the UV–vis region but, before discussing this more in detail, it can be useful to introduce some terms that are typical of this kind of spectroscopy. The list hereafter is definitely non exhaustive but it is functional to the aims of this contribution.

- A *chromophore* is a species, a part of it or a single group that is able to absorb light in the UV–vis range (unsaturated bonds, conjugated bonds, metal complexes). When it absorbs visible light it is also responsible of the colour of the compound.
- An *auxochrome* group is a saturated functional group presenting one or more lone pairs, it is attached to a chromophore and it is able to modify both its absorption wavelengths and intensity.

- A *bathochromic shift* is a change in the position of the absorption (but also transmittance or emission) band toward longer wavelengths (lower energies), it is also called *red shift*. It can be due to solvent, pH or substituents effects.
- A *hypsochromic shift* is a change in the position of an absorption (but also transmittance or emission) band toward shorter wavelengths (higher energies), it is also called *blue shift*. It can be due to solvent, pH or substituents effects.
- The *hyperchromic effect* is the increase of absorbance of a species.
- The *hypochromic effect* is the decrease of absorbance of a species.
- The *isosbestic point* is defined as a wavelength at which the absorbance of two substances, one of which can be converted into the other, is the same. Therefore at this wavelength the total absorbance of the sample does not change during the chemical reaction or the physical change of one into the other. The presence of one (or more) stable *isosbestic points*, as a consequence, is the evidence that the reaction is proceeding without forming intermediates or multiple products.

3.3 The General Absorption Characteristics of Molecules

The absorption characteristics of molecules depends on their nature since the possible electronic transitions in organic and inorganic species are different. The energetic levels and succession of molecular orbitals in organic molecules and in metal complexes have been already discussed in (Sect. 1.4), I will only recall here some fundamental features for the interpretation of an absorption spectrum.

For an organic molecule the increasing energy scale for the possible electronic transitions (Sect. 1.4.1) is: $\sigma \rightarrow \sigma^* > \pi \rightarrow \pi^* > n \rightarrow \pi^*$ (Fig. 1.4).

The $n \rightarrow \pi^*$ bands are associated with forbidden transitions and therefore they are generally weak, often covered by more intense ones, and their position in the spectrum is strongly dependent by the polarity of the solvent.

The $\pi \rightarrow \pi^*$ bands are typical of π conjugated systems, aromatic and substituted aromatic ones. These are allowed transitions and hence generally intense ones.

The $\sigma \rightarrow \sigma^*$ bands correspond to very energetic transitions and therefore they are positioned at low frequencies in the far UV, a spectral region that is not possible to investigate if not in inert atmosphere or in the void since the high atmospheric oxygen absorption in this range (from 200 nm downwards).

All the bands mentioned above are generally positioned in the UV (far and near) interval of the spectrum that is the very typical absorption range of conjugated unsaturated bonds and of aromatic rings, also presenting heteroatoms. In particular, some chromophores absorbing in the range 210–380 nm, that can be investigated using common instrumentation and in aerated solutions, will be introduced.

Ethylene and molecules with simple double bonds absorb around 150–160 nm but the conjugation of two or more of them causes a bathochromic shift of the band. This can be attributed to the decreasing energy gap between the last occupied π orbital and the first π^* one, with the increasing number of single π olefin orbitals to be combined, but only if coplanarity between them is possible. For the same reason, when cis and trans isomers are possible, the trans one always absorbs at longer wavelengths since the cis form is generally more sterically hindered and coplanarity is unfavoured. Conjugation in unsaturated systems can induce very large shifts of the absorption band to reach the visible part of the spectra as for β-carotene that, with its ten conjugated double bonds, is orange absorbing around 450 nm. Many empirical methods have been proposed to determine, in butadienic systems, the shift entity of the maximum absorption wavelength from a starting value summing constant contributions depending from the kind and the number of the bond auxochoromes. The values of these contributions are defined on statistical basis after the study of a great number of compounds. The most commonly used method is called the rule of Woodward-Hoffman, [1] and it estimates, as an example, a bathochromic shift of 30 nm for the conjugation with an additional double bond, of 5 nm for each alkyl group, and one of 60 nm for a substituent of the kind NR_2.

Another very interesting and important family absorbing in the UV range is the one of aromatic compounds. Benzene is the simplest one and presents three absorption bands in this region but only one at wavelengths >210 nm and precisely around 250 nm, but it is a forbidden band an therefore very weak. The position of these bands depends from the substituents present on the ring, and from their relative position. In general the substitution of the ring causes a bathochromic shift that can take one or more of the absorption bands in the visible range. This red shift is substantially a mesomeric effect since the presence of groups that present only and inductive effect do not cause any significant change in the maximum wavelength of the absorption spectra. The conjugation of more aromatic groups, direct or mediated by other unsaturated groups, causes even a higher bathochromic shift but only if the conjugation is possible.

As mentioned above the behaviour of inorganic molecules is quite different. They generally present significant absorptions also in the visible range and sometimes in the near IR (infra-red), like for example transition metal complexes.

Also in this case the different bands are characterized by the nature of the molecular orbitals involved in the electronic transition (Sect. 1.4.2) and two principal classes distinguished: (1) transitions that do not induce a charge transfer and that can be centred on the metal (metal centred, MC) or on the ligand (ligand centred, LC); (2) transitions that involve a charge transfer (CT) that can be from the ligand to the metal (LMCT) or vice versa from the metal to the ligand (MLCT).

The metal centred bands originates from transitions between metal orbitals ($d \rightarrow d$) that require low energies but that are forbidden for the selection rules and as a consequence characterized by low absorptions, weak bands.

On the contrary the bands due to transitions centred on the ligands are possible in complexes presenting aromatic ligands and are due to $\pi \rightarrow \pi^*$ transitions, they are positioned in the UV region and may be covered by CT ones.

Describing the metal complexes as systems where the metal centre and the peripheral ligands interact only weakly, charge transfer transitions can be seen as the addition to or the subtraction of an electron form the partially filled external orbitals of the metal. These transitions result in a change of the oxidation state of the metal of plus or minus one and they can be of two different types.

The LMCT can be observed in the UV and visible regions and their energy depends on the redox properties of both the metal and the ligand. They lay at lower and lower energy with the increasing oxidative ability of the metal and reductive ability of the ligand. When the complex is formed by all equivalents ligands the electron is assumed to come from a molecular orbital delocalized on all of them, while in case of mixed ligands the electron is given to the metal by the most reductive one.

On the contrary the MLCT bands are present when the central metal has a low ionization potential and at least one ligand possesses an empty accessible π^* orbital (CN–, CO, pyridine, phenanthroline, etc.). They are generally allowed transitions and therefore they originate intense bands with a quite high energy, lying in the UV or blue region of the visible.

3.4 Qualitative Analysis

Molecules, in general, do not possess enough energy at room temperature to reach electronically excited states since the energy difference between the ground state and the first electronically excited state is relatively high. As a consequence almost all molecules at around 298 K are in their ground state.

Absorption spectra in the visible and UV range present a few and large bands and give limited qualitative information, in comparison with, for example, IR spectra that allow to identify and discriminate many functional groups of organic molecules. In UV–vis spectroscopy the maxima of these bands are not determined by the single functional group but, on the contrary, they are dependent on the whole structure of the molecule that is absorbing light: on the number, nature and conjugation of the unsaturations, on the presence or not of transition metal ions, on the solvent, pH and temperature. This makes very difficult to univocally identify the structure of an unknown species only by its UV–vis absorption spectrum. The absorption spectrum, anyway, can confirm with certainty the identity of a substance by comparison, when the absorption spectrum of that species is already known.

The discussion reported in Sect. 3.3 about the general absorption characteristics of different families of molecules makes clear how it can be realistic that the spectra of two different substances present in the same sample show very similar profiles. In such cases, in order to distinguish between two different substances,

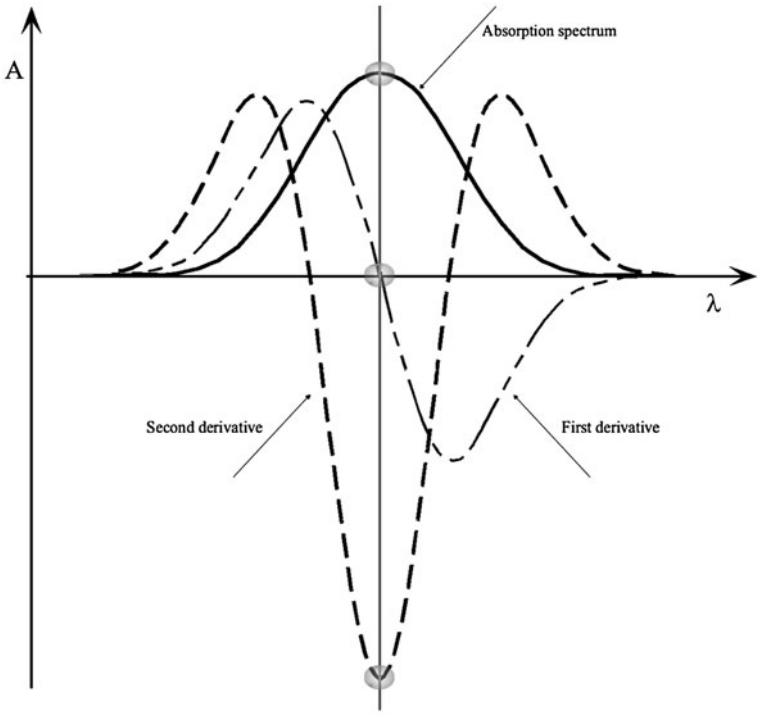

Fig. 3.3 First (— – —) and second (—) derivative of an absorption band presenting a Gaussian profile (*solid line*)

it can be useful to study the spectra of their derivatives. The use of derivates in UV–vis spectroscopy is, in fact, a very simple and valuable technique in order to enhance resolution or, sometimes, to discriminate the components of a mixture, and it can highly contribute to enhance the qualitative descriptive ability of the spectra resolving their fine structure.

The absorption spectrum is generally represented as absorbance versus wavelength, hence its first derivative ($dA/d\lambda = f'(\lambda)$) gives the extent of the absorbance variation as a function of the wavelength. The differentiation of a simple Gaussian band generates a more complex profile that assumes again the value of zero in the starting and ending points, and at the wavelength of the maximum of the absorption band. It presents therefore a negative and a positive band, with respectively the minimum and maximum at the wavelengths values corresponding to the inflection points of the initial Gaussian band (Fig. 3.3, line (— – —)).

The second derivative is generally more functional to clearly localize the absorption maximum than the first one, since it presents its characteristic minimum at the same wavelength of the maximum of the absorption band (Fig. 3.3, line (—)).

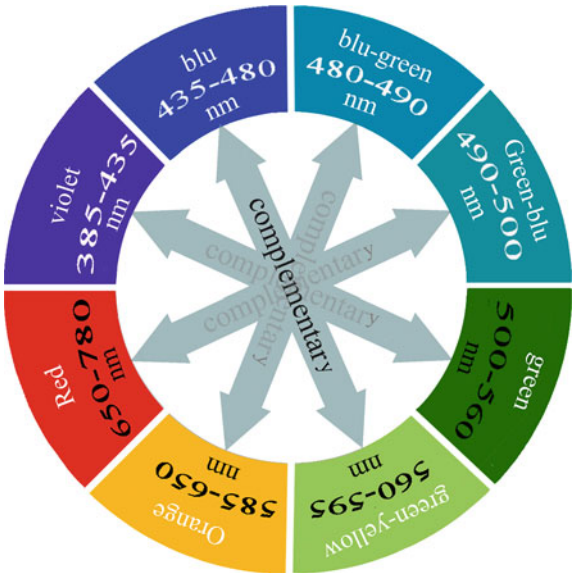

Fig. 3.4 The human eye sees the complementary radiation to the one absorbed by the sample

Moreover, in this case, the noise is generally lower than for the first derivative function.

In conclusion transforming the absorbance spectrum into its derivative (both of the first or second order) can be very useful in order to evidence differences between spectra, to solve superimposed bands in qualitative analysis and, in quantitative analysis, to decrease the effects of the interferences generated by diffusion, by the matrix or by other species that absorb in the same areas.

The most immediately perceptible characteristic of a compound is certainly its colour, that depends indeed on the visible light that it absorbs and that is therefore determined by its absorption spectrum. Generation and recognition of colours are phenomena ruled by very complex mechanisms depending on many factors, a detailed discussion on this topic is beyond the goal of this chapter but the reader, if interested, can find many texts that extensively report on this subject. [4, 5] I would like here only to clarify how the human eye perception of the colour of a compound is related to its absorption spectrum. When we look to a certain sample only the transmitted radiation can reach our eyes and this is what we see: *the complementary colour of the absorbed radiation* (Fig. 3.4).

3.5 Quantitative Treatment of the Absorption Intensity

When light passes through a sample (or it is reflected by it) the transmitted radiation will be different from the incident one. The absorbed light will be therefore given by the difference between the intensity of the incident light (I_0) and

the intensity of the transmitted radiation (I), and it can be expressed in *transmittance* or in *absorbance*.

It is named *transmittance* T (3.2) of a solution the fraction of the incident radiation transmitted by the solution:

$$T = I / I_0 \text{ or in percent } \%T = (I / I_0) \times 100 \tag{3.2}$$

The *absorbance* A (3.3) of a solution, on the contrary, is defined by the following equation:

$$A = -\log_{10} T = \log_{10} I_0 / I \tag{3.3}$$

This definition derives by the empiric relationship between the quantity of the absorbed light and the characteristics of a sample that, in the case of solutions, was independently found and proposed in different formulations by three scientists during more than a century: P. Bouguer in 1729, J. H. Lambert in 1760 and A. Beer in 1852. Experimental observations indicated that transmittance depends in an exponential way both on the *path length*, that is to say the distance the light travels through the sample, and on the concentration of the analyte. Indicating with b the path length (in centimetres), that for solutions corresponds to the length of the cuvette in which the sample is contained, and with c is the *molar concentration* of the analyte in solution, one can express the differential variation of the intensity of the light for each infinitesimal distance dx travelled through the sample as:

$$\mathrm{d}I = -\varepsilon c\, I\, \mathrm{d}x \tag{3.4}$$

The minus sign is due to the fact that the light intensity is absorbed and therefore it decreases passing through the sample, while ε indicates the proportionality constant typical of each substance, for each single wavelength in defined conditions of solvent and temperature, and it is named *molar absorption coefficient*.

The integration of this differential equation from the intensity value of the incident light I_0, to the final one revealed by the detector I, is equal to the absorbance A of the solution, and it yields the equation that is known with the name of *Lambert–Beer law* (3.7):

$$\mathrm{d}I/I = -\varepsilon c\, \mathrm{d}x \tag{3.5}$$

$$\int_{I_0}^{I} dI/I = -\int_{0}^{b} \varepsilon c \mathrm{d}x \tag{3.6}$$

$$\mathrm{A} = \log_{10} I_0 / I = \varepsilon b c \tag{3.7}$$

Consequently:

$$I = I_0 10^{-A} = I_0 10^{-\varepsilon b c} \tag{3.8}$$

$$T = I / I_0 = 10^{-\varepsilon b c} \tag{3.9}$$

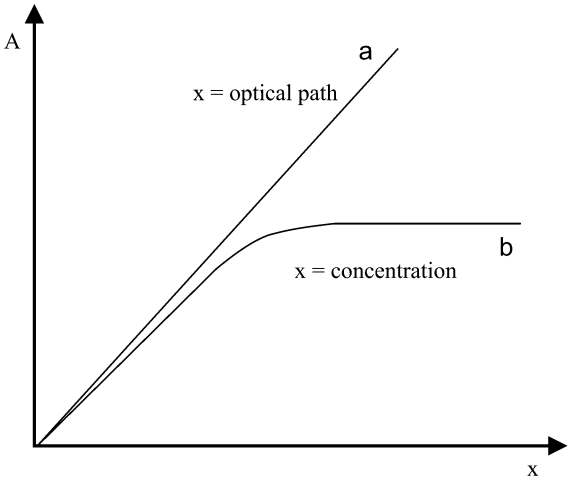

Fig. 3.5 **a** Absorbance dependence on path length; **b** absorbance dependence on the concentration of the species absorbing the incident light

The dependence of the absorbance on path length and concentration is reported in Fig. 3.5 that clearly shows how it is always linear for the first one (a), while, for concentration, it is linear only for very dilute solutions (b).

This indicates that the Lambert–Beer law is a *limit law*: it would be perfectly obeyed only at infinite dilution conditions, but it is possible to apply it in the case of dilute solutions, while it is not at all obeyed at high concentrations. It is not possible to specify a general limiting value for the applicability range, since it depends both on the analyte and on the instrumentation in use. It is anyway reasonable to consider absorbance values higher of 2–2.5 in a range of not total linearity. Moreover, significant deviations from the Lambert–Beer law, obviously, are expected when the analyte dissociates, associates or reacts in solution, yielding products presenting a different absorption spectrum.

It has to be noted that the absorbance of a solution, on the contrary of its transmittance, increases with the increasing attenuation of the incident radiation, and that for the measurement of both of them it is necessary to take into account many experimental features that we are now going to discuss more in detail.

When the analyte of interest is in a liquid solution, in order to perform the measurement the solution must be placed in a vessel that takes the name of *cell* or more precisely of *cuvette*. In order to perform a precise measurement the cuvette must be defectless, perfectly clean, and totally transparent to the incident radiation. However, even in this optimal conditions, it will never be possible to completely annul the light reflection phenomena that take place at both the interfaces air/cuvette wall and cuvette wall/solution. Moreover, very big molecules or very thin dispersed particulate in solution can induce light diffusion phenomena inside the solution itself.

This results in a significant beam attenuation that cannot be neglected. In order to take this into account the intensity transmitted by the solution containing the analyte is usually compared with the one transmitted by an identical cell containing all the components of the sample in study except for the analyte itself (*blank*), to obtain an experimental absorbance circa equal to the true one:

$$A = \log_{10} I_{\text{blank}} / I_{\text{sample}} \approx \log_{10} I_0 / I \tag{3.10}$$

A careful calibration of the instrument before the measurement is also very important in order to set the 0% of transmittance (when the incident beam is completely shielded and it does not reach the detector at all, in the modern instrumentation there is an auto-zero function), and the 100% of transmittance (the measured value obtained for the *blank*, an exactly equal sample but in absence of the analyte, that reflects the contaminations from sources external to the component in analysis).

3.6 Quantitative Analysis

Absorption spectroscopy is a very versatile technique that is extensively used in quantitative chemical analysis. It presents very interesting characteristics: (1) it can be applied to organic and inorganic systems, both in solution (topic of this chapter) and in the solid state, (2) it presents high sensitivity, (3) good accuracy, and (4) it requires not expensive and quite simple instrumentation. It is worth to noticing how spectrophotometric measurements not only allow to perform direct determinations of organic and inorganic species that present characteristic absorption bands in the UV–vis region, but also indirect quantitative measurements of species that do not absorb in this range. In these cases, in fact, one can mix these non-absorbing or weakly absorbing compounds with species able to selectively react with them to yield products presenting intense absorption bands in the region in study. The use of this kind of reagents in quantitative analysis is usually possible only when the formation reaction of the coloured compound is quantitative.

A fundamental feature of the spectrophotometric analysis is that the absorbance is an additive function. The Lambert–Beer law states that absorbance is proportional to the number or molecules that absorb the radiation at each wavelength, and this principle is valid even for different absorbing species. This means that the absorbance of a mixture at a given wavelength is equal to the sum of the absorbance of each component of the sample at that wavelength and this is at the bases of all quantitative spectrophotometric methods. Very importantly, this is no longer the case when two or more of the present species interact or react with one another.

The quantitative spectroscopic analysis methods can be divided in three classes that will be separately discussed hereafter.

3.6.1 The Method of the Standard Additions

In order to perform the quantitative investigation of a sample some initial settings are needed: the individuation of the right condition of analysis (see Sect. 3.8) and the calibration of the instrument. To this last goal it is always a good practice not to trust a single measurement of a solution of known concentration, but to prepare a calibration curve using a set of solutions with different and known concentrations, the so called *standard solutions*. These solutions should closely reproduce the global composition of the sample in analysis and span in a concentration range that includes also the one of the analyte. This is not very easy, and for very complex matrixes like soils and biological samples, it is sometimes impossible. In these cases the problem can generally be solved by following the method of the standard additions: increasing known volumes of a standard solution of the analyte are added to a precise volume of the sample in study. The graphic of the values of the absorbance of the solution in the initial conditions and after each addition versus the volumes of added standard solution gives a straight line, and the intercept is proportional to the unknown concentration of the analyte in the sample to determine.

$$A = (\varepsilon_x b V_x c_x / V_{tot}) + (\varepsilon_{standard} b V_{standard} c_{standard} / V_{tot}) \tag{3.11}$$

Equation 3.11, therefore, allows to determine c_x with a quite simple procedure, but only if all the measurements are carried on in experimental conditions of validity of the Lambert–Beer law.

3.6.2 Analysis of Mixtures of Absorbing Species

It is also possible the quantitative analysis of solutions containing mixtures of components presenting overlapping absorption spectra on the whole range of the measured wavelengths, but only if the behaviour of each component is independent from each other in the experimental conditions, and all the measurements are performed in the range of validity of the Lambert–Beer law. If this is the case, the absorbance is an additive function and therefore it is possible to solve the system reported hereafter with two unknowns, after the determination of the different ε values in standard solutions and the measurement of the absorbance value of the mixture in study at two different wavelengths (if the system presents two components, at three wavelengths for systems with three components, and so on).

$$A_1 = \varepsilon_{1x} b c_x + \varepsilon_{1y} b c_y \quad (\text{per} \lambda = \lambda_1) \tag{3.12}$$

$$A_2 = \varepsilon_{2x} b c_x + \varepsilon_{2y} b c_y \quad (\text{per} \lambda = \lambda_2) \tag{3.13}$$

3.6.3 Spectrophotometric Titrations

Spectrophotometric measurements can also be used to determine the equivalent point in a titration when the analyte, the reagent or the product of the titration absorb in the UV–vis region.

A spectrophotometric titration curve is a graphic of the absorbance values, corrected for the volume variations, versus the added quantity of the titrating agent. For example, if we titrate an uncoloured species with another uncoloured one but the product of their reaction is coloured, an immediate and liner increase of the absorbance will be detected until the complete reaction of the unknown species with the titrating agent. For further additions of the titrating agent, then, the absorbance value will not undergo any other change (if not for a pure diluting effect). This data can be used to determine the concentration of the analyte of interest in solution, and in particular the graph of the absorbance values at a single wavelength versus the added quantity of the titrating agent (expressed in equivalents, concentration or added volume) will present a profile evidencing a significant slope variation centred at the concentration value of the analyte in solution. It is common to choose for the plotting the wavelength corresponding to the maximum of the absorbance in order to monitor the point of maximum variation, minimizing the uncertainties. In order to obtain a consistent result it is necessary that all the absorbing systems follow the Lambert–Beer law, otherwise the extrapolation of the final point would be impossible in a non linearity range. As already mentioned, it is also crucial to correct the data taking into account the variations of the total volume after each addition during the titration. To this goal each experimental recorded data will be multiplied by a correction factor $(V + v)/V$ where V is the initial solution volume and v is the added volume of the titrating agent.

Since the absorbance variations are generally very sharp and easily detectable, it is possible to titrate also very dilute solutions and this makes this technique suitable to follow many different kinds of reactions: redox, acid/base, precipitations, metal ions complexation, and enzymatic ones.

3.7 Instrumentation

The equipment able to measure the transmittance and absorbance of a sample versus the wavelength of the incident radiation is called *spectrophotometer*. It is possible to outline it in the following components:

- an electromagnetic source of radiations;
- a monochromator to select a specific wavelength (or a narrow range of wavelengths) from the wide band of the radiations emitted by the source;
- a housing for the sample;
- one or more detectors to measure the intensity of the transmitted radiation.

The spectrophotometer also includes other optical parts to collimate and redirect the light inside the instrument, such as lens and mirrors of different kinds. In this respect, it is important to notice that on each optical surface, including the interfaces between the different components, there is a loss of light of circa 5–10% due to absorption or reflection phenomena, this can explain the tendency to minimize the number of optical surfaces in the modern instruments.

A synthetic description of each constituent is reported hereafter, but for a more detailed and precise information it is suggested to refer to instrumental analytic texts [6] or to the manuals that all the instrument suppliers provide to the users with the machine (usually available also on line).

3.7.1 The Light Source

The ideal electromagnetic radiation source, for this kind of instruments, would be a device able to emit radiations with a constant intensity over the whole wavelength range, presenting also a remarkable stability, long lasting, and a low noise. A light source with all these exact features does not exist, and the UV–vis spectrophotometers employ two different lamps to cover all the range of analysis, mixing their emitted light, or using a selector to pass from one to the other. The two lamps normally used are: a deuterium arc lamp for short wavelengths (180–350 nm), and a tungsten filament-halogen lamp for the longer wavelengths (330–900 nm).

The deuterium arc lamp presents a good continuity and intensity in the ultraviolet region, and a low noise level, but a poor continuity, in the visible range (Fig. 3.6). The intensity of the emitted light of these lamps decreases constantly in time and generally it becomes half of the initial one in circa 1,000 h.

The tungsten filament-halogen lamp presents a good continuity, intensity and stability over a part of the UV and the whole visible range (Fig. 3.6), moreover, it is able to guarantee a low noise and a lifetime of circa 10,000 h.

An alternative to these two light sources can be the xenon lamp, that is continuous and intense over the whole UV–vis region (Fig. 3.6) but with the important drawback of a much higher noise. For this reason it is generally mounted only in dedicated instrumentation for applications needing a very high intensity.

3.7.2 The Monochromator

Monochromators are elements able to select single wavelengths (or better to say very narrow wavelength bands) of the light emitted by the continuous sources. They deviate each single beam of a different angle, like a prism divides the sun light in the component colours of the electromagnetic spectrum, generating the so called “rainbow effect”. In modern spectrophotometers the most commonly used

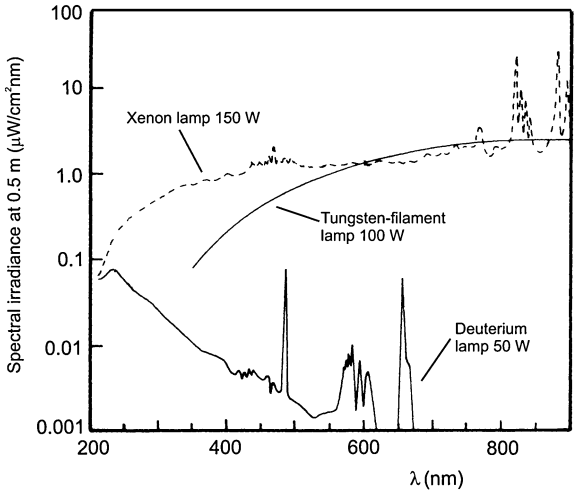

Fig. 3.6 Intensity profiles of the deuterium, tungsten filament, and xenon lamps (with permission of LOT-Oriel)

Fig. 3.7 Schematic representation of a single beam spectrophotometer

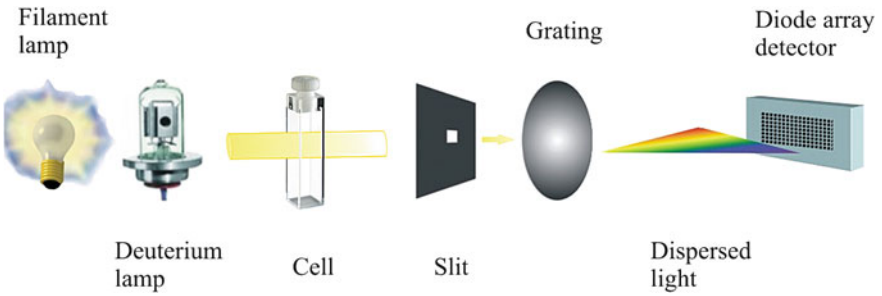

Fig. 3.8 Schematic representation of a single beam spectrophotometer with a diode array detector

monochromators are the so called holographic gratings. They are glasses patterned, via an holographic optical process, with extremely thin lines of the same order of magnitude of the wavelength of the light that they disperse. The incident light is reflected with different angles, depending on the wavelength and following an angular linear dispersion; if the grating is concave, moreover, it is able to

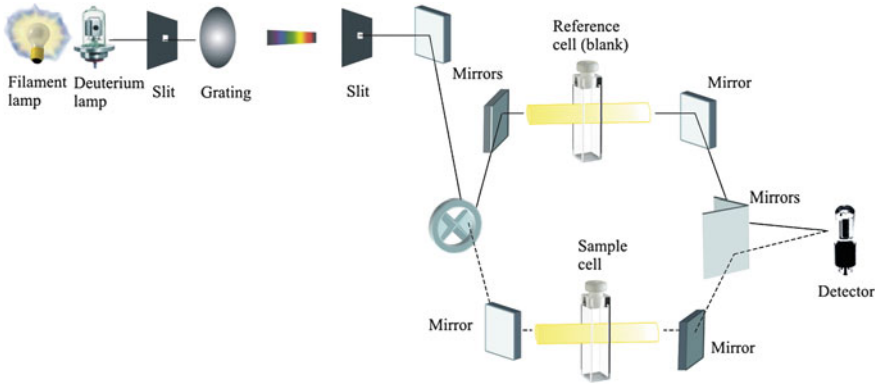

Fig. 3.9 Schematic representation of a double beam spectrophotometer

disperse and focus the light at the same time. This components present the great advantage to be insensitive to temperature.

The monochromator can be schematized with an entrance slit, a dispersing element (the grating), and an exit slit. It should transmit a monochromatic light but the passing light is always a band of wavelengths with a symmetric shape, and its width at half height is defined as spectral bandwidth (SBW). Typically a single monochromator can reach SBW of circa 5–10 nm while for more accurate spectroscopic measurements SBW of 1–2 nm, or even less, are needed and this can be obtained when two or more monochromators are used in series.

3.7.3 The Sample Holder

In the case of solutions typically the measurements are performed using plastic, glass or quartz rectangular cells with a square section (see Sect. 3.7.1 and Fig. 3.10), an optical pathway of 1 cm, and they are commonly named *cuvettes*. There are a great number of commercial cells that differ for shape, material, volume for the diverse applications: cylindrical, thermostated, flow, with optical pathways from 1 μm to 10 cm and volumes down to a few microliters, and this allows the study of a wide range of concentrations, of quantities and samples with very low or very high absorbance.

Whatever cuvette is used, it is always fundamental its location, it has to be fixed in a perfectly reproducible position both in height and orientation. Almost all modern spectrophotometers can be supplied with a series of devices for the control of the sample conditions such as thermostating, stirring, multi-sample holders or auto-samplers. Recently the possibility to study remote samples has been introduced and developed using optical fibers that are able to take the excitation signal from the light source to the remote analyte, but also the transmitted light back to the detector. This allows the measurement of both transmittance and reflectance

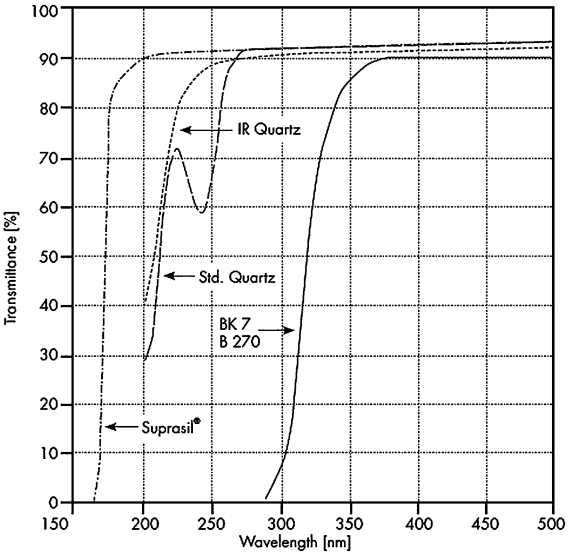

Fig. 3.10 Optical transmission of some materials used in the preparation of the cells for absorption spectroscopy (with permission of LOT-Oriel)

for analytes which are otherwise very difficult to study, for example, in paintings and artworks, or in the organs of a patient (in vivo monitoring).

There are also different and efficient solutions to locate solid samples inside the spectrophotometer to study their transmittance or their total reflectance. These housing systems allow to orient the sample at different angles with respect to the incident light to measure both the incident and diffuse reflectance. It is also possible to use the so called integrating spheres that completely surround the sample and are able to collect all the reflected light to measure the value of the total reflectance.

A deeper discussion on reflectance and solid samples goes beyond the goals of this contribution, and the interested readers can refer to the wide and dedicated literature [7].

3.7.4 The Detector

The detector is devoted to the conversion of the light signal in an electric one, ideally it should be linear in the widest range possible, and present a high sensitivity and a low noise. Generally modern spectrophotometers mount photomultiplier tubes or photodiode detectors.

The photomultiplier tubes convert the signal and, most importantly, they amplify it to such an extent that a single photomultiplier can grant a high

sensitivity in the whole UV–vis range; this sensitivity is particularly significant for low light levels.

It has to be noted, however, that in spectrophotometric measurements, a high sensitivity is necessary in conditions of low absorbance and, therefore, of high transmittance. This means in a situation of high levels of light reaching the detector, as a consequence the detector must be able to operate at high intensities with very low noise, to be able to discriminate between the blank and the sample in high dilution conditions.

Nowadays the use of photodiodes is more and more commonly spread, even if their sensitivity is much lower than that of phototubes, since they present other interesting advantages. They are, in fact, smaller, more economic, they present a wider range of detection, they do not need a high voltage to work and they are more robust in comparison with photomultiplier tubes. A photodiode is constituted by a semiconductor material that thanks to the photon absorption generates an electron flow, called photocurrent, that is proportional to the intensity of the incident light. In silicon based detectors, good operation working conditions are possible in the range 170–1,100 nm roughly. In modern instrumentation photodiodes are located in arrays one next to the other on a silicon crystal; these photodiodes work independently and they allow to measure the intensity variation on the whole range of the wavelengths of interest and, therefore, to record a complete absorption spectrum in a very short time (few seconds). These detectors are complex components but, being solid devices, they can guarantee a high reliability.

3.7.5 The Spectrophotometers

There are different types of commercial spectrophotometers presenting different configurations each with its own advantages and disadvantages. The most important and diffused ones are described and schematically represented hereafter (Figs. 3.7, 3.8, 3.9).

3.7.5.1 The Single Beam Model

The single beam configuration is the most traditional one, easy, low cost but with a high yield and sensitivity. In this configuration the polychromatic light emitted by the source is concentrated onto the entrance slit of the monochromator that selects and transmits a very narrow band of light. This band is focused on the sample and, after passing through the sample, it reaches the detector (Fig. 3.7). The absorbance of the sample is calculated measuring first the light intensity that reaches the detector when the cell contains the blank (Sect. 3.5), and then comparing it with the light intensity that reaches the detector after passing through the sample. When the detector is a photomultiplier tube, considering that the serial acquisition of the

data is a slow process, this model is suitable to measure the absorbance of a single wavelength of the spectrum, and therefore useful above all for analytical and kinetic studies.

When the detector is a diode array one (Fig. 3.8), the incident polychromatic light emitted by the source passes through the sample, and then it is concentrated, thanks to an exit slit, onto a polychromator that disperses the transmitted light in the different wavelengths before it reaches the diode array. All the diodes measure the spectrum at the same time, each of them detecting a narrow band, and therefore working as the exit slit of a monochromator. The width of the analyzed spectrum range depends on the number and the characteristics of the diodes, for example in order to measure the region between 190 and 1,100 nm with a good resolution it is typically necessary an array containing 1,024 diodes.

This configuration is called inverted optic since, with respect to the traditional configuration described above, the relative positions of the sample and the light dispersing component are inverted. Also in this case the analyte spectrum is obtained recording the differences between the light intensities that reach the detector after passing through the blank and through the sample. Due to its intrinsic nature this spectrophotometer model is suitable to measure spectra, since data are acquired at the same time on the whole range of interest, and it is consequently very fast. This configuration guarantees reliability and reproducibility, but it presents a lower sensitivity with respect with the parent model mounting a photomultiplier tube in detection.

In these instruments, in order to minimize the sample degradation and damage due to the incident light, the beam coming from the source is always blocked by a shutter strictly excepting measuring time.

3.7.5.2 The Double Beam Model

In single beam spectrophotometers, as explained above (see Sect. 3.7.5.1), the measurements of the blank and the sample are recorded one after the other, with delays that can be of seconds or minutes. This experimental methodology unavoidably exposes to the risk of possible current fluctuations, intensity variations of the lamp or other problems that could give rise to significant errors. To overcome these problems the double beam configuration has been introduced. It includes a mechanical modulator or a beam splitter along the optical pathway just after the monochromator and before the sample holders that are two in this configuration (Fig. 3.9). In the double beam spectrophotometer models the blank and the sample are measured at the same time. The modulator in fact alternates the path of the light coming from the source once to pass through the reference standard and then through the sample. Its speed is so high that it is possible to record many alternate measurements per second, avoiding the errors related to the light intensity variations of the lamp in the short and in the long period. Comparing this configuration with the single beam one, this instrumentation requires a higher

number of optical components and an overall more complex mechanic. This higher instrumental complexity could negatively influence the instrument sensitivity.

3.8 The Sample Measurement

Excluding the incorrect use of the instrumentation or its malfunctioning, the most common errors in UV–vis spectroscopic measurements are due to the composition and/or to the treatment of the sample.

3.8.1 The Cells

Speaking about liquid samples or solutions, the first thing that has to be carefully controlled is the treatment of the cuvettes used. As already anticipated, there are a great number of different commercial cells to meet the requirements of the various samples and applications (see for examples the online catalogues of specialized providers like the Hellma company). It is obvious that the first fundamental characteristic to satisfy is the transparency in the spectral range of the measurement. In Fig. 3.10 are shown the transmittances of some materials commonly used to prepare spectrophotometric cells. The figure makes clear that if the region of interest includes wavelengths below 300 nm, glass and plastic (even if resistant to the solvent in use) cells can not be used for the measurement. It is also worth noticing that all the materials present a maximum of transmittance of around 90%, this means that, in any case, the cuvette itself causes, at least, a 10% loss of the intensity of the transmitted light.

In order to obtain precise and reliable measurements the choice of the cell is very important, but also its quality that has to be very high to guarantee perfectly smooth and parallel surfaces. There is, anyway, another point at least as much important, that is to follow some essential precautions and procedures in the preparation of the sample.

First of all, it is necessary to carefully handle the cells to avoid to scratch or even only to touch the optical surfaces since any imperfection, including an imperceptible fingerprint, can absorb or diffuse light. It is therefore important to always accurately clean the outside of the cells with specific tissues or papers suitable to clean photographic instrumentation components and, in case, with some ethanol for glass or quartz cells, so as the stopper and the hole cone, if present. Moreover, when successive measurements are needed the cell must be placed in the holder always in the same direction, to be sure that the intrinsic optical effects of the cuvette influence all the measurements to the same exact extent.

To minimize the polluting risks it is anyway always better to rinse the cell with the solvent used for the measure and to control its transmittance in the spectral range of interest before the introduction of the solution in analysis.

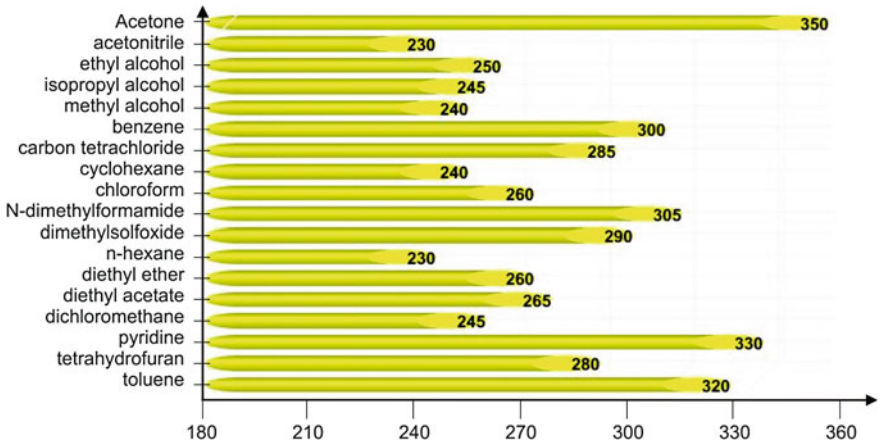

Fig. 3.11 Bar representation of the absorption intervals presenting an absorbance higher of 10% of the incident light for the most common solvents. In the intervals not covered by the bars the transmittance is higher than 90%

3.8.2 The Solvent

The solvent for the sample preparation must be able to dissolve the target analyte, it has also to be transparent for all the investigated wavelengths and, if possible, non-flammable and non-toxic solvents are always advised. Water presents all these features but, unfortunately, it is not a good solvent for many species, above all organic ones. When it is necessary to use organic solvents one has to consider, besides the transparency window, (Fig. 3.11) also their volatility. When using a very volatile solvent, in fact, it is necessary to place the sample in a closed cell to avoid concentration variations of the analyte due to solvent evaporation during the measurement.

The position and the intensity of the absorption bands of a given analyte can be influenced very much by the used solvent and they are generally correlated to its polarity. In comparative analysis it is therefore fundamental to use the same solvent for all the measurements to be evaluated, also because a change in the polarity of the solvent could induce or inhibit interspecies associations in the same sample. It is also important to consider that the use of too high concentrations could favour association processes, and, above all, take to the non linearity range of the absorbance.

To minimize the error causes, one must use only solvents labelled as suitable for UV–vis absorption measurements by the manufacturer on the packaging, this guarantees the necessary high purity degree. Since many samples are pH sensitive, these solvents must have a known and specified acidic content, again reported on the label. When the addition of a buffer is anyway necessary, it is essential to ascertain that its constituting species do not absorb in the investigation interval. Another very important point is that all solvents contain impurities and/or

stabilizing agents, including more or less relevant traces of other solvents; it is therefore necessary to always control the specifications on the bottle label to be aware of their nature and quantities, to ascertain that they would not affect the measurement.

The characteristics of the solvent can also be affected by temperature variations that can induce an expansion or a contraction of its volume, a change in its refraction index and/or influence chemical or physical equilibria. It is necessary, therefore, to use a thermostated cell all the times that these variables can significantly influence the measurement.

3.8.3 The Diffusion

Diffusion is generally caused by particles suspended in solution that disperse and deviate part of the light, that will not reach the detector causing an apparent not real absorption. The best method to solve this problem is to filter the solution before the measurement. Unfortunately, this is not always possible, moreover sometimes the particles themselves are the target analyte to measure. In such cases it is possible to take advantage from correction techniques that are reported by all the texts of experimental analytical chemistry [6] and that take into account the two different possible types of light diffusion in the UV–vis range: the *Rayleigh diffusion* and the *Tyndall effect*. The first one is possible when the particle dimensions are particularly small with respect to the wavelength of the incident light ant it depends from the inverse forth power of the wavelength. The *Tyndall effect*, on the contrary, arises when the particles present dimensions bigger than the wavelength of the incident light and it depends by the inverse of the second power of it. In the samples presenting diffusion problems, therefore, the absorption fraction due to these phenomena is proportional to the wavelength in study raised to a power that can vary in the range $-4 - -2$ ($A_{diffusion}$ is proportional to $1/\lambda^n$ con $4 < n < 2$) depending on which one of the two is the prevalent one, according to the dimensional distribution of the dispersed particles.

This takes us to conclude that the error caused by diffusion increases in an exponential way with the diminishing of the wavelength of the incident light. It is therefore the best choice possible, in these cases, to perform quantitative measurements and comparisons at a single wavelength, and to select the one corresponding to the lowest energy (the higher wavelength) possible for the sample in study.

3.8.4 The Instrumental Precision

As already outlined, the maximum measurable total absorption value strongly depends on the instrumentation, that is to say on the model of the spectrophotometer in use. Generally for the modern common spectrophotometers in research

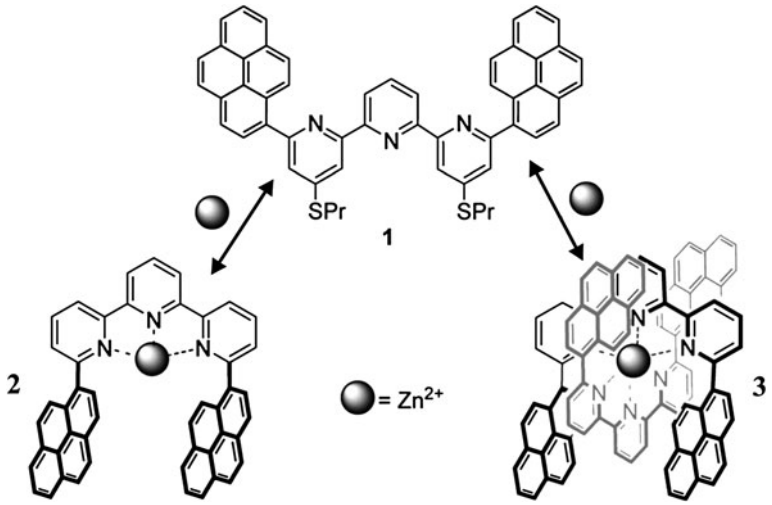

Fig. 3.12 Schematic representation of the ligand 1 and of its zinc complexes (2 and 3) (Copyright Wiley–VCH Verlag GmbH & Co. KGaA. Adapted and reproduced with permission from reference 8)

and analysis laboratories, the maximum measurable absorbance with an acceptable error is around 2–2.5. This value can vary in time since the light sources decrease their intensities with use and the optics lose efficacy, increasing the entity, and the incidence on the measure, of the diffused light. It is possible anyway to verify with a very simple experiment if the measured absorbance value is acceptable, that is to say if it still follows in a range of reasonable linearity. It is necessary to measure the absorbance of the same sample twice, in two cells with different optical pathways one can be, for example, of 1 cm, and the other one 0.5 cm. If the obtained absorbance values are exactly one the double of the other, this proves that both are in the absorbance reliability interval of the instrumentation.

3.9 Experimental Examples

Two research studies taken from the literature will be presented in this section to better clarify the investigative great potentialities of this spectroscopy in different fields.

The first example concerns a molecular dynamic device that undergoes ion triggered conformational changes from a W to a U shape, a mechanical motion that can be followed via photophysical techniques [8].

The flexible ligand bis-pyrenyl-terpyridine **1** was synthesised, and used to prepare zinc complexes (Fig. 3.12), then their photophysical properties were studied.

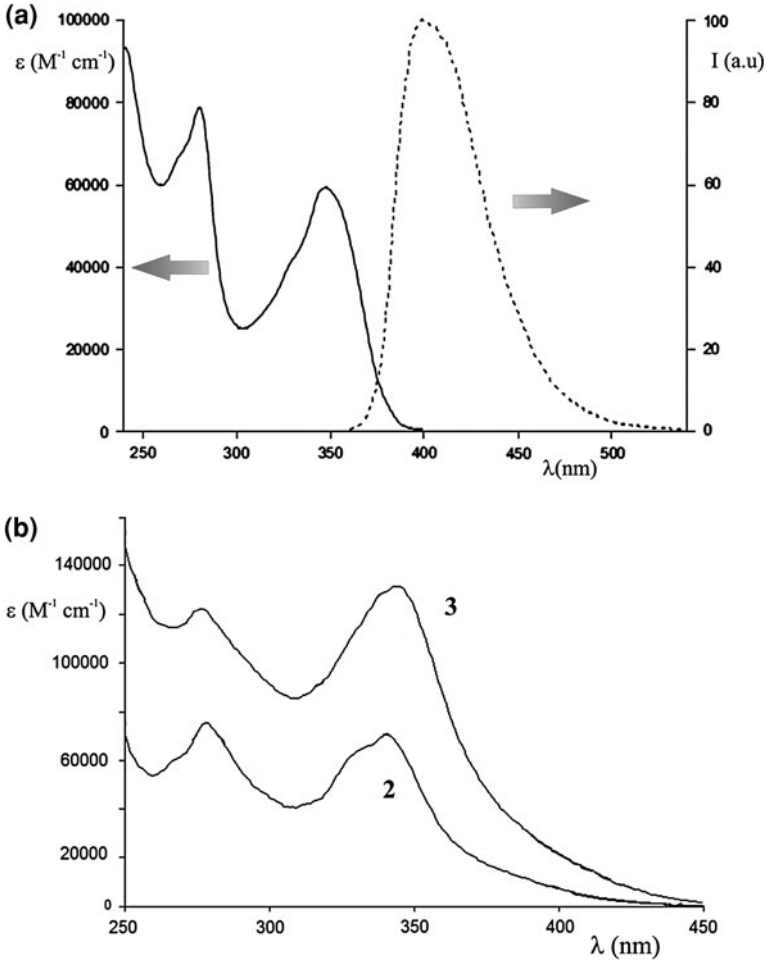

Fig. 3.13 **a** Absorption (*solid line*) and emission (*dotted line*; λexc = 348 nm) spectra of **1** in CH_2Cl_2; **b** absorption spectra of **2** and **3** in CH_2Cl_2 (Copyright Wiley–VCH Verlag GmbH & Co. KGaA. Adapted and reproduced with permission from reference 8)

Some considerations about the expected profiles of the absorption spectra of the metal complexes can be attempted a priori. They should be, in both cases, the sum of the transitions involving only the ligands, in case perturbed by the metal bonding inducing π-stacking interactions among them. This is due to the fact that the introduction of Zn^{2+} ions, that present a d^{10} configuration, does not usually introduce low-energy metal-centred or charge-transfer states, so that MC, MLCT or LMCT transition bands are not likely to be present.

The recorded spectra of **1**, **2** and **3** (Fig. 3.13) show, in fact, very similar profiles both in acetonitrile and in dichloromethane solutions. In the 320–400 nm region,

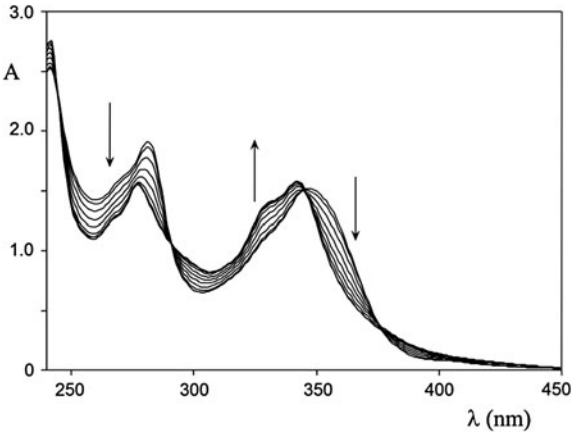

Fig. 3.14 Absorption spectra in CH_2Cl_2/CH_3CN (*v*/*v*, 1/1) of **1** upon additions of increasing amounts of $Zn(ClO_4)_2$ (Copyright Wiley–VCH Verlag GmbH & Co. KGaA. Adapted and reproduced with permission from reference 8)

in particular, the pyrene-centred band undergoes a small blueshift of its maximum (from 348 to 342 nm for both complexes), and a significant increase of the absorption tail at longer wavelengths (only for **3**). Two different phenomena have to be taken into account to explain this absorption changes. The complexation of the zinc ion decreases the electronic density on the terpy moiety and, as a consequence, perturbs the delocalisation of the electronic density to the pyrene unit, leading to the observed blueshift of the band. Moreover, this process makes the terpy unit easier to be reduced, so that a charge-transfer transition from the pyrene (E_{ox} = +1.18 V vs. SCE in acetonitrile) becomes possible. The authors hypothesize that this could be the case for **2** presenting a less pronounced tail toward the red part of the spectrum that is also solvent dependent, supporting the charge transfer nature of this band. On the other side, the metal ion complexation brings the two pyrene moieties of **1** and the terpy-type unit of the second ligand in close proximity, in the case of **3**, so that π-stacking interactions between all of them can be established. Interactions of this kind are expected to cause a broadening of the bands of the chromophores involved, as indeed observed for 3.

All this becomes much more evident when absorption measurements are used to follow the formation of the complexes during the titration of lingand **1** with increasing amounts of a solution of zinc perchlorate (Fig. 3.14).

The analysis of all the spectra taken during the titration experiment, allowed to obtain the following cumulative association constants for the different equilibria (3.14) and (3.15).

$$Zn^{2+} + \mathbf{1} \rightleftharpoons \mathbf{2}^{2+} \quad \log\beta_{11} = 8.0 \pm 0.3 \tag{3.14}$$

$$Zn^{2+} + 2 \times \mathbf{1} \rightleftharpoons \mathbf{3}^{2+} \quad \log\beta_{12} = 14.6 \pm 0.5 \tag{3.15}$$

In this case, therefore, following the variations in the absorption spectra it was possible to monitor the conversion from the W to the U shape of the bistable

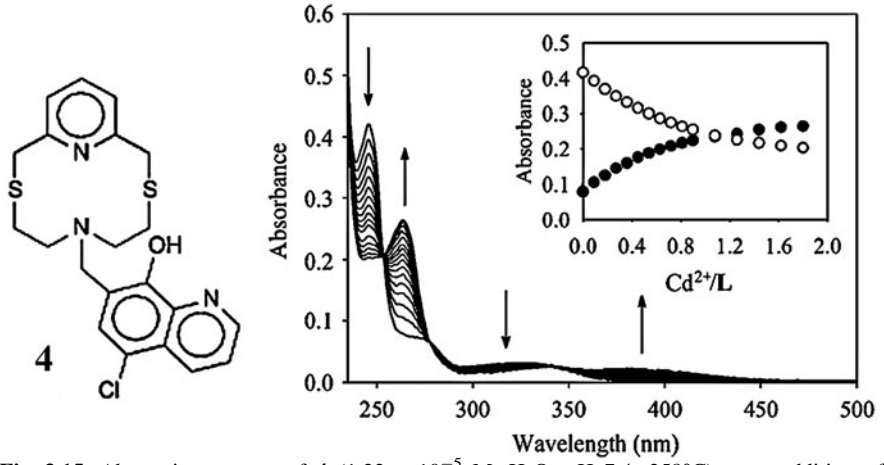

Fig. 3.15 Absorption spectra of **4** (1.22×10^{-5} M, H_2O, pH 7.4, 258°C) upon addition of increasing amounts of Cd^{2+}. *Inset*: changes in absorbance at 264 (•) and 245 nm (○) (Copyright Wiley–VCH Verlag GmbH & Co. KGaA. Adapted and reproduced with permission from reference 10)

lingand **1** upon cation complexation, and to understand which kind of electronic distribution changes this extension-compression motions caused in the total systems. It has to be underlined that the paper reports also all the photophysical characterizations of the systems in emission but their discussion is not the focus of this presentation.

As a very last comment, it is worth to point out that metal ion complexation generally causes drastic changes in the absorption profile of the ligand and this is extensively exploited in the field of sensors for the most different applications [9].

The species **4** (Fig. 3.15), for example, is a selective and nontoxic fluorescent molecular sensor proposed to probe cadmium content in living cells in case of heavy metal contamination. [10] The variation in the absorption spectrum of the ligand during the titration with increasing amounts of Cd^{2+} (Fig. 3.15) allowed to evaluate the efficacy of the complexation process calculating a log $K_{ass} \approx 6.0$ with a 1:1 stoichiometry.

In this regard it is important to highlight the presence in the set of the titration spectra of three isosbestic points (at 253, 278 and 343 nm). The presence of one (or more) stable isosbestic points, as a consequence, is the evidence that the reaction is proceeding without forming intermediates or multiple products. This is a very important indication in the study of chemical (and physical) equilibria, and the absorption spectroscopy is a very easy and straightforward instrument to obtain clear indications of the presence, or not, of multiple equilibria.

References

1. Turro NJ, Ramamurthy V, Scaiano JC (2010) Modern molecular photochemistry of organic molecules. University Science Books, Sauselito, California
2. Suppan P (1994) Chemistry and light. Royal Soc Chem, Cambridge
3. Gilbert A, Baggot J (1991) Essential of molecular photochemistry. Blakwell, Oxford
4. Ball P (2003) Bright earth. University of Chicago Press, Chicago
5. Dowling J, Stryer L, Wiesel T (eds) (1999) Colloquium of vision: from photon to perception. National Academy of Sciences, USA
6. Willard HH, Merritt LL Jr, Dean JA, Settle FA Jr (1999) Instrumental methods of analysis. Wadsworth Publishing Company, Belmont, California
7. Kortüm G (1969) Reflectance spectroscopy. priciples, methods, applications. Springer-Verlag, Berlin
8. Barboiu M, Legrand Y-M, Prodi L, Montalti M, Zaccheroni N, Vaughan G, van der Lee A, Petit E, Lehn J-M (2009) Eur J Inorg Chem 18:2621–2628
9. Fabbrizzi L (2000) Coord Chem Rev 205
10. Mameli M, Aragoni MC, Arca M, Caltagirone C, Demartin F, Farruggia G, De Filippo G, Devillanova FA, Garau A, Isaia F, Lippolis V, Murgia S, Prodi L, Pintus A, Zaccheroni N (2010) Chem Eur J 16:919–930

Chapter 4
Photochemical Techniques

Maria Teresa Gandolfi and Luca Moggi

Abstract This chapter provides information useful to perform photochemical reactions, both for spectroscopic and synthetic purposes. Main apparata required for these reactions—i.e., light sources for the UV and visible region, filters (solid or in solution) to select monochromatic or narrow band excitation light, and appropriate reaction cells—are described. The mathematical equations that allow to calculate the photoreaction quantum yield from the experimental data are then discussed. In the following section, the methods used to measure the intensity of the exciting radiation are considered: the most important chemical actinometers are described in detail, together with the recommended procedure for their use. As an example, a recent study of the authors on a photochromic compound is summarized, with particular regard to the experimental apparata and procedures used. The application of this compound as a wide range chemical actinometer is finally illustrated and a comparison with the previously reported ones is made.

4.1 Photochemical Apparata

We will illustrate here the main components of a "photochemical reactor", that is a chemical reactor useful to perform a reaction induced by light, either for spectroscopic or for synthetic purposes. We will discuss only the apparata used for the most common type of photoreactions, those which originate from "electronic"

M. T. Gandolfi · L. Moggi (✉)
Department of Chemistry "G. Ciamician", University of Bologna,
Via Selmi 2, 40126 Bologna, Italy
e-mail: luca.moggi@unibo.it

P. Ceroni (ed.), *The Exploration of Supramolecular Systems and Nanostructures by Photochemical Techniques*, Lecture Notes in Chemistry 78,
DOI: 10.1007/978-94-007-2042-8_4,

Table 4.1 Main emission lines and relative intensities of a medium pressure Hg lamp (125 W)

λ (nm)	Watt	Photons
313	33–67	28–57
365	100	100
405	24–50	27–55
436	37–84	44–100
546	33–80	49–120
577	20–74	32–117

excited states produced by means of continuous irradiation in fluid systems (pure liquid, solutions, gases).

The main components of these reactors are:

- the light source of the exciting radiation (Sect. 4.1.1);
- a system which selects the radiation of appropriate frequency (monochromator, filters, Sect. 4.1.2);
- the reaction cell (Sect. 4.1.3).

A detailed description of these components is given in [1, 2].

4.1.1 Light Sources

Electronic excited states of a chemical species are generally produced by absorption of photons in the near UV (180–400 nm) and the visible (400–800 nm) spectral regions; the light source must therefore provide radiations in this range. In practice, the most used sources are incandescent lamps, or arc lamps containing mercury or xenon as emitting gas; in particular cases, laser sources can also be used.

Incandescent lamps. They are the usual tungsten or tungsten-halogen lamps, which emit in a continuous manner from the near UV to the IR. When UV radiation is required, the bulb of the lamp must be of quartz or fused silica. The intensity of the emitted radiation depends on the electric power applied.

Low pressure (10^{-3}–10 Torr) Hg lamps. The emission spectrum of mercury lamps depends on the pressure of the gas. At low pressure, the emission consists almost exclusively of 254 and 185 nm radiations, in a ratio which depends on Hg pressure, temperature and arc current, but is generally around 10:1. Since the 185 nm radiation is only transmitted by a special type of quartz (see Sect. 4.1.4), lamps having bulbs of normal quartz are commonly used as sources of monochromatic 254 nm light.

Medium pressure (1–10 bar) Hg lamps. These lamps emit several spectral lines in the UV and in the visible, over a very weak continuum emission background. The main lines are listed in Table 4.1, together with their relative intensities, expressed as power (watt) or as number of photons. Small differences in the

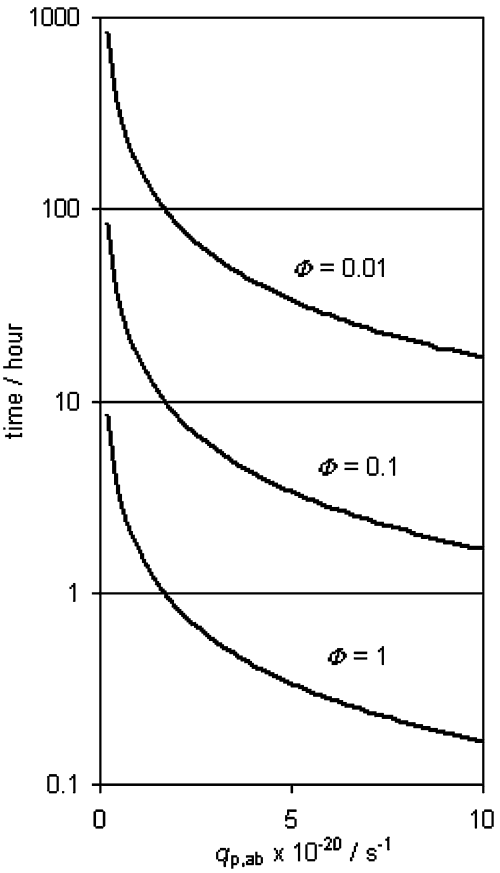

Fig. 4.1 Relation between irradiation time required to decompose one mole of reactant and absorbed photon flux, $q_{p,ab}$, for three values of the reaction quantum yield, Φ

relative intensities may occur among the commercial lamps, due to differences in the operating conditions, temperature and gas pressure.

High pressure (>20 bar) Hg lamps. An high gas pressure causes an increase of the continuum background, that may also overcome the lines, and an increase of the relative emission intensity in the visible; these lamps are therefore used as a source of visible radiation. It is to be noted that they also emit IR radiation, and so they often require an efficient cooling of the system.

Xenon lamps. The xenon lamps operate at high pressure (>20 bar) and their emission spectra are intense, continuous and almost uniform from UV to near IR. They are mainly used to provide visible light (narrow or large bands) or when sunlight-mimicking radiation is required. Also these lamps require a cooling system.

Radiant power. In a photoreaction the amount of decomposed, or produced, compound depends on the photon flux (i.e., number of photons per unit time. For the definition of this and other technical terms, see [3]) absorbed by the reacting

Table 4.2 Main lasers used in photochemistry

Laser	λ (nm)	Laser	λ (nm)
Nd:YAG (quadrupled)	266	Nd:YAG (doubled)	532
He–Cd	325	Krypton ion	568.2
Krypton ion	350.7	He–Ne	632.8
Nd:YAG (tripled)	355	Krypton ion	647.1
He–Cd	441.6	GaAlAs	750
Argon ion	488	GaAlAs	780
Argon ion	514.5	Nd:YAG	1,064

system, the duration of the irradiation and the quantum yield of the photoreaction (see Sect. 4.2); the relation among these three quantities is represented in Fig. 4.1. The absorbed photon flux is a fraction (Sect. 4.2) of the photon flux incident in the reaction cell, which, in its turn, is generally only part of the radiant power of the light source, because of losses due to:

a. emitted light not directed toward the reaction cell;
b. selection of the radiation of appropriate wavelength (Sect. 4.1.2);
c. absorption or reflection by the materials that are passed through by the light beam (Sect. 4.1.4).

The above mentioned lamps operate at various electric powers, which may range from tens to thousands of watt, at least in the case of the arc lamps, and the radiant power of the lamp increases with increasing electric power. Therefore, the electric power is one of the factors to be considered for the choice of the lamp, in order to avoid too short or too long irradiation periods. In plain words, low-power lamps (<1,000 W) are commonly used for photochemical research studies, which are generally performed on small volumes of solution; on the other hand, lamps operating at high powers are required for photochemical syntheses, where a large amount of product is desired.

Laser sources. Lasers are appropriate sources when a strictly monochromatic, or intense, or polarized radiation is required. They have the advantage of the intensity and linearity of the emitted beam, that eliminates the dispersion of light (point *a* above in this section), but present the disadvantages of the high cost and of the possible occurrence of biphotonic processes (reactions induced by the absorption of two photons by one molecule) or of reactions between two excited molecules. Some lasers that emit in the spectral region of photochemical interest are indicated in Table 4.2.

Dye lasers can also be used, which consist of a luminescent dye excited by another laser. The possibility of using several dyes emitting in different spectral ranges, combined with the possibility to select a narrow band in the emitted spectrum, allows obtaining an almost monochromatic radiation centred at any wavelength in the visible spectral region.

For a wide list of lasers, see [2, 4].

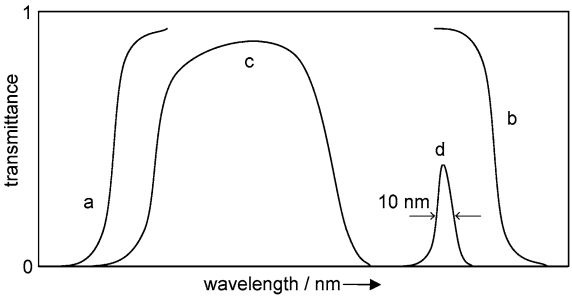

Fig. 4.2 The main types of solution and glass filters

4.1.2 Selection of the Exciting Radiation

The photochemical reactivity of a chemical species may be a function of the irradiation wavelength, so that photochemical experiments are usually performed by monochromatic light irradiation. This is not needed for photochemical syntheses, but it may be convenient to cut off radiation below a given wavelength (generally, to cut off the UV) in order to avoid photoreactions originating from high-energy excited states.

The choice of the wavelength is mainly based on the spectral characteristics of the reactant, since it must absorb the exciting radiation; thus, the radiation has to correspond to an absorption band of the reactant, possibly close to the band maximum in order to increase the absorption of the exciting light. Moreover, the exciting light must not be absorbed (or, at least, absorbed to a very low extent) by other chemical species, particularly the solvent and the photochemical products. The spectral properties of the most common solvents are reported in detail in [2].

Monochromators (gratings and prisms) may be used to select the appropriate wavelength, but solution filters and glass filters are generally preferred, because of practical and economic reasons. Four types of filters are available, that are shown in Fig. 4.2:

a. "short-wavelength cut-off" filters, that exclude the radiations below a given wavelength;
b. "long-wavelength cut-off" filters, that exclude the radiations above a given wavelength;
c. wide "band-pass" filters;
d. narrow "band-pass" filters, also known as "interference filters".

Solution filters. They are both short-wavelength cut-off or wide band-pass filters (a and c in Fig. 4.2), mainly constituted by aqueous solutions of inorganic compounds. Several of them, which cover the wavelength interval between 200 and 650 nm, have been described in detail in [2] and references therein. It is however to be noted that some of these filters may undergo thermal or photochemical reactions, so that a periodic control of their absorbance is recommended.

A combination of band-pass and cut-off filters may provide a relatively narrow band-pass filter system having high transmittance at its maximum; a compilation of these systems is reported in [4, 5].

Solution filters that absorb infrared radiations are also available: for example, the 100 g/L aqueous solution of $CuSO_4 \cdot 5H_2O$ with a 2 cm optical path. They warm up and so a cooling system must be provided.

Glass filters. Numerous filters, in quartz or glass, of the four types described above, are produced by various firms and are commercially available. They cover both the near UV and visible regions [1, 2]. Interference filters are particularly interesting because they transmit light in a very narrow spectral region (half-width, i.e., $\Delta\lambda$ at 50% maximum transmittance, around 10 nm) and are often used to select single lines of a medium-pressure Hg lamp. Unfortunately, the transmittance in the maximum is generally low (<50%) and in addition they must be strictly perpendicular to the direction of the light beam, since the nominal wavelength of the maximum depends on the angle between filter and light beam.

Neutral density filters. These are commercially available glasses able to reduce the intensity of light in an almost uniform and wavelength-independent way. They are therefore used when a reduction of the intensity of the exciting radiation is required.

4.1.3 Reaction Cells

In principle, any reaction cell can be used in photochemical experiments, provided that at least part of its surface is transparent to the exciting radiation. Photochemical studies are often accomplished on small volumes of solution and the usual spectrophotometric cells can be used as reaction cells. The optical path of the cell should be large enough to ensure a high absorption of the exciting radiation by the reactant. In order to reduce losses of light intensity, an accurate optical alignment of light source, filters and cell is recommended.

When large volumes of solution must be irradiated, the best choice is a cylindrical cell (Fig. 4.3) with a lamp immersed in the centre; in this way, the side losses of light may be completely annulled. Solution filters may be placed in a cylindrical jacket around the lamp; the same jacket may also be used for the refrigeration liquid, which, in some cases, may be the solution filter. Tubular glass filters are also commercially available.

Comparative photochemical researches can be accomplished with the so called "merry go round" apparatus, which consists of several reaction cells circularly placed around a central cylindrical lamp; an uniform irradiation is ensured by the continuous rotation of the cells around the lamp.

An exhaustive description of reaction cells can also be found in [1].

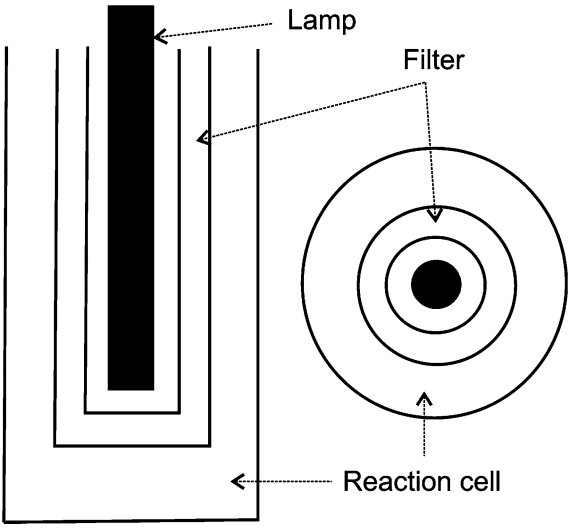

Fig. 4.3 Schematic representation of a reaction cell for the irradiation of large volumes

4.1.4 Optical Material

All the material through which the exciting radiation passes, including the reaction cell (or at least one of its faces) must obviously be transparent to the radiation; in practice, only glass or quartz are used. The normal laboratory glassware is made of a borosilicate glass (e.g., Pyrex, Duran), which transmits light above 300 nm, and so it can be used only with exciting radiations above this wavelength value. For radiation of shorter wavelength, quartz must be used, which is generally transparent above 190 nm and, in its purest form (e.g., Suprasil, 99.9% SiO_2), above 170 nm.

Note that each sheet of transparent material reflects about 10% of the incident radiation when its surface is orthogonal to the light beam, and a larger fraction for other angles; therefore, all the flat surfaces should be orthogonal to the optical path.

4.1.5 Control of Temperature and Stirring

The photoreactions that must occur at controlled, constant temperature can be performed in cells contained in a thermostat.

The stirring of the solution during the irradiation is strictly recommended, otherwise gradients of concentration can be produced that affect the photochemical process. The stirring may be accomplished by the bubbling of an inert gas or by using a magnetic stirrer.

Control of temperature and stirring should not interfere with the light beam outside and inside the cell.

4.2 Photoreaction Quantum Yield

For a photochemical or photophysical event of a chemical species caused by light excitation, the quantum yield, Φ, is defined as the ratio between the number of molecules undergoing the event in unit time and the number of photons absorbed by that species in unit time (Sect. 1.6.5). For a photochemical reaction, the quantum yield is commonly expressed in terms of disappearance of the reagent R:

$$\Phi_{\mathrm{R}} = \frac{\text{number of molecules (ions) of R decomposed in unit time}}{\text{number of photons absorbed by R in unit time}} \tag{4.1}$$

which corresponds mathematically to the equation

$$\Phi_{\mathrm{R}} = -\frac{\mathrm{d}n(\mathrm{R})/\mathrm{d}t}{q_{\mathrm{p,ab}}} \tag{4.2}$$

where $n(\mathrm{R})$ is the number of molecules (ions) of R, t is the time, $q_{\mathrm{p,ab}}$ is the photon flux absorbed by R. It is sometimes convenient to consider the quantum yield of formation of a photochemical product P, Φ_{P},

$$\Phi_{\mathrm{P}} = \frac{\text{number of molecules (ions) of P formed in unit time}}{\text{number of photons absorbed by R in unit time}} \tag{4.3}$$

The ratio between Φ_{P} and Φ_{R} in a given photoreaction is equal to the ratio between the stoichiometric coefficients of the two species.

For research purposes, the most common type of photoreaction is that performed in liquid solution and irradiated with monochromatic (or almost monochromatic) light. In this case, the quantum yield is generally determined by measuring the change of the concentration of R, [R], (or of P) in a given finite time interval. It is therefore required to integrate the differential equation

$$-\mathrm{d}n(\mathrm{R})/\mathrm{d}t = \Phi \times q_{\mathrm{p,ab}} \tag{4.4}$$

The absorbed photon flux, $q_{\mathrm{p,ab,}}$ is a fraction of the flux of photons incident in the reaction cell, $q_{\mathrm{p,in,}}$ generally time independent. If the exciting radiation is absorbed only by R, the relation between $q_{\mathrm{p,ab}}$ ad $q_{\mathrm{p,in}}$ is the Lambert–Beer law

$$q_{\mathrm{p,ab}} = q_{\mathrm{p,in}} \times \left(1 - 10^{-A}\right) \tag{4.5}$$

$$A = \varepsilon[\mathrm{R}]l \tag{4.6}$$

where A is the absorbance of the solution, ε the molar absorption coefficient of R at the excitation wavelength (L mol^{-1} cm^{-1}), [R] the molar concentration of R (mol L^{-1}) and l is the optical path in the reaction cell (cm). Thus:

$$-\mathrm{d}n(\mathrm{R})/\mathrm{d}t = \Phi \times q_{\mathrm{p,in}} \times \left(1 - 10^{-(\varepsilon[R]l)}\right) \tag{4.7}$$

Table 4.3 Fraction of absorbed light for some absorbance values

A	f_{ab}	A	f_{ab}
0.01	0.023	0.30	0.499
0.02	0.045	0.40	0.602
0.03	0.067	0.50	0.684
0.04	0.088	0.60	0.749
0.05	0.109	0.70	0.800
0.06	0.129	0.80	0.842
0.07	0.149	0.90	0.874
0.08	0.168	1.00	0.900
0.09	0.187	1.30	0.950
0.10	0.206	1.60	0.975
0.15	0.292	2.00	0.990
0.20	0.369	2.25	0.994
0.25	0.438	2.50	0.997

The ratio between the absorbance A and the fraction of absorbed light $f_{ab} = q_{p,ab}/q_{p,in} = 1–10^{-A}$ is shown in Table 4.3 and in Fig. 4.4.

Since [R] decreases during the reaction, the fraction of absorbed light and the reaction rate also decrease increasing the irradiation time, and so the differential Eq. 4.7 can be easily integrated only in two limit conditions that are clearly identifiable in Fig. 4.4.

The first condition (*a* in Fig. 4.4) occurs when $A > 2$ during the entire irradiation period; being $f_{ab} = 0.99$ for $A = 2$, $q_{p,ab}$ can be considered approximately equal to $q_{p,in}$ and the integration of Eq. 4.7 leads to

$$\Phi \approx ([\mathrm{R}]_0 - [\mathrm{R}]_t) \times \frac{V \times N_A}{q_{p,in} \times t} \tag{4.8}$$

where $[\mathrm{R}]_0$ and $[\mathrm{R}]_t$ are the molar concentrations of R at the beginning and the end of the irradiation period, V(L) is the volume of the solution, N_A the Avogadro constant, t the irradiation time (in the same units as $q_{p,ab}$ and $q_{p,in}$). V and N_A are needed in order to convert molar concentrations into number of molecules (or ions).

The second condition (*b* in Fig. 4.4) occurs if during the irradiation $A < 0.03$ ($f_{ab} < 0.07$); in these conditions, the approximation

$$1 - 10^{-A} \approx A \times \ln 10 \tag{4.9}$$

can be applied and the integration leads to

$$\Phi \approx \ln \frac{[\mathrm{R}]_0}{[\mathrm{R}]_t} \times \frac{V \times N_A}{2.303 \times q_{p,in} \times \varepsilon \times l \times t} \tag{4.10}$$

For intermediate values of A, if the change of A during the irradiation is small (we suggest no more than 10%), it can be assumed that the fraction of light absorbed by R is constant during the irradiation time and equal to the mean value

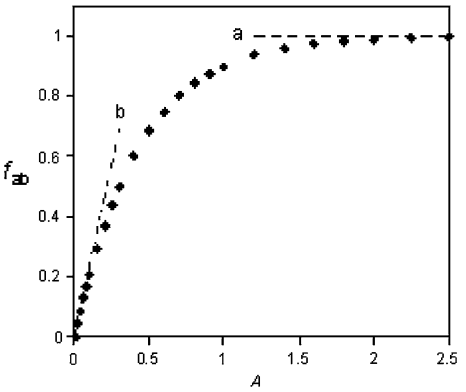

Fig. 4.4 Fraction of light absorbed by R, f_{ab}, as a function of the absorbance A. The dashed lines represent the approximations discussed in the text

$$(f_{ab})_m = \frac{(f_{ab})_0 + (f_{ab})_t}{2} = \frac{(1 - 10^{-A_0}) + (1 - 10^{-A_t})}{2} \tag{4.11}$$

where A_0 and A_t are the absorbance values at the irradiation wavelength at the beginning and end of the irradiation. Using this approximation, the following integrated equation is obtained.

$$\Phi \approx ([R]_0 - [R]_t) \times \frac{V \times N_A}{q_{p,in} \times t} \times \frac{1}{(f_{ab})_m} \tag{4.12}$$

If the photon flux is expressed in einsteins (moles of photons), the Avogadro constant, N_A, should be omitted in the integrated equations. The radiant power of a monochromatic radiation, P, may be converted into photon flux by means of the equation

$$q_p(s^{-1}) = 5.034 \times 10^{15} \times P(W) \times \lambda(nm) \tag{4.13}$$

The previous integrated equations are valid only for irradiation with monochromatic light or, approximately, with light transmitted by an interference filter sufficiently narrow to assume that the reactant has a constant molar absorption coefficient in the entire band. Otherwise, in the case of uneven absorbance of the reactant and constant emission of the lamp in the spectral range of the filter, the relation between the overall incident photon flux and the overall absorbed photon flux can be evaluated by considering a continuous sequence of very narrow (e.g., 1 nm) wavelength intervals (Fig. 4.5); in this way, the relation can be numerically calculated by means of the equation

$$q_{p,in} = q_{p,ab} \times \frac{\sum_\lambda T_\lambda}{\sum_\lambda (T_\lambda \times f_{ab,\lambda})} \tag{4.14}$$

where T_λ is the mean transmittance of the filter in one interval, $f_{ab,\lambda}$, is the mean fraction of light absorbed by the reactant in the same interval ($f_{ab,\lambda} = 1–10^{-A(\lambda)}$) and the summations are extended to the entire wavelength range of the filter.

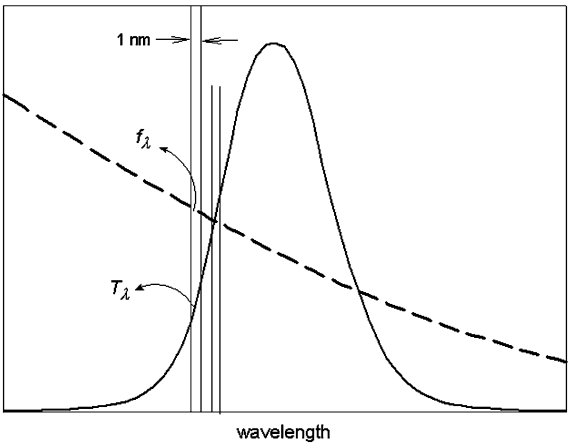

Fig. 4.5 Schematic representation of the procedure for the calculation of $q_{p,in}$ in the case of uneven absorbance by the reactant. *Solid line*: transmittance of the filter; *dashed line*: f_{ab} of the reactant

4.3 Chemical Actinometers

In the study of a photochemical reaction it is necessary to know the photon flux incident in the reaction vessel (for a specific geometry and in a well defined spectral domain), in order to determine the photochemical quantum yield; this knowledge is also necessary in a photochemical synthesis to calculate the time necessary to obtain a certain amount of photoproduct (see Fig. 4.1).

In absolute actinometric measurements a physical device (such as a photomultiplier, a photodiode, a bolometer) converts the energy or the number of the incident photons in a quantifiable electrical signal [1, 6], but there are some relevant limitations:

- impossibility to convert the measured energy in number of photons, if the incident radiation is not monochromatic;
- extreme difficulty in measuring the total flux of incident radiation, if the sensible area of the device is not coincident with the window through which the radiation penetrate the cell.

Therefore, although the physical methods remain the primary methods for determining the photon flux and are still in use in some cases (e.g., to control the relative emission intensity of the lines emitted by the mercury lamps or the transmittance of filters), the most commonly utilized method is based on a chemical actinometer, i.e., a reference substance undergoing a photochemical reaction whose quantum yield, Φ,is known, calibrated against a physical device or well characterized actinometers. The chemical actinometers are mainly fluid systems (generally solutions) irradiated for a suitable time interval; after irradiation, an analytical method allows to determine the number of decomposed molecules; by means of the equations reported in Sect. 4.2 it is possible to calculate the number of incident photons. The $q_{p,in}$ value so obtained may be used to calculate the quantum yield of other photoreactions, provided that these are

performed in the same experimental conditions (same source of light, same filters, identical reaction cell, same geometry…).

From a practical point of view, the most favourable conditions are that the actinometric solution absorbs all the exciting radiation ($A > 2$) for the entire period of time required to produce a precisely detectable change in concentration.

For a good actinometer, the following criteria should be followed, as much as possible:

- the quantum yield should be high, possibly independent of the irradiation wavelength (or at least measured for a wide wavelength interval), not dependent on the concentration, trace impurities, temperature, presence of oxygen;
- the analytical method should be simple and quick;
- the actinometric solution should be thermally stable;
- at the irradiation wavelengths the molar absorption coefficients of the actinometric compound should be high;
- the photoproducts should be photochemically stable and not absorb at the irradiation wavelength.

The photon flux, $q_{p,in,}$ measured by a chemical actinometer is assumed to be equal to that in the reaction cell of the experiment, provided that the photochemical apparatus and its geometry are the same; this implies that the two cells must be equal, or, at least, that the equality of the photon fluxes has been otherwise proved.

Several actinometers have been proposed in the literature, but none of these meets all the given criteria. A general report on chemical actinometry was prepared by the IUPAC Commission on Photochemistry [6]. Surveys on the most relevant used actinometers can be found in [1, 2, 4, 7].

In the following, we will briefly discuss only a selection of the most well characterized and widely used actinometers, with the aim of covering the entire UV and visible range of wavelengths used in photochemistry.

4.3.1 Potassium Ferrioxalate

Aqueous solutions of this salt are the most reliable and practical actinometer for UV and visible light up to 500 nm, first proposed by Hatchard and Parker in 1956 [8]. Under light excitation the potassium ferrioxalate decomposes according to the following equations:

$$\mathrm{Fe(C_2O_4)_3^{3-}} \xrightarrow{h\nu} \mathrm{Fe^{2+}} + \mathrm{C_2O_4^{\bullet -}} + 2\,\mathrm{C_2O_4^{2-}} \tag{4.15}$$

$$\mathrm{Fe(C_2O_4)_3^{3-}} + \mathrm{C_2O_4^{\bullet -}} \rightarrow \mathrm{Fe^{2+}} + 2\ \mathrm{CO_2} + 3\ \mathrm{C_2O_4^{2-}} \tag{4.16}$$

The quantity of Fe^{2+} ions formed during an irradiation period is monitored by conversion to the coloured tris-phenanthroline complex $Fe(phen)_3^{2+}$ (ε= 11,100 L mol^{-1} cm^{-1} at λ_{max} = 510 nm). The original Fe^{3+} ions are not

Table 4.4 Recommended [1, 8] $\Phi(Fe^{2+})$ values for the ferrioxalate actinometer

λ (nm)	Φ[a]	f_{ab}[b]
254	1.25	>0.99
297/302	1.24	>0.99
334	1.23	>0.99
366	1.21	>0.99
405–407	1.14	0.99
436	1.11	0.67[d]
464	0.93[c]	0.28[d]
546	0.15[c]	<0.01

[a] From [8]
[b] Fraction of absorbed light in 1 cm of the 0.012 M solution
[c] Value obtained using a 0.15 M solution
[d] $f_{ab} \geq 0.98$ for a 0.15 M solution

appreciably complexed by phenanthroline and the complex does not absorb at 510 nm. It is to note that 2 Fe^{2+} ions are produced per each $Fe(C_2O_4)_3^{3-}$ photoreacting ion. In Table 4.4 the recommended quantum yield values measured in the 220–550 nm spectral region are reported; for a complete list of all the values reported in the literature, see Table (12a-1) in [2]. Using the concentrations proposed for different excitation wavelengths (0.006 M [8], 0.012 M [9], 0.15 M [2, 8], if less than 10% of the complex is decomposed, the absorption of the exciting radiation can be considered complete in 1 cm optical path, at least up to $\lambda = 450$ nm (Table 4.4 and Fig. 4.6).

The main advantages of this actinometer are:

- the independence of the quantum yield from the temperature and the concentration;
- the small variation of Φ in the UV spectral region, that allows to measure the photon flux also if the excitation light is not monochromatic;
- the almost complete absorption of the UV exciting radiations in 1 cm optical path;
- the sensitivity of the simple analytical method.

Some drawbacks:

– the poor absorbance of the actinometric solution in the visible region;
– the quantum yield dependence on λ in the visible region.

Because of the large experimental errors, the use of the ferrioxalate actinometer for excitation wavelengths higher than 450 nm is not recommended.

Procedure—Potassium ferrioxalate can be easily synthesized as indicated in [8], and purified by recrystallization (three times).

The actinometric complex is dissolved in 0.05 M H_2SO_4; it is suggested [9] to use a 0.012 M solution, but for excitation at $\lambda > 430$ nm a 0.15 M solution is preferred [2, 10]. For the analytical determination of the Fe^{2+} ions, a solution

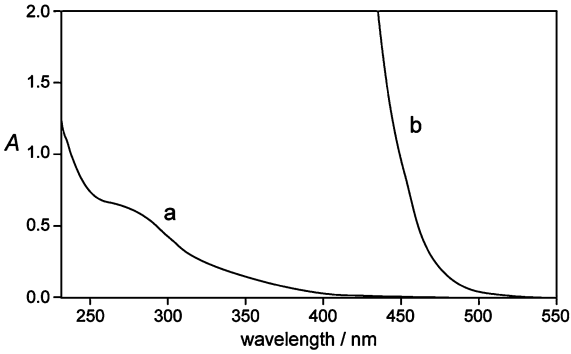

Fig. 4.6 Absorption spectra of solution of $K_3[Fe(C_2O_4)_3]$ in 0.50 M H_2SO_4: (a) 0.012 M; (b) 0.15 M

containing 1.0 g/L of phenanthroline and 225 g/L of $CH_3COONa{\cdot}3H_2O$ (as a buffer) in 0.5 M H_2SO_4 is needed. Both solutions can be stored in the dark for long periods of time.

The same amount of phenanthroline solution is added to an aliquot of the irradiated solution and to an equal volume of the actinometric solution kept in the dark and then the solutions are brought to an appropriate final volume. The difference in absorbance at 510 nm between the irradiated and dark solutions, $\Delta A(510)$, is measured. From Eqs. 4.8 and 4.12 the following equations for the incident flux are derived:

$$q_{p,in} = \frac{\Delta A(510)}{l \times \varepsilon(510)} \times \frac{V_1 \times V_3}{V_2} \times \frac{N_A}{\Phi \times t} \tag{4.17}$$

if the incident radiation is completely absorbed by the solution, and:

$$q_{p,in} = \frac{\Delta A(510)}{l \times \varepsilon(510)} \times \frac{V_1 \times V_3}{V_2} \times \frac{N_A}{\Phi \times t \times (f_{ab})_m} \tag{4.18}$$

in the case of only partial absorption of the incident light; in this second case it is necessary also to measure the absorbance of the solution at the irradiation wavelength before and at the end of the irradiation time, to obtain the factor $(f_{ab})_m$ of Eq. 4.11; V_1, V_2 e V_3 are the volume (L) of the irradiated solution, the volume of the same used for the analytical measurement, and the final volume of the analysed solution, respectively; l is the optical path (cm) of the cell used in the spectrophotometric measurements; $\varepsilon(510)$ is the molar absorption coefficient of $Fe(phen)_3^{2+}$ at 510 nm; Φ is the reaction quantum yield (see Table 4.4) and t the irradiation time. It is suggested to decompose not more than 10% of ferrioxalate. Oxygen has not to be excluded, because the quantum yield of this actinometer does not depend on the presence of oxygen [8, 10, 11, 12]. Furthermore, the quantum yield of ferrioxalate does not show a strong dependence on the temperature, as first pointed out by Hatchard e Parker [8], and subsequently carefully investigated by Nicodem et al. [13]. Stirring is recommended, although not necessary [4].

Table 4.5 *Y* factor values for various Hg lamp lines [10]

λ (nm)	$Y/10^7$	λ (nm)	$Y/10^7$
254	2.51	406	2.76
313	2.54	436	3.05
365	2.59	464	3.35

If the reaction cell is a square spectrophotometric cell of 1 cm optical path, it is convenient to adopt the so called "micro version" of the procedure, as suggested by Fisher in [9]; in this simple procedure, after the irradiation 0.5 mL of phenanthroline solution are added directly both in the reaction cell and in a cell taken in the dark and the absorbance is read at 510 nm; in this conditions the equation in the case of complete absorption of the exciting light is:

$$q_{\mathrm{p,in}} = \frac{\Delta A(510)}{t} \times Y \times N_{\mathrm{A}} \tag{4.19}$$

The *Y* factor values, repeatedly measured in the Photochemistry Laboratory of the University of Bologna (Italy), are collected in Table 4.5; for different wavelengths a linear interpolation of the quantum yield values is allowed.

4.3.2 Potassium Reineckate

This actinometer, an aqueous solution of $K[Cr(NH_3)_2(SCN)_4]$ (Reinecke's salt), is based on the photoaquation reaction:

$$[Cr(NH_3)_2(SCN)_4]^- + H_2O \xrightarrow{h\nu} [Cr(H_2O)(NH_3)_2(SCN)_3] + SCN^- \tag{4.20}$$

The number of photons are determined from the SCN^- released. These ions are complexed by addition of iron(III) nitrate

$$Fe^{3+} + SCN^- \rightarrow Fe(SCN)^{2+} \tag{4.21}$$

and the absorbance of the resulting blood-red complex is measured at $\lambda_{max} = 450$ nm ($\varepsilon = 4{,}300$ L mol^{-1} cm^{-1}).

This photoreaction has been extensively studied [14] in the spectral region 315–750 nm. The quantum yield ($\Phi = 0.29 \pm 0.03$ at 296 K and pH = 5.3–5.5) does not significantly depend on the wavelength, but is dependent on the temperature and on pH (that should be in the 5.3–5.5 range). The absorbance of the actinometric solution ($\sim$0.05 M) is almost complete up to 600 nm ($f_{ab} > 0.95$) for 1 cm optical path, but rapidly decreases at longer wavelength (Fig. 4.7).

Since the aquation reaction occurs also thermally, the same analytical analysis has to be performed on the actinometric solution kept in the dark and compared to the irradiated one.

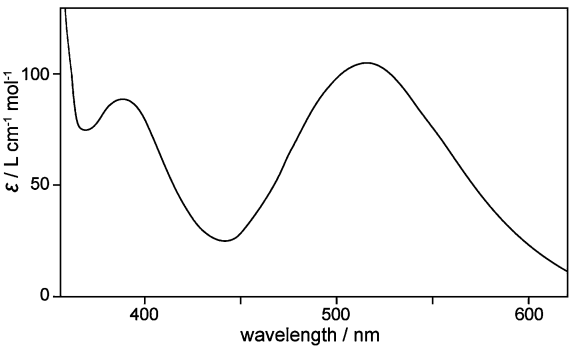

Fig. 4.7 Absorption spectrum of aqueous $K[Cr(NH_3)_2(SCN)_4]$

The advantages of this actinometer are:

- the wide spectral range of application;
- the almost constant quantum yield, that allows the use also with polychromatic irradiation sources, at least in the range 390–600 nm (for the experimental procedure and calculations in the case of polychromatic light, see [1];
- the simple analytical method, characteristic shared with other actinometers.

The drawbacks include:

– the actinometric solution cannot be prepared in advance and stored in the dark, but has to be prepared immediately before the irradiation, for the quick thermal reaction (also at room temperature), which contribution must be carefully subtracted to the photochemical one;
– the incomplete absorption of the actinometric solution and the absorbance of light by the thermal and photochemical aquation product (inner filter effects) at wavelength longer than 600 nm, that imply complicate calculations.

Procedure—Ammonium reineckate is a commercial product and can be easily transformed in the potassium salt following [14]. In the experiments, saturated solutions ($\sim$0,05 M), freshly prepared and filtered, must be used [14]. An aliquot both of the irradiated solution and of the same solution taken in the dark has to be added to a grater volume (at least 4:1) of 0.10 M $Fe(NO_3)_3$ in 0.50 M $HClO_4$. The difference in absorbance between irradiated and dark solutions, $\Delta A(450)$, is measured at 450 nm. To calculate the photon flux of the incident light the following equation is used:

$$q_{p,in} = \frac{\Delta A(450)}{l \times \varepsilon(450)} \times \frac{V_1 \times (V_2 + V_3)}{V_2} \times \frac{N_A}{\Phi \times t} \tag{4.22}$$

if the incident light is completely absorbed by the actinometric solution, or:

$$q_{p,in} = \frac{\Delta A(450)}{l \times \varepsilon(450)} \times \frac{V_1 \times (V_2 + V_3)}{V_2} \times \frac{N_A}{\Phi \times t \times (f_{ab})_m} \tag{4.23}$$

in case of incomplete absorption; in this second case, it is necessary to measure the fraction f_{ab} of absorbed light before and at the end of irradiation, to obtain the medium value, $(f_{ab})_m$, by means of Eq. 4.11; V_1, V_2 e V_3 (L) are the volume of irradiated actinometric solution, the volume taken for the analytical procedure, and the volume of the revealing solution of $Fe(NO_3)_3$, respectively; l (cm) is the optical path of the spectrophotometric cell used for the measurement of A; $\varepsilon(450)$ is the molar absorption of $Fe(SCN)^{2+}$ at 450 nm, Φ the photochemical quantum yield of the actinometric reaction and t the irradiation time.

4.3.3 Azobenzene

The *trans* isomer of azobenzene (hereafter AZB) in solution undergoes a photoisomerization reaction, that can be reversed both thermally or photochemically ([2, 6, 7] and references therein):

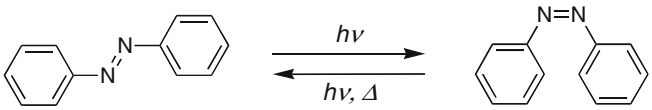

trans-AZB *cis*-AZB

This behaviour makes AZB a good actinometer in the 230–480 nm spectral region, because (i) it is possible to choose the more convenient between the two reactions

$$trans\text{ - AZB} \xrightarrow{h\nu} cis\text{ - AZB} \tag{4.24}$$

$$cis\text{ - AZB} \xrightarrow{h\nu} trans\text{ - AZB} \tag{4.25}$$

and (ii) the same solution can be used for numerous actinometric measurements, due to the reversibility of the two photoreactions. The *trans* isomer can be regenerated also thermally, at 333 K. The thermal isomerization of the *cis* isomer does not apparently interfere with the photochemical processes, if the temperature is kept low (<313 K); moreover, the quantum yield of both photoreactions seems be constant in the range 288–298 K [15].

As shown in Fig. 4.8, each isomer presents an intense absorption band in the UV and one much less intense in the visible, being photoreactive in both absorption bands. This causes two main problems in the use of azobenzene as actinometer, due to the fact that the primary photoproduct absorbs part of the exciting radiation and undergoes its own photoreaction. The first problem is that the final state obtained by irradiation will be a photostationary state containing both isomers, so that it is impossible to convert completely *trans*-AZB into the *cis* isomer. The second problem is that the inner filter effect of the photoproduct and its photoreaction render the calculation of the photon flux very complicated.

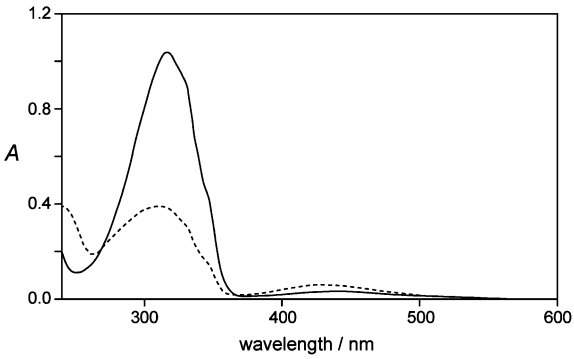

Fig. 4.8 Absorption spectra of methanolic solutions of 4.4×10^{-5} M *trans*-azobenzene (*solid line*) and of the photostationary state (about 73% of *cis*-azobenzene) obtained irradiating the *trans* isomer with light of 313 nm (*dashed line*)

To minimize these not desired effects, it is convenient to use the photoisomerization of the isomer with the higher molar absorption at the exciting wavelength. The photoreactions can be followed spectrophotometrically.

These studies have been performed in a variety of solvents, the most common being isooctane (2,2,4-trimethylpentane) or methanol. The photoreaction quantum yields are gathered in Table 4.6, from which their wavelength dependence is evident.

The main advantages of AZB actinometer are the reusability of the actinometric solution coupled with the simplicity of the analytical measurement, but for excitation at $\lambda > 340$ nm, the data processing is complicated.

Procedure—trans-Azobenzene is a commercially available product. For the 245–265 nm and 375–440 nm spectral ranges it is suggested [6] to use actinometric solutions pre-irradiated at 313 nm until the photostationary state is reached: then the *cis* → *trans* photoisomerization is used as actinometer. In the 270–375 nm spectral region solutions of *trans*-AZB should be used, thermally or photochemically regenerated, if necessary [6]; in this case the photoreaction exploited as actinometer is *trans* → *cis*.

In the irradiation experiments with light of wavelength shorter than 340 nm, the photoreaction is followed by measuring the absorbance at 358 nm. It has been suggested [17] the use of AZB concentrated solutions ($\geq 6 \times 10^{-4}$ M), that ensure the complete absorption of light also in 1 cm optical path, and to convert not more than 5% of the actinometric compound: so the inner filter effect and the reaction of the photoproduct can be disregarded. In these conditions, the incident photon flux is given by [6, 17]:

$$q_{\mathrm{p,in}} = W(\lambda) \times \frac{|\Delta A(358)|}{t} \times N_{\mathrm{A}} \times \frac{1000\,V}{l} \qquad (4.26)$$

where $|\Delta A(358)|$ is the magnitude (absolute value) of the change in absorbance at 358 nm during the irradiation, t is the irradiation time (s), V is the volume of the actinometric solution (L) and l is the optical path (cm). W is a factor that depends on the irradiation wavelength; its values for the most important Hg lamp lines [6, 17] are reported in Table 4.7.

Table 4.6 Quantum yield for the photoisomerization reaction of *trans*-AZB ($\Phi_{t \rightarrow c}$) and *cis*-AZB ($\Phi_{c \rightarrow t}$)

λ (nm)	Actinometric reaction	In isooctane[a]		In methanol[b]	
		$\Phi_{t \rightarrow c}$	$\Phi_{c \rightarrow t}$	$\Phi_{t \rightarrow c}$	$\Phi_{c \rightarrow t}$
254	$c \rightarrow t$	0.13	0.44	0.26	0.31
280	$t \rightarrow c$	–	–	0.12	0.34
313	$t \rightarrow c$	0.10	0.41/0.42	0.13	0.30[c]
334	$t \rightarrow c$	–	–	0.15	0.30
365	$t \rightarrow c$	0.12	0.48	0.15	0.35
405	$c \rightarrow t$	0.23/0.21	0.55/0.51	0.20	0.57
436	$c \rightarrow t$	0.28/0.27	0.55	0.22	0.63
546		0.24	0.40	–	–
578		0.23	0.44	–	–

[a] Data from [16] at 25°C
[b] Data from [17] at room temperature
[c] It is also reported $\Phi = 0.37$ at 20±2°C [18]

Table 4.7 Factor *W* values for selected Hg lamp lines

λ (nm)	*W* (einstein cm^{-2})
254	2.30×10^{-6}
280	4.60×10^{-6}
302	4.63×10^{-6}
313	5.30×10^{-6}
334	3.60×10^{-6}

For experiments at $\lambda > 340$ nm, the exciting radiation cannot be completely absorbed; as a consequence, the fraction of light absorbed by the product and its secondary photoreaction cannot be neglected. In this case, it is necessary to measure the absorbance of the solution at the exciting wavelength at different irradiation times and calculate the concentrations of both isomers in the photostationary state. The mathematical processing of the data based on the linear interpolation, has been proposed in [19, 20] and it can be made by computer.

4.3.4 Aberchrome 540

The pale yellow fulgide (*E*)-2-[1-(2,5-dimethyl-3-furyl)-ethylidene]-3-isopropyl-idene succinic anhydride (hereafter A(*E*)), whose commercial name was Aberchrome 540, is considered a convenient actinometer in the near UV and visible region, because of its reversible photocyclization into the deep red cyclic valence isomer 7,7a-dihydro-2,4,7,7,7a-pentamethylbenzo(b)furan-5,6-dicarboxylic anhydride (hereafter C) [21, 22]. The quantum yield of this photocyclization (0.2) is independent of the temperature ranging from 283 to 313 K and it is also claimed to

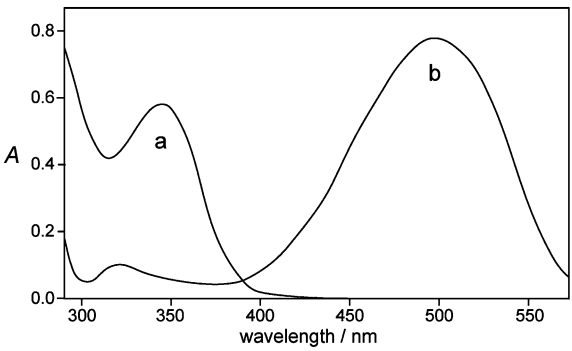

Fig. 4.9 Absorption spectrum of: *a* 1×10^{-4} M A(*E*) in toluene; *b* photostationary state reached irradiating this solution with UV light

be independent on the photocoloration/photobleaching "cycling" [22] (see however the comments below).

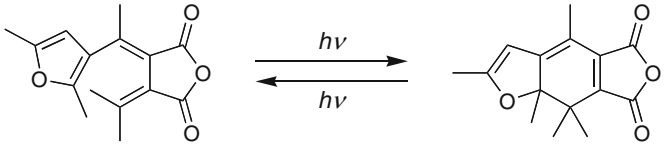

A(*E*) C

A(*E*) shows an intense absorption in the 300–400 nm UV region ($\lambda_{max} = 343$ nm in toluene), while its absorption is almost negligible at $\lambda > 400$ nm (Fig. 4.9). The direct photoisomerization reaction is proposed for measuring the photon flux in the UV spectral range, but only at λ longer than 320 nm, because at shorter wavelengths a photodegradation reaction occurs and the use as actinometer is not recommended ([22] and Gandolfi MT and Ballardini R, private communication). The opposite reaction can be exploited as actinometer in the visible region (435–545 nm): the cyclic isomer C, indeed, has an intense band in the visibile ($\lambda_{max} = 494$ nm in toluene), where A(*E*) doesn't absorb.

Thus, Aberchrome has been suggested as reusable actinometer, but, some negative comments have been reported. The reversible photoisomerization reaction

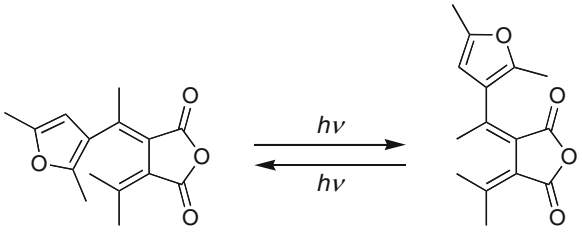

A(*E*) A(*Z*)

was found [23] to compete with the photocyclization; the quantum yields of photoisomerization at 365 nm are 0.13 (A(*E*)→A(*Z*)) and 0.12 (A(*Z*)→A(*E*)),

respectively, in toluene solution at room temperature [24]. The presence of A(*Z*), and particularly its accumulation in the actinometric solution brought up by the cyclic reuse, doesn't allow an exact evaluation of the photon flux; so, it has been suggested not to reuse the irradiated solution when the actinometer is used in the range 310–370 nm [2, 25].

The problem does not concern the use of Aberchrome 540 in the region 435–545 nm: as both A(*E*) and A(*Z*) isomers do not absorb in this spectral range, excitation in this visible region only causes the photobleaching of the cyclic form C.

In conclusion, the use of Aberchrome 540 as actinometer is particularly profitable in the visible region for the possibility to reuse many times the same solution and for the simple analytical measurements not requiring the addition of reactants.

Procedure—The actinometric fulgide A(*E*) is no longer available from Aberchromics Ltd; however, it can be synthesized following the method by Darcy et al. [21]. Some hundreds of milligrams will last for many years.

UV spectral region (310–370 nm): a 1 cm spectrophotometric cell containing a 5×10^{-3} M solution of A(*E*) in dry distilled toluene is irradiated with monochromatic light, carefully stirring; the formation of the coloured isomer C is evaluated by measuring the difference in absorbance at 494 nm before and after irradiation. In the 1 cm optical path the exciting radiation is completely absorbed. The $\varepsilon(494)$ of A(*E*) and the quantum yield value, Φ_c, for the photoreaction A(*E*)→ C originally given [22] are $\varepsilon = 8{,}200$ L mol^{-1} cm^{-1} e $\Phi_c = 0.20$, respectively; from a more recent measurement [25] on a sample of A(*E*) carefully purified, a value of $\varepsilon = 8{,}840$ L mol^{-1} cm^{-1} was obtained, involving a change of the reaction quantum yield, that becomes $\Phi_c = 0.18$. Owing to the complete absorption of the exciting light, the incident photon flux can be calculated from the equation:

$$q_{p,in} = \frac{\Delta A(494)}{l \times \varepsilon(494)} \times \frac{V \times N_A}{\Phi_c \times t} \tag{4.27}$$

where $\Delta A(494)$ is the difference in absorbance after and before irradiation, $\varepsilon(494)$ is the molar absorption coefficient of A(*E*) at 494 nm, l is the optical path (cm) of the cell used for the measurement of A, V (L) is the volume of the irradiated solution, t is the irradiation time. Do not reuse the same solution for more irradiation measurements in the UV, regenerating A(*E*).

Visible region (435–545 nm): in this spectral region it is suggested [2] to produce C by means of UV irradiation (365 nm) of A(*E*) and to use the photobleaching reaction C → A(*E*) for the actinometric measurement. The quantum yield of this reaction, Φ_a, shows a noticeable dependence on the irradiation wavelength and the solvent. In the analytical procedure, the absorbance of the irradiated solution is measured at 494 nm (C disappearance), and in toluene at 294 K the following relation has been obtained [26]:

$$\Phi_a = 0.178 - 2.4 \times 10^{-4} \times \lambda\,(\text{nm}) \tag{4.28}$$

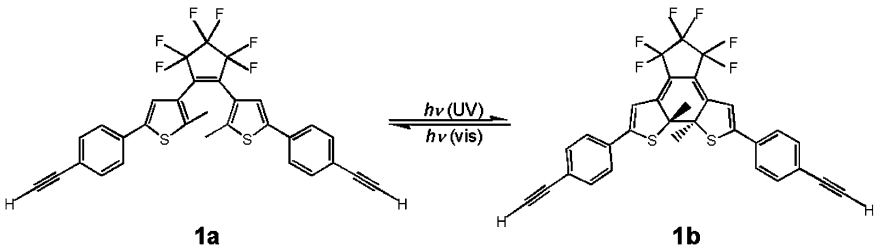

Fig. 4.10 Open-ring **1a** and closed-ring **1b** isomers of 1,2-bis(5-(4-ethynylphenyl)-2-methylthiophen-3-yl)perfluorocyclopentene **1**

From this equation $\Phi_a = 0.074$ at 435 nm and $\Phi_a = 0.047$ at 545 nm are obtained, but these values could be a little smaller, if the more recent ε(C) values are used. Since the exciting radiation could be not completely absorbed by the actinometric solution, the photon flux must be calculated by means of the equation

$$q_{p,in} = -\frac{\Delta A(494)}{l \times \varepsilon(494)} \times \frac{V \times N_A}{\Phi_c \times t \times (f_{ab})_m} \tag{4.29}$$

where the minus sign is due to the fact that $\Delta A(494)$ has negative values; for the calculation of $(f_{ab})_m$ with Eq. 4.11, the absorbance at the irradiation wavelength must be measured before and at the end of the irradiation period.

4.4 A Photochromic Diarylethene Compound

Diarylethenes are typical photochromic [3] molecules, in which the thermodynamically stable colorless open-ring isomer is converted to the colored closed-ring isomer upon irradiation (see, for example, Fig. 4.10), whereas the reverse reaction is either thermally or photochemically activated [27, 28].

The 1,2-bis(5-(4-ethynylphenyl)-2-methylthiophen-3-yl)perfluorocyclopentene diarylethene derivative (**1**), shown in Fig 4.10, has useful spectroscopic properties, since it covers a wide spectral range, and is thermally stable in both isomeric forms [28]. Therefore, the photochemical behaviour as well as the fatigue resistance properties of **1** have been recently studied in detail by us [29]; since its absorption spectrum extends in the visible up to about 700 nm and very simple practical procedures are required by photochromic actinometers, this system has also been proposed as a new chemical actinometer [29]. We report here, as an example, the experimental conditions and the actinometers used in this research, the main results obtained and the procedure suggested for the use of this compound as actinometer.

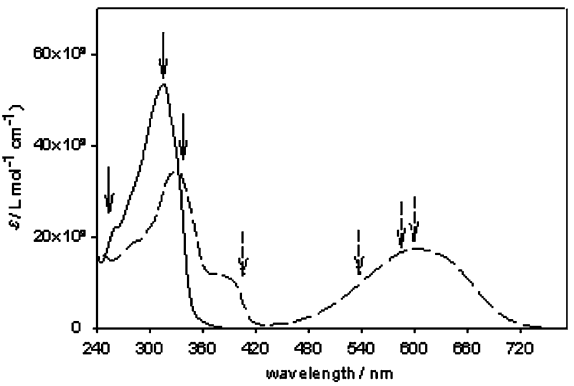

Fig. 4.11 Absorption spectra of **1a** (*solid line*) and **1b** (*dashed line*) in acetonitrile. The solid arrows indicate the wavelengths used for the irradiation of **1a** and the dashed arrows those used for the irradiation of **1b**

4.4.1 Irradiation Experiments

The photochemical behaviour of both isomers of **1** was studied in acetonitrile solutions. The electronic absorption spectra of the isomers are shown in Fig 4.11; **1a** exhibits only one absorption band with maximum at 313 nm with a shoulder at about 255 nm and no absorption in the visible, while the spectrum of **1b** shows a band with maximum at 329 nm, a shoulder at 376 nm and a second broad band with maximum at 600 nm. The absorbance in the visible is a very useful tool for monitoring both the photocoloring (ring-closure, **1a** → **1b**) and photobleaching (ring-opening, **1b** → **1a**) reactions.

According to the spectral properties of the two isomers, the photocoloring reaction can only be induced by UV irradiation, while the photobleaching is more conveniently produced by irradiation with visible light, where no absorption by **1a** is present. The following lines of Hg lamps were chosen (see the arrows in Fig. 4.11) for quantum yield measurements: 254, 313, 334 nm for the first reaction and 404, 549, 586, 609 nm for the reverse one. The lamps and the filters used in the experiments are summarized in Table 4.8; in the case of the 334 nm radiation a cut-off filter was added to the interference filter in order to block the much more intense 365 nm line. The chemical actinometers (Sect. 4.3) used to measure the photon flux are also summarized in Table 4.8; when possible a second actinometer was also used as a control. For the 586 and 606 nm radiation the procedure described at the end of Sect. 4.2 and Eq. 4.14 had to be used, since the absorbance of the Reinecke's salt is not constant in the wavelength interval of the filters. The reaction cells used for both experiments and actinometric measurements were sealable quartz spectrophotometric cells, 1 cm optical path, and the stirring was accomplished magnetically.

The quantum yields were evaluated by measuring the absorbance changes at 600 nm, i.e., the production (reaction **1a** → **1b**) or the disappearance (reaction **1b** → **1a**) of **1b** and by using an equation analogous to (4.12). Unfortunately, the UV light used to cause the photoreaction of **1a** is partially absorbed by the product **1b** (see Fig. 4.11), so that the quantum yield progressively decreases with the

Table 4.8 Lamps, filters and actinometers used in the photochemical experiments

λ (nm)	Lamp	Filter, half-width	Actinometer
254	Low pressure Hg, 15 W	Nil	Ferrioxalate
313	Medium pressure Hg, 125 W	Interference, 12 nm	Ferrioxalate
334	Medium pressure Hg, 125 W	Interference + cut-off	Ferrioxalate
404	Medium pressure Hg, 125 W	Interference, 12 nm	Ferrioxalate
549	Medium pressure Hg, 125 W	Interference, 18 nm	Reinecke's salt Aberchrome 540
589	Halogen incandescent	Interference, 14 nm	Reinecke's salt
609	Halogen incandescent	Interference, 7 nm	Reinecke's salt

irradiation time, since it is calculated on the basis of the total light absorbed by the solution. This problem was overcome by measuring the quantum yield for several consecutive time intervals: extrapolation to $t = 0$ gave the corrected quantum yield of reaction **1a** → **1b** [29]. This procedure was not required for the photoreaction **1b** → **1a**, since the product **1a** does not absorb visible light.

The photochemical reactions that imply the rearrangement of chemical bonds are often accompanied by side or secondary reactions that lead to irreversible products. This represents a disadvantage when photochromic systems would be utilized for practical applications which require a repetitive use of the system, such as, for example, optical memories, photochemical switches and also chemical actinometers; these reactions, in fact, cause a progressive chemical degradation of the system with a loss of performance over time. This effect, that is commonly called "fatigue of the system", is quantified by the "fatigue resistance", that is the number of complete cyclic interconversion of the two forms of the system causing the loss of 20% of the photochromic compound [27, 28]. Since spectrophotometric measurements have demonstrated the presence of a secondary photoreaction in system **1**, caused by UV excitation of **1b**, the fatigue resistance of the system was therefore investigated by performing several consecutive cycles of interconversion between **1a** and **1b**: **1a** was completely converted into **1b** by 313 nm irradiation and then **1b** was reconverted to **1a** by irradiation with polychromatic visible light of $\lambda > 500$ nm, obtained from a halogen incandescent lamp combined with a short-wavelength cut-off filter.

4.4.2 Photochemical Behaviour

Irradiation of a solution of **1a** with 313 nm light causes an increase of absorbance in the visible region; the changes in absorbance at 600 nm are shown in Fig. 4.12.

The increase of absorbance is due to the formation of **1b**, while the very slow progressive decrease observed for long irradiation times is due to a secondary photoreaction of **1b,** which practically may be observed only after the

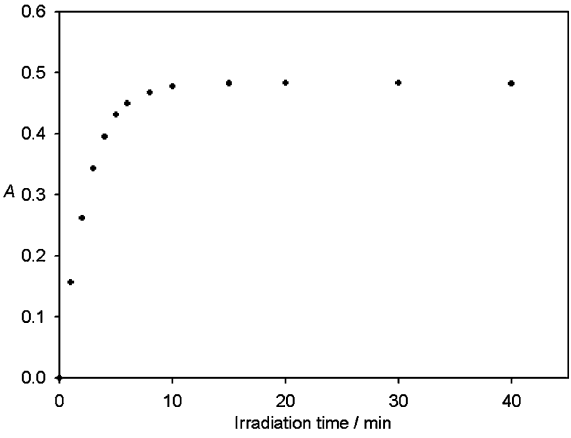

Fig. 4.12 Changes of absorbance at 600 nm during the irradiation of **1a** with 313 nm light, in acetonitrile

Table 4.9 Quantum yields of the photoreactions of **1**[a]

λ (nm)	Φ(**1a**)	λ (nm)	Φ(**1b**)
254	0.92 ± 0.03	404	0.016 ± 0.001
313	0.71 ± 0.03	549	0.0064 ± 0.0003
334	0.72 ± 0.03	589	0.0052 ± 0.0002
		609	0.0015 ± 0.0001

[a] In deareated acetonitrile solutions; data from [29]

photochemical conversion of **1a** into **1b** is completed. Thus, the general scheme of the photoreactions that occur in a solution of **1** may be:

$$\mathbf{1a} \underset{h\nu(\text{vis})}{\overset{h\nu(\text{UV})}{\rightleftharpoons}} \mathbf{1b} \xrightarrow{h\nu(\text{UV})} \mathbf{X}$$

The quantum yield of **1a** → **1b** reaction, Φ(**1a**), and that of **1b** → **1a** reaction, Φ(**1b**), are summarized in Table 4.9. Φ(**1b**) depends linearly on the irradiation wavelength and can be calculated by means of the equation

$$\Phi(1\text{b}) = 0.0440 - 6.94 \times 10^{-5} \times \lambda\,(\text{nm}) \qquad (4.30)$$

which has been experimentally tested in the 400–610 nm range, but most likely is applicable up to 700 nm.

For the reaction **1b** → **X** in aerated acetonitrile solution irradiated at 313 nm a quantum yield value of the order of 10^{-3} has been estimated [29].

As far as the fatigue resistance is concerned, Fig. 4.13 shows a progressive slow decrease of the absorbance with the increasing number of cycles performed. From the linear regression of this and analogous plots we evaluated [29] that the number

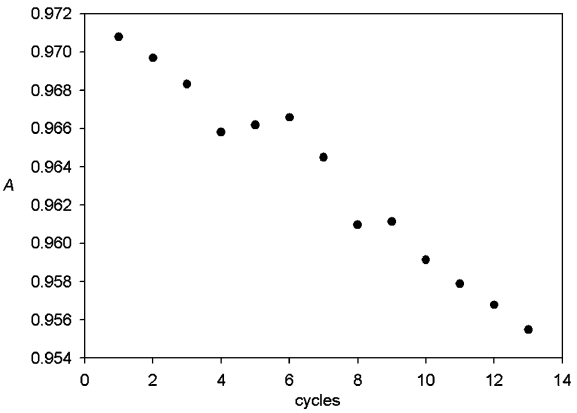

Fig. 4.13 Consecutive photocoloring/photobleaching cycles of a solution of **1** in aerated acetonitrile: absorbance values at 329 nm at the end of the photocoloring step of each cycle

of cycles required to reduce the absorbance to 80% of its initial value is about 180 for deaerated solutions and about 150 for the aerated ones.

4.4.3 Compound 1 as Actinometer

The reversible photocyclization reaction which compound **1** undergoes when irradiated with UV or visible light, offers the possibility to use it as a chemical actinometer. Its positive features are:

- compound **1** can be used to measure light intensity both in the UV (250–340 nm, reaction **1a** → **1b**) where other actinometers are also available, and, albeit the small quantum yield values, in the visible (400–620 nm, reaction **1b** → **1a**) where only a few actinometers can be used and with severe limitations;
- the analytical procedure is rapid, consisting of only a few spectrophotometric measurements before and after irradiation directly in the reaction cell;
- the fatigue resistance of the system is rather large; since in the actinometric procedure suggested (see below) only a small fraction of reactant is transformed, it has been evaluated [29] that the amount of secondary products produced during a single measurement is of the order of 10^{-10} mol L^{-1} and of 10^{-8} mol L^{-1} for UV-light and visible-light intensity evaluation, respectively; thus, one actinometric solution can be used about 500 times with a less than 10% consumption of compound **1**.

Therefore, compound **1** appears to be a very convenient, simple and reusable actinometer.

Procedure—Compound **1** can be synthesized as indicated in [29]. An approximately 1×10^{-4} mol L^{-1} solution of **1** is prepared in spectrophotometric grade acetonitrile and a known volume of this solution is put in a sealable quartz

spectrophotometric cell; a magnetic bar is used to stir the solution during irradiation. Deoxygenation of the solution is suggested, to improve the fatigue resistance of the system. The actinometric solution must be stored in the dark, better in the **1a** form.

UV region. Read the absorbance at both the excitation wavelength and 600 nm, before and after irradiation. The increase in absorbance at 600 nm (0.1–0.2 is sufficient) enables the photon intensity incident in the cell to be calculated using the Eq. 4.31,

$$q_{p,in} = \frac{\Delta A(600) \times V \times N_A}{\Phi(\mathbf{1a})_\lambda \times (f_{ab})_m \times f(\mathbf{1a})_\lambda \times \varepsilon(600) \times l \times t} \tag{4.31}$$

where ΔA (600) is the increase of absorbance at 600 nm in the irradiation period t, V the volume of irradiated solution (L), N_A the Avogadro constant, $\Phi(\mathbf{1a})_\lambda$ the ring-closure (reaction **1a** → **1b**) quantum yield at the excitation wavelength, $(f_{ab})_m$ the mean fraction of light absorbed by the solution in the irradiation period (calculated by means of Eq. 4.11), $\varepsilon(600)$ the molar absorption coefficient of **1b** at 600 nm (17,400 L mol^{-1} cm^{-1}), l the optical path of the actinometric cell (cm) and t the irradiation period. $f(\mathbf{1a})_\lambda$ represents the mean fraction of the light absorbed by the solution that is actually absorbed by **1a,** and it can be calculated by means of the equation

$$f(\mathbf{1a})_\lambda = 1 - \frac{[\mathbf{1b}]_m \times \varepsilon_\lambda \times l}{A_\lambda} \tag{4.32}$$

where $[\mathbf{1b}]_m$ is the mean molar concentration of **1b** in the irradiation period (obtained from the absorbance values at 600 nm), ε_λ is the molar absorption coefficient of **1b** at the excitation wavelength and A is the total absorbance of the solution at the excitation wavelength (mean value in the irradiation period). Note that if no more that 10% of **1a** is converted to **1b**, in the spectral range 250–340 nm $f_\lambda(\mathbf{1a})$ is larger than 0.94; moreover, for $l \geq 1$ cm, the excitation light is almost completely absorbed by the solution (98.5% at 254 nm), so that the term $(f_{ab})_m$ can be neglected in Eq. 4.31.

For $\lambda > 340$ nm, the molar absorption coefficient of **1b** is larger than that of **1a** and so the fraction of light absorbed by **1b** is high even for small conversions (e.g., at 365 nm **1b** absorbs 59% of the light after 10% conversion). The use of **1** as actinometer in the 340–400 nm spectral region is, therefore, discouraged.

Visible region (400–620 nm, likely extendible to 700 nm). To obtain a suitable actinometric solution, the starting solution of **1a** is irradiated with UV light until the absorbance at 600 nm reaches a sufficiently high value (1.0–1.5); it is convenient to use light of wavelength close to the absorption maximum of **1a** (313 nm), in order to minimize the light absorption by **1b** and increase the fatigue resistance. A final value of 1.0 of the absorbance at 600 nm (corresponding to $[\mathbf{1b}] = 5.8 \times 10^{-5}$ mol L^{-1}) is a convenient compromise between a high absorption of visible light by the actinometric solution (90% at 600 nm) and the fraction of light absorbed by **1b** in the UV; we recommend to reach the 1.5 value

Table 4.10 Properties of the most used chemical actinometers

	Ferri-oxalate	Reinecke's salt	AZB	Aberchrome	Compound 1
Thermal reactivity	No	Yes	Yes, at T > 40°C	No	No
Inner filter of the product	No	Yes at $\lambda > 600$ nm	Yes	No	Yes, in the UV
Φ dependence on λ	Yes, in the visible	No	Yes	Yes, in the visible	Yes
Φ dependence on T	No	Yes	No	A little	Not observed
Reusability	No	No	Yes	Yes, in the visible	Yes

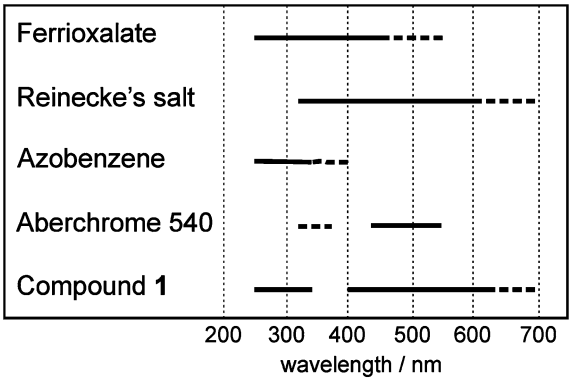

Fig. 4.14 Spectral range of availability of the most common actinometers: the dashed lines indicate the wavelength ranges where the use is possible, but not recommended or simple

only for actinometric measurements around the minimum of **1b** spectrum (430 nm). Now the solution is ready for irradiation at the chosen visible wavelength: read the absorbance at 600 nm and at the excitation wavelength and measure again these values after a suitable irradiation period; the decrease in absorbance at 600 nm can now be used to calculate the incident photon flux using the equation

$$q_{\mathrm{p,in}} = \frac{\Delta A(600) \times V \times N_{\mathrm{A}}}{\Phi(\mathbf{1b})_{\lambda} \times (f_{\mathrm{ab}})_{\mathrm{m}} \times \varepsilon(600) \times l \times t} \tag{4.33}$$

where ΔA (600) is now the decrease of absorbance at 600 nm in the irradiation period t, $\Phi(\mathbf{1b})_{\lambda}$ is the ring-opening (reaction **1b** → **1a**) quantum yield at the excitation wavelength, which can be derived from Eq. 4.30, and the other symbols have the same meaning as for Eq. 4.31.

Table 4.10 and Fig. 4.14 allow comparing compound **1** with the actinometers described in Sect. 4.3.

References

1. Braun AM, Maurette MT, Oliveros E (1991) Photochemical technology. Wiley, Chichester
2. Montalti M, Credi A, Prodi L, Gandolfi MT (2006) Handbook of photochemistry. CRC Press, Boca Raton
3. Braslavsky SE (2007) . Pure Appl Chem 79:293–465
4. Scaiano JC (ed) (1989) Handbook of organic photochemistry, vol 1. CRC Press, Boca Raton
5. Calvert JG, Pitts JN (1966) Photochemistry. Wiley, New York
6. Kuhn HJ, Braslavsky SE, Schmidt R (2004) Pure Appl Chem 76:2105–2146
7. Favaro G (1998) In: Albini A, Fasani E (eds) Drugs: photochemistry and photostability. Spec Publ Royal Soc Chem 225. Cambridge, pp 295–304
8. Hatchard CG, Parker CA (1956) Proc Roy Soc (London) A235:518–536
9. Fisher E (1984) EPA Newsletters 21:33–34
10. Moggi L, Juris A, Gandolfi MT (eds) (2006) Manuale del fotochimico. Bononia University Press, Bologna
11. Demas JN, Bowman WD, Zalewski EF, Velapoldi RA (1981) J Phys Chem 85:2766–2771
12. Bunce NJ (1989) In: Scaiano JC (ed) Handbook of organic photochemistry, vol 1. CRC Press, Boca Raton, pp 241–259
13. Nicodem DE, Cabral MLPF, Ferreira JCN (1977) Mol Photochem 8:213–238
14. Wegner EE, Adamson AW (1966) J Am Chem Soc 88:394–404
15. Birmbaum PP, Style DWG (1954) Trans Faraday Soc 50:1192–1196
16. Zimmerman G, Chow L-Y, Paik U-J (1958) J Am Chem Soc 80:3528–3531
17. Gauglitz G, Hubig S (1985) J Photochem 30:121–125
18. Siampiringue N, Guyot G, Monti S, Bortolus P (1987) J Photochem 37:185–188
19. Gauglitz G (1976) J Photochem 5:41–47
20. Gauglitz G, Hubig S (1981) J Photochem 15:255–257
21. Darcy PJ, Heller HG, Strydom PJ, Wittall J (1981) J Chem Soc Perkin I:202–205
22. Heller HG, Langan JR (1981) J Chem Soc Perkin II:341–343
23. Yokoyama Y, Goto T, Inoue T, Yokoyama M, Kurita Y (1988) Chem Lett 2:1049–1052
24. Uhlmann E, Gauglitz G (1996) J Photochem Photobiol A 98:45–49
25. Boule P, Pilichowski JF (1993) J Photochem Photobiol A 71:51–53
26. Glaze AP, Heller HG, Whittall J (1992) J Chem Soc Perkin II:591–594
27. Irie M (1996) Pure Appl Chem 68:1367–1371
28. Irie M (2000) Chem Rev 100:1685–1716, and references therein
29. Santos AR, Ballardini R, Belser P, Gandolfi MT, Iyer VM, Moggi L (2009) Photochem Photobiol Sci 8:1734–1742

Chapter 5
Spectrofluorimetry

Luca Prodi and Alberto Credi

Abstract Photoluminescence spectroscopy, because of the versatility and sensitivity it can offer, is finding applications in fields of great social and economical impact such as molecular electronics, food technology, environmental sciences, medical diagnostics, and cell biology. Unfortunately, luminescence measurements are often not as easy as they seem at first glance, since the electric signal produced by a spectrofluorimeter is related to the total luminescence intensity (i.e., to the number of emitted photons) through a number of instrumental factors and, in addition, can often hide subtle artifacts. A superficial approach can thus lead to major mistakes; this section has been then conceived to give the reader all the information needed for the correct handling of the instrumentation and of experimental data, even for solid samples. An example taken from the world of supramolecular chemistry is also described in order to evidence all the steps required for comparing luminescence intensities obtained in different experimental conditions. Moreover, in this section it is possible to find information about the main standards for fluorescence quantum yield determination.

L. Prodi · A. Credi (✉)
Dipartimento di Chimica "G. Ciamician", Università di Bologna, via Selmi 2, 40126 Bologna, Italy
e-mail: alberto.credi@unibo.it

L. Prodi
e-mail: luca.prodi@unibo.it

P. Ceroni (ed.), *The Exploration of Supramolecular Systems and Nanostructures by Photochemical Techniques*, Lecture Notes in Chemistry 78,
DOI: 10.1007/978-94-007-2042-8_5,

5.1 Introduction

Photoluminescence spectroscopy is one of the most versatile and sensitive techniques for the detection of chemical species in solution. Nowadays, standard UV–VIS–NIR spectrofluorimeters are low-cost, compact instruments usually interfaced to a PC, very easy to use and largely employed in research and analytical laboratories. Luminescence spectroscopy has been shown to have application in growing fields of great social and economical impact such as molecular electronics, food technology, environmental sciences, medical diagnostics, and cell biology. The main reasons that explain the large interest for this analytical technique can be summarized underlining that photoluminescence spectroscopy offers:

a. a very high sensitivity even in complex matrices, so that, in special conditions, even single molecule detection is possible;
b. a linear response in a very wide concentration range;
c. a very high versatility, that is due to the possibility to choose both the emission and the excitation wavelength, to analyze sample both in solid and in solution, and to use devices such as optical fibres allowing to perform analysis almost everywhere, including, for example, inside human body.

Furthermore, although in this chapter we will mainly deal with photoluminescence (i.e., luminescence arising from an excited state created by the absorption of light), it is important to underline at this point that (electro-)chemiluminescence (luminescence arising from an excited state generated by an (electro-)chemical reaction), has made analytical potentials even stronger.

Unfortunately, luminescence measurements are often not as easy as they could seem at a first glance [1–5], since they can hide often subtle artifacts. Furthermore, while the electric signal produced by a spectrophotometer represents a physical quantity (the absorbance) that can be expressed in an absolute scale, the electric signal produced by a spectrofluorimeter is related to the total luminescence intensity (i.e., to the number of emitted photons) through a number of instrumental factors (intensity of the exciting source, instrument optics, signal amplification) and to the sample characteristics. The observed intensity can be related to sample concentration only if corrected in order to take into account all these factors. It should be stressed that luminescence intensity measurements carried out with standard spectrofluorimeters are never absolute, and the intensity values must be expressed in a relative scale even after corrections. As a consequence, the number given by the instrument has no physical meaning; rather, only the ratios between measurements performed exactly in the same experimental conditions can have a significance to analysts working with other equipments and in other conditions.

It is also important to note here that, as it will be discussed in detail later on, there are instrumental factors that can deceive users not familiar with this technique, by making bands appear in the emission (or excitation) spectrum that

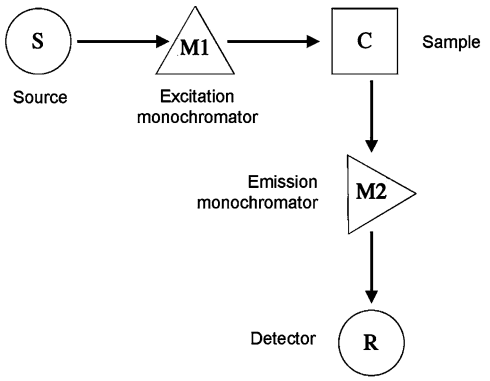

Fig. 5.1 Simplified optical diagram for a spectrofluorimeter

have nothing to do with the real luminescence of the substance being examined, such as Rayleigh and Raman bands.

In conclusion, (photo)luminescence techniques can offer a very promising solution (if not the only one) when it is necessary to have very high sensitivity, with the plus of requiring a generally cheap and easy-to-use instrumentation. However, a superficial approach can lead to major mistakes, and for this reason to interpret the data obtained it is important to know the instrumental technique in detail. This chapter has been conceived with this aim in mind.

5.2 The Instrumentation for Measuring Luminescence

Luminescence measurements can have different purposes:

1. measuring the intensity of the luminescence at various wavelengths (emission spectra),
2. determination of the dependence of the intensity of luminescence on the excitation wavelength (excitation spectra),
3. identification of the nature of the luminescent excited state, including its spin multiplicity (thus, identifying if the emission observed is a fluorescence or a phosphorescence),
4. determination of the quantum yields of luminescence,
5. qualitative and quantitative analytic determinations.

For this, spectrofluorimeters are needed. Figure 5.1 contains a block diagram of a modern spectrofluorimeter, while Fig. 5.2 contains the optical diagram of a Perkin–Elmer LS55 spectrofluorimeter. We will first explain the various components and, then, discuss the possibilities offered by this type of instrumentation and the techniques necessary for performing the most precise analysis possible.

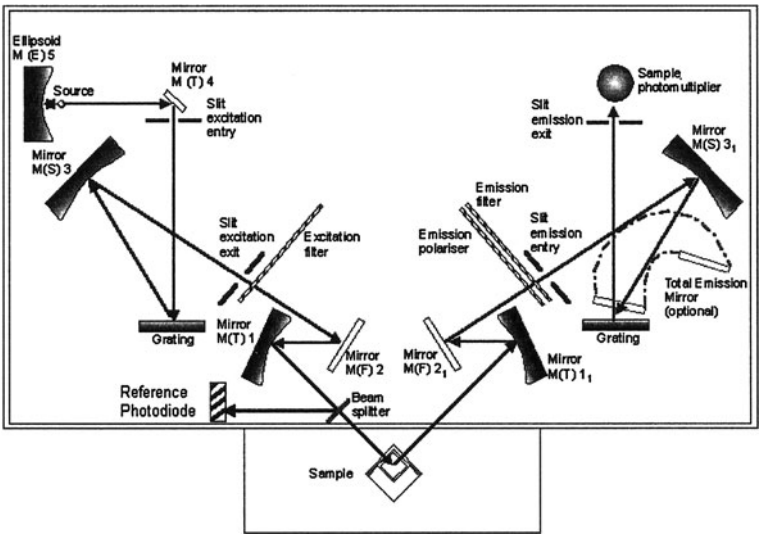

Fig. 5.2 Optical diagram of a Perkin–Elmer LS55 spectrofluorimeter

5.2.1 Light Source S

This is necessary for exciting the sample under examination, i.e., for generating the excited states whose emission we want to observe when exploiting photoluminescence. When the excited state is generated through chemical reactions, such as in the case of chemiluminescence and bioluminescence, the light source must, instead, be turned off. In conventional instrumentation, the source is generally a Xenon lamp whose spectrum, shown in Fig. 5.3 for the region between 250 and 700 nm, is continuous from 250 to over 1,000 nm. However, as it can be seen, the lamp's intensity is not constant with the wavelength and this fact must be taken into account when working with a spectrofluorimeter. In fact, as one can see from Eq. 5.1, the quantity of photons emitted (I_l) by a sample is directly proportional to the number of photons absorbed (I_a), which, at equal absorbance, is directly proportional to the intensity of the incident light on the sample I_i (λ_{exc}), which is precisely dependent on the wavelength selected.

$$I_l(\lambda_{exc}) = \Phi \cdot I_a(\lambda_{exc}) = \Phi \cdot I_i(\lambda_{exc}) \cdot (1 - 10^{-A(\lambda exc)}) \tag{5.1}$$

If a sample has, for example, the same absorbance at 250 and 450 nm, the number of emitted photons that reach the detector is much greater (and, thus, the signal is higher) if you excite at 450 nm rather than at 250 nm. Moreover, the nature of the lamp's spectrum is the main reason for the need to correct excitation spectra, a subject that will be discussed further below.

You can currently find spectrofluorimeters on the market with continuous light sources (usually 150 or 450 W), i.e., whose intensity is constant over time, or

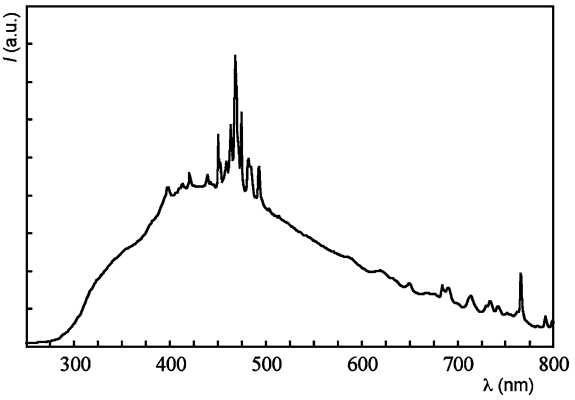

Fig. 5.3 Emission spectrum of a 450 W Xenon lamp

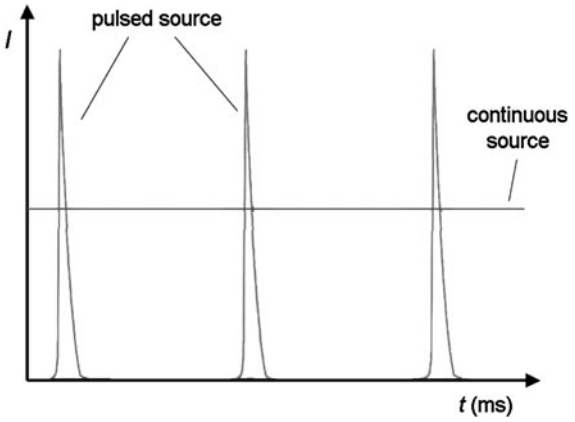

Fig. 5.4 Intensity profile versus time of a pulsed lamp compared to a continuous one

pulsed, a characteristic that is achieved by discharging a condenser through a lamp at regular intervals. Typically, the pulsed lamps in the most common spectrofluorimeters generate light pulses at the frequency of the power grid (50 Hz, i.e., every 20 ms) with a duration of a few microsecond (Fig. 5.4). In addition, their energy consumption is lower (8–15 W), a characteristic that can reduce the effect of any photochemical reaction of the sample and the heating of the optical parts of the instrument. Finally, they also offer the possibility of determining lifetimes longer than 10 μs (generally up to about 100 s) and of resolving spectra over time, whose most common application is that of separating the spectrum of phosphorescence from that of fluorescence. The principle on which this latter possibility is based is discussed in Sect. 5.2.2. In any case, it should be stressed that the sensitivity of instruments with a continuous 450-W source is generally higher than that offered by instruments with pulsed sources.

Since the intensity of the lamp of a spectrofluorimeter can vary over time (variations in the power grid, aging, etc.), the most modern spectrofluorimeters take a small part of the ray coming from the lamp after it is dispersed by the excitation

monochromator M1; this portion of light is then sent to a photomultiplier of reference that automatically corrects the intensity output by the detector for the variations of intensity of the source (see Fig. 5.2). This mode is often called "ratio mode".

Finally, it should be emphasized how some instruments provide the possibility of exciting the sample with a laser source by having the light enter downstream from the monochromator (since laser light is monochromatic, in this case, this device is not necessary). The possibility of using laser light allows a significant increase in the sensitivity of the instrument, an increase in the incident light and a decrease in noise, especially due to the decrease of the diffused light.

5.2.2 Excitation and Emission Monochromators M1 and M2

Excitation monochromator M1 is used to select the wavelength that excites the sample from the light coming from the lamp; the emission monochromator M2, instead, selects the wavelength emitted by the sample that is, then, sent to the detector. In the most recent spectrofluorimeters, there are gratings that minimize the effects due to diffused light (see below); however, as we will see, they have the disadvantage of leading to the appearance of higher-order bands in the emission and excitation spectra, a disadvantage that can easily be eliminated with the appropriate use of filters. It should be noted that, even for monochromators, the percentage of light transmitted depends on the wavelength selected.

5.2.3 Sample-Holder C

The arrangement most frequently used for the analysis of solutions provides the geometry described in Figs. 5.2 and 5.5, in which the luminescence is measured with an angle of 90° with respect to the exciting light so as to minimize the quantity of exciting light that hits the detector.

In any case, this quantity can never be completely avoided due to the scattering caused by the molecules themselves (solvent and solute), the presence of small suspended particles (such as dust) and the change of the refraction index at the air-cell wall and wall-solution interface. To partly eliminate this latter problem, the cell is generally masked so that only the light coming from the center area of the cuvette (and, thus, not from the lateral faces of the cell) is conveyed to the detector (Fig. 5.5b). The use of this 90° arrangement has, as we will see below, an important effect on the dependence of the signal on the concentration of the analyte, since the fraction of the exciting light that reaches the part of the cell "observed" by the detector is not linear with respect to the absorbance of the solution. For analyses of solids, solutions of high optical density and very cloudy

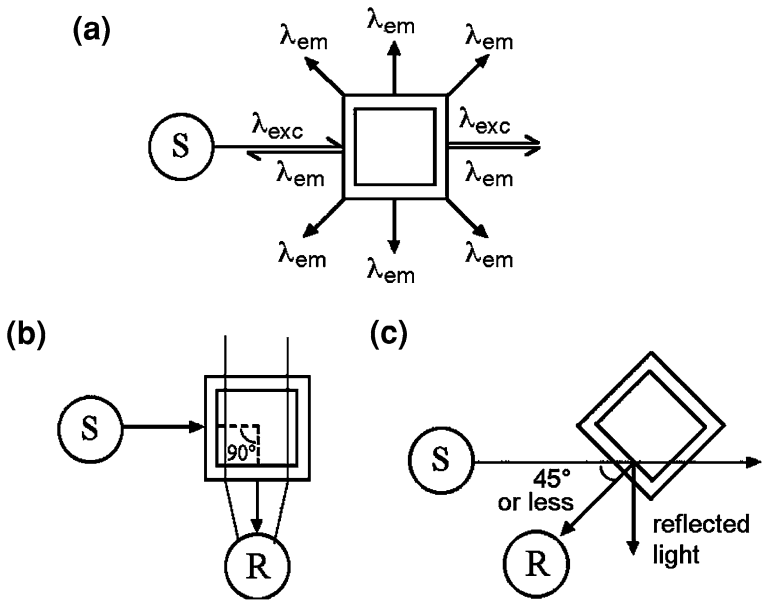

Fig. 5.5 **a** Differences among the propagation of excitation and emitted light; **b** Geometrical representation of a sample-holder for dilute solution; **c** Geometrical representation of a sample-holder for solids or concentrated solutions

samples, a geometry of 45° or 37° is used instead (Fig. 5.5c). In fact, in these cases, all the exciting light would be absorbed or diffused in the first layer of the sample and, with a 90° geometry, only a very small part of the light would fall in the cone of observation of the detector.

5.2.4 Detector R

Conventional spectrofluorimeters normally use photomultipliers as detectors. The sensitivity limit of a photomultiplier is normally related to the level of dark current, which is the signal coming from the detector phototube even when no light is falling on it. The dark current is caused by the thermal activation of electrons in the phototube and can be decreased by cooling. It must be stressed that the sensitivity of photomultipliers depends on the wavelength of the incident photons (Fig. 5.6) and, for this reason, in order to meet different investigative needs, manufacturers produce photomultiplier with different response curves depending on the wavelength range explored. For this reason, it is fundamentally important for the user to choose from among the photomultipliers available on the market those most suitable to his needs, especially if red light ($\lambda > 600$ nm) is to be detected.

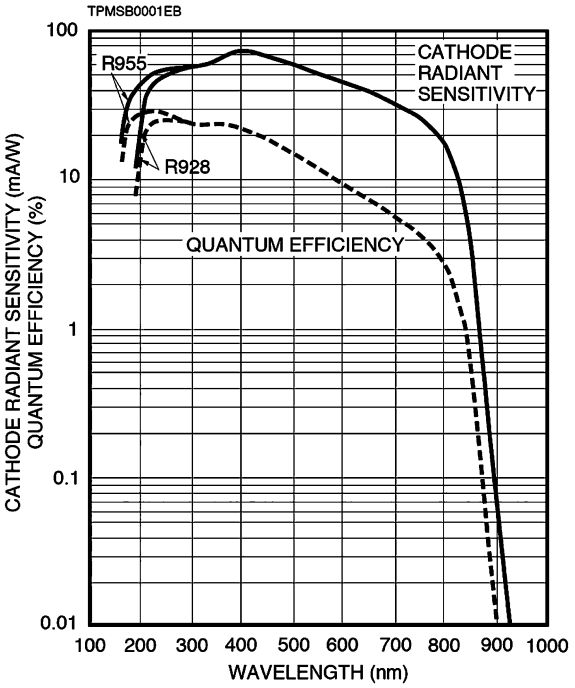

Fig. 5.6 Cathode radiant sensitivity and quantum efficiency of two widely diffused photomultipliers (Hamamatsu R955 and R928) having high sensitivity up to 800 nm

In fact, the incorrect choice of this component could result in a failure to observe signals that are otherwise easily visible. The strong dependence of the sensitivity of photomultipliers on the wavelength, to which is added, in lesser measure, the non-linear response of the emission monochromator, is the main cause of the fact that, as we will see in the next section, experimentally-obtained emission spectra must be "corrected", i.e., they must be multiplied by an instrumental factor in order to be compared with spectra obtained under other experimental conditions.

5.3 Emission and Excitation Spectra and Their Correction

5.3.1 Emission Spectra

Emission spectra can provide important information about the nature and energy of the emitting excited state and can, obviously, be used in analytical chemistry, both qualitative (the emission spectrum is characteristic of the luminophore) and quantitative (the intensity depends on the concentration, as we will see below). To record an emission spectrum, the sample is excited at a fixed wavelength, λ_{exc}, at which it absorbs and, by moving the emission monochromator, we measure how

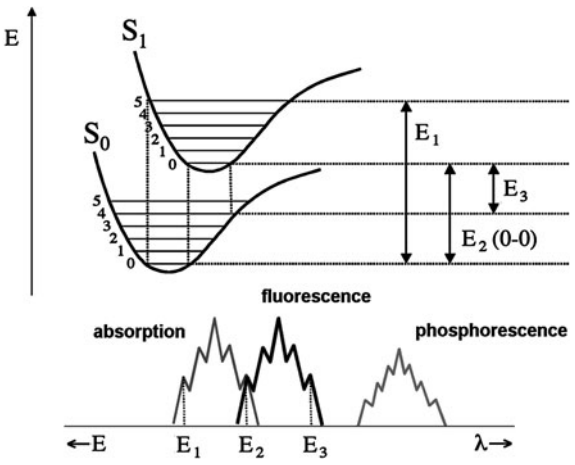

Fig. 5.7 Potential energy curves for the ground and excited state of a generic diatomic molecule

the intensity of the luminescence varies with the emission wavelength λ_{em}. It is important to emphasize that, in this specific case (recording emission spectra), the excitation monochromator (M1, Fig. 5.1) is fixed at a certain wavelength, while the emission monochromator (M2, Fig. 5.1) examines a more or less broad interval of wavelengths. Now, let's consider making the emission spectrum of substance A by exciting with light of λ_1, i.e., by exciting in the first band of excited singlet S_1. The substance can either emit from S_1 and, in that case, we will have the emission of fluorescence or it can give intersystem crossing to T_1 and, in this latter case, we have phosphorescence. So, at most, we can observe two emission bands (fluorescence + phosphorescence), or only one band (fluorescence or phosphorescence) or no band (the substance emits neither fluorescence nor phosphorescence). Where will these emission bands fall with respect to the absorption bands? Always to the right of the last absorption band. In the most common cases, i.e., when the excited state is distorted with respect to the ground state (Sect. 1.5), at most one part of the last absorption band overlaps the emission band. In other words, if we consider, for example, the energy potential curves of a generic biatomic molecule (Fig. 5.7) and keeping in mind that the Franck–Condon principle applies in both absorption and emission, we see that:

a. In absorption, the 0–0 transition is the one having the minimum energy and, thus, corresponds to the origin of the absorption band at longer wavelengths. If, however, the ground state and the excited state are sufficiently distorted from one another so as to not have an overlap of the 0–0 in absorption with emission, this origin of the absorption band is only an upper limit.
b. In fluorescence, the 0–0 transition is the one having the maximum energy, thus corresponding to the origin of the band of fluorescence at shorter wavelengths. However, it should be noted that, if the two ground and excited states are sufficiently distorted, the origin of the band of fluorescence by the short λ corresponds to a lower limit. If, as represented by the diagram in Fig. 5.7, we

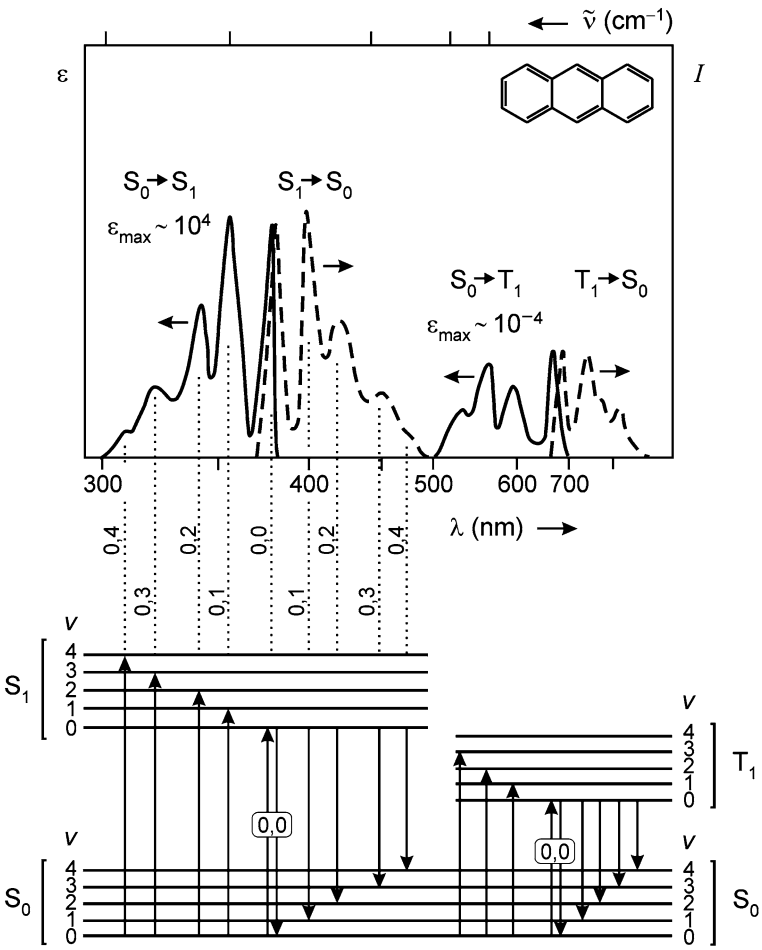

Fig. 5.8 Absorption (*dashed line*) and emission (*full line*) spectra of anthracene in solution

had the resolved vibrational spectrum, we would see that the band of fluorescence looks like the mirror image of the lowest energy absorption band ($S_0 \rightarrow S_1$) because the vibrational spacing of the ground and excited states is often similar. The same could be said of the phosphorescence with respect to the absorption $S_0 \rightarrow T_1$, but this last band is usually highly prohibited (very small ε) so as to be practically never visible in the absorption spectrum. With the absorption spectrum (transitions $S_0 \rightarrow S_n$), the phosphorescence thus has no relation, except that it must fall well beyond the last band. A good example for these considerations is that offered by anthracene (Fig. 5.8).

If the spectrofluorimeter is working in ratio mode (and, thus, corrects for the variations of emission intensity of the lamp), the only two instrumental factors that must be considered for the correction of the spectra are the different response of

the photomultiplier (see Sect. 5.2.4) and the different transmission of the monochromator with the varying of λ_{em}. In the absence of suitable corrections, there can be errors in the positions of the maximums of the band, in maximum–maximum and maximum–minimum relationships and, in general, in the shape of the band itself. This distortion is even more accentuated the more the response of the photomultiplier changes as the wavelength varies.

The most precise system for correcting emission spectra uses a calibrated lamp, i.e., one whose emission spectrum is known with precision (quanta s^{-1} nm^{-1}), supplied by the manufacturer of the lamp. This is compared with the emission spectrum obtained from our instrument by directly sending the light from the calibrated lamp to the emission monochromator (taking care to attenuate the signal, also using small slits and a low photomultiplier voltage); by determining the ratio between the two spectra, we obtain the values, wavelength by wavelength, for which we need to multiply the spectra to correct. It should be stressed that this factor includes the dependency on λ_{em} of both the response of the phototube and the transmission of the emission monochromator. Since the response of the photomultiplier can change with use, it is useful to obtain the correction curve with a certain frequency (at least every 6 months) and, naturally, every time that the photomultiplier is replaced. Sometimes this correction curve is supplied with the instrument's software; however, it is important to remember that it is prepared for the model of photomultiplier with which the instrument is assembled (i.e., for the average response that the model of detector offers and not for the specific detector mounted on the instrument, which could be slightly different), which becomes obsolete with use and that, finally, loses all value when the model of photomultiplier is changed.

If you do not have a calibrated lamp, one simple and fairly reliable method is to obtain the necessary correction factor by comparing the emission spectrum of a standard substance obtained with your own instrument with that of the spectrum of the same substance, but corrected, as shown in the literature. The main standards and their corrected spectra, which cover the region between 300 and 800 nm, are listed in [1].

5.3.2 Excitation Spectra

To execute an excitation spectrum, it is necessary to fix the emission monochromator (M2, Fig. 5.1) at a certain wavelength (λ_{em}) in correspondence with the emission band of the sample (generally the maximum or at a slightly higher wavelength), while the excitation monochromator is moved, exploring the spectral interval in which the sample absorbs. After the due corrections are made, the signal obtained is proportional to the probability that, by sending a photon of a suitable wavelength, the excited state responsible for the emission to be observed will be populated. If you are observing a solution containing a single luminescent species (or a single peak in the HPLC) in suitable experimental conditions

(primarily, as we will see, $A < 0.1$ in the entire region that is the object of investigation), and if the conversion of the excited states higher in energy than the one responsible for the emission is complete (by far and away the most common case), the corrected excitation spectrum is proportional to the absorption of the species being examined. It should be kept in mind that this proportionality only implies that the two spectra have the same shape: as was said in Sect. 5.1, the intensity values obtained with spectrofluorimetric measurements and, thus, even excitation spectra, have no physical significance. One analytical implication is that you could obtain the excitation spectrum of solutions whose absorbance is so low that it not possible to execute a normal absorption spectrum. Given the proportionality between excitation and absorption spectra, you can, in this way, obtain additional information about the nature of the chromophore. Excitation spectra also play a very important role in the analysis of mixtures. In this case (in the absence of energy transfer processes, as we will see later), we obtain an excitation spectrum that will be proportional to the absorption spectrum of just the chromophore whose emission is under investigation (helping, in this way, to identify it), since the absorption of the light by other species will not lead to photon emission at λ_{em}. It should also be remembered that, if the analyte of interest has a high quantum yield, you can obtain an excitation spectrum of it even when its absorption is negligible with respect to the other components of the mixture.

Given the dependence of the intensity of the exciting source and of the intensity transmitted by the monochromator on λ_{exc}, it should be noted that, by simply recording the emission intensity as a function of the wavelength of excitation, we obtain incorrect excitation spectra; so, it is necessary to make suitable corrections for excitation spectra as well. Nowadays, spectrofluorimeters are normally equipped to automatically correct excitation spectra for these two instrumental factors (even if somewhat imperfectly, especially where the emission of the lamp changes dramatically with the wavelength).

As an alternative, the most common method for obtaining the spectral irradiance of the excitation system (which, thus, takes into account both the lamp and the monochromator) as a function of the excitation wavelength is to use a quantum counter, i.e., a relatively concentrated solution (normally rhodamine B, 3 g/l in ethylene glycol, $\Phi \cong 1$) of a fluorescent substance having a high, constant quantum yield with the variation of the excitation wavelength. At the indicated concentrations, quantum counters have the property of absorbing all the incident light in the interval of wavelengths for which they are recommended (220–580 for rhodamine B, but with hexamethyl-indotricarbocyanine, 8 g/l in acetonitrile, the interval is 320–800 nm) [1], so that the light emitted, measured at a suitable emission wavelength, is proportional to the flow of the incident photons. In this way, we obtain the spectral irradiance of the instrument. The excitation spectrum of the substance being examined can now be corrected by dividing it by the profile of the lamp thus obtained. At this point, it is important to remember, even thought it will be taken up again in Sect. 5.4.1, that to have a correct excitation spectrum, it is absolutely necessary that the absorbance of the solution is <0.1 or, even better,

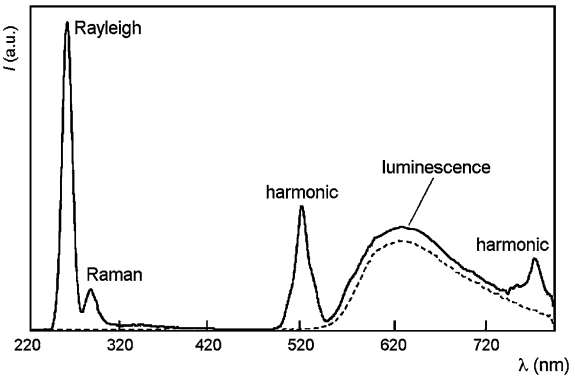

Fig. 5.9 Emission scan of a dilute $[Ru(bpy)_3]^{2+}$ solution in water, exciting at 260 nm, using (*dashed line*) or not (*full line*) a cut-off filter ($T \approx 50\%$ at 385 nm)

<0.05 (the error in this case will be less than 5%) since in this range, emission intensity is proportional to the absorbance at the excitation wavelength.

Finally, the excitation spectrum can serve to quantify the presence of any energy transfer process between the compound A whose emission we are observing and another compound B present in the solution. In fact, as was already said, in the absence of such processes, the excitation spectrum is proportional to the absorption spectrum of A. Similarly, if this process has a unitary efficiency (i.e., every photon absorbed by B is transferred to A), the excitation spectrum will, in this case, be proportional to the sum of the absorption of A and B. In intermediate cases, the excitation spectrum will, instead, be proportional to the absorption spectrum of A, plus a fraction of the absorption of B, equal to the efficiency of the energy transfer.

5.3.3 Presence of Spurious Bands in Spectra

To conclude this paragraph, it is necessary to mention other factors that could deceive users not familiar with this technique, by making bands appear in the emission (or excitation) spectrum that have nothing to do with the real luminescence of the substance being examined (Fig. 5.9).

5.3.3.1 Rayleigh–Tyndall Bands

These bands are due to the fact that the incident light on the sample being examined is not just absorbed or transmitted but is also diffused in all directions (thus even arriving at the emission monochromator) by the molecules themselves (solvent and solute), by the air-wall and wall-solution interfaces of the cell (Rayleigh scattering) or by the presence of small suspended particles (such as dust, Tyndall scattering). This type of diffused light is always observed when you are

forced to use the instrument in conditions of great amplification because, for example, the concentration of the luminophore is very low or because its quantum yield is very small.

These phenomena cause the detector to collect part of the exciting radiation together with the emitted radiation. The fraction of diffused light depends on the absorbance at λ_{exc} and will be as small as the absorbance is large. The width of the scattering band depends on the slits and, in the case in which the luminescence band observed is very close to the excitation wavelength, it can generate an overlap of the two signals with consequent distortion of the emission band itself. If possible, in this case it is a good idea to move the λ_{em}, in the case of excitation spectra, or the λ_{exc}, in the case of emission spectra, and/or narrow the slits.

5.3.3.2 Raman Bands

These bands derive from the interaction of the photons of the exciting radiation with the vibrational levels of the molecules of the solvent to which they transfer a constant fraction of their energy. These bands are generally not intense and, for this reason, the contribution of the solute is normally negligible. For the same solvent, the difference between the λ_{exc} and the maximum of the Raman band is constant in terms of energy but *not in terms of wavelength*. The wavelength at which the Raman band appears in the emission spectrum always depends on the λ_{exc} and, for this reason, unlike a "real" emission, it moves as the excitation varies. All solvents with C–H or O–H bonds normally show Raman bands moved by about 2,800 and 3,400 cm^{-1}, respectively. So, when observing a band with an energy difference of less than 3,400 cm^{-1}, it is a good idea to check if it is a Raman band either by executing a spectrum of the solvent alone and/or by varying the excitation (if it moves with the exciting wavelength, it will, with all probability, be a Raman band). It should also be kept in mind that Raman bands can also be observed in excitation when the λ_{exc} assumes a value such that the energy difference between it and the λ_{em} equals a Raman transition. If the Raman band and the luminescence band in a spectrum are very close, it could be a good idea to move the λ_{em}, in the case of excitation spectra, or the λ_{exc}, in the case of emission spectra.

5.3.3.3 Higher-Order Harmonic Bands

These bands are connected to the use of gratings as monochromators, which work based on the phenomenon of diffraction. We have already seen that part of the diffused light, together with any real emission from the sample, arrives at the emission monochromator, whose orientation (angle) selects the wavelength that reaches the photomultiplier. If, for example, we excite at 250 nm, and we scan a sample containing only the solvent between 220 and 800 nm, at 250 nm we observe a signal that is due to the scattering of the light. When the emission

monochromator M2 reaches 500 nm, due to the laws of diffraction, in addition to the light of this wavelength, it also sends light with $\lambda = 500/m$ (where m is an integer number). So, even if, nominally, we are observing the light at 500 nm, light of 250 nm is also coming to the photomultiplier ($\lambda/2$), *if it strikes the* gratings. So, in our spectrum, in addition to the Rayleigh at 250 nm, we are observing a band, called harmonic (because on the order of $m > 1$), at 500 nm, of an intensity that is, in any case, less than the first (in fact, intensity decreases as m increases). This, it should be emphasized, does not mean that light with $\lambda = 500$ nm is really reaching the photomultiplier, but only that, when the instrument is adjusted to see light at 500 nm, it also sees light whose wavelength is one of its whole fractions. As we continue scanning, we again observe a peak at 750 nm ($m = 3$). To summarize, in the emission spectrum (but, reversed, the same is true for excitation spectra), if suitable techniques are not used, in addition to the real emission (if it's there), it is possible to observe the passing band, the Raman band and other bands with maxima that are whole multiples of the excitation wavelength (and that, therefore, unlike the "real" emissions, move with this, which is a very important characteristic for recognizing them).

What can be done to eliminate these spurious bands? We simply need to avoid the diffused exciting light reaching the emission monochromator and this is achieved by interposing suitable cut-off filters between the sample and the emission monochromator (i.e., only transparent at wavelengths greater than a certain value, depending on the type of filter), as it is shown in Fig. 5.9. Some instruments have a filter set incorporated, selectable by computer, even if it can be a good idea to get a set of external filters so that you will have more options available. Obviously, the filter must be selected so as not to cut-off the real emission, which means that the wavelength below which the filter absorbs all the light must be between the excitation wavelength (which is the one to mask) and that in which we starts to observe the emission of the sample (which, instead, must not be absorbed by the filter).

5.4 Quantitative Measurements at Fixed Wavelength

5.4.1 Correction for the Sample Absorption at the Excitation Wavelength

In this section we deal with quantitative steady-state luminescence intensity determination in solution, at a fixed emission wavelength, using a commercial spectrofluorimeter with right-angle excitation (perpendicular geometry). These kind of measurements are particularly important in analyte detection, titrations, quenching and sensitization experiments, photoreaction and photoluminescence quantum yield determination, and whenever a luminescence signal is used to monitor a chemical process.

In the introduction of this chapter we pointed out that a crucial advantage of spectrofluorimetry is the possibility of obtaining a linear response over a wide concentration range. In general, a linear relationship between luminescence intensity and concentration is observed only if effects related to the absorption of the exciting and emitted light can be neglected; this condition is always fulfilled with extremely dilute samples. Measurements on highly dilute samples, down to 10^{-10} M, is a most important challenge for fluorimetric techniques in analytical chemistry. However, experiments are often carried out on far more concentrated solutions, for which the observed luminescence intensity does not scale linearly with concentration; such a lack of linearity, if it is not correctly understood, can indeed pose problems in the interpretation of the data.

Figure 5.10 shows a plot of the emission intensity of a luminescent species in solution as a function of its absorbance—and hence of its concentration. For very low absorbance values (approximately lower than 0.1), the luminescence intensity increases linearly upon increasing the absorbance. For higher absorbances the emitted intensity increases in a nonlinear manner, until it reaches a maximum (usually around $A = 1$). Finally, for even higher absorbance values, the luminescence intensity decreases upon increasing the sample concentration. This experimental behavior arises from the combination of two distinct factors: one of mathematical and one of "geometric" nature.

The mathematical factor can be understood from the analysis of Eq. 5.1, which states that the number of photons emitted by a sample (I_l) is equal to the number of photons absorbed (I_a) times the emission quantum yield. The number of absorbed photons, resulting from the difference between the number of incident and transmitted photons, is not linearly related to the absorbance, and hence to concentration; as shown in the equation, the relationship contains the term $[1-10^{-A(\lambda exc)}]$. As a matter of fact, this term can be expanded in series, and orders higher than 1 can be neglected if $A(\lambda_{exc})$ is reasonably small (usually <0.05 or, if a larger error can be tolerated, <0.1); in other words, the luminescence intensity observed for solutions whose absorbance at λ_{exc} is smaller than 0.05 (or 0.1) is linearly proportional to $A(\lambda_{exc})$. This is also the reason why the excitation spectrum of an emitting species, to be quantitatively compared with the absorption spectrum, must be recorded on a solution with very low absorbance (see Sect. 5.3.2). The term $[1-10^{-A(\lambda exc)}]$ tends to unity at increasingly larger absorbance values: for $A = 0.5$ it is 0.68, for $A = 1$ it is 0.90, for $A = 2$ it is 0.99, for $A = 3$ it is 0.999, and so on. In summary, such a mathematical factor accounts for the fact that the initial part of the curve in Fig. 5.10 can be approximated to a straight line; it does not explain, however, the trend at higher absorbance values. In fact, according to the above relation, upon increasing the absorbance the curve should reach a plateau, not a maximum and a successive decrease of the intensity. This phenomenon can be interpreted only by taking into account the second factor, that is, the geometric one.

To understand the origin of the geometric factor it is useful to recall the description of the instrumentation earlier in this chapter. When the luminescence is measured at an angle of 90° with respect to the excitation direction in commercial

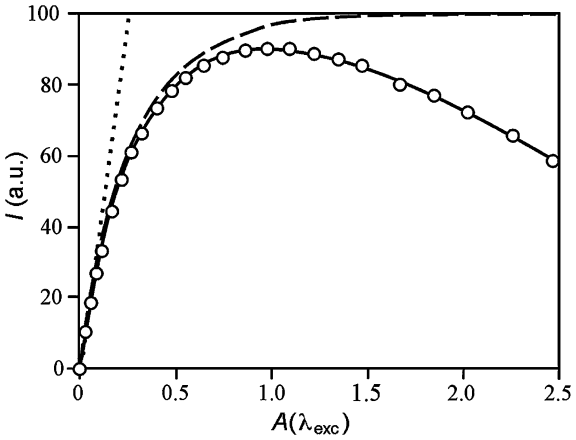

Fig. 5.10 Experimental calibration curve obtained by plotting the luminescence intensity observed for quinine sulfate solutions at different concentrations in H_2SO_4 0.5 M (*empty circles*, *full line*). Instrumental conditions: Perkin–Elmer LS-50 spectrofluorimeter, $\lambda_{exc} = 350$ nm, $\lambda_{em} = 450$ nm, bandpass 5 nm. The *dashed line* shows the luminescence intensity versus absorbance relationship expected on the basis of the sole mathematical factor. The *dotted line* is the tangent to the experimental curve for $A(\lambda_{exc}) \rightarrow 0$, and evidences the linear relationship between luminescence intensity and absorbance for $A < 0.1$

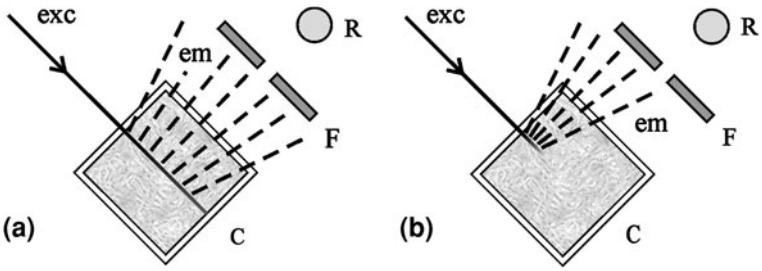

Fig. 5.11 Schematic representation of the sample geometry for a photoluminescence experiment on a square cell containing solutions with different absorbance at the excitation wavelength: **a** low absorbance (<0.1) and **b** high absorbance (>2.0). Legend: exc, exciting light; em, emitted light; C, cell; F, slit; R, detector

spectrofluorimeters (in order to avoid artifacts arising from scattered light at the air-cell and cell-solution interfaces), the cell is positioned such that the detector monitors only the central part of the illuminated solution, and not its side portions (Fig. 5.5b). Hence, it is not only important *how much* light is emitted but also *where* it is emitted inside the solution cell. If the solution is sufficiently dilute, the excitation beam is able to cross the entire cuvette before being considerably attenuated (i.e., the absorbed light is negligible with respect to the incident light, Fig. 5.11a), and the excited states are uniformly produced along the excitation beam path. Under this condition, Eq. 5.1 holds and no geometric effect is present.

The situation is completely different at high absorbance values: most of the light is absorbed (and emitted) in the first millimeters of the cell, i.e., in a sector that is not monitored by the detector. This fact leads to the paradox that more emitted photons generate less signal, an effect which occurs for analyte concentrations above a certain threshold, and is increasingly more evident upon increasing the absorbance at the excitation wavelength (Fig. 5.11b). It should be stressed that this phenomenon is related to the total absorbance of the sample, including the possible contribution from chromophores other than the fluorophore under investigation.

The shape of an instrument calibration curve, such as that shown in Fig. 5.10, depends on the specific equipment and the employed instrumental parameters (e.g., slit widths), and not on the fluorophore, unless it undergoes concentration-dependent phenomena such as aggregation or self-quenching. In fact, by using a different fluorophore, the emitted intensity values will be different (because of the different luminescence quantum yields of the various emitting species), but the overall shape of the curve will not be affected. The complex $[Ru(bpy)_3]^{2+}$ in water turned out to be a suitable species for constructing the instrument calibration curve. The curve can be constructed by preparing a number of solutions with increasing concentrations, and measuring for each solution the absorbance at the excitation wavelength (with a spectrophotometer) and the luminescence intensity at the emission maximum upon excitation at λ_{exc} (with a spectrofluorimeter). As the geometric factor depends—although not dramatically—on the width of the slits, it may be useful to construct different calibration curves for the most commonly used slit widths. The data points (from 20 to 30 points in the absorbance range comprised between 0 and 2.5) can be plotted as shown in Fig. 5.10, and interpolated by means of an appropriate polynomial function. The function obtained, $F_g(A(\lambda_{exc}))$, contains both the mathematical and the geometrical dependence of the intensity measured by the detector, I_{obs} (not the total intensity Il as expressed in Eq. 5.1), versus $A(\lambda_{exc})$, as shown in Eq. 5.2:

$$I_{obs}(\lambda_{exc}, \lambda_{em}) \propto \Phi \times I_i(\lambda_{exc}) \times F_g(A(\lambda_{exc})) \tag{5.2}$$

From an analytical point of view it is important to establish a linear relationship between the signal and the concentration: to this aim the intensity observed with a spectrofluorimeter should be multiplied by a correction factor P defined in Eq. 5.3, so that a corrected intensity value (I_{corr}) is obtained (Eq. 5.4).

$$P(\lambda_{exc}) = A(\lambda_{exc})/F_g(A(\lambda_{exc})) \tag{5.3}$$

$$I_{corr}(\lambda_{exc}, \lambda_{em}) = I_{obs}(\lambda_{exc}, \lambda_{em}) \times P(\lambda_{exc}) \tag{5.4}$$

Upon substitution of Eqs. 5.2 and 5.3 into 5.4 one obtains Eq. 5.5:

$$\begin{aligned} I_{corr}(\lambda_{exc}, \lambda_{em}) &= I_{obs}(\lambda_{exc}, \lambda_{em}) \times P(\lambda_{exc}) \\ &\propto \Phi \times I_i(\lambda_{exc}) \times F_g(A(\lambda_{exc})) \times A(\lambda_{exc})/F_g(A(\lambda_{exc})) \\ &= \Phi \times I_i(\lambda_{exc}) \times A(\lambda_{exc}) \end{aligned} \tag{5.5}$$

As it can be seen, the corrected intensity obtained in this manner is proportional to the absorbance of the sample (and, in the absence of other species, to its concentration) through two constant factors—Φ, for the chosen fluorophore, and $I_i(\lambda_{exc})$, for the chosen instrument and excitation wavelength. It can be shown, however [6], that the same relationship between emitted intensity and sample concentration is obtained when other species absorbing the excitation wavelength are present; in such a case, the absorbance of the solution at λ_{exc} should be used to compute the correction factor $P(\lambda_{exc})$ in Eq. 5.3.

Although the procedure described above may appear complicated at a first glance, the correction of the emission data for the factors related to the absorbance of the solution at the excitation wavelength is relatively easy. Specifically, the procedure can be summarized in the following four steps:

1. Determination of the instrument calibration curve as previously described. This operation must be performed for every single instrument available in the laboratory and, preferably, for the slit widths utilized in the experiments. It is advisable to perform the experimental calibration procedure at least once a year.
2. Measurement of the absorbance of the solution at the excitation wavelength; this value will be introduced directly in Eq. 5.3, and also employed to determine the value of $F_g(A(\lambda_{exc}))$ from the equation resulting from the interpolation of the data obtained in step 1.
3. Measurement of the emission intensity.
4. Determination of the corrected emission intensity by using Eq. 5.4.

The procedure is convenient because step 1 requires some time but it has to be carried out only occasionally, whereas steps 2–4 are easy and quick.

The advantage of the corrected intensity is that two solutions of the same luminophore at concentrations C_1 and C_2 will exhibit corrected emission intensities whose ratio corresponds to the ratio of the respective concentrations, according to Eq. 5.6:

$$\frac{C_1}{C_2} = \frac{I_{1,corr}}{I_{2,corr}} \tag{5.6}$$

Therefore, in order to determine the concentration of an unknown solution of a luminophore, one has to (i) prepare a solution with a known concentration of the same luminophore in the same solvent, (ii) measure the luminescence intensity with the same excitation and emission wavelength, (iii) perform the appropriate correction, and (iv) apply Eq. 5.6.

5.4.2 *Correction for the Sample Absorption at the Emission Wavelength*

In addition to the issues related to the absorption of the exciting light, it is necessary to perform a correction of the observed luminescence intensity also in case

the solution absorbs light at the wavelength selected for monitoring the emission. In fact, in luminescence measurements it is rather common that the absorbance of the solution in the spectral region of the luminophore emission is not zero. In such a case, part of the light emitted by the luminophore is reabsorbed by the solution and is not detected by the instrument. The reason is easily understood: a photon emitted from a luminophore species inside the cuvette has to travel across the solution on a path of a certain length b in order to get out from the cell and reach the detector; the presence of a compound (be it the luminophore itself or another species) that can absorb the emitted photons reduces the probability that these photons reach the detector. Such a phenomenon, known as trivial energy transfer, does not involve electronic interactions between the energy donor and acceptor; hence, it cannot be considered as a quenching process, and falls into the category of the so-called inner filter effects.

The effect of the reabsorption of the emitted light is of great importance in the determination of luminescence quantum yields and of the correct shape of a luminescence band. Of course, in fixed emission wavelength measurements, the best precaution is to read the luminescence intensity at a wavelength where the absorbance of the solution is small or zero. This favorable situation, however, is sometimes impossible to achieve, and a correction for the reabsorption of the emitted light must be done. Such a correction takes into account an absorption phenomenon and is obviously based on the Lambert–Beer law. Specifically, the fraction $T(\lambda_{em})$ of emitted light that is transmitted through the solution—which can therefore be detected by the instrument—is expressed by Eq. 5.7:

$$T(\lambda_{em}) = 10^{-A(\lambda_{em})\times b} \tag{5.7}$$

The intensity value corrected for reabsorption effects is obtained by dividing the luminescence intensity (possibly corrected for the effects described in the previous section) by $T(\lambda_{em})$. Therefore, if one considers all the correction factors together, the complete formula for obtaining the corrected intensity is:

$$\begin{aligned} I_{corr}(\lambda_{exc}, \lambda_{em}) &= I_{obs}(\lambda_{exc}, \lambda_{em}) \times P(\lambda_{exc})/T(\lambda_{em}) \\ &= I_{obs}(\lambda_{exc}, \lambda_{em}) \times A(\lambda_{exc})/F_g(A(\lambda_{exc})) \times 10^{A(\lambda_{em})\times b} \end{aligned} \tag{5.8}$$

As one can see from Eq. 5.8, the value of b—that is, the path length of the emitted photon across the solution—must be known in order to calculate the correction. As shown in Fig. 5.12, the path length of a specific emitted photon depends on the position where the excited state is generated; therefore, only an average value of the optical path length can be determined. Some authors [1] suggested the adoption of $b = 0.5$ for 1-cm spectrofluorimetric cells with central illumination. It should be noted, however, that this is an approximation which is often not satisfactory: on the basis of our experience, this value can be more than 40% higher (consider that this error propagates in an exponential manner on the corrected intensity!). The value of the distance b can be estimated with good confidence by means of a simple experiment. What is needed is a solution containing a

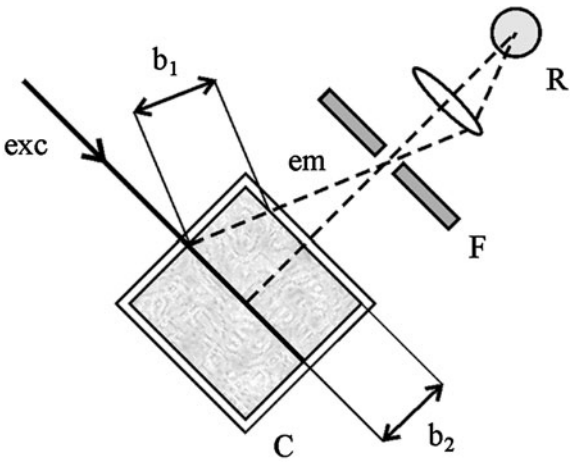

Fig. 5.12 Schematic representation of the sample geometry in which the optical path lengths b_1 and b_2 travelled by two light beams emitted in different positions inside the cell are indicated. Legend: exc, exciting light; em, emitted light; C, cell; F, slit; R, detector

luminophore L, characterized by intense and well separated absorption and luminescence bands, and an "inner filter" species W exhibiting high absorbance in the emission region of L, and preferably low absorbance in the absorption region of L. In this manner, the addition of W to a solution of L changes substantially the absorption of the solution at the emission wavelength (thereby effectively acting as an inner filter), while affecting only slightly the absorption at the excitation wavelength (thus keeping to a minimum the correction for this effect, which is also a source of error). Obviously, under the conditions employed, no interaction should occur between L and W (leading to, e.g., non-trivial energy transfer or electron-transfer processes). The choice of species with large molar absorption coefficients enables the study of very dilute solutions, in which dynamic processes are negligible; in case of doubt, the occurrence of such processes can be monitored by luminescence lifetime measurements. The system L = 1,5-dimethoxynaphthalene and W = anthracene in acetonitrile solution fulfills all these requirements.

From an experimental viewpoint, increasing amounts of the filter W are added to a solution of the luminophore L; after each addition one has to record the absorption spectrum of the solution (particularly, the absorbance values at λ_{em} and λ_{exc}), and measure the emission intensity at the selected wavelength, λ_{em}. If dilution effects can be neglected, according to Eq. 5.6 the corrected intensity must remain constant throughout the experiment because the luminophore concentration does not change. Hence, Eq. 5.8 can be rewritten in the following form:

$$I_{corr}(\lambda_{exc}, \lambda_{em}) \times 10^{A(\lambda_{em})\times b} = I_{obs}(\lambda_{exc}, \lambda_{em}) \times A(\lambda_{exc})/F_g(A(\lambda_{exc})) \qquad (5.9)$$

which, in logarithmic form, becomes

$$\text{constant} - A(\lambda_{em}) \times b = \log[I_{obs}(\lambda_{exc}, \lambda_{em}) \times A(\lambda_{exc})/F_g(A(\lambda_{exc}))] \qquad (5.10)$$

Therefore, by plotting the right term of the equation as a function of $A(\lambda_{em})$ one obtains a straight line (Fig. 5.13) whose slope is $-b$, that is, the parameter we are

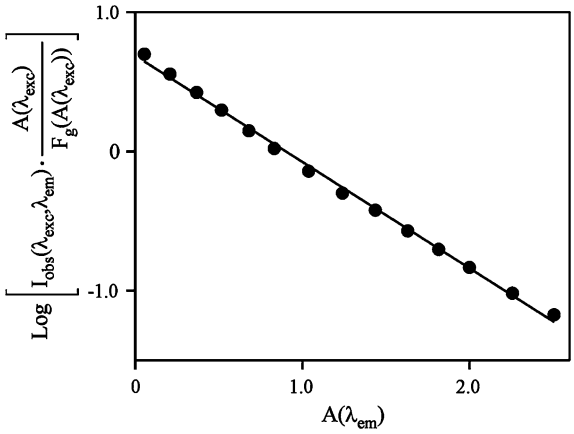

Fig. 5.13 Plot of the logarithm of the luminescence intensity of L at λ_{em} upon excitation at λ_{exc}, corrected for the absorption effects at the excitation wavelength, as a function of the absorbance of the solution at λ_{em} (due to the presence of the inner filter W). L, 1,5-dimethoxynaphthalene; W, anthracene; solvent, acetonitrile; 1-cm cell; $\lambda_{exc} = 311$ nm; $\lambda_{em} = 346$ nm. From the slope of the *straight line* a value of $b = 0.76$ cm is obtained

looking for. This parameter does not need to be re-determined frequently (once a year or less; it is advisable to re-determine b after a lamp replacement), but it has to be measured for every single spectrofluorimeter in the laboratory (even if there are identical models).

In conclusion, it should be emphasized that the corrections discussed in this section are affected by errors that are often difficult to estimate and can be quite large. The corrected data should be utilized with care, particularly when the extent of the correction is relevant in comparison with the observed intensity value. For example, the effect of the reabsorption of the emitted light can easily require huge corrections, often larger than 100%! The best practice is therefore to avoid performing heavy data corrections, whenever possible, by a wise choice of the experimental and instrumental conditions.

5.4.3 Determination of the Stability Constant of a [2]Pseudorotaxane

[2]Pseudorotaxanes are supramolecular host–guest complexes comprising one macrocyclic ring threaded by an acyclic component [7]. Their most important feature is that changes in the relative position of their molecular components can be induced by external stimuli [7, 8]; this could be of interest for the development of molecular machines [9], and for processing information at the molecular level [10, 11].

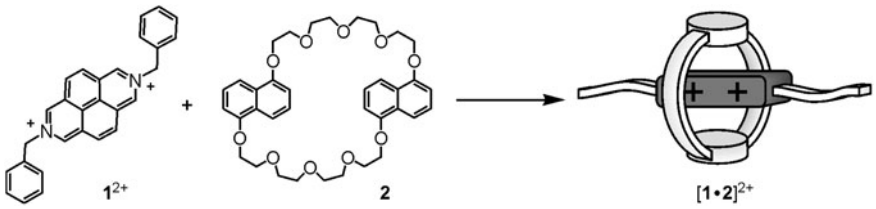

Fig. 5.14 The self-assembly of the 2,7-diazapyrenium dication $\mathbf{1}^{2+}$ and the crown ether **2** to give the pseudorotaxane $[\mathbf{1}\bullet\mathbf{2}]^{2+}$

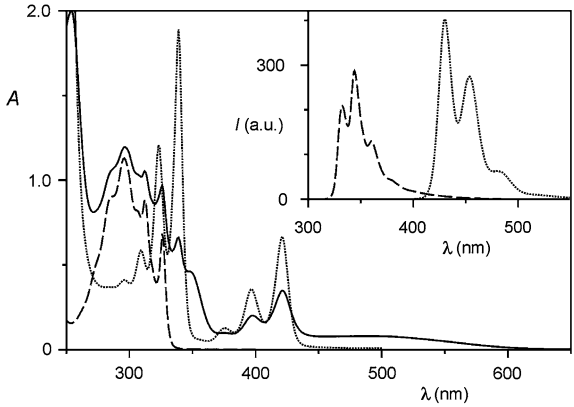

Fig. 5.15 Absorption spectra (acetonitrile, 298 K) of 5.0×10^{-5} M $\mathbf{1}^{2+}$(*dotted line*), 6.4×10^{-5} M **2** (*dashed line*), and their mixture (*full line*). Note the charge-transfer band ($\lambda_{max} = 510$ nm) due to the formation of the pseudorotaxane. The *inset* shows the luminescence spectra observed for the above mentioned solutions of $\mathbf{1}^{2+}$ (*dotted line*, $\lambda_{exc} = 371$ nm) and **2** (*dashed line*, $\lambda_{exc} = 295$ nm)

The [2]pseudorotaxane $[\mathbf{1}\bullet\mathbf{2}]^{2+}$ is obtained in acetonitrile solution by self-assembling of the 2,7-dibenzyldiazapyrenium dication $\mathbf{1}^{2+}$ with the crown ether **2** based on 1,5-dioxynaphthalene units (Fig. 5.14) [12]. The main driving force of this self-assembly process is a charge-transfer (CT) interaction from the π-electron donor naphthoxy units of **2** to the π-electron acceptor diazapyrenium group of $\mathbf{1}^{2+}$.

Upon formation of the [2]pseudorotaxane $[\mathbf{1}\bullet\mathbf{2}]^{2+}$, the CT interaction leads to (1) the appearance of a weak and broad absorption band in the visible region (Fig. 5.15) and (2) the disappearance of the luminescence characteristic of the two components (Fig. 5.15, *inset*). The latter result is due to the presence of low-energy charge-transfer excited states which offer fast radiationless decay to the upper-lying luminescent states of the molecular components $\mathbf{1}^{2+}$ and **2** [12].

The quenching of the luminescence of the molecular components when they are threaded in the pseudorotaxane structure can be used to estimate their association constant. In fact, the residual luminescence of $\mathbf{1}^{2+}$ and **2** in a solution containing both these species is related to the concentration of uncomplexed $\mathbf{1}^{2+}$ and **2**, respectively, through Eq. 5.12, that are directly derived from Eq. 5.6:

$$\frac{I_{\mathbf{1}^{2+},\mathrm{corr}}(\lambda_{\mathrm{em}})}{I^0_{\mathbf{1}^{2+},\mathrm{corr}}(\lambda_{\mathrm{em}})} = \frac{C_{\mathbf{1}^{2+}}}{C^0_{\mathbf{1}^{2+}}} \qquad \frac{I_{\mathbf{2},\mathrm{corr}}(\lambda_{\mathrm{em}})}{I^0_{\mathbf{2},\mathrm{corr}}(\lambda_{\mathrm{em}})} = \frac{C_{\mathbf{2}}}{C^0_{\mathbf{2}}} \tag{5.12}$$

where $C_{\mathbf{1}}{}^{2+}$ and $C_{\mathbf{2}}$ are the concentration of the uncomplexed molecular components, and $C^0_{\mathbf{1}^{2+}}$ and $C^0_{\mathbf{2}}$ are their total (i.e., analytical) concentration. Of course, $C^0_{\mathbf{1}^{2+}}$ and $C^0_{\mathbf{2}}$ are known from the preparation of the solution. $I^0_{\mathbf{1}^{2+},\mathrm{corr}}(\lambda_{\mathrm{em}})$ and $I_{\mathbf{1}^{2+},\mathrm{corr}}(\lambda_{\mathrm{em}})$ are the corrected luminescence intensities of $\mathbf{1}^{2+}$ in a solution containing $\mathbf{1}^{2+}$ alone at a concentration of $C^0_{\mathbf{1}^{2+}}$, and in a solution containing $C^0_{\mathbf{1}^{2+}}$ $\mathbf{1}^{2+}$ and $C^0_{\mathbf{2}}$ **2**, respectively. $I^0_{\mathbf{2},\mathrm{corr}}(\lambda_{\mathrm{em}})$ and $I_{\mathbf{2},\mathrm{corr}}(\lambda_{\mathrm{em}})$ are the corrected luminescence intensities of **2** in a solution containing **2** alone at a concentration of $C^0_{\mathbf{2}}$, and in a solution containing $C^0_{\mathbf{1}^{2+}}$ $\mathbf{1}^{2+}$ and $C^0_{\mathbf{2}}$ **2**, respectively. The stability constant of the pseudorotaxane $[\mathbf{1}\bullet\mathbf{2}]^{2+}$, that is, the constant of the association equilibrium between $\mathbf{1}^{2+}$ and **2**, is

$$K = \frac{C_{[\mathbf{1}\cdot\mathbf{2}]^{2+}}}{C_{\mathbf{1}^{2+}} C_{\mathbf{2}}} = \frac{C_{[\mathbf{1}\cdot\mathbf{2}]^{2+}}}{(C^0_{\mathbf{1}^{2+}} - C_{[\mathbf{1}\cdot\mathbf{2}]^{2+}})(C^0_{\mathbf{2}} - C_{[\mathbf{1}\cdot\mathbf{2}]^{2+}})} \tag{5.13}$$

where $C_{[\mathbf{1}\cdot\mathbf{2}]^{2+}}$ is the concentration of pseudorotaxane.

It should be noticed that to calculate K it is sufficient to measure the luminescence quenching of only one component, because the concentration of pseudorotaxane $C_{[\mathbf{1}\cdot\mathbf{2}]^{2+}}$ can be evaluated independently as both $(C^0_{\mathbf{1}^{2+}} - C_{\mathbf{1}^{2+}})$ and $(C^0_{\mathbf{2}} - C_{\mathbf{2}})$. In the present case both components of the complex are luminescent, thereby enabling the determination of K from two independent series of emission measurements. The comparison of the results of these two experiments, which of course must be consistent with one another, can be useful for checking the validity of the corrections that have been made. As one can see from Fig. 5.15, the absorption spectrum of the solution containing $[\mathbf{1}\bullet\mathbf{2}]^{2+}$ and its free components $\mathbf{1}^{2+}$ and **2** is rather complex; in particular, it is impossible to excite **2** selectively, and luminescence of both $\mathbf{1}^{2+}$ and **2** (Fig. 5.15, *inset*) is reabsorbed by the solution. Therefore, considerable corrections of the observed luminescence intensities are necessary.

In our experiment, $C^0_{\mathbf{1}^{2+}}$ and $C^0_{\mathbf{2}}$ were 5.0×10^{-5} M and 6.4×10^{-5} M, respectively; the emission of $\mathbf{1}^{2+}$ was observed at 453 nm upon excitation at 371 nm, whereas the emission of **2** was observed at 344 nm upon excitation at 295 nm. The observed absorbance and luminescence intensity values are gathered in Tables 5.1 and 5.2, together with the correction parameters and the corrected

Table 5.1 Data for correction of the luminescence intensity of $\mathbf{1}^{2+}$

Solution	$A(371)$	$F_g(371)$	$I_{obs}(371,453)$	$A(453)$	$T(453)$	$I_{corr}(371,453)$
5.0×10^{-5} M $\mathbf{1}^{2+}$	0.123	0.46	273	0.012	0.98	69.0
5.0×10^{-5} M $\mathbf{1}^{2+}$ + 6.4×10^{-5} M **2**	0.123	0.46	37.5	0.076	0.86	11.7

Table 5.2 Data for correction of the luminescence intensity of **2**

Solution	$A(295)$	$F_g(295)$	$I_{obs}(295,344)$	$A(344)$	$T(344)$	$I_{corr}(295,344)$
6.4×10^{-5} M **2**	1.121	0.92	287	0.008	0.98	357
5.0×10^{-5} M $\mathbf{1}^{2+}$ + 6.4×10^{-5} M **2**	1.190	0.90	37.3	0.481	0.39	126

luminescence intensities calculated according to Eq. 5.8 (in our conditions b was determined to be 0.85 cm).

From the measurement of the luminescence intensity of $\mathbf{1}^{2+}$ (Table 5.1) one obtains

$$C_{\mathbf{1}^{2+}} = C^0_{\mathbf{1}^{2+}} \frac{I_{\mathbf{1}^{2+},corr}(453)}{I^0_{\mathbf{1}^{2+},corr}(453)} = 5.0 \times 10^{-5} \frac{11.7}{69.0} = 8.5 \times 10^{-6}\,\text{M} \tag{5.14}$$

$$C_{[1\cdot2]^{2+}} = C^0_{1^{2+}} - C_{1^{2+}} = 4.15 \times 10^{-5}\,\text{M} \tag{5.15}$$

$$C_{\mathbf{2}} = C^0_{\mathbf{2}} - C_{[\mathbf{1}\cdot\mathbf{2}]^{2+}} = 2.25 \times 10^{-5}\,\text{M} \tag{5.16}$$

$$K = \frac{C_{[\mathbf{1}\cdot\mathbf{2}]^{2+}}}{C_{\mathbf{1}^{2+}} C_{\mathbf{2}}} = 2.2 \times 10^{5}\,\text{M}^{-1} \tag{5.17}$$

while the measurement of the luminescence intensity characteristic of **2** (Table 5.2) leads to

$$C_2 = C^0_{\mathbf{2}} \frac{I_{\mathbf{2},corr}(344)}{I^0_{\mathbf{2},corr}(344)} = 6.4 \times 10^{-5} \frac{126}{357} = 2.26 \times 10^{-5}\,\text{M} \tag{5.18}$$

$$C_{[\mathbf{1}\cdot\mathbf{2}]^{2+}} = C^0_{\mathbf{2}} - C_2 = 4.14 \times 10^{-5}\,\text{M} \tag{5.19}$$

$$C_{\mathbf{1}^{2+}} = C^0_{\mathbf{1}^{2+}} - C_{[\mathbf{1}\bullet\mathbf{2}]^{2+}} = 8.6 \times 10^{-6}\,\text{M} \tag{5.20}$$

$$K = \frac{C_{[\mathbf{1}\cdot\mathbf{2}]^{2+}}}{C_{\mathbf{1}^{2+}} C_{\mathbf{2}}} = 2.1 \times 10^{5}\,\text{M}^{-1} \tag{5.21}$$

The values of the pseudorotaxane concentration (Eqs. 5.15 and 5.19) are substantially similar, indicating that the correction factor is reasonable. This example

demonstrates that luminescence spectroscopy can provide a simple and quick method for studying supramolecular equilibria in high dilution conditions.

5.5 Determination of Luminescence Quantum Yields

In order to determine whether a given species is a good luminophore, its emission quantum yields has to be measured:

$$\Phi = \frac{\text{number of emitted photons}}{\text{number of absorbed photons}}$$

The simplest method for the measurement of the luminescence quantum yield of a luminophore is based on the comparison with a standard species with known quantum yield. The luminescence quantum yield of such reference compounds are practically independent on the excitation wavelength, hence they can be utilized for the whole spectral range of their absorption.

In practice, the quantum yield is generally determined by comparing the emission spectrum of the examined luminophore with that of a suitably selected standard, both recorded under the same instrumental conditions (excitation wavelength, excitation and emission slits, detector settings, etc.). The comparison involves the emission intensities of the two species (sample and reference) integrated over the whole wavelength range, that is, the areas underneath the respective emission spectra, measured from the baseline.

It should be noted that modern spectrofluorimeters utilize gratings as monochromators and thus perform a linear dispersion of the radiation with respect to wavelength. Hence, the values of the area of the emission spectra to be used in the calculation of the quantum yield must be obtained on a spectrum reported as a function of λ and not, e.g., frequency or wavenumber. The two luminescence spectra to be compared should exhibit similar shape and occur on the same wavelength range; if these conditions cannot be fulfilled, the spectra must be corrected before the comparison (See [1, 13, 14] and Sect. 5.3.1 above). If the same excitation wavelength is used for the sample and reference solutions, the unknown luminescence quantum yield can be obtained from the formula [1, 15, 16]:

$$\Phi = \Phi_R \frac{S}{S_R} \frac{A_R}{A} \frac{n^2}{n_R^2} \tag{5.22}$$

in which Φ is the emission quantum yield, S is the area underneath the spectrum for the whole emission wavelength range, A is the absorbance at the excitation wavelength, and n is the refraction index of the solvent. The subscript R in the formula denotes the quantities referred to the luminophore with known quantum yield used as a reference standard.

Equation 5.22 can be utilized only for solutions whose absorbance at the excitation wavelength is lower than 0.1; such a limit is also useful to minimize

inner filter effects (reabsorption of the emitted light) that must be taken into consideration when the lowest energy absorption band overlaps with the luminescence band (see, e.g., anthracene in Fig. 5.8).

When sufficiently dilute solutions cannot be used (i.e., $A \geq 0.1$), the previous expression must include the factor F_g, which comprises both the mathematical and the geometric dependences of the luminescence intensity versus the absorbance (see Sect. 5.4.1).

$$\Phi = \Phi_R \frac{S}{S_R} \frac{F_{g,R}}{F_g} \frac{n^2}{n_R^2} \tag{5.23}$$

In case the sample and reference solutions exhibit the same absorbance at the excitation wavelength—a condition that can be easily obtained in most cases by adjusting the concentrations of the solutions—the equation reduces to

$$\Phi = \Phi_R \frac{S}{S_R} \frac{n^2}{n_R^2} \tag{5.24}$$

The presence of the ratio of the refraction indexes of the solvents employed accounts for the fact that the intensity emitted by a point source in a medium of refraction index n_i and monitored with a detector in a medium with refraction index n_o is modified by the factor $(n_i/n_o)^2$ (see [1], p. 53).

5.5.1 *Reference Standards for the Determination of Fluorescence Quantum Yields*

Fluorescence quantum yield measurements are usually performed on fluid solutions at room temperature. The solvents must be of appropriate purity and suitable for fluorescence measurements; it is advisable, however, to verify the absence of spurious emissions due to the solvent itself or to other dissolved species (impurities and/or stabilizers) under the conditions used.

Finally, the choice of the common excitation wavelength for the sample and reference solutions, corresponding to isoabsorptive points, is of the highest importance for a high quality measurement of the quantum yield. This wavelength should be selected in a region where both absorption curves are not steep, in order to avoid errors related to small differences in the values of λ (e.g., because of a slightly different calibration of the employed spectrophotometer and spectrofluorimeter) and of the slit widths. Commonly used reference standards for the determination of fluorescence quantum yields are listed in Table 5.3. Other similar tables can be found in [1, 6, 16, 17].

In order to facilitate the choice of the reference standard on the basis of the spectral region of interest and the band shape, the fluorescence spectra of the most popular standards are reported in Figs. 5.16, 5.17, 5.18.

Table 5.3 Reference standards for the determination of fluorescence quantum yields

Emission range (nm)	Compound	Solvent	Φ[a,b]	Ref.
280–330	Phenol	H_2O	0.14	[1, 18, 19]
		Cyclohexane	0.08	[19]
300–400	Naphthalene	Cyclohexane	0.23; 0.036[c]	[19, 20], Credi A (private communication)
		EtOH	0.21	[13, 21]
310–400	Terphenyl	Cyclohexane	0.93; 0.82[c]	[19, 20], Credi A (private communication)
315–480	2-Aminopyridine	H_2SO_4 0.05 M	0.60[d]	[22]
		H_2SO_4 0.05–0.5 M	0.66[e]	[23]
360–480	Anthracene	EtOH	0.27	[19, 21, 24]
			0.21[f]	[20], Credi A (private communication)
390–500	9,10-Diphenyl anthracene	Cyclohexane	0.90; 0.95	[23, 25, 26]
		EtOH	0.81; 0.88	[24, 26]
380–580	Quinine sulfate[g,h]	H_2SO_4 0,5 M	0.55; 0.54	[21, 24]
		H_2SO_4 0,05 M	0.53	[27]
400-600	β-Carboline[i]	H_2SO_4 0,5 M	0.60	[1, 28]
430–560	Perylene	EtOH	0.92	[15]
		Benzene	0.89; 0.99	[21, 24]
480–650	Fluorescein[g,j]	NaOH 0,1 M	0.92; 0.95	[29, 30]
550–700	Rhodamine 101	EtOH	1.00	[31]
550–700	Rhodamine 6G	EtOH	0.94[g]	[32]
550–700	$[Ru(bpy)_3]^{2+}$ [k]	H_2O	0.042, 0.028[l]	[33]
		MeCN	0.059[m]	[34]
580–780	Cresyl violet[n]	MeOH	0.54[l]	[35]
600–850	$[Os(bpy)_3]^{2+}$ [k]	MeCN	0.005	[36]
600–900	$[Os(phen)_3]^{2+}$ [k]	MeCN	0.021	[36]

[a] Room temperature; absolute values, or values obtained using reliable reference standards; deoxygenated solutions, unless indicated otherwise

[b] See the specific references for the experimental errors

[c] Value obtained in aerated solution using naphthalene in deoxygenated solution as a reference standard

[d] Relative value, using both quinine sulfate and 9,10-diphenylanthracene as reference standards

[e] Measured with an integrating sphere, using quinine sulfate as a reference standard

[f] Aerated solution, with substantial oxygen quenching [19]; for other comments, see [15]

[g] No oxygen quenching [15]

[h] Sensitive to quenching by halogens; only sulfuric acid of the highest available purity should be used [37].[i] 9H-Pyrido[3,4-*b*]indole

[j] Deoxygenated by nitrogen bubbling to avoid photodegradation [15]

[k] These compounds are characterized by a phosphorescence emission with a relatively short lifetime, making them more similar to fluorescence emitters; for this reason they are included in this table [1]. Aerated solution

[m] For other polar solvents, see [34]

[n] Perchlorate salt

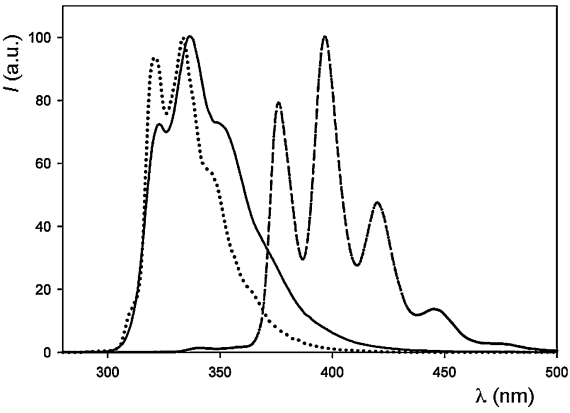

Fig. 5.16 Uncorrected emission spectra at ambient temperature of reference standards suggested for the emission range 300–500 nm: naphthalene in cyclohexane (*dotted line*), terphenyl in cyclohexane (*full line*), and anthracene in ethanol (*dashed line*)

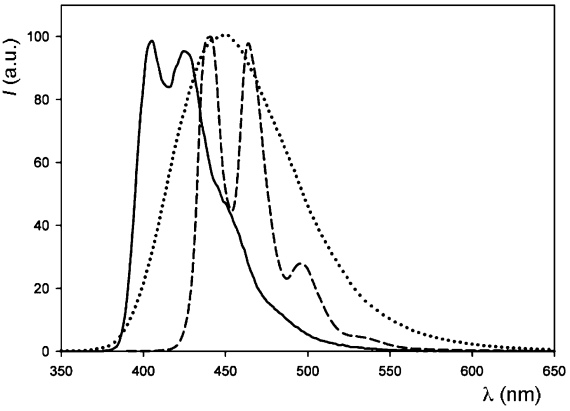

Fig. 5.17 Uncorrected emission spectra at ambient temperature of reference standards suggested for the emission range 350–650 nm: 9,10-diphenylanthracene in cyclohexane (*full line*), quinine sulfate in H_2SO_4 0.5 M (*dotted line*), and perylene in cyclohexane (*dashed line*)

5.5.2 Reference Standards for the Determination of Phosphorescence Quantum Yields

Phosphorescence emission is due to a spin forbidden radiative transition between two electronic states characterized by different spin multiplicities. In most cases (e.g., for organic molecules), the transition takes place from the lowest triplet excited state to the singlet ground state. Phosphorescence emission can hardly be observed in fluid solutions because bimolecular quenching processes of a long lived emitting excited state are very likely. Hence, phosphorescence experiments have to be carried out either on solid matrices at room temperature, or at low temperatures (e.g., under liquid nitrogen at 77 K) on frozen matrices. The same recommendations on solvents given in the previous section are valid also for phosphorescence measurements. A list of organic solvents that give rise to transparent matrices when frozen at 77 K can be found in [6].

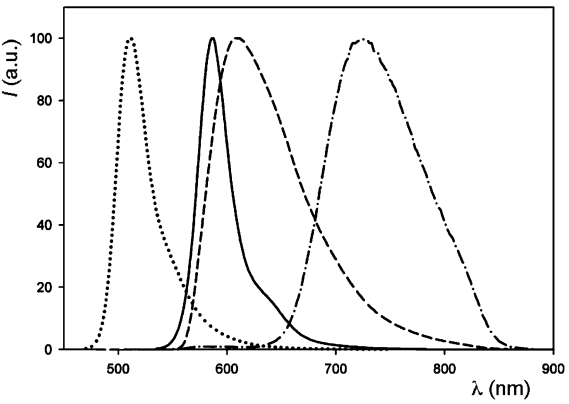

Fig. 5.18 Uncorrected emission spectra at ambient temperature of reference standards suggested for the emission range 450–900 nm: fluorescein in NaOH 0.5 M (*dotted line*), rhodamine 101 in ethanol (*full line*), $Ru(bpy)_3Cl_2$ in water (*dashed line*), and $Os(bpy)_3(PF_6)_2$ in acetonitrile (*dashed–dotted line*)

Highly absorbing solutions ($A > 0.1$) can be used to determine phosphorescence quantum yields because inner filter effects are generally negligible due to the large Stokes shift of the emission band. Some secondary reference standards for an approximate ($\pm 15\%$) determination of phosphorescence quantum yields are indicated in Table 5.4 [6, 16].

5.6 Luminescence Measurements on Solid Samples

5.6.1 Introduction

Luminescence measurements on solid samples do not differ substantially from measurements on solutions but they can be complicated by factors related to the inhomogeneity and opacity of the material, or the high concentration of the emitting species. Very intense luminescent signals *not arising* from the emitting species are frequently observed; therefore the interpretation of luminescence spectra of solid samples is generally not straightforward.

5.6.2 Front-Face and Right-Angle Geometries

As previously discussed, a sample geometry characterized by an angle of 90° between the excitation beam and the monitoring direction (right-angle geometry, Fig. 5.5b) is the most popular and convenient one for fluorescence measurements on dilute solutions. For samples with a high absorbance or opacity, however, such a geometry is not appropriate because the portion of the sample that is monitored by the instrument is not significantly excited. In these cases, a configuration in which the above described angle is smaller than 90° (front-face

Table 5.4 Reference standards for the determination of phosphorescence quantum yields

Emission range (nm)	Compound	Solvent	Φ[a]	Ref.
340–450	Benzene[b]	EPA[c]	0.23; 0.18	[38–40]
400–550	Benzophenone[b]	EPA	0.74	[38, 39, 41]
		Freon 113 (298 K)	~0.01	[42]
400–550	Xanthone[b]	EtOH-Ether	0.44	[41]
460–560	Naphthalene[b]	EPA	0.04	[40]
500–650	Biacetyl[b]	Hexane	~0.05[d]	[42]
1,062	Tris(1,1,1,5,5,5-hexafluoro acetylacetonato) neodymium(III)	THF-d_8	0.003[d]	[43]

[a] Values obtained at 77 K, unless indicated otherwise
[b] Reference standards suggested in [16]
[c] Ethanol/isopentane/ether (2:5:5)
[d] 298 K

geometry, Fig. 5.5c) should be adopted. Albeit angles of 45° or 37° are often used, sample-holders that permit the adjustment of the angle in order to optimize the signal and minimize the contribution from spurious emissions are preferable. The main interference in luminescence experiments on solids is represented by the scattering of the exciting light; in fact, monochromators are not able to provide fully monochromatic light even when narrow band widths are used. The presence of stray light at the same wavelength of the investigated luminescence emission can become significant under conditions in which the scattering from the sample causes this radiation to impinge on the detector. This kind of interference can be reduced using lasers to obtain a strictly monochromatic excitation.

The samples are usually prepared as thin films deposited on a suitable support (e.g., a glass slide), plates, or powders. However, by utilizing special accessories (e.g., optical fiber probes) and instrumental setups, in principle one can perform photoluminescence experiments on any object. As a consequence of the front-face geometry and the low transparency of the sample, it is often the case that luminescence measurements on solids involve only the outer part of the sample, for a depth on the order of a few micrometers or less. Therefore, particularly in the case of powdered samples, it is important to obtain a homogeneous dispersion of the granules and deposit it as a thin layer on a transparent support, such as glass or quartz, potentially utilizing an inert medium like mineral oil.

5.6.3 Sample Inhomogeneity

In the case of substantially inhomogeneous samples, very different signals may be measured depending on the sample positioning. The measured signal, in fact, arises from the portion of the sample corresponding to the intersection between the

excited surface and that monitored by the detector. If such an intersection is small, the instrument response will be very sensitive to the position of the sample, and able to detect an inhomogeneous spatial distribution of the luminescence. It must be recalled, however, that the measured luminescence intensity is also strongly dependent on the sample positioning for purely geometric reasons.

5.6.4 Concentration Effects

The comparison of the properties of a luminophore in the solid state (or dispersed in a solid matrix) with those of the same luminophore in solution often reveals remarkable differences. A common reason is related to the fact that for many luminescent molecules the emission decreases upon aggregation. This phenomenon, which takes place also in dimers or small aggregates, is known as self-quenching and is typical of several organic fluorophores. Self-quenching processes are always dependent on concentration and on the type of aggregation.

References

1. Lakowicz JR (2006) Principles of fluorescence spectroscopy, 3rd edn. Springer, Singapore
2. Mielenz KL (ed) (1982) Optical radiation measurements. Academic Press, New York
3. Rendell D (1987) Fluorescence and phosphorescence. Wiley, Chichester
4. Harris DA, Bashford CL (eds) (1987) Spectrophotometry and spectrofluorimetry. IRL, Oxford
5. Turro NJ, Scaiano JC, Ramamurthy V (2010) Modern molecular photochemistry of organic molecules. University Science Books, Mill Valley
6. Montalti M, Credi A, Prodi L, Gandolfi MT (2006) Handbook of photochemistry, 3rd edn. CRC Press, Boca Raton
7. Amabilino DB, Stoddart JF (1995) Chem Rev 95:2725–2828
8. Ashton PR, Ballardini R, Balzani V et al (1997) Chem Eur J 3:152–170
9. Silvi S, Venturi M, Credi A (2009) J Mater Chem 19:2279–2294
10. Credi A, Balzani V, Langford SJ et al (1997) J Am Chem Soc 119:2679–2681
11. Semeraro M, Credi A (2010) J Phys Chem C 114:3209–3214
12. Ballardini R, Balzani V, Credi A et al (1996) Angew Chem Int Ed Engl 35:978–981
13. Parker CA, Joyce TA (1966) Trans Faraday Soc 62:2785–2792
14. Hofstraat JW, Latuhihin MJ (1994) Appl Spectrosc 48:436–447
15. Demas JN, Crosby GA (1971) J Phys Chem 75:991–1024
16. Scaiano JC (ed) (1989) Handbook of organic photochemistry, vol 1. CRC Press, Boca Raton
17. Eaton DF (1988) Pure Appl Chem 60:1107–1114
18. Chen RF (1967) Anal Lett 1:35–42
19. Berlman IB (1971) Handbook of fluorescence spectra of aromatic molecules, 2nd edn. Academic Press, New York
20. Biagini M (2003) Diploma thesis. Dipartimento di Chimica "G Ciamician", Università di Bologna
21. Dawson WR, Windsor MW (1968) J Phys Chem 72:3251–3260
22. Rusakowicz R, Testa AC (1968) J Phys Chem 72:2680–2681

23. Meech SR, Phillips D (1983) J Photochem 23:193–217
24. Melhuish WH (1961) J Phys Chem 65:229–235
25. Hamai S, Hirayama F (1983) J Phys Chem 87:83–89
26. Mardelli M, Olmsted J III (1977) J Photochem 7:277–285
27. Adams MJ, Highfield JG, Kirkbright GF (1977) Anal Chem 49:1850–1852
28. Ghiggino KP, Skilton PF, Thistlethwaite PJ (1985) J Photochem 31:113–121
29. Shen J, Snook RD (1989) Chem Phys Lett 155:583–586
30. Brannon JH, Magde D (1978) J Phys Chem 82:705–709
31. Karstens T, Kobs K (1980) J Phys Chem 84:1871–1872
32. Fischer M, Georges J (1996) Chem Phys Lett 260:115–118
33. Nakamaru K (1982) Bull Chem Soc Japan 55:2697–2705
34. Nakamaru K (1982) Bull Chem Soc Japan 55:1639–1640
35. Magde D, Brannon JH, Cremers TL et al (1979) J Phys Chem 83:696–699
36. Kober EM, Caspar JV, Lumpkin RS, Meyer TJ (1986) J Phys Chem 90:3722–3734
37. Miller JN (ed) (1981) Standards in fluorescence spectrometry. Chapman & Hall, London
38. Gilmore EH, Gibson GE, McClure DS (1952) J Chem Phys 20:829–836
39. Gilmore EH, Gibson GE, McClure DS (1955) J Chem Phys 23:399
40. Li R, Lim EC (1972) J Chem Phys 57:605–612
41. Hunter TF (1970) Trans Faraday Soc 66:300–309
42. Turro NJ (1978) Modern molecular photochemistry. Benjamin, Menlo Park, pp 117–118
43. Iwamuro M, Wada Y, Kitamura T et al (2000) Phys Chem Chem Phys 2:2291–2296

Chapter 6
Absorption and Emission Spectroscopy with Polarized Light

Alberto Credi and Marco Montalti

Abstract In the first part of this chapter we will illustrate circular dichroism and we will discuss the optical activity of chemical compounds with respect to light absorption which is at the basis of this technique. Moreover, we will introduce the phenomena that lie behind the technique of optical rotatory dispersion. We thought appropriate to include a brief description of linear dichroism spectroscopy, although this technique has nothing to do with optical activity. In the final part of the chapter we will introduce the basic principles of the luminescence techniques based on polarized (either circularly or linearly) excitation. The experimental approach to the determination of steady-state and time resolved fluorescence anisotropy will be illustrated. For all the techniques examined in this chapter the required instrumentation will be schematically described. A few examples of application of these techniques to molecular and supramolecular systems will also be presented.

6.1 Linear and Circular Dichroism Spectroscopy

6.1.1 Introduction

Since the time of Louis Pasteur it was known that if a beam of linearly polarized light goes through one enantiomer of a chiral species, the polarization plane undergoes a rotation of a certain angle [1, 2]. This phenomenon is known as

A. Credi · M. Montalti (✉)
Dipartimento di Chimica "G. Ciamician", Università di Bologna,
via Selmi 2 40126 Bologna, Italy
e-mail: marco.montalti2@unibo.it

A. Credi
e-mail: alberto.credi@unibo.it

P. Ceroni (ed.), *The Exploration of Supramolecular Systems and Nanostructures by Photochemical Techniques,* Lecture Notes in Chemistry 78,
DOI: 10.1007/978-94-007-2042-8_6,

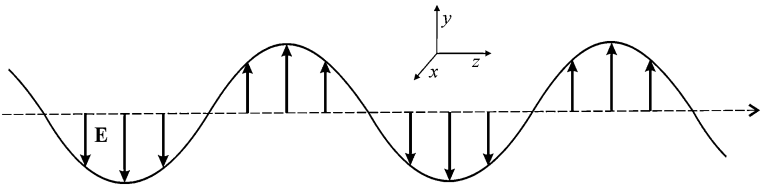

Fig. 6.1 Oscillation of the electric field vector of a wave linearly polarized on the *yz* plane and propagating along the *z* axis. The polarization direction of the wave is that of the *y* axis. Each arrow represents the electric field vector at the same time in contiguous positions, or in the same position at successive times (in such a case the time is reported on the *z* axis)

optical rotation. Each enantiomer rotates the polarization plane of light of the same angle, but in the opposite direction as that of the other enantiomer. For this reason the two enantiomers of a chiral species are also referred to as optically active compounds.

The optical activity of chiral molecules stems from the fact that they interact in a different manner with the two circularly polarized components of light. The various manifestations of optical activity can be categorized depending on whether they are based on radiation dispersion, absorption, or emission phenomena. In this Section we will illustrate the optical activity of chemical compounds with respect to light absorption, which is at the basis of the circular dichroism technique. Moreover, we will discuss the effects that lie behind the technique of optical rotatory dispersion. We thought appropriate to include a brief description of linear dichroism spectroscopy, although this technique has nothing to do with optical activity. A few examples of application of these techniques to molecular and supramolecular systems will also be presented. Before going into more details it is worthwhile to recall some fundamental concepts of electromagnetic radiation and the aspects of polarization.

6.1.2 Polarized Light

Generally speaking, an electromagnetic radiation is composed of a packet of waves. Each wave comprises an electric and a magnetic field oscillating in mutually perpendicular planes and propagating in a direction orthogonal to such planes (Fig. 6.1). These fields move at a speed $v = c_0/n$, where c_0 is the speed of light in vacuum (about 3×10^8 m s^{-1}) and n is the refractive index of the material in which the radiation is travelling across. As the electric and magnetic field vectors are always perpendicular to one another, in most cases it is sufficient to consider only one of the two (usually, the electric field vector) to describe the properties of the radiation. The plane defined by the oscillation direction of the electric field and the travelling direction of the wave is the *polarization plane* of the wave (Fig. 6.1).

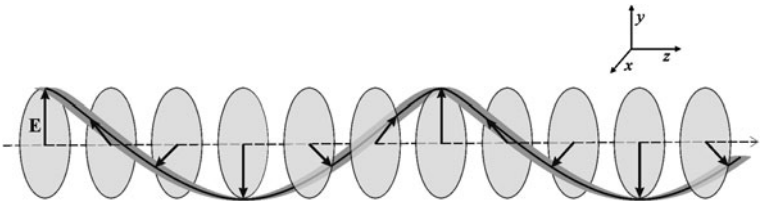

Fig. 6.2 Oscillation of the electric field vector of a wave with left circular polarization that propagates along the z axis. Each arrow represents the electric field vector at the same time in contiguous positions, or in the same position at successive times (in such a case the time is reported on the z axis)

The light generated by common sources (sun, lamps) is composed of an ensemble of waves whose polarization planes are randomly oriented around the travelling direction. A radiation of this type is said to be *unpolarized*. Conversely, if all the waves that constitute the radiation possess the same polarization plane, the wave is linearly polarized (Fig. 6.1). The oscillation direction of the electric field is called polarization direction—or simply polarization—of the wave.

A wave with circular polarization is characterized by the fact that the electric field vector rotates around the propagation axis while it is travelling (Fig. 6.2). During the period of the wave the electric field vector does not change its intensity but it does change its direction while maintaining itself perpendicular to the travelling axis. In other words, in the case of circular polarization it is the direction of the electric field vector that oscillates, whereas the length of the vector remains constant.

Circular polarization of a wave can occur in two directions: right or left. For a right circularly polarized wave, the rotation of the electric field vector observed in the direction towards the source occurs in a clockwise sense; the tip of the vector draws a right-handed helix while propagating in space. In the case of a left circularly polarized wave, the rotation of the electric field vector observed in the direction towards the source is counterclockwise; the tip of the propagating vector draws a left-handed helix (Fig. 6.2). Therefore, a circularly polarized wave can be considered as a radiation possessing chirality.

It is easy to show that a circularly polarized wave can be obtained from the combination of two waves with the same frequency and amplitude, linearly polarized on perpendicular planes and presenting a phase difference of $\pi/2$. In this manner when the electric field vector of the first wave reaches its maximum, that of the second wave is zero.

For the sake of the following discussion it is important to observe that, conversely, a linearly polarized wave can be constructed by combining together two waves with the same frequency and amplitude, and exhibiting opposite circular polarization (Fig. 6.3). The phase difference between the two circularly polarized waves determines the orientation of the polarization plane of the resulting linearly polarized wave.

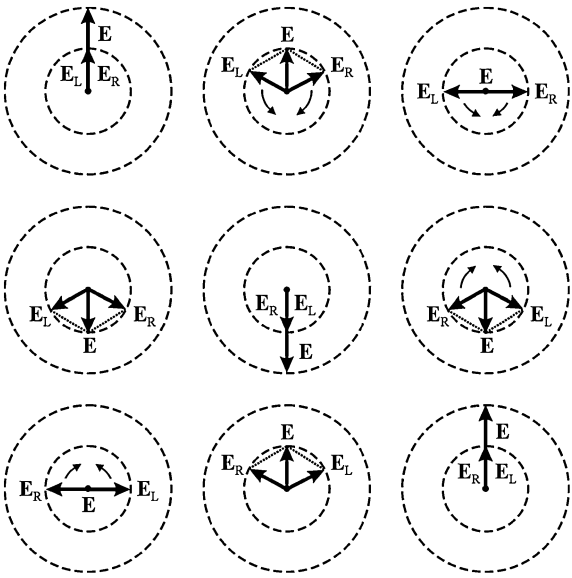

Fig. 6.3 Composition of the electric field vectors $\mathbf{E}_L$ and $\mathbf{E}_R$ of two waves with the same frequency and amplitude, and opposite circular polarization. The resulting vector **E** oscillates on a plane perpendicular to the direction of propagation, giving rise to a linearly polarized wave

6.1.3 Birefringence and Circular Dichroism

Generally speaking, the phenomenon of optical activity can be explained considering that a chiral species interacts in a different manner with the two chiral—namely, circularly polarized—components of linearly polarized light. In particular, the optical rotation arises from the fact that left and right circularly polarized radiations propagate in the optically active medium with different velocities (circular birefringence). In other words, $n_L(\lambda) \neq n_R(\lambda)$, in which $n_L(\lambda)$ ad $n_R(\lambda)$ are the refractive indexes for the radiation of wavelength λ with left and right circular polarization, respectively.

Let us consider a linearly polarized radiation, composed of two waves with opposite circular polarization, impinging on an optically active medium. While travelling across the medium, one of the two circularly polarized components propagates faster than the other one, and when they come out of the medium their phase difference has changed. Therefore, the resulting wave is still linearly polarized but its polarization plane is rotated by some angle with respect to that of the incident wave. Such an angle depends on the difference between the refractive indexes n_L and n_R, the thickness of the sample, and the wavelength of the radiation. The study of the change of the optical rotation as a function of the wavelength is known as *optical rotation dispersion* (*ORD*) [1].

In its absorption spectral region, an optically active sample may absorb the two circularly polarized components of a linearly polarized radiation to different extents. In such a case the species exhibits different absorption coefficients for left- and right-handed light, that is, $\varepsilon_L(\lambda) \neq \varepsilon_R(\lambda)$. This phenomenon is called *circular dichroism* (*CD*) [3, 4]. When circular dichroism occurs, the two circularly

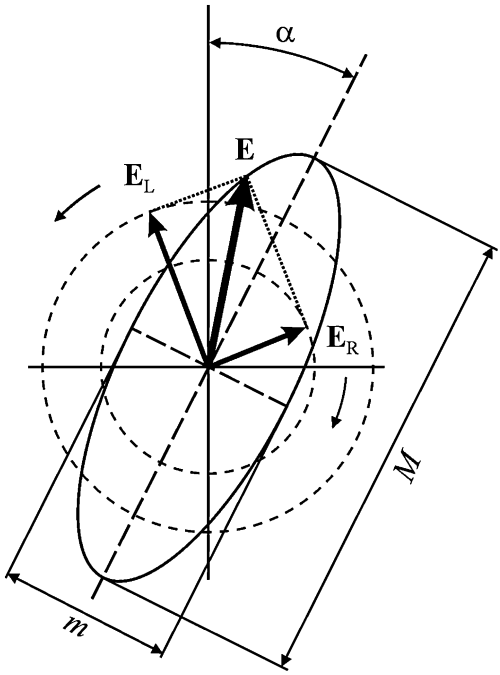

Fig. 6.4 Composition of the electric field vectors of two waves with the same frequency, opposite circular polarization and different amplitude ($|\mathbf{E}_L| \neq |\mathbf{E}_R|$). The resulting wave is said to be elliptically polarized

polarized components emerging from the sample possess not only a phase difference but also different amplitudes. The polarization of the radiation arising from their composition is no longer circular but elliptical: the tip of the corresponding electric field vector, projected in a plane perpendicular to the travelling direction of the wave, now describes an ellipse (Fig. 6.4). The major axis of the ellipse and the polarization direction of the incident light determine the angle of optical rotation (α in Fig. 6.4) due to the different refractive indexes for left- and right-handed light.

The different absorption experienced by the two circularly polarized components is expressed by means of the ellipticity θ, defined as the angle whose tangent is equal to the ratio between the minor (m) and the major (M) axes of the ellipse (Fig. 6.4).

$$\tan\ \theta = m/M \tag{6.1}$$

As it will be shown in the next paragraph, the value of ellipticity is related to the absorption difference for the two linearly polarized components, and depends on the wavelength of the radiation. The aim of CD spectroscopy is the measurement of the ellipticity as a function of wavelength. Although this kind of spectroscopy can be carried out in several spectral regions, the most popular case is that of CD in the UV-visible region, which arises from electronic transitions in molecules. Infrared CD spectroscopy, involving vibrational transitions, is less common yet used in several research laboratories.

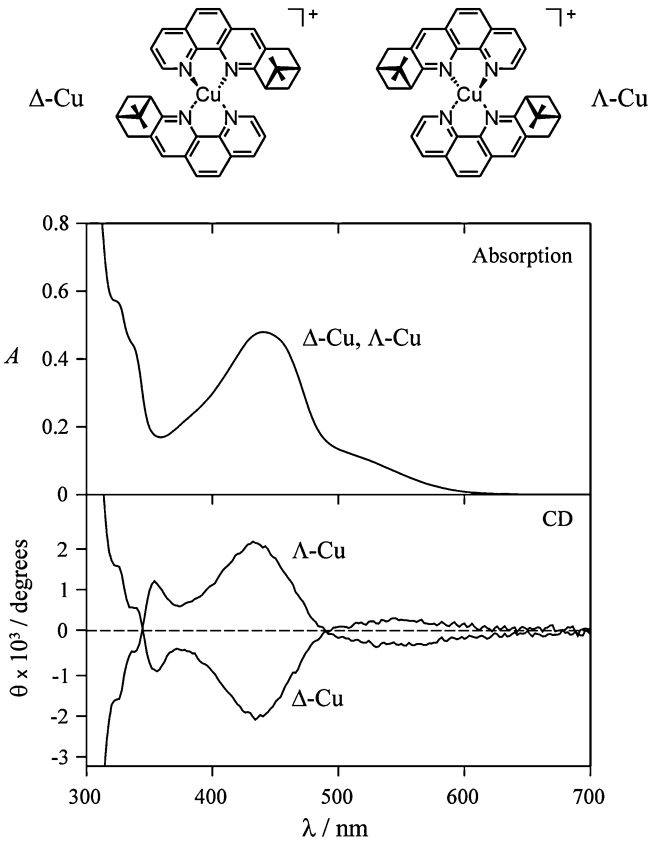

Fig. 6.5 Absorption (*top*) and circular dichroism (*bottom*) spectra of two enantiomeric complexes of Cu(I) in 1.0×10^{-4} M CH_2Cl_2 solution at 298 K [5]. Notice that the two enantiomers exhibit the same absorption spectra, and CD spectra with the same shape but opposite sign

Similarly to the isotropic absorption spectrum (i.e., recorded using non-polarized light), the circular dichroism spectrum of a chemical species in solution is constituted by bands. There is, however, an important difference between absorption and CD spectra: while the former exhibit only positive signals, the latter can show both positive and negative signals, because CD bands are due to absorption differences (Fig. 6.5).

The optical rotation dispersion and circular dichroism are caused by the same phenomenon—namely, the different interaction of left- and right-handed light with an optically active species; hence, it is not surprising that a strict relationship exists between ORD and CD spectra of the same compound. In fact, the ORD spectrum can be obtained from the CD spectrum, and vice versa, by using the so-called Kramers–Krönig transformations. Usually the ORD spectrum is recorded in

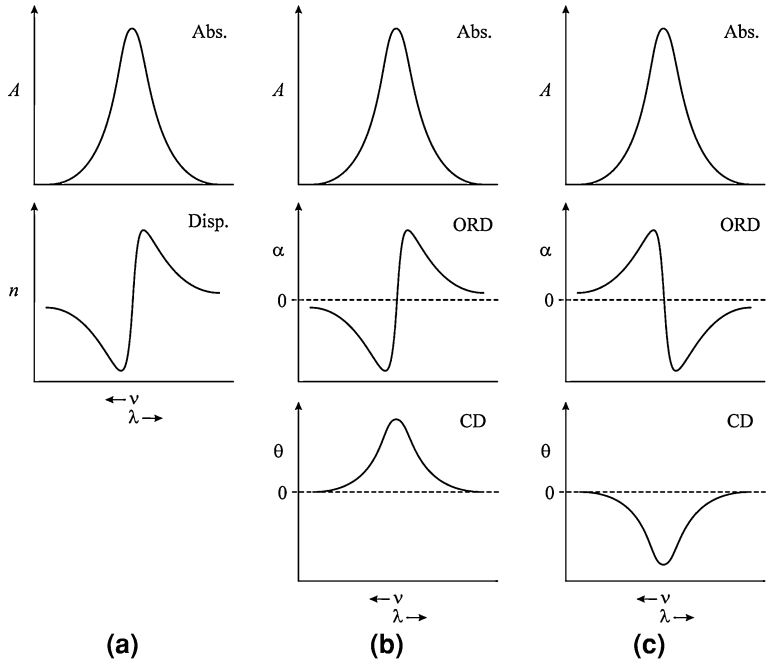

Fig. 6.6 Relation between the isotropic absorption spectrum and the dispersion spectrum (**a**), and relation between the absorption, ORD and CD spectra in the case of positive (**b**) and negative (**c**) Cotton effect

spectral regions in which the examined sample does not exhibit absorption bands; conversely, the sample will show a CD spectrum in its absorption region.

From a qualitative point of view, the relationship between ORD and CD spectra is reminiscent of that existing between the dispersion spectrum (change of the refractive index as a function of wave frequency) and the isotropic absorption spectrum (Fig. 6.6a). One can observe that in the region of absorption bands, particularly the sharp ones, the refractive index increases on increasing frequency (i.e., on decreasing λ) until it suddenly drops to a minimum around the wavelength of the absorption maximum. Upon further increase of the frequency, the refractive index grows again.

A similar wavelength-dependent behavior is observed for the optical rotation (difference in the refractive indexes for left- and right-handed light) and the dichroism (difference in the absorption coefficients). Such a behavior for ORD is referred to as Cotton effect and can be either positive or negative. In the positive Cotton effect the optical rotation dispersion shows the same wavelength dependence as the refractive index in the isotropic case and occurs in the region of a positive CD band (Fig. 6.6b). Conversely, the negative Cotton effect takes place in the region of a negative CD band (Fig. 6.6c). It can be noted that the wavelength at which the optical rotation vanishes corresponds to the maximum of the ellipticity.

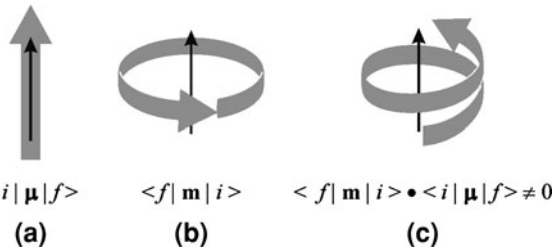

Fig. 6.7 Schematic representation of the change in electronic distribution induced in a molecule by the electromagnetic field in the case of an electric dipole transition (**a**), a magnetic dipole transition (**b**) and a transition possessing a rotatory strength (**c**). In the latter case the transition is associated with the phenomenon of optical activity

The origin of the circular dichroism phenomenon should be discussed using quantum mechanical arguments; such a task, because of its complexity, is beyond the scope of this paper. Nevertheless, it is worthwhile recalling that any electronic transition from an initial state i to a final state f is characterized by a rotator strength, $R_{i\to f}$. This parameter determines the intensity of the circular dichroism spectrum and it can be calculated from the integration of the CD spectrum in the spectral region of the examined transition. In the absence of a preferential orientation of the molecules in the sample, the rotator strength associated with the transition corresponds to the imaginary part of the scalar product between the electric dipole moment $\boldsymbol{\mu}$ and the magnetic dipole moment $\mathbf{m}$ induced on the molecule by light (transition moments, Fig. 6.7).

In the case of a non-isotropic distribution of molecular orientations, the expression of $R_{i\to f}$ becomes considerably more complex. As previously discussed, circular dichroism is observed for chiral species, i.e., species lacking a plane or a center of symmetry because stereogenic atoms are present or because they are inherently asymmetric for structural (e.g., sterically hindered compounds such as 1,1′-binaphthyl or octahedral metal complexes with three bidentate ligands), conformational (e.g., helical proteins), or topological (e.g., molecules with the shape of a trefoil knot) reasons. For a given transition, the rotation strength of an enantiomer has the same intensity and opposite sign as that of the other enantiomer. In achiral molecules, for symmetry reasons, it happens that the $\boldsymbol{\mu}$ and $\mathbf{m}$ vectors are either mutually perpendicular or one of them is zero; hence $R_{i\to f} = 0$ and there is no circular dichroism. Of course, not all the isotropic absorption bands of an optically active compound give necessarily rise to circular dichroism: for some of them, in fact, the absorption coefficients ε_R and ε_L could exhibit the same value.

In the presence of a static magnetic field any sample becomes optically active in a direction parallel to that of the magnetic field, and exhibits a circular dichroism to an extent proportional to the intensity of the applied field. Such an effect has nothing to do with molecular chirality and is called *magnetic circular dichroism* (*MCD*). Differently from what discussed for natural circular dichroism, the two

enantiomers of a chiral molecule and their racemic mixture possess the same MCD spectrum. Moreover, as the MCD signal changes sign upon inverting the direction of the magnetic field with respect to the travelling direction of light, the MCD effect vanishes if the radiation is sent through the sample twice in opposite directions. As a matter of fact, this is a simple and effective method for distinguishing magnetic and natural circular dichroism phenomena.

A circular dichroism signal may be observed also for achiral molecules immersed in chiral environments (for example, dissolved in a chiral solvent or complexed by chiral receptors) [6]. This effect is known as *induced circular dichroism* (ICD) and is generally very weak [7]. ICD spectroscopy is frequently used in supramolecular chemistry to study the complexation of an achiral guest by a chiral host [8]. An example of this kind is represented by the association of optically inactive organic chromophores with cyclodextrins, that are macrocyclic receptors possessing a chiral cavity [9, 10].

The measurement of the circular polarization of the light *emitted* by a sample is at the basis of the circularly polarized luminescence spectroscopy (CPL) technique, which will be described in Sect. 6.2. This technique can be considered as the emission equivalent of circular dichroism.

6.1.4 Linear Dichroism

LD spectroscopy is a technique based on the interaction between linearly polarized radiation and chemical species [3]. Such a technique has no relation with molecular chirality and circular dichroism. It relies on the fact that the probability of inducing an electronic transition with electromagnetic radiation is proportional to the cosine square of the angle between the transition dipole moment and the polarization direction of the radiation (which coincides with the direction of oscillation of the electric field). Therefore, if a linearly polarized radiation is employed, the probability of a transition to occur is maximum when the corresponding dipole moment is parallel to the polarization direction, while the probability is zero when the transition dipole moment is oriented perpendicularly to the polarization direction. The dependence of the absorption of a sample on the polarization direction of the light is called linear dichroism.

In an isotropic sample (e.g., a solution) the molecules, and hence the transition moments, can exhibit all possible orientations. In order to observe linear dichroism the sample molecules must be all or in part oriented along a certain direction, as it can happen for instance in crystals, polymers, thin films, gels and liquid crystals. In some cases, the molecules of an isotropic sample can be oriented by applying an electric field.

The linear dichroism spectrum is a diagram reporting the difference between the absorption of the radiation with parallel polarization ($A_{\parallel}$) and that of the radiation with perpendicular polarization ($A_{\perp}$) with respect to the direction of preferential orientation of the molecules, as a function of wavelength.

$$\Delta A_{\mathrm{LD}}(\lambda) = A_{\parallel}(\lambda) - A_{\perp}(\lambda) \tag{6.2}$$

The measurement of the linear polarization of the light emitted by a sample constitute the subject of the luminescence anisotropy technique that will be discussed in Sect. 6.3. As discussed above for CPL and CD spectroscopies, luminescence anisotropy can be considered as the emission equivalent of the linear dichroism technique.

6.1.5 Observables in Circular Dichroism Spectroscopy

As discussed previously, the different absorption exhibited by an optically active sample for the two circularly polarized components of a linearly polarized wave confers an elliptical polarization to the emerging radiation. The extent of such a polarization is expressed by means of the ellipticity θ (in degrees or millidegrees):

$$\theta = \arctan\ m/M \tag{6.3}$$

in which m and M are the minor and major axes of the ellipse, respectively (Fig. 6.4).

The quantity measured experimentally in CD spectroscopy is the difference between the absorbance of left- (A_{L}) and right-handed (A_{R}) light at a given wavelength λ:

$$\Delta A_{\mathrm{CD}}(\lambda) = A_L(\lambda) - A_R(\lambda) \tag{6.4}$$

For any wavelength, the ellipticity is related to the absorbance difference ΔA by the following equation:

$$\theta = 180/4\pi\ \ln 10\, \Delta A = 32.98\, \Delta A \tag{6.5}$$

In the case of an enantiomerically pure species dissolved in solution, the Lambert–Beer law can be written as

$$\Delta A = \Delta\varepsilon\, c\, l \tag{6.6}$$

in which $\Delta\varepsilon = \varepsilon_L - \varepsilon_R$ (usually expressed in L mol^{-1} cm^{-1}) at the considered wavelength, c is the concentration of the absorbing species in mol L^{-1}, and l is the optical path length of the radiation in cm.

Occasionally, in particular for the biological area, circular dichroism spectra report the molar ellipticity $[\theta]$, expressed in degrees L mol^{-1} cm^{-1}, in the place of $\Delta\varepsilon$:

$$[\theta] = \theta/c\, l \tag{6.7}$$

The relationship between the molar ellipticity and the differential molar absorption coefficient is quite simple:

$$\Delta\varepsilon = [\theta]/32.98 \tag{6.8}$$

For historic reasons, the molar ellipticity can sometimes be reported in degrees $cm^2\ dmol^{-1}$; in such a case $\Delta\varepsilon$ is obtained dividing $[\theta]$ by 3,298.

The ratio between $\Delta\varepsilon$ and ε at a given wavelength yields the absorption dissymmetry factor:

$$g_{abs}(\lambda) = \Delta\varepsilon(\lambda)/\varepsilon(\lambda) \tag{6.9}$$

in which $\varepsilon(\lambda) = [\varepsilon_L(\lambda) + \varepsilon_R(\lambda)]/2$. The analysis of the function $g_{\mathrm{abs}}(\lambda)$ and of the corresponding emission dissymmetry factor $g_{\mathrm{em}}(\lambda)$, obtained from circularly polarized luminescence measurements (Sect. 6.2.2), enables the investigation of the structural differences between the ground and excited electronic states, as well as the nature and properties of the molecular vibration in these two states.

6.1.6 Instrumentation and Experimental Procedures

Circular dichroism spectra are recorded with an instrument called CD spectropolarimeter. A spectropolarimeter is basically a spectrophotometer capable of measuring the absorbance difference A_{L}–A_{R} at any wavelength in the explored spectral region. Therefore, besides the components of a conventional spectrophotometer (lamp, monochromator, sample holder, detector), it must possess a circular polarizer (Fig. 6.8). The simplest way to make a circular polarizer (or analyzer) is to couple a linear polarizer with an optical element that can introduce a phase shift between two radiations polarized linearly on perpendicular planes. This is because, as discussed above, a circularly polarized wave is composed of two waves linearly polarized on perpendicular planes and having a phase shift of $\pi/2$, that is, $\lambda/4$. The dephasing element is usually a photoelastic modulator (PEM) composed of an isotropic material which becomes optically anisotropic upon application of an electric potential. The non-polarized light coming from the source is first linearly polarized, then it goes through the photoelastic modulator (whose main axis must be tilted by 45° with respect to the direction of the linear polarizer) which transforms it into circularly polarized light. On changing the electric potential that drives the PEM at a certain frequency f, the phase shift introduced between the two linearly polarized input components can be modulated between $+\pi/2$ and $-\pi/2$. In such a way the polarizer converts the non-polarized light into radiation whose circular polarization oscillates between left- and right-handed with a frequency f. This radiation is sent through the sample and successively measured by a detector coupled with a lock-in amplifier operating at the frequency f, which directly detects the difference between the left-handed and right-handed transmitted intensities. ΔA is straightforwardly obtained from these data.

In UV-visible spectrophotometers the detector is usually a photomultiplier tube. The circular dichroism signal is generally quite weak ($\Delta\varepsilon$ is small compared with

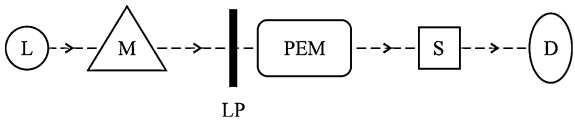

Fig. 6.8 Block diagram of a CD spectropolarimeter. *L* lamp; *M* monochromator; *LP* linear polarizer; *PEM* photoelastic modulator; *S* sample; *D* detector

ε), and in the process of polarization of the analyzing light a substantial fraction of the intensity emitted by the source is lost. Therefore, spectropolarimeters must be equipped with powerful sources, generally xenon lamps with a power of 150 W or higher. The mid-UV spectral region (ca. 250–180 nm) is very important in CD spectroscopy, particularly for biological studies (for example, the CD signals of the $\pi\pi^*$ and $n\pi^*$ transitions of proteins fall in the region comprised between 180 and 220 nm), oxygen must be removed from the interior of the spectropolarimeter by means of a continuous nitrogen stream. The O_2 molecule, in fact, absorbs in the above region: this phenomenon is detrimental because it decreases the sensitivity of the instrument in the UV, and because it generates ozone which can damage the optical components.

In the absence of an optically active sample, the instrument must obviously measure $\Delta A = 0$ for any wavelength. It is therefore necessary to record the baseline on a blank sample; in the case of measurements on solutions, the blank is represented by the cell containing the solvent alone. Common spectrophotometric and spectrofluorimetric cells can be used in UV-visible CD spectroscopic experiments, although it is advisable that they are tested for use in polarimetric measurements.

In order to obtain a good signal-to-noise ratio, the expedients to be adopted in a CD experiment are the same as those for a conventional absorption experiment. In particular, the absorbance of the solutions in the spectral region of interest should not be too large (preferably below 1 and never higher than 2). In case of photoluminescent samples, because of the high intensity of the analyzing light of the spectropolarimeter, the CD spectrum may be affected by the light emitted from the sample. This effect can be kept to a minimum or totally removed by, e.g., diluting the sample or using a cut-off filter to prevent the emitted light from reaching the detector.

If necessary, the spectropolarimeter can be calibrated by using compounds with a known CD spectrum [11, 12]. To be used as calibration standards, these compounds must be stable, easily available in high purity samples, soluble in water or in common solvents, harmless, and exhibiting an intense and characteristic CD spectrum. The choice of the standard is essentially dictated by the spectral region in which a calibration is needed. Pantolactone [13] is a good standard for the region comprised between 180 and 250 nm, while for the 250–350 nm region the compounds ammonium-10-camphorsulfonate [14] or 10-camphorsulfonic acid [11, 15] can be used (the latter is a primary standard). Calibration in the visible region can be performed with the complexes cobalt(III) tris-ethylenediamine [16]

or ruthenium(II) tris-2,2′-bipyridine [17], both in their enantiomerically pure forms.

An interesting variation of CD spectroscopy is *fluorescence detected circular dichroism* (FDCD). This technique is based on the measurement of the difference in the fluorescence intensity produced when an optically active fluorescent sample is excited with left- and right-handed circularly polarized radiations. The FDCD measurement is performed with a spectropolarimeter, placing the photomultiplier at an angle of 90° with respect to the optical path of the polarized light, and introducing a cut-off filter or a monochromator in order to prevent scattered light from impinging on the detector. Similarly to conventional CD spectroscopy, the FDCD technique gives information on the chirality of molecules in their ground state, because the chiral discrimination occurs in the absorption process. The use of fluorescence to reveal circular dichroism has two important advantages: firstly, the differential absorption is measured through a high-sensitivity technique such as fluorescence detection. Secondly, one can study the dichroic properties of specific fluorophores in molecules or supermolecules that contain several chromophoric groups.

Linear dichroism can be observed by applying a linear polarized to a UV-visible spectrophotometer. By orienting the polarizer at 0° and 90° with respect to the sample, the two absorbance values, $A_{\parallel}$ and $A_{\perp}$, can be measured. The use of a spectropolarimeter for LD experiments, however, gives better results in terms of sensitivity and accuracy. LD signals can be measured by changing a few parameters of the linear polarizer/PEM ensemble, an option available in most modern spectropolarimeters.

Commercially available CD spectropolarimeters, either stand-alone or with specific accessories, are capable of recording isotropic absorption and luminescence, ORD, LD, FDCD and MCD spectra. Moreover, they can also be equipped with thermostatic modules, flow cells, automatic titration devices, and stopped flow systems for the measurement of reaction kinetics. CD instruments are also employed as detectors in HPLC chromatography with chiral stationary phases.

6.1.7 Applications

Taking advantage from the study of spectra-structure relationships, the analysis of CD and ORD spectra enable the investigation of the stereochemistry of chiral molecules and determine the absolute configuration of enantiomers [18]. Moreover, interchromophoric interactions such as exciton coupling can be evidenced, and the distance and orientation of the involved chromophore can be determined [19].

CD Spectroscopy has become popular especially because of its application in the biological area [4, 20]. This technique is employed to investigate conformations and folding/unfolding processes—under both thermodynamic and kinetic viewpoints—of polypeptides, proteins and nucleic acids, enzyme kinetics and other biochemical reactions. CD Spectra are of particular utility to determine the

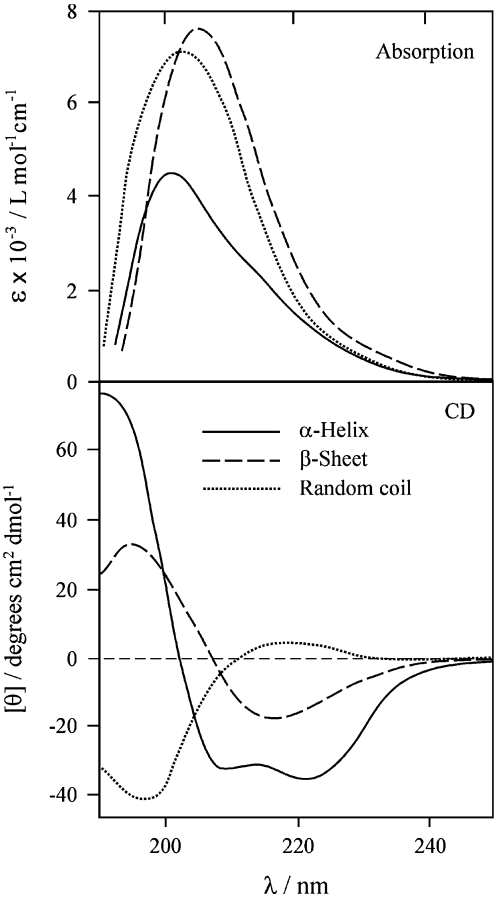

Fig. 6.9 UV Absorption (*top*) and circular dichroism (*bottom*) spectra of poly-L-lysine in aqueous solution in the α-helix (*full line*), *β*-sheet (*dashed line*) and random coil (*dotted line*) conformations

occurrence of the various types of secondary structures (α-helix, *β*-sheet, random coil, etc.) in proteins in their native form [20]. Figure 6.9 shows the UV absorption and circular dichroism spectra of poly-L-lysine with various secondary structures.

Structural and conformational changes caused by interactions involving chiral molecules can be studied with CD spectroscopy. These experiments deal with, for example, the formation of host-guest complexes between asymmetric species, whose association constant can be determined from CD titrations. The case of an achiral chromophore (thus lacking a natural CD signal) that interacts with a chiral molecule is of particular interest. The resulting complex is obviously chiral and can exhibit circular dichroism in the absorption region of the achiral chromophore.

Curve (a) in Fig. 6.10 shows the CD spectrum in aqueous solution of a molecule comprising a ferrocene unit (achiral) functionalized with chiral D-glucopiranose units [21]. Curves (b–d) represent the spectral changes observed upon addition of *β*-cyclodextrin, a well known chiral macrocycle. In water, ferrocene forms an inclusion complex with *β*-cyclodextrin. As in the examined spectral region only the

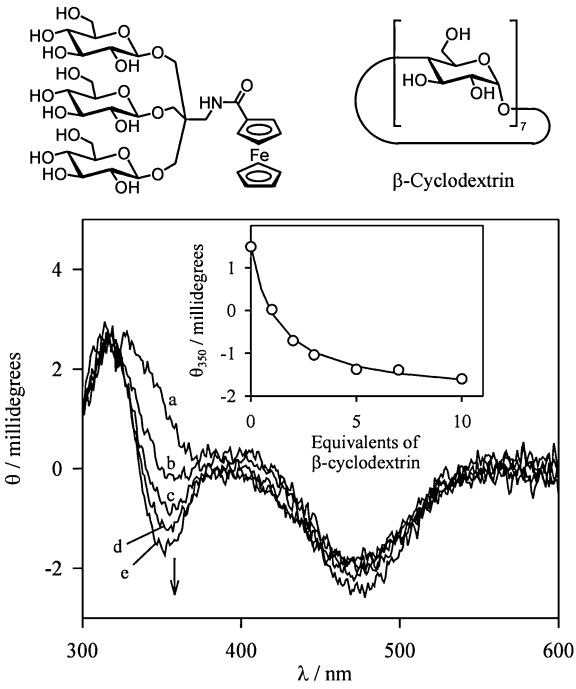

Fig. 6.10 CD spectral changes of a glucopyranose derivative of ferrocene (1×10^{-3} M, H_2O, 295 K) in the absence (**a**) and in the presence of increasing amounts of β-cyclodextrin (**b-d**) [21]. Notice that neither the D-glucopyranose units nor β-cyclodextrin exhibit absorption bands in the examined spectral region. From the titration curve obtained by plotting the ellipticity at 350 nm as a function of the added equivalents of β-cyclodextrin (*inset*) the stability constant of the complex can be determined

ferrocene unit absorbs light, the CD bands observed in curve (a) are induced on the achiral ferrocene chromophore by the presence of the chiral substituent. The addition of β-cyclodextrin causes changes in the circular dichroism induced on the ferrocene absorption bands, because of the formation of a host-guest complex in which the ferrocene unit occupies the cavity of the chiral macrocycle [21].

The analysis of the CD spectrum induced on the achiral chromophore can provide insights on its orientation relatively to the chiral molecule. For example, a rule of thumb exists for cyclodextrin inclusion complexes: the CD induced on a certain electronic transition of the guest chromophore is positive if the corresponding transition dipole moment is parallel to the main axis of cyclodextrin, while it is negative if the transition dipole moment is oriented perpendicularly [22].

Circular dichroism is largely employed to investigate interactions among different biomolecules (protein–protein, protein–nucleic acid, etc.), and among biomolecules and other ligands (for examples, molecules of medicinal interest). Also in this case, not only thermodynamic (association constants, reaction enthalpy and entropy) and kinetic (reaction rates and activation barriers) parameters can be determined, but also different association modes (e.g., DNA intercalation or association in the minor or major groove of the double helix) can be distinguished. Finally, CD spectroscopy is applied in analytical sciences to determine the purity of optically active compounds.

Linear dichroism spectroscopy is used to study the orientation of molecules in an anisotropic sample. It is usually performed in the UV-visible (LD of electronic transitions) and in the infrared (vibrational LD) spectral regions.

6.2 Circularly Polarized Luminescence Spectroscopy

6.2.1 Introduction

As described in the previous section, chiral species—or achiral species in a chiral environment—can absorb the two circularly polarized components of light with different probabilities, giving rise to circular dichroism. Similarly, chiral luminescent species—or achiral but immersed in a chiral environment—can emit left- and right-handed radiations with different probabilities. Because of this phenomenon, the emitted light exhibit elliptical polarization (Fig. 6.4). It should be noted that in the present discussion only spontaneous emission will be considered.

The differential emission of left and right circularly polarized light from luminescent molecular systems is called *circularly polarized luminescence* (CPL), and is at the basis of the corresponding spectroscopic technique (CPL spectroscopy) [23–25]. CPL spectroscopy should not be confused with fluorescence detected circular dichroism (see Sect. 6.1.6); in the latter technique the differential absorption of the circularly polarized components is detected through fluorescence measurements, owing to the different extent of photoexcitation that left- and right-handed light can produce on a chiral molecule.

Any chiral molecular or supramolecular system can exhibit circular dichroism in its absorption region; similarly, molecular or supramolecular species in a luminescent excited state are potentially characterized by CPL. This observation holds also for achiral species placed in chiral environments (for example, dissolved in a chiral solvent or complexed by a chiral host), or subjected to a magnetic field; these cases are referred to as induced CPL (ICPL) and magnetic CPL (MCPL).

As noted above, CPL spectroscopy can be considered as the emission equivalent of circular dichroism spectroscopy. In summary, the CPL phenomenon can occur in the following cases, even upon excitation with unpolarized or linearly polarized light:

- Chiral molecules, either enantiomerically pure or in mixtures with an enantiomeric excess;
- Achiral molecules in the presence of chiral species (ICPL);
- Achiral molecules subjected to a magnetic field (MCPL); the emission of light with circular polarization takes place in a direction parallel to that of the applied magnetic field.

One can also observe CPL by exciting a racemic mixture with circularly polarized light. In this case, the ensemble of excited molecules is no longer racemic because of the photoselection brought about by the differential absorption of polarized light exhibited by the two enantiomers.

6.2.2 Observables in CPL spectroscopy

The measured quantities in CPL spectroscopy are the difference of intensity (ΔI) of the left handed (I_L) and right handed (I_R) circularly polarized components of the emitted light, and the total luminescence intensity (I) emitted by the sample:

$$\Delta I(\lambda) = I_L(\lambda) - I_R(\lambda) \tag{6.10}$$

$$I(\lambda) = I_L(\lambda) + I_R(\lambda) \tag{6.11}$$

in which $I_L(\lambda)$ and $I_R(\lambda)$ are the intensities of left and right handed circularly polarized components of the light emitted at the wavelength λ. The quantity $\Delta I(\lambda)$ is called differential circular luminescence intensity or simply CPL intensity, whereas $I(\lambda)$ is called total luminescence (TL) intensity.

As discussed in the previous section, if CPL occurs the values $I_L(\lambda)$ and $I_R(\lambda)$ are different and the total luminescence shows a partial circular polarization (the emitted light is elliptically polarized). In a CPL experiment one can either measure directly $\Delta I(\lambda)$ or determine $I_L(\lambda)$ and $I_R(\lambda)$ separately. In both cases the key problem of the experiment is to make a reliable measurement, because the difference between $I_L(\lambda)$ and $I_R(\lambda)$ is usually very small.

The emission dissymmetry factor, $g_{em}(\lambda)$, can be calculated from these quantities:

$$g_{em}(\lambda) = 2\Delta I(\lambda)/I(\lambda) \tag{6.12}$$

The experimental determination of the emission intensity in absolute units is quite complex; as it commonly happens in luminescence measurements, $I(\lambda)$ and $\Delta I(\lambda)$ are often measured in arbitrary units, which are dependent on the equipment and the experimental conditions adopted. The dissymmetry factor $g_{em}(\lambda)$ is a significant quantity because it is a ratio of emission intensities and is therefore unaffected by the instrumental and experimental parameters. Its value gives an absolute quantification of the chirality of the emitting excited state.

The emission dissymmetry factor can be compared with the absorption dissymmetry factor, g_{abs}, obtained from circular dichroism measurements (Sect. 6.1.5) [24]. As an example, Fig. 6.11 shows the absorption, CD and CPL spectra of an optically active polypyridine complex of osmium(II) together with the corresponding values of g_{abs} and g_{em}. In general, g_{abs} and g_{em} depend on the same aspects of electronic structure of molecules. Circular dichroism, however, is a property of molecules in their electronic ground state, whereas circularly polarized luminescence arises from electronic excited states. According to the Franck-Condon

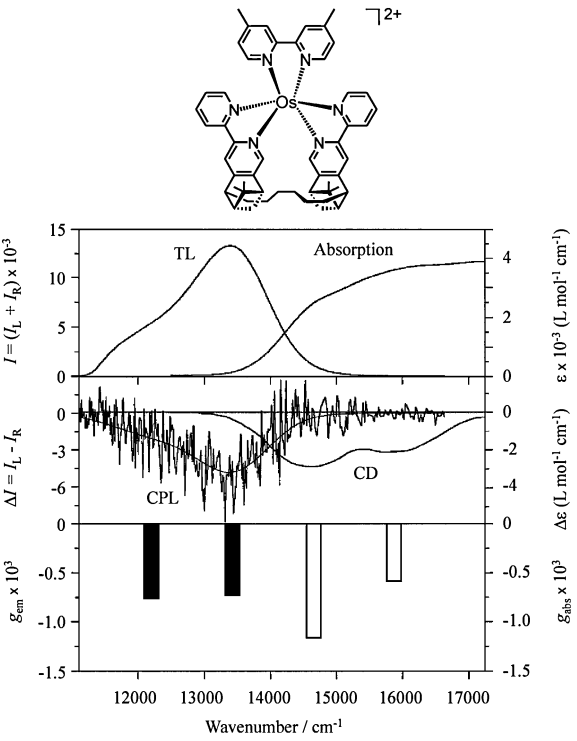

Fig. 6.11 Absorption, total luminescence (TL), circular dichroism (CD), and circularly polarized luminescence (CPL) spectra of a chiral Os(II) polypyridine complex in the spectral region comprised between 11,100 and 17,200 cm^{-1} (CH_3CN, 293 K) [33]. The CPL signal is noisy because it is very weak. The lower part of the figure shows the values of the absorption and emission dissymmetry factors measured at specific frequencies

principle, the CD and CPL spectra reflect the molecular structure in the ground state and in the luminescent excited state, respectively. The information obtained from CD to CPL spectroscopies is therefore redundant for molecular species that possess the same geometry in the ground and in the luminescent excited states.

As noted for circular dichroism (Sect. 6.1.3), the extent of circular polarization of a luminescence band is proportional to the rotatory strength of the corresponding electronic transition(s). The emission dissymmetry factor for a sample of molecules isotropically distributed both in the ground and in the excited state has the following expression:

$$g_{em} \propto R_{if}/D_{if} \tag{6.13}$$

in which R_{if} is the rotatory strength of the $i \rightarrow f$ transition, in its turn depending on the scalar product of $\boldsymbol{\mu}_{if}$ and $\mathbf{m}_{if}$ (electric and magnetic transition moments), and D_{if} is the dipolar strength, that is proportional to $|\boldsymbol{\mu}_{if}|^2 + |\mathbf{m}_{if}|^2$. In other words, R_{if} determines the CPL intensity and D_{if} determines the total luminescence intensity. For most electronic transitions in non-centrosymmetric molecules, $|\boldsymbol{\mu}_{if}| \gg |\boldsymbol{\mu}_{if}|$ hence, it can be concluded that the emission transitions exhibiting a strong circular polarization are generally those characterized by a significant magnetic moment and a not too large electric dipole moment.

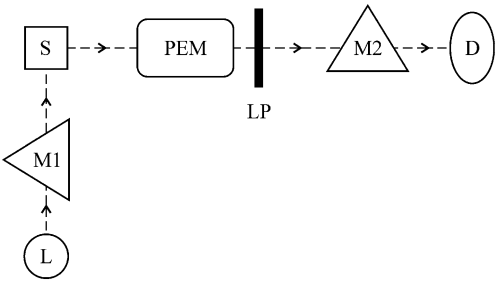

Fig. 6.12 Block diagram of a CPL spectrofluorimeter. *L* lamp; *M*1 excitation monochromator; *S* sample; *PEM* photoelastic modulator; *LP* linear polarizer; *M*2 emission monochromator; *D* detector

6.2.3 Instrumentation and Experimental Procedures

CPL spectroscopy is not as popular as luminescence or circular dichroism spectroscopies, and is much less diffused in research laboratories. This is the reason why stand-alone instruments for CPL measurements are not commercially available. The scheme of a CPL spectrofluorimeter, however, is not very complicated. In analogy with the spectropolarimeter, which is essentially a spectrophotometer capable of detecting circular dichroism, a CPL spectrofluorimeter is in fact a normal spectrofluorimeter equipped with a circular polarization analyzer (Fig. 6.12).

The sample is excited with a lamp coupled with an excitation monochromator or, better, with a laser (because the CPL signal is weak and a powerful excitation source will enhance the signal-to-noise ratio). The emitted light is sent through a PEM oscillating at a frequency f, whose task is to convert the circularly polarized radiation into a linearly polarized one (see Sect. 6.1.6). The latter is then selected with the passage through a linear polarizer oriented at 45° with respect to the main axis of the PEM. In this way the detector "sees" alternately, at a frequency f, the light emitted with left handed and right handed polarization. By connecting the detector to a lock-in amplifier that operates at the frequency f one can directly measure ΔI. The total luminescence intensity is obtained from the total output current of the photomultiplier. A suitable calibration is however necessary to quantitatively correlate the signal coming from the lock-in amplifier, proportional to ΔI, and that corresponding to the total intensity [26]. The most common calibration standard in CPL spectroscopy is *tris*(3-trifluoroacetyl-*d*-camphorate) europium(III). It is used as an NMR shift reagent and can be easily found in high purity samples. More details are available in specialized papers [24].

The scheme shown in Fig. 6.12 can also be adapted to a single-photon counting system. An advantage of such a system is that it does not require a calibration because it measures directly the photon count corresponding to ΔI and I, whose ratio yields straightforwardly g_{em}.

If the excitation on the spectrofluorimeter is performed by a lamp-monochromator system, CPL excitation spectra can be recorded. CPL spectrofluorimeters can also be modified to make time-resolved measurements, obviously utilizing a pulsed excitation source. In this case, it should be noticed that the time

resolution of the technique is limited by the duration of the photoelastic modulation cycle. In most cases, PEMs are modulated at 50 kHz, therefore the time response of the instrument cannot be faster than tens of microseconds. Because of this limitation, time-resolved CPL measurements can be carried out only on long-lived luminescence signals, like phosphorescence of organic chromophores or formally forbidden electronic transitions in metal complexes (e.g., complexes of the lanthanide ions).

In most cases the CPL component is a very little fraction of the emitted light (typically below 1%). The exclusion of any source of error or artifact in CPL experiments is therefore of the highest importance. The most dangerous interference, because it is difficult to spot out, is the presence of linearly polarized light in the sample emission [24]. This can happen if the excited states are anisotropically distributed as a consequence, for example, of a non isotropic distribution of the molecules in the ground state, or of the photoselection effect operated by the incident radiation.

6.2.4 Applications

The analysis of the CPL spectra constitutes a straightforward method for the study of the chirality of molecules in their luminescent excited states. By means of comparative CD/CPL measurements one can investigate the geometrical differences between the ground and excited states. The observation of CPL has the problems and limitations already described in the previous sections. In particular, the molecular or supramolecular species must contain a luminophore exhibiting a sufficiently high emission quantum yield. CPL spectroscopy, however, has a number of advantages in terms of specificity and selectivity that can be extremely useful in supramolecular chemistry, namely:

- The possibility of examining emission transitions that end in an electronic level not accessible by thermal activation, which cannot be investigated by absorption/CD spectroscopies;
- The observation of excited states that cannot be easily produced by direct light absorption;
- The study of dynamic processes involving luminescent excited states (e.g., energy- or electron-transfer processes);
- The study of complex multichromophoric systems, for which the interpretation of the spectra is facilitated because emission usually takes place exclusively from one of the chromophores.

As mentioned above, CPL spectroscopy can be used to distinguish a racemic mixture of a chiral species from an achiral one, through the photoselection effect brought about by exciting the sample with circularly polarized light. Such an experiment requires that the examined species is luminescent, and that any racemization process is slower than the decay time of the excited state under investigation.

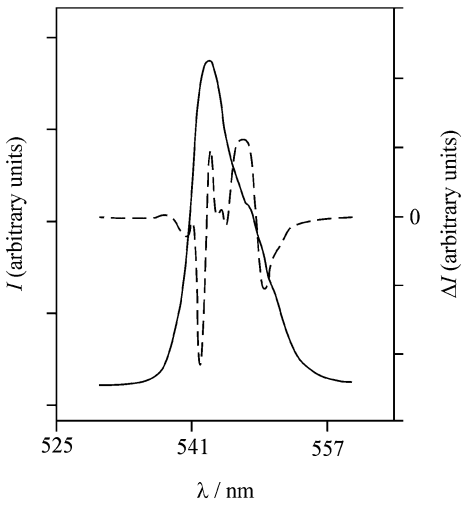

Fig. 6.13 Total luminescence spectrum (*full line*) and CPL spectrum (*dashed line*) of an aqueous solution at pH 5.6 containing Tb^{3+} ions and D-(+)-mannose in a 1:3 ratio. The Tb^{3+} concentration is 0.01 M and the excitation wavelength is 488 nm

In many cases, the chemical species studied with CPL spectroscopy are complexes of lanthanide ions, particularly those of Eu(III) and Tb(III) [27–30]. In fact the *f–f* electronic transitions of these ions possess a strong magnetic dipole character and a modest electric dipole moment, and give rise to very narrow emission bands. Such transitions were exploited to investigate the interaction between these metal ions (or their complexes) and other species, for examples molecules of biological interest [31, 32]. Figure 6.13 shows the CPL band corresponding to the $^7F_5 \leftarrow {}^5D_4$ transition of Tb^{3+} induced by the interaction with D-(+)-mannose in aqueous solution.

CPL investigations on transition metal complexes [33], molecular trefoil knots [34], organic species in solution [35, 36] and in thin films [37], and biological systems [24, 25] including protein aggregates [38] have been reported. Recent studies demonstrated that the CPL properties of optically active organic molecules can be affected by the solvent and can be controlled photochemically [36]. The change of CPL properties arising from supramolecular complexation in the solid state was also described [39].

Time-resolved CPL spectroscopic experiments have been employed to study the stereoselectivity of electronic energy-transfer processes among optically active species [34, 40, 41].

6.3 Steady State and Time Resolved Fluorescence Anisotropy

6.3.1 Introduction

Fluorescence anisotropy (FA) is a very versatile technique which can be exploited to investigate phenomena of different nature: indeed any kind of process that

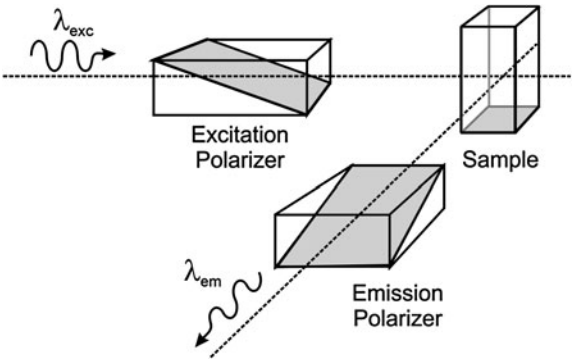

Fig. 6.14 Schematic representation of the instrumental configuration used for FA measurements

causes a change of the orientation of the dipole moment associated to the electronic distribution of a fluorescent excited state can be, at least in principle, investigated by FA. Nevertheless the processes which are most commonly studied (and are discussed in detail in this section) are fluorophore rotation [42, 43] and homo-energy transfer (namely energy transfer from an excited fluorophore to an identical one at the ground state) [44]. As far as rotation is concerned, the constant rate and the degrees of freedom are strongly dependent on the properties of the fluorophore, such as the mass and the structure, and of the surrounding environment. This is why FA is traditionally used to investigate phenomena which lead to configurational or structural changes of the fluorescent system (such in the case of protein denaturation) but also for the characterization of microenvironments allowing, for example, to determine the mobility of a specific fluorophore into a membrane. Beside steady state (SS) FA is a technique suitable to investigate phenomena related to excited fluorophore reorientation, the study of energy transfer processes requires fast time resolved (TR) FA measurements.

The final aim of this section about FA is to discuss the basis of this technique and to give to the reader the basic knowledge of the procedures to be used for spectra and decay recording. A more detailed description of the most sophisticated aspects of FA can be found elsewhere [45].

6.3.2 Definition of Fluorescence Anisotropy

FA is used to measure the degree of polarization of the fluorescence coming from a sample excited with polarized light. It can be measured using the experimental configuration depicted in Fig. 6.14. The sample is excited with vertically polarized light which is obtained by interposing a polarizer (the excitation polarizer) between the excitation source and the sample holder. The fluorescence is analyzed using a second polarizer (the emission polarizer). The FA is calculated from the intensities measured when the emission polarizer is vertical (parallel to the excitation one) and horizontal (perpendicular to the excitation one) and is defined as:

$$r = \frac{I_{\parallel} - I_{\perp}}{I_{\parallel} + 2I_{\perp}} \tag{6.14}$$

The instruments used for FA measurements are usually conventional fluorimeter equipped with a pair of polarizers inserted in the excitation and emission beams, respectively. The kind of measurement performed hence depend on the operative modality of the instruments. A single value of FA can be measured by selecting specific values for the excitation and emission monochromators. FA spectra can be measured by recording the FA in a given wavelength range either in emission (FA emission spectra) or in excitation (FA excitation spectra). The meaning of these two kinds of spectra will be discussed below.

6.3.3 Fluorescence Polarization

The term polarization has been used in the previous paragraphs in a generic way, to indicate a specific spatial orientation either of an electromagnetic field or a transition moment. Indeed this word had, when associated to fluorescence a specific meaning being a size alternative to FA. Fluorescence polarization is defined as:

$$P = \frac{I_{\parallel} - I_{\perp}}{I_{\parallel} + I_{\perp}} \tag{6.15}$$

and was commonly used in the past. More recently for practical reasons FA was preferred to polarization. Conversion between anisotropy and polarization can be easily performed:

$$P = \frac{3r}{2 + r} \quad r = \frac{2P}{3 - P} \tag{6.16}$$

6.3.4 Fluorescence Anisotropy and Electronic Transition

The origin of FA is the polarization of electronic transition of molecules: to each transition is associated a vector called transition moment (see Sect. 1.5) which as a given orientation with respect to the molecular structure, In Fig. 6.15, the absorption transitions $S_0 \rightarrow S_1$ and $S_0 \rightarrow S_2$ of perylene are depicted. Transition $S_1 \rightarrow S_0$ responsible for the fluorescence is almost parallel to $S_0 \rightarrow S_1$. In general, when the deactivation of an excited state takes place radiatively, the emitted photon is polarized parallel to the transition moment. Hence, if a single molecule is observed, the polarization of the emitted light is parallel to the direction defined by the transition responsible for the fluorescence.

From the practical point of view, fluorescence measurements are carried out on a large number of molecules simultaneously; molecules which are randomly

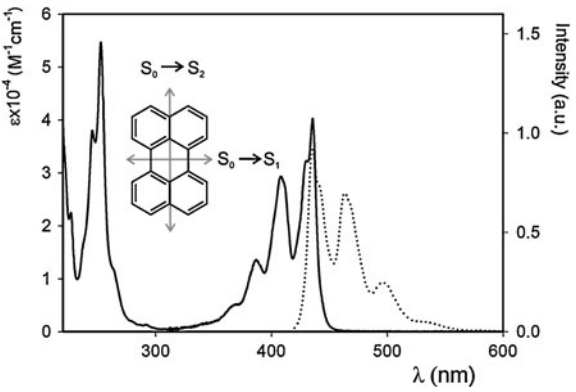

Fig. 6.15 Orientation of the electronic transition of perylene responsible for the two bands observed in the absorption spectrum (*continuous line*). The *dashed line* is the fluorescence spectrum of perylene (transition $S_1 \rightarrow S_0$)

oriented and free to rotate. Nevertheless, if excitation is performed with polarized light it is possible to observe polarized emission. This effect is the result of a preferential excitation of those molecules which have a suitable orientation with respect to the direction of the polarization of the incoming light. In order to understand better this phenomenon, it is useful to start with analyzing a simplified model namely a situation in which the fluorescent units are immobilized in a very viscous medium and are quite far from each other so that their mutual electronic interaction is very weak. If such model system is excited with non polarized light all the molecules have the same probability to be excited independently on their orientation. The situation is different in the case of polarized excitation. As in the case of the emitting dipole, also the transition moment involved in the absorption of the excitation light has a defined orientation with respect to the skeleton of the fluorophore; moreover the probability of the transition will be proportional to the component of the electric field of the excitation radiation in the direction of the dipole. As a consequence, in the case of polarized excitation, those molecules which have the transition dipole oriented parallel to the excitation field will have the highest probability to be excited while those perpendicular will have zero probability to absorb a photon (Fig. 6.16). The overall effect is the production of a population of excited fluorophores which have a preferential orientation with respect to the direction of the polarization of the excitation light. As a consequence also the emitting dipole will be oriented preferentially in a given direction (which generally is not the same of the excitation polarization) and the emitted light will be polarized. It is worth noticing that even the emission of the immobilized model system will be not polarized if the excitation is performed with unpolarized light. In that case in fact no selection is performed in the excitation and the resulting population of excited state is randomly oriented; as a consequence the electromagnetic field of the overall emission has no preferential orientation. Going more into the detail, in the case of polarized excitation, the light emitted by our model system will be polarized parallel to the excitation when the two transition moments $S_0 \rightarrow S_1$ and $S_1 \rightarrow S_0$ are parallel. More generally the angle between the direction

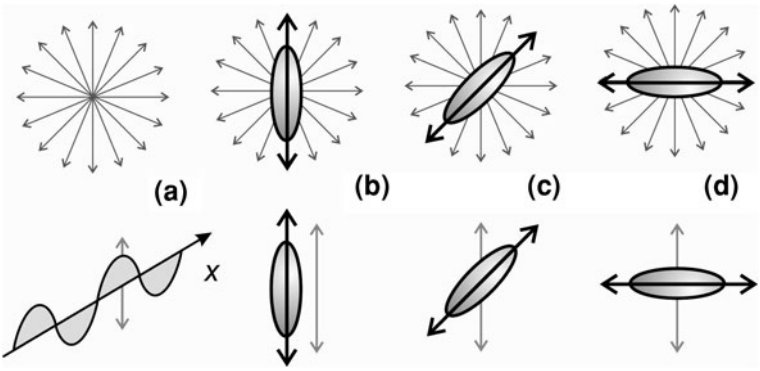

Fig. 6.16 Excitation with unpolarized (*top*) and polarized (*bottom*) light. In the former case the excitation probability is the same independently on the dipole orientation. Upon polarized excitation excitation probability is maximum in the case (**b**), zero in the case (**d**) and intermediate for (**c**)

of the polarization of the emission and of the polarization of the excitation will be the same measured between the two transition moments $S_0 \rightarrow S_1$ and $S_1 \rightarrow S_0$.

Going back to the case of perylene, for example, two transitions can be observed in the absorption spectra: the $S_0 \rightarrow S_1$ absorption band has its maximum in the blue region and a typical vibrational structure. The $S_0 \rightarrow S_2$ transition takes place in the UV and has a transition moment perpendicular to the one of $S_0 \rightarrow S_1$ which is parallel to $S_1 \rightarrow S_0$. As a consequence, if perylene is excited with polarized light in the UV region the emitting state is formed via an internal conversion process $S_2 \rightarrow S_1$ and the emitting dipole moment of the molecule is perpendicular to the polarization of the excitation. In a similar way, a different orientation of the emitting dipole for the transition $S_1 \rightarrow S_0$ with respect to the absorption one (transition $S_0 \rightarrow S_1$) can be observed in a molecule when the excited state is strongly distorted with respect to the ground state; in this case the process which causes the change of the polarization is the same that leads to the distortion, namely the vibrational relaxation. From the experimental point of view, the discussed immobilized model system can be achieved, for example, by freezing the solvent. In these conditions fluorescence anisotropy measurements allow to calculate the angle between a given transition and the one involved in the radiative deactivation. On the basis of simple geometric considerations, it becomes in fact possible to calculate what is the expected anisotropy value for an ensemble of molecules randomly oriented and unable to rotate as a function of the angle β between the excitation and emission transition:

$$r_0 = \frac{2}{5}\left(\frac{3\cos^2\beta - 1}{2}\right). \tag{6.17}$$

This value, indicated as r_0 is called fundamental anisotropy. It is worth noticing that the maximum possible value for this parameter is 0.4 and it can be observed in

the case of perfect parallelism of the two transition moment ($\beta = 0$). The minimum value, on the other hand, can be observed in the case of perpendicularity $\beta = \pi/2$ and it is -0.2. Fluorescence anisotropy values very close to 0.4 and -0.2 can be indeed measured for perylene in propylene glycol at -70 °C upon excitation of the transitions $S_0 \rightarrow S_1$ and $S_0 \rightarrow S_2$ respectively.

It is worth noting that in the case of a single fluorophore having a vertical emission transition moment, the emitted radiation is perfectly vertically polarized and, in the case of parallelism of the excitation and emission transition moment, the fluorescence anisotropy is expected to be as high as 1. The limiting value of 0.4 is hence due to the random orientation of the fluorophores. In disordered systems in fact the possibility to observe fluorescence anisotropy is due to the selective excitation performed by polarized light. Nevertheless, such selectivity is preferential but not exclusive, and also fluorophores which have a component of the transition moment parallel to the direction of polarization of the excitation different from zero are indeed excited. The emission of these fluorophore on the other hand will be polarized in a direction different with respect to the excitation. In conclusion 0.4 is the limiting value for the anisotropy of random oriented fluorophores. Value higher than 0.4 can be measured experimentally and they reveal a non random and hence preferential orientation of the fluorophore.

6.3.5 Depolarization due to Rotation

In most real systems molecules are free to diffuse and to rotate in space; this does not prevent their selective excitation with polarized light. Rotation, on the other hand, strongly influences the degree of polarization of the emitted light. During the time interval that lapse between the excitation and the emission, in fact, Brownian motion allows a reorientation of the molecule. As a consequence, the population of molecules selectively excited for their orientation becomes, after some time, a random oriented one. In particular, if excited state deactivation is much slower than rotation, most of the emission is due to this random distribution of fluorophores. The resulting phenomenon is called (together with all those processes that causes a decrease of polarization) depolarization. The deactivation rate of the excited state is conventionally indicated by the excited state lifetime τ. For a large population of molecules a fraction 1/e excited states deactivate in a time shorter than τ. In a similar way the rate of rotation can be indicated by θ which is called rotational correlation time and which is dependent on the rotational diffusion coefficient D. The dependence of the FA on these parameters is expressed by the Perrin equation and for a spherical rotor is

$$\frac{r_0}{r} = 1 + \frac{\tau}{\theta} = 1 + 6D\tau \tag{6.18}$$

where r_0 is the fundamental anisotropy.

6.3.6 Depolarization due to Energy Transfer

Energy transfer between equal fluorophores (homo-energy transfer) is an important depolarization mechanism. As a consequence, this process which does not lead to any change of photophysical properties such as fluorescence quantum yield or excited state lifetime can be investigated using FA. As in the case of rotation, homo energy transfer becomes relevant in causing depolarization only when it is faster than excited state deactivation. Also in the case of energy transfer it is possible to use FA measurements to calculate the rate constant of the process.

6.3.7 Emission Anisotropy Spectra

Equation 6.14 suggests that emission anisotropy spectra can be obtained starting from two emission spectra recorded with the excitation polarizer vertically oriented and the emission one vertical (I_{VV}) and horizontal (I_{VH}), respectively. The FA can be hence calculated supposing that $I_{VV} = I_{\parallel}$ and $I_{VH} = I_{\perp}$. Indeed, from the practical point of view, if the FA spectrum of a sample with no FA is measured in such a way, a false spectrum with FA different from zero is obtained. This deviation is caused by an instrumental effect due to the intrinsic anisotropy of the analysis system. The emission monochromator in particular is a strongly anisotropic object which has a different response to light depending on its polarization. As a consequence, in the case in which the vertical and horizontal components of the emission have the same intensities, two different signal for the two components are indeed measured. It becomes hence necessary to correct the intensities of the vertical and horizontal components in order to take into account the instrumental anisotropy. The correction can be done introducing two correction factor S_V and S_H in such a way that:

$$\frac{I_{VV}}{I_{VH}} = \frac{S_V I_{\parallel}}{S_H I_{\perp}} = G\frac{I_{\parallel}}{I_{\perp}} \tag{6.19}$$

From the practical point of view it is not necessary to determine the value of both S_V and S_H since only their ratio (conventionally referred to as G factor) appears in the expression of the FA.

$$r = \frac{I_{VV} - GI_{VH}}{I_{VV} + 2GI_{VH}} \tag{6.20}$$

Once G is defined and determined it becomes possible to express r as a function of the two experimental spectra I_{VV} and I_{VH}. Of course G is a wavelength dependent factor which is characteristic of the instruments and once it has been determined for a sample it can be used to correct the FA of other samples.

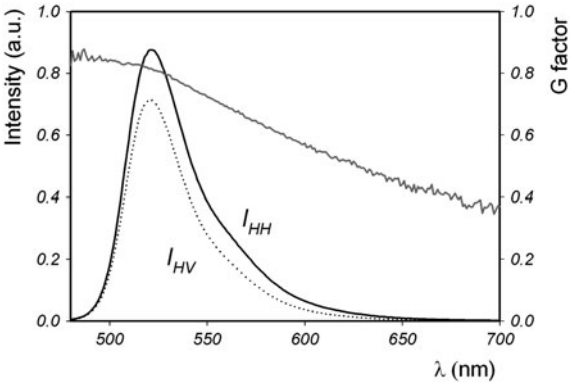

Fig. 6.17 G factor calculated for a propylene glycol solution of fluorescein (1×10^{-5} M) at room temperature. Fluorescence spectra were recorded with a fluorimeter Edinburgh FLS920P

6.3.8 The G Factor

As already mentioned G is purely an instrumental factor which must be known in order to perform correct FA measurements. Its determination is quite simple thanks to the fact that when excitation is performed with horizontally polarized light (instead than vertical) the vertical and horizontal component of the emitted light are expected to be equal, independently on the properties of the sample. A difference between the measured intensities is hence, in this excitation condition, due exclusively to instrumental effect and it can be used to obtain the G factor.

$$G = \frac{I_{HV}}{I_{HH}} \tag{6.21}$$

It is hence possible to calculate the G factor in a given spectral range by recording the fluorescence spectra of a sample which emits in that spectral window keeping the excitation polarizer in the horizontal position and the emission one first horizontal and then vertical. Indeed it is usually convenient to measure the G factor using the same sample under investigation. In this case it is necessary to record four different luminescence spectra exactly in the same experimental conditions changing the orientation of the two polarizer in all the possible combination. Two of the four spectra are used to calculate the G factor (Eq. 6.21) and the other two to calculate the anisotropy. In alternative it is possible to express the anisotropy as a function of the four spectra.

$$r = \frac{I_{VV}I_{HH} - I_{VH}I_{HV}}{I_{VV}I_{HH} + 2I_{VH}I_{HV}} \tag{6.22}$$

Figure 6.17 shows the dependence of the G factor on the wavelength. The curve was obtained using a solution of fluorescein in propylene glycol. This solvent is often used to study fluorescence anisotropy because of its high viscosity which slows down depolarization processes due to rotation allowing to investigate them

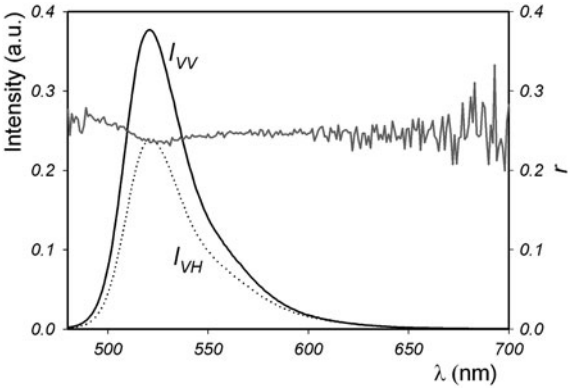

Fig. 6.18 FA spectrum of a propylene glycol solution of fluorescein (1×10^{-5} M) at room temperature ($\lambda_{exc} = 470$ nm). Fluorescence spectra were recorded with a fluorimeter Edinburgh FLS920P and combined using the G factor of Fig. 6.17

even with steady state techniques. In the case of fluorescein (see Fig. 6.18) fluorescence anisotropy in propylene glycol is quite high $r = 0.24$ near the fluorescence maximum. Knowing the excited state lifetime $\tau = 3.6$ ns and the value of the fundamental anisotropy $r_0 = 0.375$ it is possible from Eq. 6.18 to calculate the rotational correlation time $\theta = 6.5$ ns.

6.3.9 Calculation of the Emission Anisotropy Spectra

In order to get the anisotropy spectra it is possible to combine the fluorescence intensity ones either manually or automatically. The manual procedure required the setting of the polarizers in the four combinations reported above and their elaboration with a suitable software. In the case of the automatic acquisition it is the same software that control the instrument that set the sequential acquisition of the spectra controlling the polarizers and giving, at the end, directly the anisotropy spectrum. The direct acquisition of anisotropy is available for several instruments and is surely convenient from the operative point of view. Nevertheless, it is important to examine critically the anisotropy spectra obtained in such automatic modality.

In particular, it is very important to consider that anisotropy is calculated starting from fluorescence intensities spectra according to Eqs. 6.20 or 6.22 and it is significant only in those spectral regions where these signals are due to the samples and not to instrumental effects. Noise due to the detector and scattering produce signals that when combined give anisotropy values completely different from those of the sample. In the case of scattering of the excitation beam, for example, the diffused light which reached the detector is strongly polarized and if its contribution is relevant in the emission spectral window anisotropy is overestimated. Background signal, on the other hand, usually is not subtracted by the acquisition software during the calculation of the anisotropy. Its contribution can become dominant when the fluorescent signal is weak.

6.3.10 Effect of Concentration and Scattering on the Anisotropy

A bad alignment of the polarizer can cause errors in the determination of FA. In general, the use of efficient polarizers, the control of the alignment and the correction for the G factor allow to avoid false measurements due to instrumental effects. Some other aspects related to the sample must be considered in order to get reliable FA measurements. In particular, re-absorption and scattering cause a trivial depolarization of the fluorescence. Fortunately these effects can be reduced simply by diluting the samples. Errors in the determination of the FA can also be caused by saturation of the detector. Since the signals combined to calculate FA have usually very different intensities it is necessary to check that the saturation of the photomultiplier is avoided in each of the configurations of the polarizers. Saturation can be easily avoided by reducing the sizes of the slits. It is worth noting that FA measurements, in the absence of re-absorption and scattering and in the case of non interacting molecules do not depend on the concentration.

6.3.11 Instrumental Configurations

The L configuration is typically used in commercial fluorimeters and can be used to measure FA simply by equipping the instruments with a pair of polarizer. In this configuration a single detection channel is available. The different spectra necessary to calculate the FA are recorded sequentially. As a consequence, the FA spectra obtained with an L configuration are the combination of intensity spectra measured in different moments. It is hence necessary in order to have reliable results to use exactly the same experimental conditions. AT configuration, on the other hand allows simultaneous detection of two intensity signals. The required instrumentation is more complicated and more expensive since it requires two emission polarizer and two independent detectors. Compact commercial fluorimeter usually cannot be set in T configuration which, on the other hand, can be achieved with modular instruments.

6.3.12 Fluorescence Anisotropy of a Mixture of Fluorophores

The FA spectrum of a solution in which are present different fluorescent molecules is an average of the FA spectra where a weight factor f_i is introduced which takes into account the fraction of light intensity emitted by the i-th species in the considered experimental conditions

$$\langle r \rangle = \sum\nolimits_i f_i r_i. \tag{6.23}$$

6.3.13 Excitation Anisotropy Spectra

As previously discussed the value of FA, if depolarization due to rotation and energy transfer are prevented, just depend on the angle between the excitation and the emission dipole moments according to Eq. 6.17. The ideal situation of an ensemble of non interacting fluorophores randomly oriented and immobilized in space can be achieved with good approximation by freezing diluted solution of the species under investigation. In this conditions it is possible to obtain information about the relative orientation of the different transition of a molecule with respect to the emitting dipole by collecting an excitation r spectrum. The procedure followed to obtain such a spectrum is analogous to the one used for emission r spectra with the only difference that in this case the emission monochromator is set to a fixed value while the excitation wavelength is changed in a given range.

From the experimental point of view the most critical point is the preparation of the sample. Only solvents that form a limpid matrix (such as propylene glycol at −70°C) can be used since scattering would seriously interfere with the measurement. Figure 6.19 shows the excitation spectrum of fluorescein in this solvent. Despite the spectrum has been recorded at room temperature for simplicity, it is possible to observe clearly the strong dependency of the anisotropy on the excitation wavelength. Thanks to the high viscosity of the medium in fact the rotation rate is low and a negative value of the anisotropy about −0.1) can be measured in the UV region while r reached a quite high value (about 0.25) upon excitation in the visible. The spectrum has been corrected for the G factor at the emission wavelength (550 nm). It is worth to recall that G does not depend on the excitation wavelength.

6.3.14 Time Resolved Fluorescence Anisotropy

In the previous paragraphs we have discussed the basic aspects of steady state fluorescence anisotropy. It is, on the other hand possible to investigate the time dependency of the FA anisotropy of a system excited with a pulsed source [46] This technique allows to study the rate of the operating depolarization processes and becomes very useful especially in those cases in which excited states deactivation is much slower than depolarization. In such a situation, in fact, most of the light emitted is not polarized and steady state techniques give poor information.

6.3.15 Fluorescence Anisotropy Decay

Steady state anisotropy measurements are usually performed using a continuous excitation source. Such measurements are quite simple and require inexpensive instrumentation. Nevertheless SS techniques do not allow actually to follow the

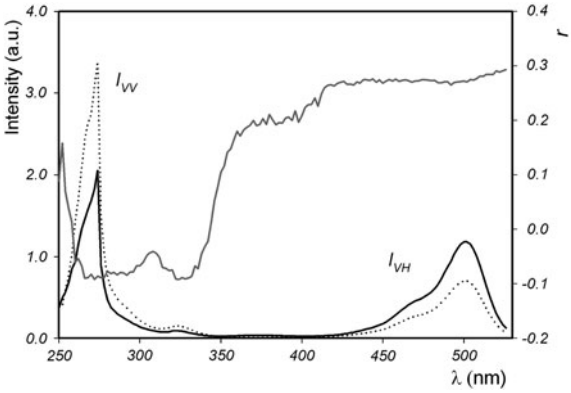

Fig. 6.19 FA excitation spectrum of a propylene glycol solution of fluorescein (1×10^{-5} M) at room temperature ($\lambda_{em} = 550$ nm). Fluorescence spectra were recorded with a fluorimeter Edinburgh FLS920P and combined using the G factor of Fig. 6.17

depolarization kinetics and give results that cannot always be univocally interpreted. In particular when depolarization is very fast, the fraction of polarized light is so small to become unimportant in comparison to the unpolarized component and zero anisotropy is measured. This is what happens in the case of many fluorophores in solution. Going back to fluorescein, when the high viscosity solvent is replaced by water the value of θ decreases enormously and the ratio r_0/r in Eq. 6.18 greatly increases giving a value of r very close to zero. As already mentioned FA decay can be investigated using pulsed technique. This approach allows to obtain results that, for simple systems, can be easily interpreted and discussed. The excitation is performed with a light pulse vertically polarized and the decays of the vertical and horizontal components of the emitted light are recorded sequentially (in the case of a L geometry) or simultaneously (T geometry). The two decays are then combined to calculate the anisotropy decay.

$$r(t) = \frac{I_{\parallel}(t) - I_{\perp}(t)}{I_{\parallel}(t) + 2I_{\perp}(t)} \tag{6.24}$$

The two components can be recorded with a 'pump and probe' system or with a time correlated single photon counting (TCSPC) device. As in the case of SS FA the correction due to the G factor must be taken into consideration.

$$r(t) = \frac{I_{VV}(t) - GI_{VH}(t)}{I_{VV}(t) + 2GI_{VH}(t)} \tag{6.25}$$

6.3.16 *Fundamental Fluorescence Anisotropy in Time-Resolved Measurements*

As already discussed for SS FA, polarized excitation produces a population of preferentially oriented excited states. As a consequence, if the excitation pulse is

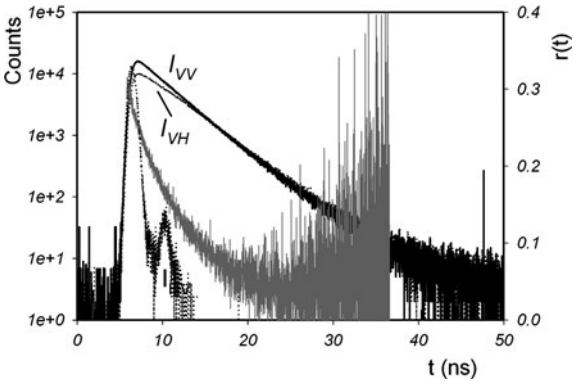

Fig. 6.20 FA decay (in *gray*) of a propylene glycol solution of fluorescein (1×10^{-5} M) at room temperature ($\lambda_{em} = 550$ nm). Fluorescence spectra were recorded with a fluorimeter Edinburgh FLS920P and combined using the G factor of Fig. 6.17

short enough, the anisotropy measured during the excitation will be the one of the system before depolarization takes place and hence the fundamental FA r_0 as defined in Eq. 6.17. Nevertheless depolarization process are often very fast and instruments with very short response are needed. Figure 6.20 shows the anisotropy decay observed for fluorescein in water together with the instrumental response to the excitation pulse. The initial value of the anisotropy is significantly lower than r_0. In this case in fact the instrumental profile is broader than the time constant of the anisotropy decay and the FA averaged in a time interval long enough to allow depolarization. As for excited state lifetime measurements the actual profile can be recovered by deconvolution.

6.3.17 Acquisition of the Decay

FA decay can be acquired using a TCSPC equipped with two polarizers for the excitation and emission respectively. Also in this case two signals are measured setting the polarizer first parallel and then perpendicular. The decay of the anisotropy is calculated from the two intensity decays. If an L geometry is used and the two traces are measured sequentially it is important to use the same experimental conditions and in particular the same acquisition time for both measurements.

6.3.18 Interpretation of the Results

The interpretation of the anisotropy decay can be, in the case of multi-coponent systems, very complicated and require the use of specific software especially when deconvolution is needed. Nevertheless in the case of depolarization due to rotation

and approximating the fluorophore to a spherical rotor a quite simple model can be used to interpolate the experimental decay.

$$r(t) = r_0 e^{-t/\theta} \tag{6.26}$$

This simple model have been used to interpolate the decay of fluorescein of Fig. 6.20 giving $\theta = 6.3$ ns, in good agreement with the SS measurement.

References

1. Djerassi C (1960) Optical rotatory dispersion: applications to organic chemistry. McGraw-Hill, New York
2. Mason SF (1982) Molecular optical activity and the chiral discriminations. Cambridge University Press, Cambridge
3. Rodger A, Norden B (1997) Circular dichroism and linear dichroism. Oxford University Press, Oxford
4. Berova N, Nakanishi K, Woody RW (eds) (2000) Circular dichroism: principles and applications, 2nd edn. Wiley-VCH, New York
5. Riesgo EC, Credi A, De Cola L, Thummel RP (1998) Inorg Chem 37:2145–2149
6. Gawroński J, Grajewski J (2003) Org Lett 5:3301–3303
7. Mason SF (1975) Chem Phys Lett 32:201–203
8. Mendicuti F, González-Álvarez MJJ (2010) Chem Ed 87:965–968
9. Marconi G, Mezzina E, Manet I, Manoli F, Zambelli B, Monti S (2011) Photochem Photobiol Sci 10:48–59
10. Gao G, Ma X, Zhang Q, Wang Q, Qu D, Tian H (2011) Org Biomol Chem 9:1126–1132
11. Schippers PH, Dekkers HPJM (1981) Anal Chem 53:778–782
12. Norden B, Seth S (1985) Appl Spectrosc 39:647–650
13. Konno T, Meguro H, Tuzimura K (1975) Anal Biochem 67:226–232
14. Takakuwa T, Konno T, Meguro H (1985) Anal Sci 1:215–218
15. DeTar DF (1969) Anal Chem 41:1406–1408
16. McCaffery AJ, Mason SF (1963) Mol Phys 6:359–362
17. Belser P, Daul C, Von Zelewsky A (1981) Chem Phys Lett 79:596–598
18. Lightner DA, Gurst JE (2000) Organic conformational analysis and stereochemistry from circular dichroism spectroscopy. Wiley-VCH, New York
19. Harada N, Nakanishi K (1983) Circular dichroic spectroscopy. exciton coupling in organic stereochemistry. University Science Books, Mill Valley
20. Fasman GD (ed) (1996) Circular dichroism and the conformational analysis of biomolecules. Plenum, New York
21. Ashton PR, Balzani V, Clemente-Leon M, Colonna B, Credi A, Jayaraman N, Raymo FM, Stoddart JF, Venturi M (2002) Chem Eur J 8:673–684
22. Connors KA (1997) Chem Rev 97:1325–1357
23. Richardson FS, Riehl JP (1977) Chem Rev 77:773–792
24. Riehl JP, Richardson FS (1986) Chem Rev 86:1–16
25. Dekkers HPJM (2000) Circularly polarized luminescence: a probe for chirality in the excited state. In: Berova N, Nakanishi K, Woody RW (eds) Circular dichroism: principles and applications, 2nd edn. Wiley-VCH, New York, pp 185–215
26. Steinberg I, Gafni A (1972) Rev Sci Instrum 43:409–413
27. Thompson NC, Parker D, Schmitt-Willich H, Suelzle D, Muller G, Riehl JP (2004) Dalton Trans 12:1892–1895
28. Mamula O, Lama M, Telfer SG, Nakamura A, Kuroda R, Stoeckli-Evans H, Scopelitti R (2005) Angew Chem Int Ed 44:2527–2531

29. Gawryszewska P, Sokolnicki J, Dossing A, Riehl JP, Muller G, Legendziewicz J (2005) J Phys Chem A 109:3858–3863
30. Gregolinski J, Starynowicz P, Hua KT, Lunkley JL, Muller G, Lisowski J (2008) J Am Chem Soc 130:17761–17773
31. Coruh N, Riehl JP (1992) Biochemistry 31:7970–7976
32. Meskers SCJ, Dekkers HPJM (2001) J Phys Chem A 105:4589–4599
33. Gunde KE, Credi A, Jandrasics E, von Zelewsky A, Richardson FS (1997) Inorg Chem 36:426–434
34. Meskers SCJ, Dekkers HPJM, Rapenne G, Sauvage J-P (2000) Chem Eur J 6:2129–2134
35. Field JE, Muller G, Riehl JP, Venkataraman D (2003) J Am Chem Soc 125:11808–11809
36. van Delden RA, Huck NPM, Piet JJ, Warman JM, Meskers SCJ, Dekkers HPJM, Feringa BL (2003) J Am Chem Soc 125:15659–15665
37. Marletta A, Goncalves D, Oliveira ON, Faria RM, Guimaraes FEG (2001) Synth Met 119:207–208
38. Gussakovsky EE, Salakhutdinov BA, Shahak Y (2002) Funct Plant Biol 29:955–963
39. Imai Y, Kawano K, Nakano Y, Kawaguchi K, Harada T, Sato T, Fujiki M, Kuroda R, Matsubara Y (2008) New J Chem 32:1110–1112
40. Metcalf DH, Snyder SW, Wu S, Hilmes GL, Riehl JP, Demas JN, Richardson FS (1989) J Am Chem Soc 111:3082–3083
41. Maupin CL, Meskers SCJ, Dekkers HPJM, Riehl JP (1996) Chem Commun 2457–2458
42. Horng ML, Gardecki JA, Maroncelli M (1997) J Phys Chem A 101:1030–1047
43. Montalti M, Dolci LS, Prodi L, Zaccheroni N, Stuart MCA, van Bommel KJC, Friggeri A (2006) Langmuir 22:2299–2303
44. Rampazzo E, Bonacchi S, Juris R, Montalti M, Genovese D, Zaccheroni N, Prodi L, Rambaldi DC, Zattoni A, Reschiglian P (2010) J Phys Chem B 114:14605–14613
45. Jameson DM, Ross JA (2010) Chem Rev 110:2685–2708
46. Suhling K, French PMW, Phillips D (2005) Photochem Photobio Sci 4:13–22

Chapter 7
Time-Resolved Luminescence Techniques

Alberto Juris and Mauro Maestri

Abstract This chapter provides an overview of the principles and techniques used to measure the excited state lifetime of luminescent species. After a brief review of general concepts (simple decay scheme for an excited state, first order kinetic equations), the most important experimental methods used for lifetime measurement are illustrated, considering both *time-domain techniques* (single flash, gated sampling, time correlated single photon counting) and *frequency-domain techniques* (phase shift). Appropriate examples are given to illustrate the peculiarities of the different techniques. A practical example taken from the literature is detailed, to show how lifetime measurements can help investigation of supramolecular systems. A list of standard compounds commonly used to check the performance of the equipment is given.

7.1 General Concepts

As already discussed in Chap. 1, a generic excited state *A can follow any of the three deactivation pathways shown in Fig. 7.1: (1) *photochemical reaction*, i.e. a chemical reaction where *A is transformed into the generic product P; (2) *radiationless deactivation*, a process where the excitation energy contained in *A is dissipated in the surrounding medium as vibrational energy and is transformed into

A. Juris (✉) · M. Maestri
University of Bologna, "G. Ciamician" Chemistry Department, via Selmi 2,
I-40126 Bologna, Italy
e-mail: alberto.juris@unibo.it

M. Maestri
e-mail: mauro.maestri@unibo.it

P. Ceroni (ed.), *The Exploration of Supramolecular Systems and Nanostructures by Photochemical Techniques*, Lecture Notes in Chemistry 78,
DOI: 10.1007/978-94-007-2042-8_7,

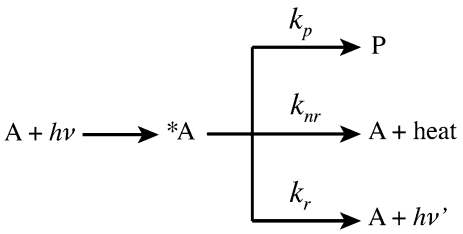

Fig. 7.1 A generic excited species *A can decay following three main deactivation paths

heat; and (3) *radiative deactivation*, a process giving rise to *luminescence*: the surplus energy of the excited state is released by emitting a photon whose energy is $h\nu$'.

The observed luminescence can be characterized using two types of measurements. The most common one characterizes the energy profile of the emission by measuring its intensity as a function of wavelength. In this way, emission and/or excitation spectra can be recorded, as previously illustrated in Chap. 5. The second type of measurement is less common, because it requires a more sophisticated instrumentation, and defines the temporal characteristics of the emission by measuring its intensity as a function of time.

The processes shown in Fig. 7.1 are governed by their monomolecular rate constant (k_p, k_r, and k_{nr}). Typically, the three processes are in competition among themselves, and the value of the rate constants will determine the actual behavior of the excited molecule. In cases such as that outlined here, each of the three processes follows a first-order kinetics, and thus the concentration of the excited state also decays following a first-order kinetics, with a *lifetime* (τ), which is defined as

$$\tau = \frac{1}{\sum k} = \frac{1}{k_p + k_r + k_{nr}} \tag{7.1}$$

As it can easily be seen, the lifetime τ is the time required to reduce the excited state concentration by an e factor. Indeed, simple kinetic treatment of the reaction scheme of Fig. 7.1 leads to Eq. 7.2. Integration of Eq. 7.2 gives rise to Eq. 7.3, where it can be seen that $[^*A]/[^*A]_0 = 1/e$ is obtained when $t = \tau$.

$$\frac{d[^*A]}{dt} = -(k_p + k_r + k_{nr})[^*A] = -\sum k[^*A] \tag{7.2}$$

$$[^*A] = [^*A]_0 \exp(-\sum kt) \tag{7.3}$$

Figure 7.2 illustrates graphically the decay of the excited state concentration following Eq. 7.3.

The lifetime of an excited state can be calculated by measuring its concentration as a function of time. Most lifetime-measuring techniques are indeed based on the recording of the excited state concentration as a function of time, and are collectively referred to as *time-domain measurements*. The techniques described

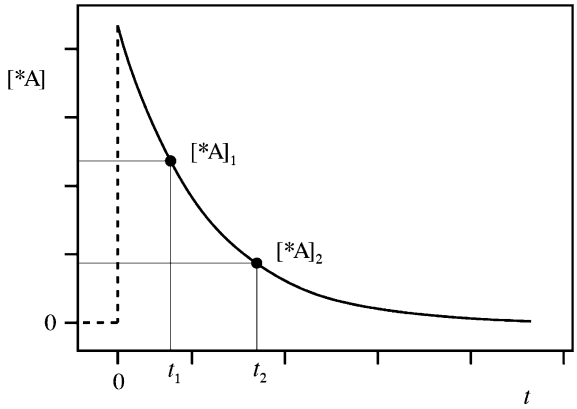

Fig. 7.2 Variation of the concentration of the excited species *A as a function of time. Following an ideally instantaneous excitation, *A is formed at $t = 0$ (*dashed line*). Then, the concentration of *A decays exponentially, in accordance with a first order kinetics (*continuous line*). After a lifetime $\tau = t_2 - t_1$ the excited state concentration is reduced by an e factor ($[*A]_2 = [*A]_1/e$)

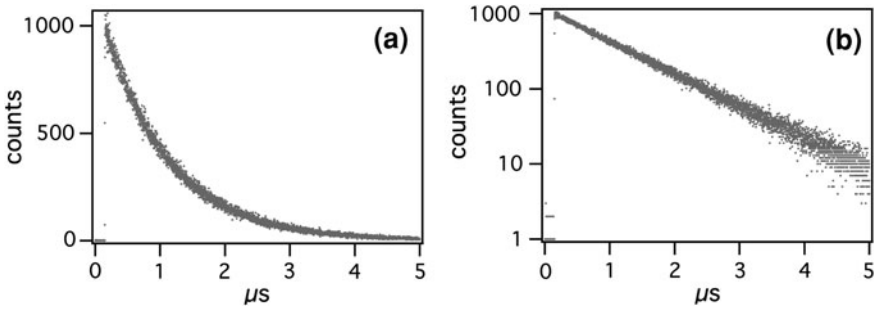

Fig. 7.3 Emission decay of $[Ru(bpy)_3]^{2+}$ in deaerated acetonitrile solution, at room temperature. Excitation at 355 nm and emission at 610 nm. The same data are represented with a linear (**a**) or logarithmic (**b**) emission intensity scale

herein try to rebuild the decay curve by measuring the luminescence emission of the excited state as a function of time, as at any time a direct proportionality exists between the number of emitted photons and the number of excited states present. Thus, taking into account that $\Sigma k = 1/\tau$ (from Eq. 7.1), and substituting the excited state concentration with the emission intensity, Eq. 7.3 can be rewritten as Eq. 7.4, or also as Eq. 7.5 in logarithmic form:

$$I(t) = I_0 \exp(-t/\tau) \tag{7.4}$$

$$\ln I(t) = \ln I_0 - t/\tau \tag{7.5}$$

Equation 7.5 reveals that a logarithmic plot of the decay intensity as a function of time gives a straight line whose slope is $-1/\tau$. Figure 7.3 shows the different appearance of these plots using a linear or logarithmic scale for the emission intensity.

It is worth noting that the equations introduced above are based on the assumption that the excited state decays following a first order kinetics. In more complex cases, multi-exponential or non-exponential decays can also be observed; such cases are briefly mentioned in Sect. 7.3. Moreover, it must be underlined that lifetime depends on temperature, being a quantity derived from kinetics. Thus, temperature must always be specified together with the lifetime values obtained.

In addition to the time-domain techniques, a luminescence lifetime can be measured also using the so-called *frequency-domain techniques*, based on the phase shift occurring between excitation and emission when the excitation intensity is suitably modulated.

In any case, taking into account both time-domain and frequency-domain techniques, there are basically four methods to measure the lifetime of an excited state, as described in detail in the next Sect. 7.2. The first three methods use the time-domain approach to rebuild the intensity-time curve; the fourth one uses the frequency-domain approach and is based on the phase shift between excitation and emission.

7.2 Experimental Methods for Lifetime Measurements

7.2.1 Single Flash

This is the most direct way to measure a lifetime. The excited species *A is generated with a single flash of exciting radiation, and its luminescence is then monitored as a function of time using a photomultiplier. It is therefore essential that the excitation source is intense enough to create a concentration of excited states that can be detected by the analysis system, and that the pulse duration is shorter than the lifetime to be determined. Nowadays, the signal-to-noise ratio is often improved by averaging the signal acquired following n (4, 10, 32, or even more) single excitation flashes.

Figure 7.4 illustrates the block diagram of a typical equipment for the measurement of lifetimes ranging from nanoseconds to microseconds (and also longer). For this time range several kinds of exciting lasers are available, with a pulse duration of 5–50 ns (see Chap. 3 and Refs. [1, 2]). For example, the Nd/YAG laser is a very versatile possibility, featuring a pulse duration of the order of 10 ns, and an excitation wavelength that can be selected among the following values: 1064 (fundamental line), 532, 355, and 266 nm. A conventional photomultiplier can be used as a detector, and digital oscilloscopes with a time response appropriate for the lifetime to be determined are also commercially available. The experimental data

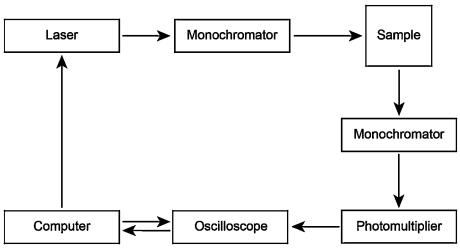

Fig. 7.4 Block diagram of the single flash lifetime equipment

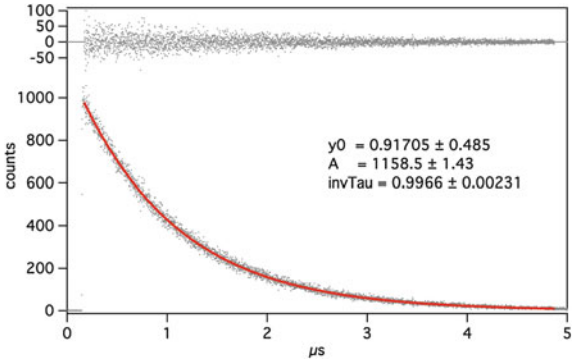

Fig. 7.5 Luminescence decay of $[Ru(bpy)_3]^{2+}$ in deaerated acetonitrile solution at room temperature. Excitation at 355 nm (Nd/YAG laser), emission at 610 nm; average of 32 laser pulses

acquired by the oscilloscope are usually analyzed with a computer, by means of software supplied with the apparatus.

An example of this kind of measurement is illustrated in Fig. 7.5, where the room-temperature luminescence decay of $[Ru(bpy)_3]^{2+}$ in deaerated acetonitrile solution is shown, collecting and averaging the signal of 32 laser pulses. The measured luminescence intensity (gray data) decays exponentially, as the intensity scale is linear. Analysis of this data with an exponential fit gives the results shown in the figure, which correspond to the curve overlapping the experimental points. The lifetime value is calculated as 1/invTau = 1.0034 μs (see Fig. 7.5), and this result must be reported as $\tau = 1.00$ μs. Analysis of the residuals is shown in the upper part of the figure; this is a plot of the difference between calculated and experimental intensity values. When the fit is good, as in this case, the residuals are randomly and evenly distributed around zero.

Lifetimes shorter than a nanosecond can be measured using picosecond lasers with suitable detectors (streak camera) [3], bearing in mind that, as a rule of thumb, the cost of the equipment is inversely proportional to its time resolution. However, the measurement of lifetimes shorter than a nanosecond is most commonly performed with a single photon apparatus (see Sect. 7.2.3). Lasers with pulse duration shorter than 100 femtoseconds (1 fs = 1×10^{-15} s) are also available, but with such equipment the sample emission cannot be monitored for technical reasons, and transient absorption must be measured instead (see Chap. 8).

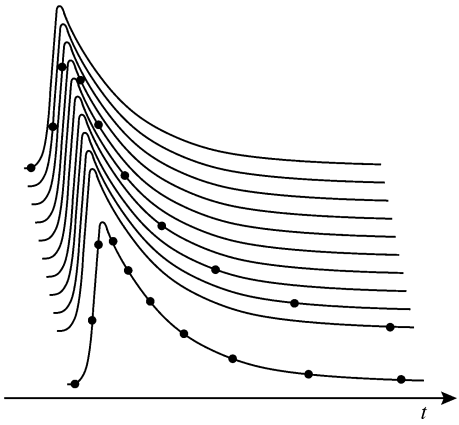

Fig. 7.6 Operating principle of a gated sampling acquisition. The decay curve (*bottom curve*) is recovered by plotting the emission intensity as a function of the delay time with respect to excitation pulse

7.2.2 Gated Sampling

The block diagram of this kind of equipment is essentially the same of the previous case (Fig. 7.4), but the method requires a repetitive source and uses gated sampling. Following excitation, the emission intensity of the sample is measured after a certain *delay time* t_1 during a time window Δt (*gate time*), which must be short with respect to the sample lifetime. Usually, this acquisition is performed by collecting and averaging the signal of many excitation pulses, in order to improve the signal-to-noise ratio. The measurement is then repeated several times, by shifting the acquisition window Δt towards delay time values (t_2, t_3, … t_n) that are gradually increasing with respect to excitation. The shape of the decay curve is then recovered by plotting the emission intensity values as a function of the delay time, as illustrated in Fig. 7.6.

Sources featuring good frequency and intensity stability are necessary to recover a reliable decay curve. The time resolution of the equipment is affected by time duration of the pulse and by time resolution of the oscilloscope. At present, a time resolution of about 20 ns can be achieved.

The gated sampling approach is used also in commercial spectrofluorimeters, if the excitation source is a pulsed lamp; in this case lifetime values ranging approximately from 0.1 ms to 100 s can be determined. Such spectrofluorimeters can also perform time-resolved spectroscopy, and can thus easily record the emission spectrum of long-lived excited states by suppressing the emission from short-lived species. For example, phosphorescence spectra can be easily separated from fluorescence spectra. In medical diagnostics these instruments are suitable for techniques such as fluroimmunoassay with lanthanides (for details see Ref. [3]).

Figure 7.7 illustrates an example of a lifetime measurement performed on a Perkin-Elmer LS-50 spectrofluorimeter. The sample is biacetyl at room temperature. Emission intensity is recorded at 525 nm, gate time is 0.1 ms. The decay

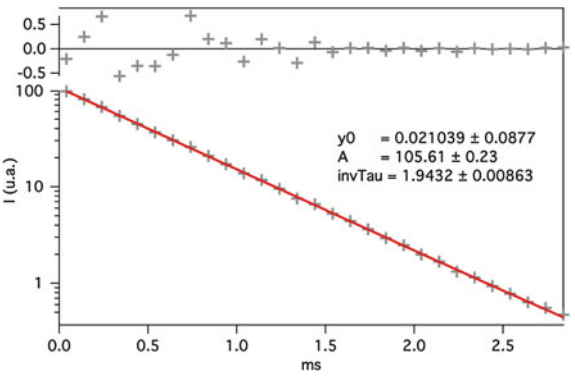

Fig. 7.7 Phosphorescence decay of biacetyl in deaerated dichloromethane solution at room temperature, emission at 525 nm. Experiment performed on a Perkin-Elmer LS-50 spectrofluorimeter

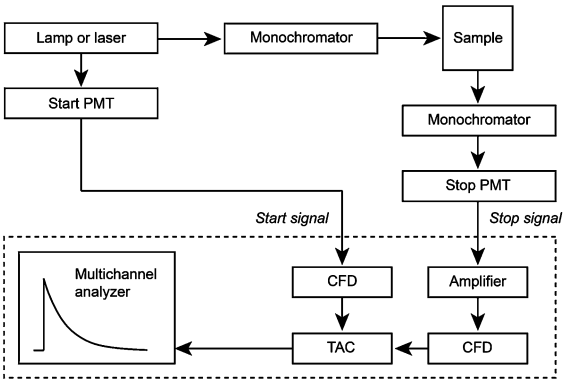

Fig. 7.8 Schematic block diagram of a "single photon" counting apparatus. See text for the abbreviations used

appears linear on a logarithmic scale; data analysis confirms the monoexponential nature of the decay. The lifetime obtained from data fitting is 0.515 ms; it is worth noting that lifetimes in this time range cannot be measured with single photon techniques, see next section.

7.2.3 Single Photon

The technique known as "time correlated single photon counting" is based on the probability that one (single) photon emitted by a luminescent sample could be detected by a highly sensitive photomultiplier. This probability is statistically bound with the change in the emitting excited state concentration with time by a specific operative procedure.

A block diagram of a "time correlated single photon counting" apparatus is shown in Fig. 7.8; there is the housing of a pulsed light source directly connected to a light detector (called start photomultiplier, start PMT), an optional (exciting)

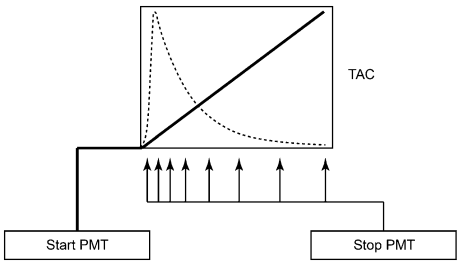

Fig. 7.9 Working principle of the time-to-amplitude-converter. For details, see text

monochromator, a sample holder, an optional but useful (emitting) monochromator, a second light detector (usually a photomultiplier called stop PMT) and a complex electronic system for a proper treatment of the photomultiplier's signals. At a first glance it looks like an usual instrument for luminescence detection; but it actually differs for (i) the properties of the exciting light source; (ii) the presence of the start PMT; (iii) the properties of the stop PMT; (iv) an unusual treatment of the PMT signals made by the final electronic system.

The exciting light source is usually a low pressure lamp where the discharge between two electrodes in a gas atmosphere (nitrogen, deuterium, hydrogen, etc.) produces light pulses with high repetition rate (frequency 1–100 kHz), short duration (1–5 ns), very low intensity and high stability. At present, small lasers are used with similar pulse characteristics.

The start PMT, usually a side on photomultiplier, displays electric signals (pulses) having the same frequency of the light source with which it is optically connected. Each pulse starts a time cycle whose duration is selected a priori and always lies within two consecutive pulses. The optimum time cycle duration is approximately 5–6 times the emission lifetime of the sample under investigation.

The stop detector, usually a high gain ($>10^{12}$) photomultiplier (nowadays also a microchannel plate), displays an electric signal (a pulse) when hit by the first (and lonely) photon; this pulse stops the time cycle initiated by the start signal; then the detector quits until a subsequent start signal begins a new excitation-emission cycle.

The final electronic system, inside the dashed rectangle in Fig. 7.8, incorporates two constant fraction discriminators (CFD), a time-to-amplitude-converter (TAC) and a multichannel analyzer (MCA).

The two CFD, one for the start and one for the stop signals, do not allow the cycle to be considered when one of the two signals (mainly the stop) does not reach a threshold value. This procedure reduces dark current effects.

The TAC is the heart of the instrumentation and it works like a stopwatch, even though very sophisticated; indeed, by elaborating the signals coming from the start and stop photomultipliers, the TAC measures, within a single excitation-emission cycle, the time difference (Δt, usually in nanoseconds range) between the stop and start signals, i.e. the delay between the exciting photons (start signal) and the specific, single (and lonely) photon causing the stop signal.

Finally, the MCA receives (and collects) the time delays (Δt) from TAC organizing them in a plot showing the number of times that a single photon is seen by the stop PMT at a given Δt.

Ultimately, the apparatus works as follows; the exciting lamp fires a light flash, the start PMT sees it and send an electric signal to the TAC where it starts a time cycle of a selected (predetermined) duration by generating, in a proper circuit, an electric potential (voltage) which increases linearly with time (Fig. 7.9). The electric potential increase can be stopped only by two events: (i) the end of the selected time cycle; (ii) an electric signal from the stop PMT. In the former case nothing else happens, while in the latter the TAC sends a signal to the MCA that records it simply as an event occurring at a time defined by the electric voltage at which the TAC has been stopped. Then, in both cases, the TAC is reset so as to wait for a new start signal beginning another time delay measurement. This procedure is repeated a number of times, depending on the time frequency of the exciting source, and allows the accumulation of a huge number of points in a plot showing the number of emitted photons versus time delay. It should be pointed out that this plot closely describes the time decay curve of an emitting excited state only if the stop/start signals ratio is $\leq$0.02, i.e. only when the 98% of the cycles go to the end time without any interruption of the potential increase in the TAC by stop signals (98% of the times the stop PMT does not see emission from the excited sample). In other words, by setting the stop/start signals ratio at $\leq$0.02 we faithfully reproduce the excited state decay because in this way each single emitted photon has the same probability to be seen independently of the emission moment. No matter if, for practical, operational reasons the selected time cycle only allows the detection of the first photons, 98% of the time is allowed for the possible detection of laggard photons, i.e. even a photon emitted well out of the selected time cycle would have a finite probability of being seen by the stop PMT if it would not be blind.

Indeed, working at stop/start ratio higher than 0.02 the first emitted photons have a greater possibility of being seen with respect to those emitted later, thus causing a shortening of the emission lifetimes. As a limiting case, for a stop/start ratio of 1, the decay curve would reduce to a line close to the excitation light flash, since the only photon seen by the stop PMT would be the first one emitted by the sample immediately after its excitation. Experimentally, the correct stop/start ratio ($\leq$0.02) can be achieved by controlling (mainly closing) the excitation and emission slits.

This technique, when used correctly, provides accurate emission decay curves so that analysis of multiple decays is possible, and, more important, it allows, by means of the so-called "deconvolution", lifetime measurements in a time range lower than that of the duration of the excitation pulse, which is usually the resolution limit for lifetimes measurement apparatus. Indeed, when the emission process occurs in a time shorter than or similar to the excitation time, the exciting flash light becomes the rate determining step of the whole excitation-emission process and the excitation time strongly affects the emission lifetime.

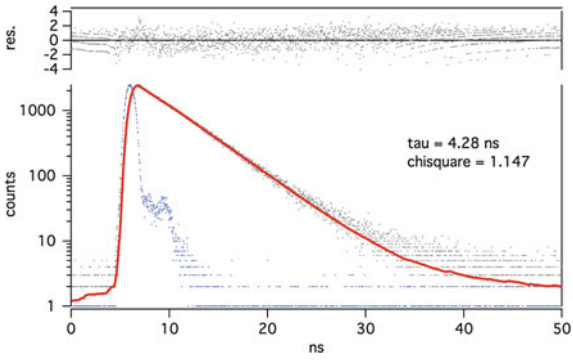

Fig. 7.10 Emission lifetime determination by "deconvolution" of a fluorescein aqueous solution at pH = 7.0, at room temperature. The emission is collected at 525 nm. The observed emission decay is *gray*, the time behavior of the excitation laser flash is *blue*, and the fitting function is *red*

The "deconvolution" is a calculation technique, that by using a suitable software, "subtracts" the contribution of the exciting light flash from the emission decay curve thus leaving the "pure" emission behavior which allows the calculation of the actual emission lifetime. A mandatory requirement for the application of the "deconvolution" procedure is the availability of the time profile of the flash with great accuracy and precision, which can be obtained by means of the very good reproducibility of the exciting source. Figure 7.10 shows an example of a lifetime determination by means of the "deconvolution".

The "time correlated single photon counting" technique allows the measurement, with great accuracy, of the luminescence emission lifetimes in a temporal range spanning from hundreds of picoseconds to tens of microseconds. As we have seen the shorter lifetimes are accessible by using the "deconvolution" procedure while the longer lifetimes are measurable by a suitable reduction of the excitation lamp frequency in order to avoid the presence of two or more excitation pulses within the selected excitation-emission time cycle.

Thus, the "time correlated single photon counting" technique is a very sophisticated but a very accurate and precise procedure that makes use of an expensive and reliable apparatus with a large time range of applications that can be extended by using the "deconvolution" procedure. For more details see Ref. [3].

7.2.4 Phase Shift

In contrast to the emission lifetime determination techniques reported above, the "phase shift" does not require the collection of the excited states decay curve. Indeed this frequency-domain technique provides emission lifetimes by measuring unusual parameters.

The peculiarity of an instrumentation based on this technique is the exciting source, that, contrary to what was previously seen for other instrumentation, exhibits continuum light emission although variable in intensity with time (it goes from a maximum to a minimum, being never zero). Thus, the light source is

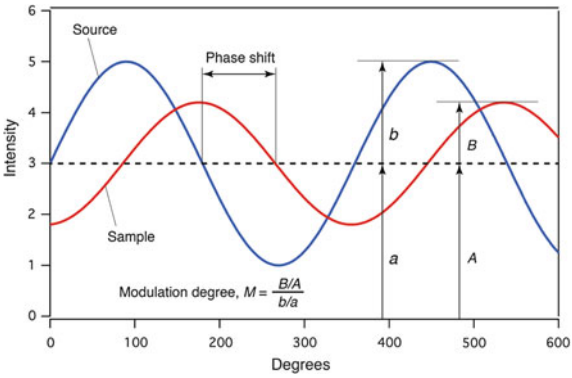

Fig. 7.11 The exciting light (source) and the emission from sample differ in phase and intensity as a function of the sample lifetime. Phase shift and modulation degree are used to quantify the difference

modulated in intensity (it follows a sinusoidal behavior, see Fig. 7.11) with a frequency that can be changed from some hundreds of hertz to tens of gigahertz.

The method is based on the fact that when a light source sinusoidally modulated in intensity is used to excite a luminescent molecule, a modulated emission is observed exhibiting the same frequency of the excitation source. If the emission lifetime is faster with respect to a single excitation wave of the modulated source, the emission profile matches the excitation behavior both in intensity and time. On the contrary, when the emission lifetime is slower than the single excitation wave, the sample emission, although keeping the same frequency of the source, is shifted in time and lowered in intensity with respect to the former case (see Fig. 7.11). The phase shift and the intensity decrease depend on the emission lifetime of the sample, increasing with the increasing emission lifetime.

The relationship between the emission lifetime and the two parameters phase shift (δ) and intensity reduction percentage or modulation degree (M) are as follows:

$$\tan \delta = \omega\tau \tag{7.6}$$

$$M = (1 + (\omega\tau)^2)^{-1/2} \tag{7.7}$$

where $M = \cos \delta$; δ = shift angle (phase shift) between excitation and emission (0°–90°); ω = modulation frequency of the light source; M = modulation degree (100–0%, see Fig. 7.11).

Practically, to measure the excited state lifetime of an emitting sample, one has to measure the phase shift δ and the modulation degree M at various frequency modulation of the exciting source. The measurement starts at a relatively high modulation frequency, at which, with the emission lifetime being faster than a single excitation wave, the emission profile matches the excitation behavior ($\delta = 0$, $M = 100\%$). Then, the modulation frequency is progressively increased and at a certain frequency the emission becomes shifted ($\delta > 0$) and the intensity decreases ($M < 100\%$).

Then, the emission lifetime is evaluated by a best-fitting procedure (non-linear least-squares analysis) over the shift angles and the modulation degrees obtained at

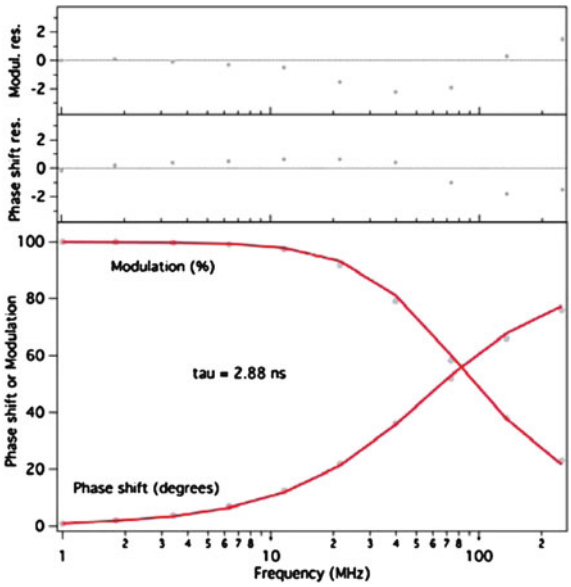

Fig. 7.12 Example of a lifetime measurement with the phase shift method. The sample is eosin in dichloromethane at room temperature. As the frequency increases, the phase shift increases, and the modulation decreases

all the frequency modulations used. In order to get the difference between the excitation and the emission behaviors it is mandatory to have the correct excitation profiles at all the possible frequency modulations. This is obtained by monitoring, at each frequency change, the emission of a very fast emitting sample (emission lifetime $\tau \leq 1\ ps$) or a high light scattering non-transparent solution.

As a consequence of what reported, it is evident that the time resolution of the technique depends on the modulation frequency achievable by the instrument light source, indeed the higher the frequency modulation the shorter the measurable emission lifetime will be. For example, to measure luminescence emission lifetimes of 1 μs, 10 ns or 100 ps, a light modulation frequency of ca 1 MHz, 200 MHz, 2 GHz, respectively, is needed.

Figure 7.12 shows the graphical aspect of the data exhibited by a "phase shift" instrumentation: the grey points are the experimental values obtained for δ and M at various modulation frequency of the light source. The full line is the best-fitting equation resulting from the treatment of the data (non-linear least-squares analysis) as a monoexponential decay. In the present day, computational facilities also allow accurate treatment of multiexponential decays. For more details, see Ref. [3].

7.3 Analysis of Decay Data

Usually, analysis of recorded data is performed by means of software supplied with the apparatus. Examples concerning the visual aspect of the experimental decay, and different ways to analyze the data have already been illustrated in Sect. 7.2.

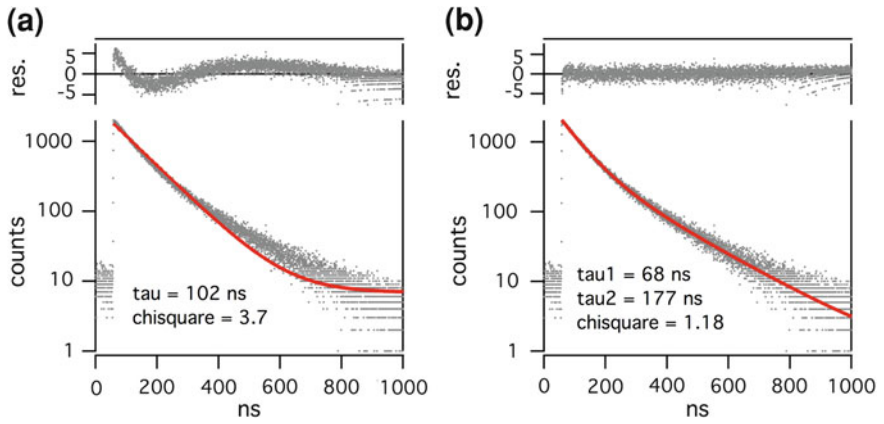

Fig. 7.13 Luminescence decay at 650 nm of an aerated acetonitrile solution containing $[Os(phen)_3]^{2+}$ and $[Ru(bpy)_3]^{2+}$, at room temperature. Measurement performed with a single photon counting apparatus. Fit performed using either a single (**a**) or a double (**b**) exponential analysis

In the following discussion, a few considerations will be added for an appropriate analysis of the decay data, especially if "time domain" measurements are to be dealt with.

Usually, it is very convenient to start displaying the intensity decay data by means of a logarithmic scale, as illustrated in Fig. 7.3b. There are two possibilities:

(1) The decay looks linear. In this case the simple model discussed in Sect. 7.1 is usually taken for granted. The data are then analyzed by a monoexponential fit (Eq. 7.5), which should result in a picture similar to Fig. 7.5. Irrelevant differences may be present, depending on the particular software used; for example, the intensity scale could be logarithmic. If a good match exists between the experimental data and the fitted function, the simple monoexponential model appears adequate, and there is no reason to examine more complex models.
(2) The decay does not look linear (in this case it is usually a curve with upward concavity), or the monoexponential fit was not satisfying. In this case a more complex model should be looked for, taking into account the peculiarities of the investigated system. Only one example will be illustrated; for a more detailed discussion, see Ref. [3].

Most commonly, the decay of the total emission intensity is fit as a sum of two exponential terms:

$$I(t) = A_1 \exp(-t/\tau_1) + A_2 \exp(-t/\tau_2) \tag{7.8}$$

Here, τ_1 and τ_2 are the lifetime values, and A_1 e A_2 are their respective emission intensity at $t = 0$ (the so-called *pre-exponential factors*). The meaning of these terms depends on the particular system under investigation.

If the system contains two different and independent luminescent compounds (consider always the possibility of an unwanted impurity), τ_1 and τ_2 are their lifetime values, and A_1 e A_2 are their emission intensity at $t = 0$. In such a case, the pre-exponential factors are determined by the emission quantum yield of the two compounds, by their emission intensity at the monitored wavelength, and by their concentration. Figure 7.13 illustrates a pertinent example.

The sample is an acetonitrile solution containing the two complexes $[Os(phen)_3]^{2+}$ and $[Ru(bpy)_3]^{2+}$, which feature monoexponential lifetimes of 64 and 160 ns, respectively, as individually determined. The luminescence decay observed is not linear in a logarithmic scale when both complexes are present in the same solution, indicating that a monoexponential fitting is not appropriate. Figure 7.13a shows indeed that a monoexponential analysis does not fit the data. As it can be noted, there is no match between the experimental data and the fitted function, and the residuals are not randomly distributed around zero. This behaviour is typical, and indicates that the monoexponential model chosen is not appropriate. Figure 7.13b shows the result of a fit using a two-exponential model: the match between experimental data and fitted function looks good, and the residuals are evenly distributed around zero. The goodness of the fit can be evaluated also using the statistical parameter χ^2, but normally a visual examination is conclusive. As indicated in Fig. 7.13b, the two calculated lifetime values are 68 and 177 ns, in good agreement with the values determined on the individual compounds.

Multi-exponential decays can also be observed from a single luminescent compound. For example, the compound under examination can be present in two (or even more) different chemical environments (e.g., due to different solvent shielding), producing species with different lifetimes. Normally the radiative constant of a luminescent species is independent of the chemical environment, and in such a case the pre-exponential factors are related to the fraction of species experiencing different environments. In biochemical research it is very common to consider that a multiexponential decay can result from different conformers of a single biological molecule.

If even a bi-exponential model fails to fit the experimental data, more complex models with three (or even more) exponential terms can be sought. Certainly, from a mathematical viewpoint any decay can be fitted by increasing the number of exponential terms. However, from a chemical viewpoint there is the difficulty to relate the data obtained to individual components of the system under investigation.

7.4 Example of Lifetime Measurements on a Supramolecular System

A very nice example of how lifetime measurements can be used to study supramolecular systems is shown in the following paper where time-resolved luminescence measurements were employed to investigate the photophysical behavior

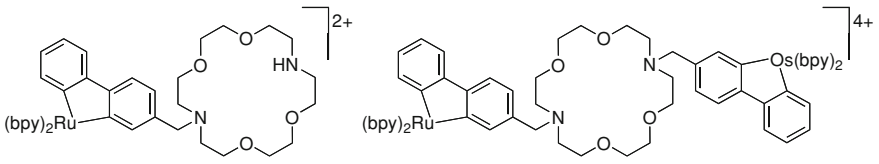

Fig. 7.14 Structures of the model compound $[(bpy)_2RuL]^{2+}$ and of the dinuclear complex **1**. The species **1(Ba)** is obtained by addition of Ba^{2+} to a solution of **1** (Ba^{2+} is hosted inside the macrocyclic cavity)

Table 7.1 Photophysical properties[a]. Data from Ref. [4]

Compound	λ_{em}, 610 nm		λ_{em}, 740 nm		k_{en},[b] s^{-1}	d_{MM},[c] Å
	τ_1, ns	τ_2, ns	τ_1, ns (A_1)	τ_2, ns (A_2)		
Ru model	190[d]	–				
1	186[e]	9[f]	40 (0.110)	8[g] (–0.050)	1.1×10^8	13.5
1(Ba)	205[e]	20[f]	42 (0.127)	17[g] (–0.045)	4.5×10^7	15.5

[a] Air-equilibrated acetonitrile solvent; when necessary a dual-exponential analysis was employed, $I(t) = A_1 \exp(-t/\tau_1) + A_2 \exp(-t/\tau_2)$. [b] $k_{en} = 1/\tau_2 - 1/\tau_1$; lifetimes as observed at 610 nm. [c] Inter-metal separation, evaluated according to the Förster mechanism [6]. [d] The luminescence quantum yield was $\phi = 0.018$. [e] Corresponding to small amounts (<5%) of unquenched Ru-based luminescence. [f] From the quenched luminescence of the Ru-based component. [g] Rise-time for the Os-based decay

of the supramolecular systems **1**, **1(Ba)** and of the model compound $[(bpy)_2RuL](PF_6)_2$ (see Fig. 7.14). The work [4] has been done with the aim of understanding if and how the addition of Ba^{2+} affects the photophysical properties of **1**.

The mononuclear Ru(II) complex $[(bpy)_2RuL](PF_6)_2$, used as model, exhibits a ^{3}MLCT emission at 610 nm with a lifetime of 190 ns (Table 7.1). The attachment of the $[Os(bpy)_2]^{2+}$ unit to give **1**, results in a decrease of the Ru-based emission both in intensity and lifetime ($\tau = 9$ ns), with a concomitant increase in intensity of the Os-based emission at 740 nm. Moreover, the Os-based emission shows dual-exponential behavior with an initial rise-time of 8 ns and a subsequent decay-time of 40 ns (typical of the Os-based luminophore) [5], Table 7.1. Figure 7.15 shows the decay profiles of the Ru- and Os-based emission of **1**.

The almost coincident Ru-based emission lifetime (9 ns) and Os-based emission rise-time (8 ns) is a clear evidence of the connection between these two processes; indeed, they are the two different sides of the same, efficient photoinduced energy-transfer process occurring between the Ru (the donor) and Os (the acceptor) units in **1**. Moreover, from the lifetimes determined at 610 nm in the model compound (τ_1) and in **1** (τ_2) it is possible to calculate ($k_{en} = 1/\tau_2 - 1/\tau_1$) an

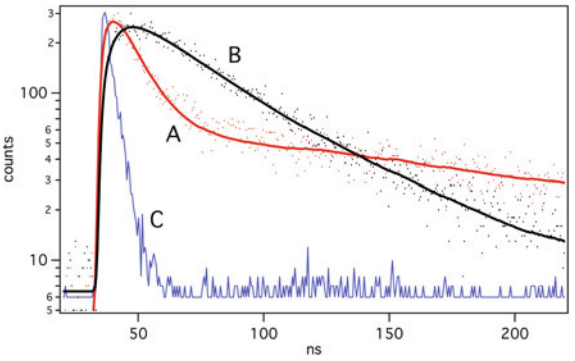

Fig. 7.15 Luminescence decay of **1** detected at 610 nm (emission from Ru unit, A) and 740 nm (emission from Os unit, B). Excitation is performed with a N_2-filled lamp (profile C). Data from Ref. [4]

Table 7.2 Selected standards for luminescence lifetime measurement[a]

Compound	Solvent	λ_{em} (nm)	τ	References
Erythrosin	H_2O	580	66 ps[b]	[8]
Rose bengal	MeOH	580	550 ps[b]	[8]
Rose bengal	EtOH	580	800 ps[b]	[8]
2,5-Diphenyloxazole	Cyclohexane	370	1.28 ns[b–d]	[9]
Rhodamine B	EtOH	600	2.85 ns[b]	[9]
Coumarin 450	EtOH	460	4.3 ns[b]	[8]
Anthracene	EtOH	>400	5.1 ns[b]	[9]
1-Methylindole	Cyclohexane	330	6.24 ns[c]	[9]
9,10-Diphenylanthracene	EtOH	[e]	8.8 ns	[10]
1-Cyanonaphthalene	Hexane	345	18.2 ns[b, c]	[9]
2-Methylnaphthalene	Cyclohexane	320	59 ns[b]	[11]
Naphthalene	Cyclohexane	320	96 ns[b]	[11]
Pyrene[f]	Cyclohexane	390	450 ns	[12–14]
$[Ru(bpy)_3]^{2+}$	H_2O	610	650 ns	[15]
	MeCN[g]	610	1.10 μs	[16]
Benzophenone	EPA[i], 77 K	450	6 ms[h]	[17]
Naphthalene	EPA[i], 77 K	–[e]	2.35; 2.6 s	[18, 19]
Benzene	EPA[i], 77 K	350	6.3 s[h]	[19]

[a] The table is ordered according to increasing lifetime value; room temperature, deaerated solution, unless otherwise noted; see individual references for the errors and for the exact temperature values. [b] Recommended by Eaton [20]. [c] Recommended by O'Connor and Phillips [21]. [d] Air-equilibrated solution. [e] See individual references. [f] Very dilute solution is recommended ($<10^{-5}$ mol L^{-1}) to avoid excimer formation. [g] For other polar solvents, see Ref. [15]. [h] Recommended by Eaton in Ref. [22]. [i] EPA = ethanol/isopentane/diethyl ether 2:5:5

energy-transfer rate constant of 1.1×10^8 s^{-1}, corresponding to a quenching efficiency greater than 95%. The addition of Ba^{2+} (which is hosted in the macrocyclic cavity acting as a spacer between the Ru and Os moieties) leads to **1(Ba)**. In this compound the lifetime of the residual Ru(II) emission increases to 20 ns and the rise-time of the sensitised Os-based luminescence approximately doubles, to 17 ns (Table 7.1) indicating a less efficient quenching of the Ru-based emission

by the Os(II) centre; indeed, an energy-transfer rate constant of $4.5 \times 10^7\ s^{-1}$ can be calculated, corresponding to a quenching efficiency of 90%.

The significant decrease in the efficiency of Ru → Os photoinduced energy-transfer can be ascribed to an increase in the Ru–Os separation in **1(Ba)** with respect to **1**, most likely due to electrostatic reasons.

In fact some calculations based on the very plausible assumption of a Förster type energy-transfer mechanism (see Sect. 2.5.1) [6] and on the energy-transfer rate values measured in the two cases leads to an estimated increase of the Ru–Os separation from 13.5 Å in **1** to 15.5 Å in **1(Ba)**.

The conclusion of this paper [4] clearly shows that lifetimes measurements not only enable the study of the photophysical behavior of molecules, but also allow a glance at structural changes in supramolecular systems.

7.5 Luminescence Lifetime Standards

Several standard compounds are available to check the performance of the equipment for various decay ranges. Selected standards are listed in Table 7.2; a more exhaustive list can be found in Ref. [7].

Solutions of standard compounds must be prepared using the highest grade purity samples and solvents, taking into account the presence and concentration of any possible quencher (i.e. oxygen). This is crucial for lifetimes longer than ~100 ns. For lifetimes longer than ~1 μs only a few standards are listed in the table, both in fluid solution at room temperature and in rigid matrix at 77 K.

References

1. Andrews DL (ed) (1997) Lasers in chemistry: third completely revised and enlarged edition. Springer, Berlin
2. Telle HH, Ureña AG, Donovan RJ (2007) Laser chemistry: spectroscopy, dynamics and applications. Wiley, Chichester
3. Lakowicz JR (2006) Principles of fluorescence spectroscopy, 3rd edn. Springer, New York
4. Paul RL, Morales AF, Accorsi G, Miller TA, Ward MD, Barigelletti F (2003) Inorg Chem Commun 6:439–442
5. Kober EM, Caspar JV, Sullivan BP, Meyer TJ (1988) Inorg Chem 27:4587 and references therein
6. Balzani V, Maestri M (1992) Intramolecular electron and energy transfer. In: Kalyanasundaram K, Graetzel M (eds) Catalysis by metal complexes. Kluwer Academic Press, Dordrecht
7. Montalti M, Credi A, Prodi L, Gandolfi MT (2006) Handbook of photochemistry, 3rd edn. CRC, Boca Raton
8. Zimmerman HE, Penn JH, Carpenter CW (1982) Proc Natl Acad Sci USA 79:2128–2132
9. Lampert RA, Chewter LA, Phillips D, O'Connor DV, Roberts AJ, Meech SR (1983) Anal Chem 55:68–73
10. Mardelli M, Olmsted J III (1977) J Photochem 7:277–285

11. Berlman IB (1971) Handbook of fluorescence spectra of aromatic molecules, 2nd edn. Academic Press, New York
12. Birks JB, Dyson DJ, Munro IH (1963) Proc Royal Soc A275:575–587
13. Birks JB (1970) Photophysics of aromatic molecules. Wiley, New York
14. Patterson LK, Porter G, Topp MR (1970) Chem Phys Lett 7:612–614
15. Nakamaru K (1982) Bull Chem Soc Jpn 55:1639–1640
16. Juris A, Balzani V, Belser P, von Zelewsky A (1981) Helv Chim Acta 64:2175–2182
17. Murov SL (1967) Ph. D. Thesis, University of Chicago
18. Heinrich G, Güsten H (1979) Z Phys Chem (Wiesbaden) 118:31–41
19. Li R, Lim EC (1972) J Chem Phys 57:605–612
20. Eaton DF (1988) Pure Appl Chem 60:1107–1114
21. O'Connor DV, Phillips D (1984) Time-correlated single photon counting. Academic Press, London
22. Scaiano JC (ed) (1989) Handbook of organic photochemistry, vol 1. CRC Press, Boca Raton

Chapter 8
Transient Absorption Spectroscopy

Sandra Monti and Claudio Chiorboli

Abstract The concepts at the basis of transient absorption measurements were illustrated with particular reference to nanosecond kinetic spectrophotometry and femtosecond pump and probe methods. The main features of the typical experimental setups for both techniques were illustrated as regards optical parts, geometrical layout of components and light detection systems. Examples of application of transient absorption spectroscopy were illustrated for the elucidation of photoinduced processes in supramolecular systems like a fullerenepyrrolidine–oligophenyleneethynylene hybrid derivative, a drug–protein complex and a tri-chromophoric system consisting of two porphyrins and one perylene bisimide.

8.1 Introduction

One of the most powerful tools in photochemistry and photophysics is represented by the *flash photolysis* method. The fundamental idea is to use an intense light pulse with a suitably short time duration to perturb the equilibrium of a system and follow the appearance and the evolution of photochemically formed transients by detecting, in particular, their electronic absorption. This technique was developed

S. Monti (✉)
Istituto per la Sintesi Organica e la Fotoreattività (ISOF), Consiglio Nazionale delle Ricerche (CNR), Area della Ricerca, Via Piero Gobetti 101,
40129, Bologna, Italy
e-mail: sandra.monti@isof.cnr.it; monti@isof.cnr.it

C. Chiorboli
Sez. di Ferrara, Via Borsari 46, 44121,
Ferrara, Italy
e-mail: chc@unife.it

P. Ceroni (ed.), *The Exploration of Supramolecular Systems and Nanostructures by Photochemical Techniques*, Lecture Notes in Chemistry 78,
DOI: 10.1007/978-94-007-2042-8_8,

more than 60 years ago by Manfred Eigen, Ronald G. W. Norrish and George Porter, awarded in 1967 for this important achievement with the Nobel Prize in Chemistry [1, 2]. They firstly developed experimental apparatus with millisecond time resolution based on extremely powerful arc flash lamps as excitation sources. Later on the time resolution was progressively improved and, with the introduction of pulsed lasers, extended to the nanosecond [3], picosecond [4, 5] and, more recently, femtosecond [6, 7] time domains. In this chapter we will describe two typical apparatus for transient absorption spectroscopy and the relevant experimental methods, one with nanosecond and the other one with femtosecond time resolution. These two apparatus can typically cover a time window from 10^{-13} to 10^{-2} s allowing to monitor the most significant photophysical and photochemical processes, either intramolecular or intermolecular, that follow the absorption of a photon by a molecule. We will illustrate with few examples their application to the study of the photobehaviour of supramolecular species in solution. For a more detailed illustration of all the technical aspects of the transient absorption detection we address to relevant specialistic reports [5, 8–10].

When a ground state molecule absorbs a photon it is promoted to an excited state. From this higher energy state the molecule can relax back to the ground state via some other intermediate excited state of singlet or triplet spin multiplicity or chemically react to form products. Intermediate excited states or products can be monitored by detecting their absorption spectrum in suitable wavelength windows, typically in the UV–Vis–NIR. Flash photolysis systems with nanosecond resolution allows detection of triplet states, diradicals, radicals, ions and bimolecular processes controlled by diffusion in solution. Longlived photoisomers and other metastable species can also be monitored. With femtosecond resolution excited singlet states and unimolecular processes like internal conversion, intersystem crossing, bond dissociation, proton transfer, charge and energy transfer in single or multicomponent systems can be approached.

8.2 Transient Absorption with Nanosecond Resolution

The typical nowadays system for the detection of transient absorption in solution has the optical scheme represented in Fig. 8.1. It is based on single beam spectrophotometric time resolved detection of light transmitted by the sample at single wavelengths (kinetic spectrophotometry).

There are (i) a pulsed laser source of 5–20 ns for the excitation of the sample; (ii) a steady lamp source of white analysing light, monitoring the excited sample at right angle geometry; (iii) an optical system composed by lenses, filters and a monochromator along with the path of the monitoring light; (iv) an electronic detection system for the measure of the transmitted light. The detection system is made by a photomultiplier tube (PMT), fast enough to follow the temporal change of the transmitted light, and a digital oscilloscope coupled to a computer for recording the time dependent PMT electric signal.

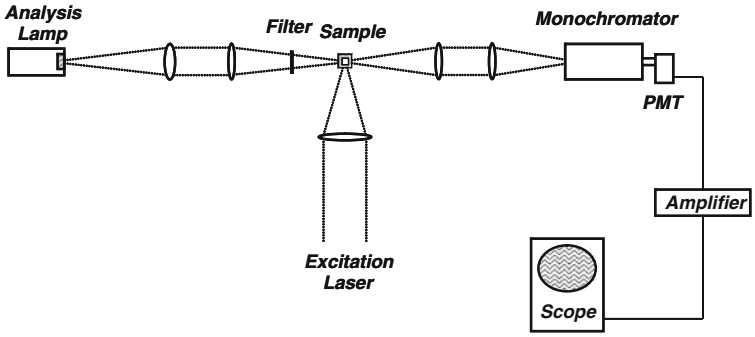

Fig. 8.1 Scheme of a nanosecond flash-photolysis system for transient absorption (PMT: photomultiplier tube)

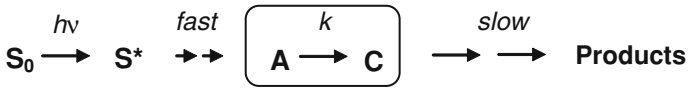

Fig. 8.2 Temporal sequence of events in a typical flash-photolysis measurement: photoinduced generation of intermediate **A** upon photoexcitation of $\mathbf{S_0}$ and conversion of **A** into a subsequent intermediate **C**, along the path to final products

8.2.1 Measure of Absorbance Change

The photons of the laser pulse at λ_{exc} are absorbed by the ground state $\mathbf{S_0}$ of the solute molecule and produce an excited state **S***. From **S*** a series of physical and/or chemical processes in temporal sequence take place (Fig. 8.2).

Some of them can occur in the accessible temporal window (typically 10^{-3}–10^{-8} s) and be detectable. Thus, for example, while the conversion of **A** into **C** may be observed with rate $k = 1/\tau\,(s^{-1})$, both the fast processes leading to **A** and the slow processes along the reaction path converting **C** into the final products may escape. The species **A** and **C** are characterized by means of their *transient absorbance* and the rate of their decay and formation. For the observation of very fast or very slow processes special requirements for the analysis light and the detection system are needed.

The goal of a flash photolysis experiment is to reveal the changes in the sample absorbance A at a given wavelength λ and time t, $A(\lambda, t)$, changes induced by the partial or total absorption of the excitation pulse photons. The intensity I of the incident analysing beam at a given wavelength λ, ($I_{\text{incident}}\,(\lambda)$), is transmitted by the sample according to the Lambert–Beer law in Eq. 8.1:

$$I(\lambda, t) = I_{\text{incident}}(\lambda) \times 10^{-A(\lambda,t)}. \tag{8.1}$$

Immediately before the excitation laser pulse the transmitted light intensity is $I_0(\lambda)$:

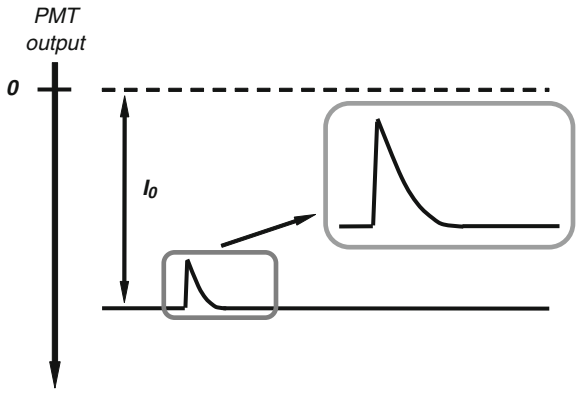

Fig. 8.3 Change in the intensity of the light transmitted by the sample upon laser excitation, as monitored by the PMT-scope system

$$I_0(\lambda) = I_{\text{incident}}(\lambda) \times 10^{-A_0(\lambda)}. \tag{8.2}$$

Immediately after the laser pulse the sample absorbance $A(\lambda, t)$ appears to have changed because a change $\Delta A(\lambda, t)$ is produced by the absorbed photons and adds to the initial absorbance value $A_0(\lambda)$:

$$A(\lambda, t) = A_0(\lambda) + \Delta A(\lambda, t). \tag{8.3}$$

The transmitted light thus becomes

$$I(\lambda, t) = I_{\text{incident}}(\lambda) \times 10^{-[A_0(\lambda)+\Delta A(\lambda,t)]} = I_0(\lambda) \times 10^{-\Delta A(\lambda,t)} \tag{8.4}$$

where

$$\Delta A(\lambda, t) = -\log_{10}[I(\lambda, t)/I_0(\lambda)] \tag{8.5}$$

or

$$\Delta A(\lambda, t) = -\log_{10}[1 + \Delta I(\lambda, t)/I_0(\lambda)] \tag{8.6}$$

where

$$\Delta I(\lambda, t) = I_0(\lambda) - I(\lambda, t). \tag{8.7}$$

Thus, monitoring the intensity of the transmitted analysing light before the laser pulse, ($I_0(\lambda)$), and its variation after the laser pulse, $\Delta I(\lambda, t)$, allows the *transient absorbance* $\Delta A(\lambda, t)$ to be calculated.

It is worth noticing that in the Eqs. 8.5 and 8.6 ΔI and I_0 appear as a ratio, thus there is no need of an absolute measurement of the transmitted light and its variation, but a relative measure of them (as electrical current or voltage across a resistance R_L) is enough for the determination of $\Delta A(\lambda, t)$. In Fig. 8.3 a schematic representation of a typical PMT signal output suitable to measure $I_0(\lambda)$ and $\Delta I(\lambda, t)$ is given.

If the transient has concentration c and molar absorption coefficient $\varepsilon(\lambda)$ the value of the transient absorbance change for a pathlength l is

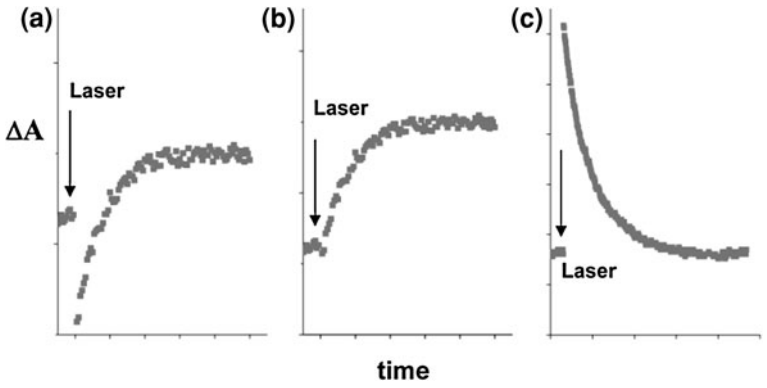

Fig. 8.4 Absorbance change profiles at: (**a**) λ_1 where $\varepsilon_A < \varepsilon_{S_0}$ and $\varepsilon_C > \varepsilon_{S_0}$;(**b**) λ_2 where $\varepsilon_A = \varepsilon_{S_0}$ and $\varepsilon_C > \varepsilon_{S_0}$;(**c**) λ_3 where $\varepsilon_A > \varepsilon_{S_0}$ and $\varepsilon_C = \varepsilon_{S_0}$

$$\Delta A(\lambda, t) = (\varepsilon(\lambda) - \varepsilon_{S_0}(\lambda)) \times l \times c \tag{8.8}$$

where $\varepsilon_{S_0}(\lambda)$ is the absorption coefficients of $\mathbf{S_0}$ at the observation wavelength. Equation 8.8 evidences the differential nature of the flash photolysis measurements and accounts for the dependence of the shape of the kinetic profiles $\Delta A(\lambda, t)$ on the difference between the absorption coefficients of $\mathbf{S_0}(\varepsilon_{S_0}(\lambda))$ and those of the involved transients. More in general the absorbance change profiles for a reaction scheme as that in Fig. 8.2 can be very differentiated at various observation wavelengths, as shown with the example in Fig. 8.4.

The molar absorption coefficient of **A** is lower than that of the ground state at λ_1, thus an initial decrease is observed (a); the ground state $\mathbf{S_0}$ and **A** are isosbestic at λ_2, thus the absorbance does not initially change (b) the molar absorption coefficient of **A** is higher than that of the ground state at λ_3, thus the absorbance increases immediately upon formation of **A** (c); product **C** in (a) and (b) has higher absorption coefficients than $\mathbf{S_0}$, thus formation of **C** leads to an increase of the absorbance. Absorption change profiles at different wavelengths at any delay after the laser pulse in the explored time window allows to reconstruct the evolution of the differential absorption spectra, revealing the fingerprints of different transients and affording insights into the photoreaction mechanism. We will see later on some applications to the study of photoinduced processes in supramolecular systems.

8.2.2 The Sample Compartment

The typical sample consists in a 1 cm fluorimetric cell, filled with 3–4 ml solution of the compound under study, on which the laser pulse incides after being focused and shaped to have a rectangular section with a cylindrical lens. The analysed volume is a front cylindrical portion of the excited solution placed at right angle geometry, as represented in Fig. 8.5.

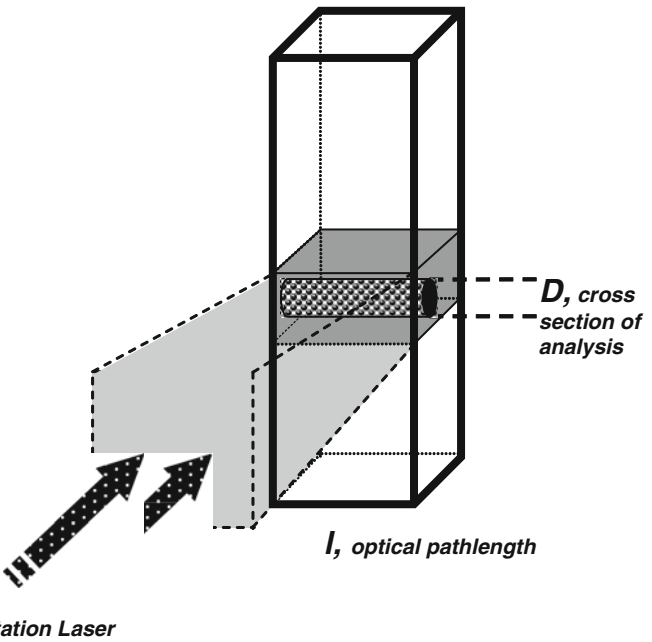

Fig. 8.5 90°-geometric layout of the excitation and analysis beams for detection of transient absorbance (l = pathlength, D = base of the analysed cylindrical volume)

The concentration of the transient species **A** generated in the analysed volume depends on the quantum yield of the **A** formation process, on the laser incident energy per cm^2 and on the ground state absorbance at the excitation wavelength, $A_0(\lambda_{exc})$. For quantitative measurements the concentration of the transients must be fairly homogeneous in the analysed volume and this requires $A_0(\lambda_{exc})$ is not too high. A good compromise between precision and sensitivity is $A_0(\lambda_{exc}) \approx 0.3$–$0.5$ over 1 cm, so that in the frontal analysed part of the excited solution only $\leq$20% of the incident photons are absorbed. For qualitative measurements higher $A_0(\lambda_{exc})$ can be used. Other geometries of excitation and analysis beams are also possible. Anyhow, in order to avoid distortions in the spectra and erroneous molar absorption coefficients and quantum yields determinations, care must be taken for obtaining a good overlap between excitation and analysis and not analysing unexcited solution portions.

8.2.3 The Optical System

The excitation source is typically a solid state laser, most frequently a Nd-YAG source, able to deliver high energy pulses ($\geq$100 mJ) with full width at half maximum (FWHM) $\leq$20 ns at 1,064, 532, 355 and 266 nm, with repetition rate

≤20 Hz. The high energy 355 nm output can be used to pump an Optical Parametric Oscillator (OPO), able to provide tunability of the excitation wavelength in the interval 410–710 nm. A mechanical shutter protects the sample cell from laser light out of the measurement time. The analysing light comes typically from a high pressure 150 W Xenon arc lamp with emission ranging from 200 nm to the NIR region. The lamp, normally running at ≤10 A current, can be supplied by a voltage pulse to reach a current up to 200 A for a short time (e.g. a millisecond). An increase of a factor of 10–100 in the brightness of the analysing beam can be obtained, this improving significantly the signal-to-noise (*S/N*) ratio in the measurement of $\Delta I(\lambda, t)$. Accumulation and averaging techniques make lamp pulsing not strictly necessary for signal-to-noise ratio optimization. A mechanical shutter protects the sample from analysing light out of the measurement time. The optically collimated analysing beam goes through the *D* photolysis cross section (Fig. 8.5) and after passing through the sample is collected to form an image of *D* on the monochromator entrance slit. The monochromator has typically a focal length of 25 cm, several gratings for UV, Vis and NIR performance optimization, a dispersion ≤4 nm/mm. It is important to select the analysing light before the sample and before the entrance slit of the monochromator using cut-off filters, to reduce as much as possible the perturbation of the PMT signal by stray light and scattered laser light. Slit width must be adjusted for the measure of the absorption spectra to get the correct bandwidth and kinetics and, again, for the minimization of signal distortions by stray light and laser scattered light. Laser induced fluorescence is a further source of strong perturbation, because it reflects in the PMT anode current as apparent transmitted light. This perturbation can be minimized using narrow monochromator entrance slits and pulsing the analysing light.

8.2.4 The Electronic Detection System

The measurement of the light intensity is typically performed with a device based on a PMT as photodetector, with basic circuit schematized in Fig. 8.6. The circuit shows the output current of the device going to earth connected through a resistor R_L. The value of R_L may range from 50 Ω to several KΩ. Change in the light intensity caused by transient absorbing species results in change of the anode photocurrent and hence of the voltage across R_L. This voltage is fed into a voltage monitoring device, usually an oscilloscope.

Standard PMTs have a lateral photocathode (side-on window), spectral response from 200 to 800 nm and a few connected dynodes (typically five out of twelve) for a faster response. The operating voltage *V* (typically $V = -950 \div -1{,}250$ V) controls the overall gain (i.e. the dynode amplification of the photoelectric signal initially generated by the photocathode). The variations in the light transmitted by the sample due to absorption by a transient may be very small. Thus for good *S/N* value the PMT must sustain high light fluxes while the anode current versus the light intensity keeps linear. In the pulsed operation mode,

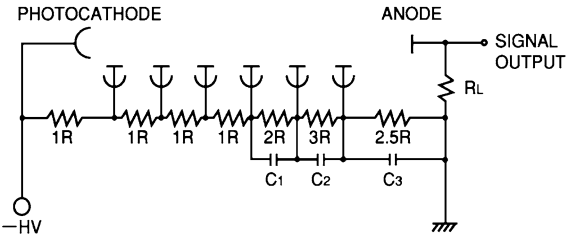

Fig. 8.6 Basic photomultiplier circuit

normally used for kinetic measurements, the anode current of standard PMTs can keep linear up to ≈ 4 mA for exposures of about one millisecond (if the photocathode exposure is steady the saturation current is normally 100 times lower). An important parameter of the PMT is also the rise time, i.e. the time taken by the anode to respond to an ultrafast optical signal. As mentioned above a first condition for short rise time is the connection of few dynodes, while increasing the dynode to dynode voltage. The basic photomultiplier circuit is shown in Fig. 8.6.

Above 800 nm the typical photodetectors are photodiodes. They can cover a large spectral window (up to 1,700 nm) and have fast response (∼ 5 ns). They are generally supplied by a low voltage (∼ 10 V) and provide a photocurrent linearly dependent on the light intensity. Hereto the photocurrent is transformed into a voltage signal across a resistance R_L ($R_L = 50\ \Omega$ for the best time response). Although photodiodes possess lower amplification capability than PMTs, they are irreplaceable in the NIR region.

As already pointed out the variation in the transmitted light due to absorption by a transient may be as low as ≈ 1% of the total steady light. This means that the signal to be measured is superimposed onto a continuous level which may be up to 100-fold greater. To analyse such a small change with a normal oscilloscope an useful method is to provide a device known as back-off circuit [11]. This arrangement makes the steady anode current I_0 be continuously compensated by a $-I_0$ current, so the voltage across R_L is always *zero*. The I_0 current is measured just before the laser pulse, stored in memory, and maintained for a time much longer than the duration of the chemical reaction. By this way the oscilloscope sensitivity can be very high without any problem of input saturation in order to see the small voltage change due to transient absorption.

A triggering system controls the timing of all the important steps of the transient absorption measure: (i) opening of the monitoring light shutter, (ii) measuring and storing of I_0 for back-off compensation, (iii) opening of the laser shutter for arrival of the excitation pulse on the sample, (iv) triggering of oscilloscope.

As mentioned above a first condition for fast response of the detection system is the rise time of the photodetector. A second condition is relevant to the load resistance R_L. The fall time t_f of the anode current depends on the values of the resistance R_L and the capacitance C, the latter due essentially to stray capacitances and the input capacitance of the oscilloscope, according to Eq. 8.9

$$t_f = R_L C \tag{8.9}$$

Thus for $R_L = 50\ \Omega$, the value generally used for nanosecond detection, C must be below 40 pF to have $t_f \leq 2$ ns. Other crucial parameters are the bandwidth (BW) of the oscilloscope amplifier, which for nanosecond resolution must be ≥350 MHz

$$t_r(\text{ns}) = \frac{0.350}{\text{BW(MHz)}}. \tag{8.10}$$

The electric signal is stored in digital form. The time axis is typically described by a multiple of 256 channels and each channel (time) is associated to a number proportional to the light intensity transmitted by the sample. Accurate reconstruction of a signal (with a limited frequency band) depends on the number of samples taken at T intervals within the signal time profile and on the interpolation method used to fill in the spaces between the samples. Using linear interpolation the sampling frequency f_s should be at least 10 times the highest frequency signal component, i.e.

$$f_s(\text{sample/s}) = 1/T \geq 10 \times f_{\max}. \tag{8.11(a)}$$

If this condition is not fulfilled, especially for a single event signal, the reconstructed waveform does not correspond to the original one, because the information relevant to the high frequency components has been lost in the digitalization process. For example, for 2 ns resolution the sampling frequency f_s of the digital oscilloscope must be $\geq 5 \times 10^9$ sample/s.

Nanosecond kinetic measurements need wide amplifier bandwidths which limit electronic filtering of high frequency noise. Thus noise is high. Further the statistical fluctuations in the number of photoelectrons, the so called "shot noise" of the PMT photocathode, is large because the number of incident photons is low in the short time intervals explored. In these conditions the *S/N* ratio is:

$$S/N \propto I^{1/2} \tag{8.11(b)}$$

and can be improved using light levels as high as possible for the analysing light and/or accumulating and averaging over many signals. Other noise sources are the fluctuations in the analysing light, which on long time scales may lead to instability of the baseline (I_0).

8.3 Transient Absorption Spectroscopy in Supramolecular Systems

8.3.1 Fullerene Derivatives

Typical species that can be detected by laser flash photolysis with nanosecond resolution are molecular triplet states. In Fig. 8.7 the differential absorption of the lowest triplet state of fullerene, $^3C_{60}$, in dichloromethane is reported [12].

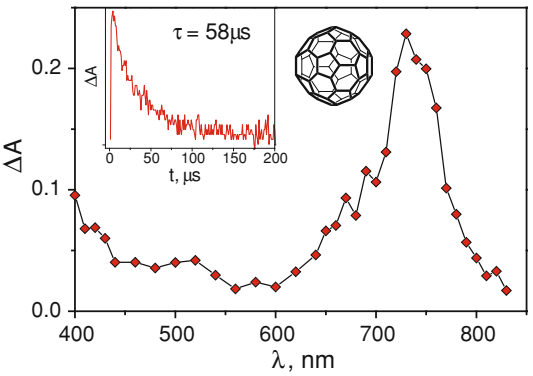

Fig. 8.7 End-of-pulse differential absorption spectrum of fullerene C_{60} in dichloromethane ($A_{355} = 1.1$, $l = 1$ cm). *Inset*: Decay profile at 730 nm. Excitation at 355 nm, pulse FWHM 20 ns, energy 1 mJ (From Armaroli et al. [12])

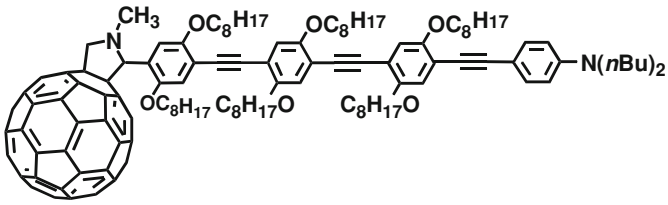

Fig. 8.8 Fullerenepyrrolidine–oligophenyleneethynylene hybrid derivative (C_{60}-OPE)

The transient, produced by laser excitation at 355 nm, exhibits a monoexponential decay (profile at $\lambda_{max} = 730$ nm in the inset of Fig. 8.7), describing the deactivation of the excited state back to the ground state C_{60}. Indeed in this molecule no intermediates other than the triplet state are formed by laser excitation.

On the contrary in the fullerenepyrrolidine–oligophenyleneethynylene hybrid derivative (C_{60}-OPE) (Fig. 8.8), where there is a terminating amino-aromatic donor unit, no fullerene triplet was formed in benzonitrile [13]. A completely different transient absorption profile was recorded in the near IR region (Fig. 8.9), indicating that an electron transfer occurs in the system leading to the charge-separated C_{60}^{-}-OPE^{+} state, recognizable in the sharp peak at 990 nm, assigned to the fulleropyrrolidine anion, and the broad band peaking at ca. 1,200 nm, ascribed to the cation of the $PhN(Bu)_2$ unit. The same fullerene hybrid derivative in toluene exhibits a transient spectrum with $\lambda_{max} = 700$ nm, clearly due to formation of $^3C_{60}$. In the inset of Fig. 8.9 the decay profile at 1,000 nm in benzonitrile points to a relatively shortlived charge separated state (lifetime ca. 390 ns), likely deactivating by intramolecular charge recombination; at 700 nm in toluene the triplet appears to be a longerlived species, relaxing to the ground state with time constant of ca. 12 μs.

This example shows how time resolved absorption measurements result to be very informative on the photoreactivity of the supramolecular dyad and clearly

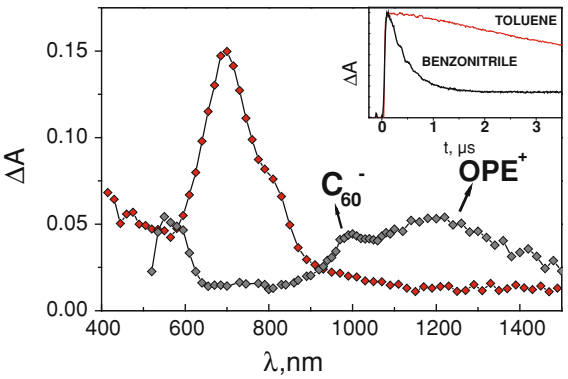

Fig. 8.9 Differential absorption spectrum of C_{60}-OPE in benzonitrile (*dark grey*) and in toluene (*grey*). *Inset*: Decay profiles at 700 nm in toluene and at 1,000 nm in benzonitrile. Excitation at 532 nm, pulse FWHM 5 ns, T = 295 K (From Clifford et al. [13])

evidences that the fate of the excited state in these systems is largely controlled by the medium polarity.

8.3.2 Ligand–Protein Complexes

Transient absorption measurements can be used to gain an insight into the photoreactivity of a ligand in a protein environment. In the following example the ligand is the antibacterial drug nalidixic acid (NAH) and the protein is serum albumin, a very important carrier for drugs in the circulatory stream and a biomolecule largely used for model studies [14]. Nalidixic acid with either bovine (BSA) or human serum albumin (HSA) forms drug:protein adducts of 1:1 and 2:1 stoichiometry. The binding sites of the drug are located in the protein subdomain IIIA (primary site) and subdomain IIA (secondary site). Conformational calculations (Molecular Mechanics and Molecular Dynamics) and circular dichroism provide insights into the binding geometry in the primary site (see Fig. 8.10 for HSA). The drug faces Tyrosine 411 at an average distance of 4.24 Å and a strong interaction between the two molecular units can be expected.

355 nm laser excitation of 1.4×10^{-4} M nalidixic acid in 0.01 M Ar-saturated phosphate buffer at pH 7.4, where the drug is in the form of nalidixate anion NA^-, leads to an intense end-of-pulse absorption with $\lambda_{max} = 370$ and 620 nm which is assigned to the triplet state of the nalidixate anion ($^3NA^{-*}$). The triplet decay is exponential with a lifetime $\tau_{triplet} = 2.1$ μs (Fig. 8.11).

In the presence of 1.4×10^{-4} M HSA or BSA the end-of-pulse absorption is weaker and exhibits two bands peaking at 410 nm and ~630 nm, the latter with a marked shoulder in the 650–700 nm region. Both the 410 and 630 nm bands disappear exponentially with time constant of a few tens of nanoseconds (ca. 45 ns for BSA, see Fig. 8.11), suggesting they are relevant to a single species.

The 410 nm band exhibits the well known fingerprints of the tyroxyl radical TyrO·; the 630–640 nm band is assigned to the reduced $NA^{2-\cdot}$ radical

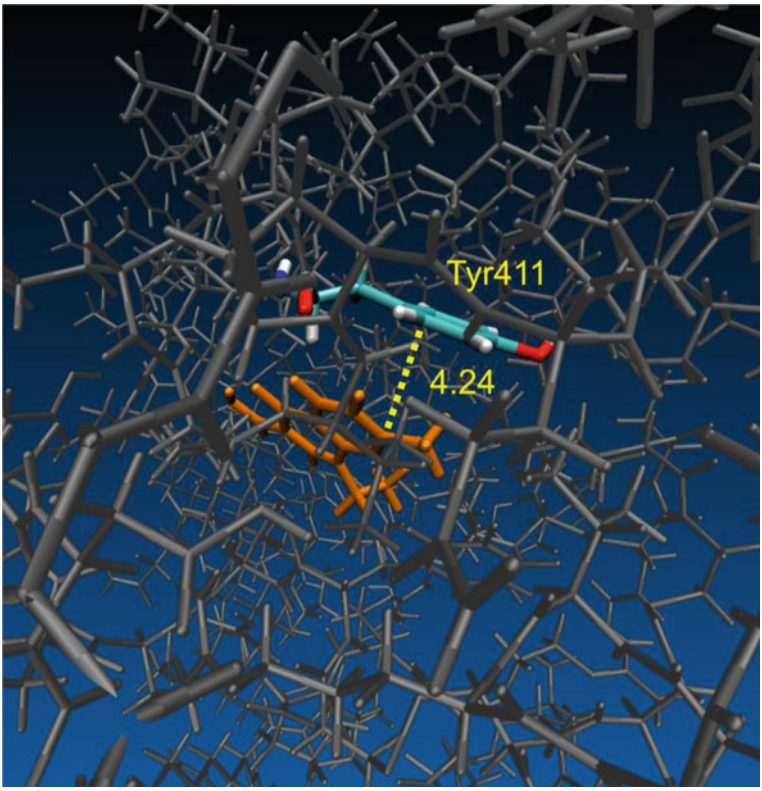

Fig. 8.10 Calculated structure of the complex of nalidixic acid with HSA-subdomain IIIA

($\lambda_{max} = 650$ nm in buffer). The initial concentration of the radical pair in BSA is estimated to be 1.22×10^{-5} M, using an $\varepsilon_{max} = 3{,}200 \pm 200\ M^{-1}\ cm^{-1}$ at 410 nm for Tyr–O$^{\cdot}$. Considering that the concentration of the excited 1:1 complex in the experiment is ca. 3.01×10^{-5} M, the quantum yield of the radical pair results to be $1.22 \times 10^{-5}/3.01 \times 10^{-5} = 0.41$. In relation to the complex structure the transient spectra of Fig. 8.12 indicate that a fast electron transfer from tyrosine (Tyr–OH) to NA^{-*} occurs, leading to the formation of a radical pair consisting of the Tyr–$OH^{+\cdot}$ radical cation and the $NA^{2-\cdot}$ radical. Fast deprotonation of the tyrosyl radical cation, according to the mechanism in Eq. 8.12, leads to the formation of the observed radical pair:

$$NA^{-*} + \ TyrOH \rightarrow NA^{2-\cdot} + Tyr{-}O^{\cdot} + H^{+}. \qquad (8.12)$$

No precursor excited state is detected and no growing-in of radical absorption is observed in these experiments, thus it can be concluded the radical pair forms within the 20 ns duration of the laser pulse. The electron is transferred to NA^{-*} within the excited 1:1 drug:protein complex, but the experiments limited to nanosecond resolution do not allow assignment of the photoreaction to either the

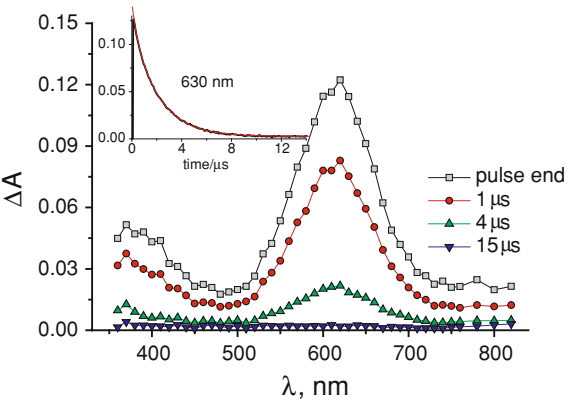

Fig. 8.11 Difference absorption spectra generated after laser excitation at 355 nm of a deaerated solution of 1.4×10^{-4} M NAH, in 0.01 M phosphate buffer at pH 7.4 at 22 °C. Delay: pulse end (*filled square*), 1 μs (*filled circle*), 4 μs (*filled triangle*), 15 μs (*filled inverted triangle*). *Inset*: experimental decay profile at 630 nm and exponential best fit (in *red*) with $\tau_{Triplet} = 2.1$ μs

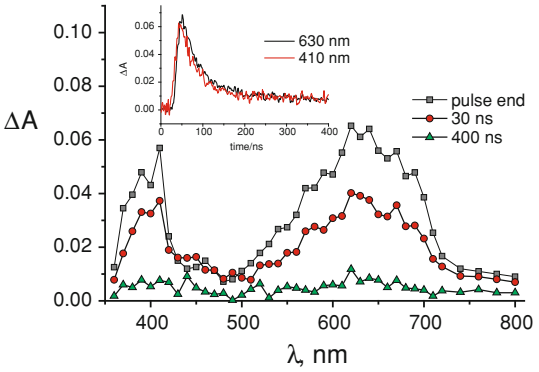

Fig. 8.12 Difference absorption spectra generated after laser excitation at 355 nm of a deaerated solution of 1.4×10^{-4} M NA in presence of 1.4×10^{-4} M BSA, in 0.01 M phosphate buffer at pH 7.4 at 22 °C. Delay: pulse end (*filled square*), 30 ns (*filled circle*), 400 ns (*filled triangle*). *Inset*: experimental decay profiles at 630 nm and 410 nm

excited singlet or the lowest triplet state of the complex. The decay of the radical pair Tyr–O·–$NA^{2-\cdot}$ follows first order kinetics with rate constant $\approx 10^7$ s^{-1}, pointing to a cage combination reaction. The process leads to an irreversible modification of the biomolecule consisting in covalent binding of the drug. Formation of photoinduced covalent drug–protein adducts is actually confirmed by HPLC. On the basis of the information obtained from transient absorption measurements the photochemical reactivity of nalidixic acid in the protein matrix can be fully understood.

8.4 Sub-Nanosecond Transient Absorption

The laser flash photolysis experiments, as we have seen, consist of two basic operations in sequence: generation of short-lived species using pulses of laser light (transient generation) and their detection (transient detection). The first stage (generation) must be shorter than the phenomena to be investigated in order to avoid interference from the excitation light with the test species. For example,

if we have a laser pulse of 30 ps, we can try to detect phenomena that occur on a scale of not less than 40 ps. The relevant parameters for the excitation source are: the wavelengths available, the duration, the frequency and the energy of the laser pulse. The second phase (detection) must be completed in the time between an excitation pulse and the other to avoid overlapping of events and signals, in practice, with repetitive laser (e.g. Nd: YAG) with pulse frequency of 1–20 Hz, the length of periods of time exploring falls in the range 1 to 0.05 s. The relevant parameters of the devices for the analysis of transient absorption signals are: the temporal resolution, the spectral window explored and the sensitivity. The development of sub-nanosecond laser pulses (pico or femtosecond) has pioneered the exploration of the events that occur on these time scales, but has required a radical change in the detection techniques.

8.4.1 Shortening the Laser Pulse

In order to achieve short and intense laser pulses in the domain of sub-nanosecond the mode-locking techniques are commonly used. We provide a brief discussion of mode locking and the regenerative mode locking technique employed with the Ti:Sapphire laser, by far the most widely used laser source for transient spectroscopy studies in the sub-nanosecond time domain. To briefly explain the principle must be observed that the laser light, despite being the most coherent form of light, is not made up of photons of only one frequency (or wavelength). In any laser system, the allowed oscillating wavelengths (or frequencies) are determined by two factors: the longitudinal modes determined by the laser cavity (subject to threshold conditions) and the gain-bandwidth of the laser medium. In a laser cavity, the electric field of the oscillating optical frequencies must repeat itself after one round-trip: i.e., the oscillating wavelengths must satisfy a standing wave condition in the laser cavity or an integral number of half-wavelengths must exactly fit between the end mirrors. The small group of frequencies that satisfy this condition are the longitudinal modes of the laser. The gain-bandwidth of the laser medium is determined by its atomic or molecular energy levels. The phases of the oscillating modes vary randomly over time, so out of the cavity, the laser intensity varies randomly due to the interference between modes, although the average power remains approximately constant. Conversely, if the modes are forced to maintain a fixed relationship between the respective phases, the laser output becomes a well-defined periodic function of time and the laser is said mode-locked. In a mode-locked laser, the longitudinal modes must be "locked" in phase, such that they constructively interfere at some point in the cavity and destructively interfere else-where in order to create a single circulating pulse. Each time this intracavity pulse reaches the partially reflective output coupler, an output pulse is produced. The time between the output pulses is the time it takes for the cavity pulse to make one complete round trip. For a Ti:Sapphire system, this corresponds to about 12.5 ns. The output pulse frequency, or repetition rate (rep. rate), is about 80 MHz.

8.4.2 Ti: Sapphire Laser

The Ti^{3+} titanium ion is responsible for the laser action of Ti:Sapphire. Ti:Sapphire is a crystalline material produced by introducing Ti_2O_3 into a melt of Al_2O_3. The electronic ground state of the Ti^{3+} ion is split into a pair of vibrationally broadened levels. Absorption transitions occur over a broad range of wavelengths from 400 to 600 nm. Fluorescence transitions occur from the lower vibrational levels of the excited state to the upper vibrational levels of the ground state. Although the fluorescence band extends from wavelengths shorter than 600 nm, the long wavelength side of the absorption band overlaps the short wavelength end of the fluorescence spectrum. Therefore, the laser action is only possible at wavelengths longer than 660 nm. An additional weak absorption band that overlaps the fluorescence spectrum further reduces the tuning range.

8.4.3 Chirped Pulse Amplification

Solid state amplifiers, such as Ti:Sapphire, have high saturation fluorescence, making it possible to extract relatively high energies from modest scale laser systems. Ti:Sapphire also has a large gain-bandwidth needed to amplify sub-picosecond pulses. A limitation comes from the tendency of bright beams to self focus destructively (a result of non-linearity in the index of refraction), which makes it necessary to limit the intensity present in amplifiers of reasonable length to less than 10 GW/cm^2. The technique of Chirped Pulse Amplification (CPA) removes this obstacle. Briefly, the idea is to initially generate a very short duration pulse. The next step is to stretch its pulse duration, thus significantly reducing its brightness (or peak power). This low brightness optical pulse is then amplified, with the probability of self-focusing induced damage significantly reduced. Following amplification, the pulse is recompressed to near its original duration. The fundamental relationship, existing between laser pulse width and bandwidth, requires that a very short pulse exhibits a broad bandwidth. For a Gaussian pulse, this relation is $\Delta v \times \Delta t > 0.441$, where Δv is the bandwidth and Δt is the laser pulse width (for a 100 fs duration pulse, at $\lambda = 800$ nm, the corresponding bandwidth is more than 9 nm). A device which delays certain frequencies relative to others can, in principle, stretch a short pulse over a longer time or, alternatively, compress a long pulse into a shorter one. A diffraction grating, which disperses different frequencies in different space, can serve as a basis for such a device. A grating can be arranged, with some other optical components, in such a way to delay the higher frequency (bluer) light over a longer path than the lower frequency (redder) light, stretching out the pulse. Such a pulse has a positive Group Velocity Dispersion (GVD), or is described as being Positively Chirped. Conversely, delaying the redder light more than the blue reverses the process, thus compressing the pulse (Fig. 8.13).

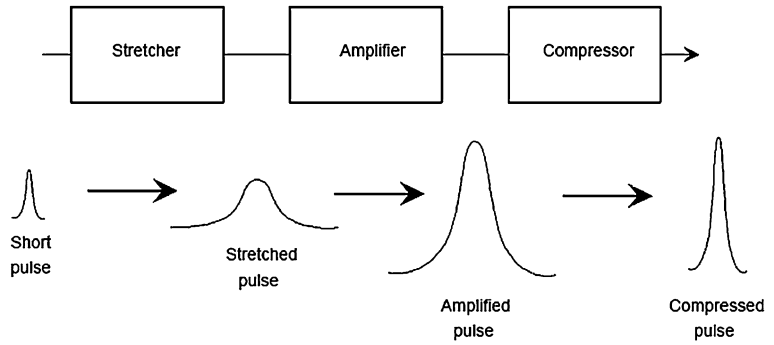

Fig. 8.13 Principle of CPA

A low energy, short duration pulse is initially stretched, by as much as 10,000 times, using a single grating pulse stretcher. A Ti:Sapphire regenerative amplifier, increases the pulse energy up to 10^6 times. A single grating compressor then recompresses the pulse to near its original duration.

8.4.4 Regenerative Amplification

Regenerative amplifiers, seeded by low energy laser pulses, are an extremely efficient means of obtaining high energy and high peak power pulses. The principle of regenerative amplification is to confine, by polarization, a single pulse (selected from a mode-locked train), amplify it to an appropriate energy level, then cavity dump the output. Typically an input pulse of energy only a few nanojoules can be amplified to over 1 mJ in a single Ti:Sapphire laser rod. This represents an overall amplification of greater than 10^6. The amplification takes place as the optical pulse passes through the laser rod, which has been optically excited by a pulse from an Nd:YLF laser. Normally the amplification of the laser rod is small, only about 3–4 in single pass, however the regenerative amplification technique enables the pulse to multi-pass the rod resulting in a much higher overall gain.

8.5 Ultrafast Transient Absorption Spectroscopy

8.5.1 Femtochemistry

Branch of physical chemistry that studies what happens in a chemical reaction in time intervals in the order of 10^{-12} to 10^{-15} s. It has enabled the detection of the transition state and reaction intermediates for formation–dissociation of bonds,

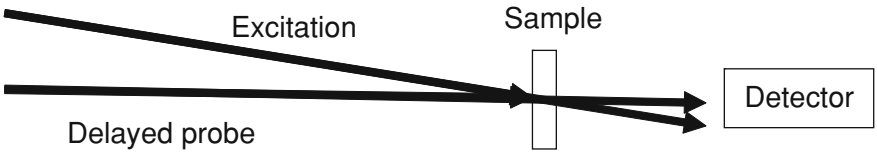

Fig. 8.14 Pump beam and analysis beam are overlapped on the sample

intramolecular electron and proton transfer. For pioneering studies of this type the Nobel Prize for chemistry was awarded to Ahmed H. Zewail in 1999 [15].

8.5.2 Pump and Probe Experiments

In the systems for femto-picosecond transient spectroscopy it is used a special detection technique, known as "pump and probe". The idea behind this technique is to use the same laser source to generate the excitation pulse (PUMP), and the analysis beam (PROBE). The path of the PROBE beam is varied in length by a delay line, i.e. a mobile platform on which are mounted mirrors that reflect the laser beam with high efficiency. The change in the optical path allows the control of the temporal distance between excitation and analysis (Fig. 8.14).

Several combinations of pump and probe experiments are possible: (i) UV–Vis pump/visible single wavelength probe, types of the data generated are absorption changes at a certain wavelength; (ii) UV–Vis pump/white light probe, types of the data generated are time-resolved absorption spectra (Fig. 8.15).

Scheme 8.1 shows the schematic layout of an apparatus to measure the femto-picosecond transient absorption spectra. It uses amplified Ti:Sapphire femtosecond laser as the laser source. This system comprises a seed laser (mode-locked Ti:Sapphire pulsed laser), a pump laser (Q-switched Nd:YLF laser), a stretcher, a Ti:sapphire regenerative amplifier, and a compressor. The output of the system consists of pulses of 800 nm, 1 mJ, 100 fs (FWHM) at a repetition rate of 1 kHz. The output is first split (50%) in two beams. One of these (PUMP) is converted to useful excitation wavelengths by coupling it into a second-harmonic (SHG) or third-harmonic (THG) generator (for 400- or 266-nm excitation) or into an optical parametric amplifier (OPA, for tunable wavelengths in the region 320–700 nm). The other (PROBE) is first passed through a computer-controlled delay line, and then focussed on a crystal plate (usually sapphire or CaF_2) in order to generate a white light continuum (WLG, useful range, 450–750 nm sapphire, 350–750 nm CaF_2). The pump beam is passed through a computer controlled optical chopper, and focused, on the sample cell. The white light continuum probe beam is collimated and focused into the sample cell, superimposed to the pump beam, at an angle of ca 5°. In order to minimize the temporal chirp in the spectrum, parabolic mirrors are used to collimate and focus the white light probe beam. After passing through the sample cell, the white continuum is coupled into a 100 μm optical

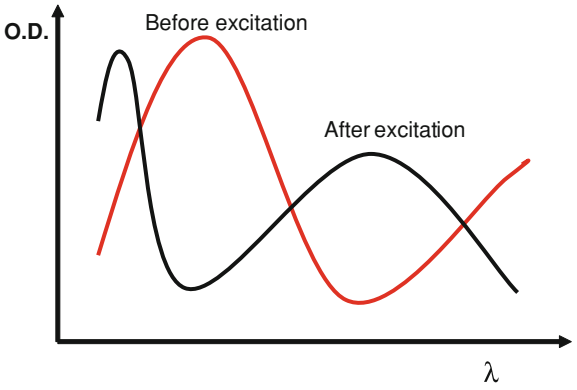

Fig. 8.15 Example of the difference in the absorption spectra of a sample before and after the excitation with a laser pulse

fiber connected to a CCD spectrograph. The delay line, the CCD spectrograph and the chopper are computer-controlled. Commercially available routines allow automatic spectral acquisition at any selected delay-line settings. Kinetic traces at chosen wavelengths can be extracted from the accumulated transient absorption data.

With 100-fs pump and probe pulses, the effective time resolution of the ultrafast spectrometer, i.e., the rise time of an "instantaneous" signal, is ca. 300 fs. The temporal chirp over the 450–750 nm range of the white light probe pulse is ca. 200 fs. The maximum temporal window of the experiment, limited by the optical delay stage dimension, for commercially available system goes from 0–1,000 ps to 0–4,000 ps.

8.6 Photoinduced Electron Transfer in a Multichromophoric System

The amount of information that can be achieved with this type of instrumentation is illustrated for the trichromphoric system consisting of two porphyrins and one perylene bisimide $(H_2P)_2PBI$ (Scheme 8.2). The transient spectral changes obtained upon excitation at 585 nm of $(H_2P)_2PBI$ (Scheme 8.2) are shown in Fig. 8.16 [16].

The spectral variations are clearly triphasic, with different spectral changes taking place in the 0–10 ps (Fig. 8.16a), 10–200 ps (Fig. 8.16b), and 200–1,000 ps (Fig. 8.16c) time ranges. The initial spectrum of Fig. 8.16a, taken immediately after the excitation pulse, is the typical spectrum of the perylene bisimide singlet state, showing, besides positive absorption in the long and short wavelength region, ground-state bleaching in the 500–600 nm range and stimulated emission at 600–700 nm range. In the spectral changes of Fig. 8.16a, the disappearance of

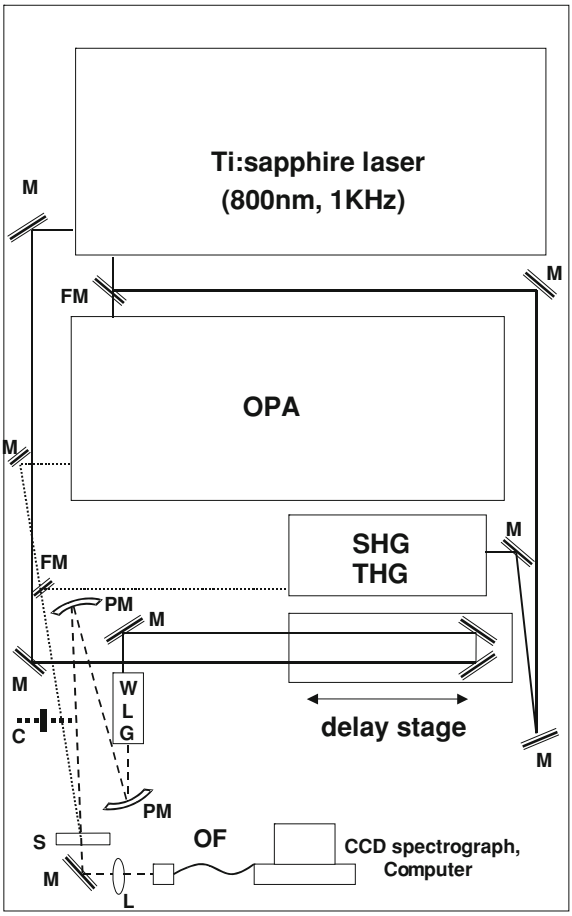

Scheme 8.1 Schematic layout of an ultrafast spectroscopy setup. Continuous line, fundamental (800 nm); *dashed line* white light continuum probe; *dotted line* pump beam; *M* mirror; *PM* parabolic mirror; *L* lens; *OF* optical fiber; *S* sample; *C* chopper; *FM* flipping mirror; *OPA* optical parametric amplifier; *WLG* white light generator, *SHG–THG* second harmonic and third harmonic generators

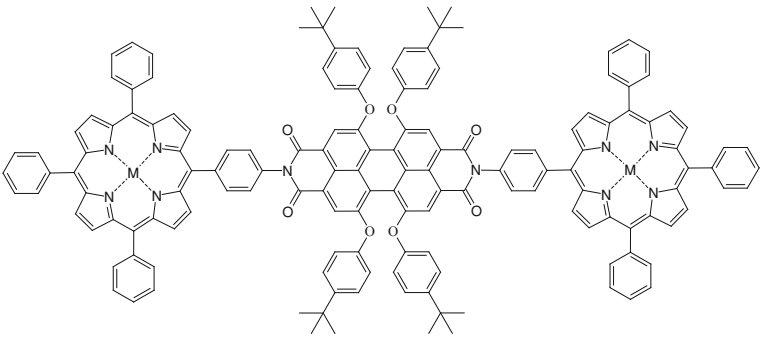

Scheme 8.2 The $(H_2P)_2PBI$ diad

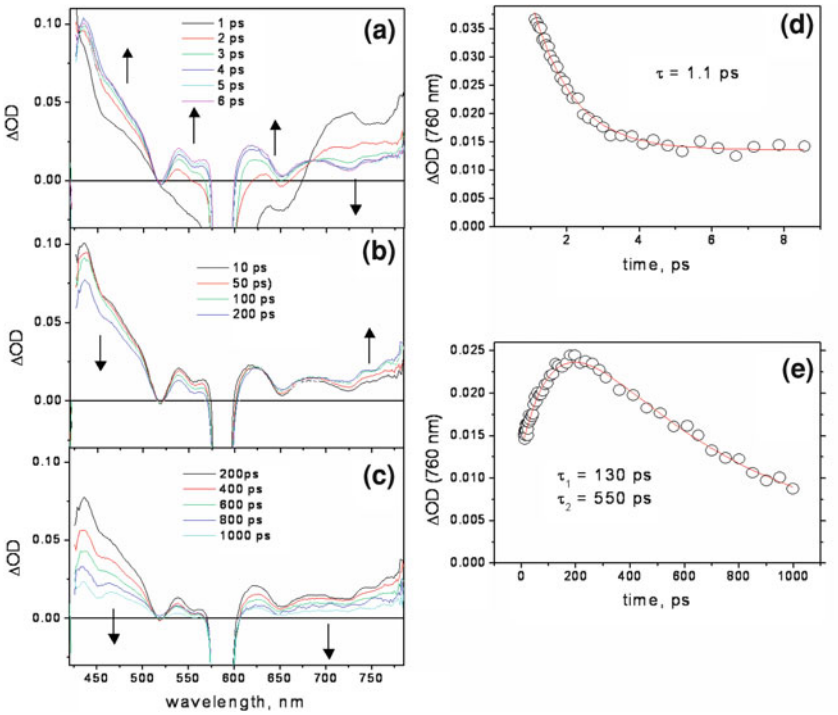

Fig. 8.16 Ultrafast spectroscopy of $(H_2P)_2PBI$ in dichloromethane (excitation at 585 nm). Time-resolved spectra: **a** $t < 10$ ps **b** $10 \leq t \leq 200$ ps **c** $t \geq 200$ ps. Kinetics: **d** $t < 10$ ps **e** $t > 10$ ps

the perylene bisimide excited state is accompanied by the formation of typical spectrum of the singlet excited state of the free-base porphyrin, characterized by bleaching of the four ground-state Q-bands at 520, 550, 590 (hidden within laser pump), and 650 nm and by an apparent bleaching at 720 nm corresponding to stimulated emission of porphyrin superimposed on a relatively positive absorption. This provides direct evidence for the singlet energy transfer process $^*PBI(S_1) \rightarrow {}^*H_2P(S_1)$, (Scheme 8.3). Kinetic analysis of the spectral changes of Fig. 8.16a at 760 nm (Fig. 8.16d) yields a time constants for singlet energy transfer of 1.1 ps. The spectral changes in the 10–200 ps time scale (Fig. 8.16b) are indicative of a charge separation process leading to $PBI–H_2P^+$, (Scheme 8.3). The bleaching of the ground-state Q-bands persists (these features are common to the excited state and the radical cation of the porphyrin) while stimulated emission at 720 nm disappears and the typical absorption of the perylene bisimide radical anion grows in at 700–800 nm. The kinetic analysis of this process (Fig. 8.16e) gives a time constant of 130 ps for the charge separation process. On a longer time scale (Fig. 8.16c) the transient spectrum decays uniformly at all wavelengths, indicating disappearance of the charge separated state by charge recombination to

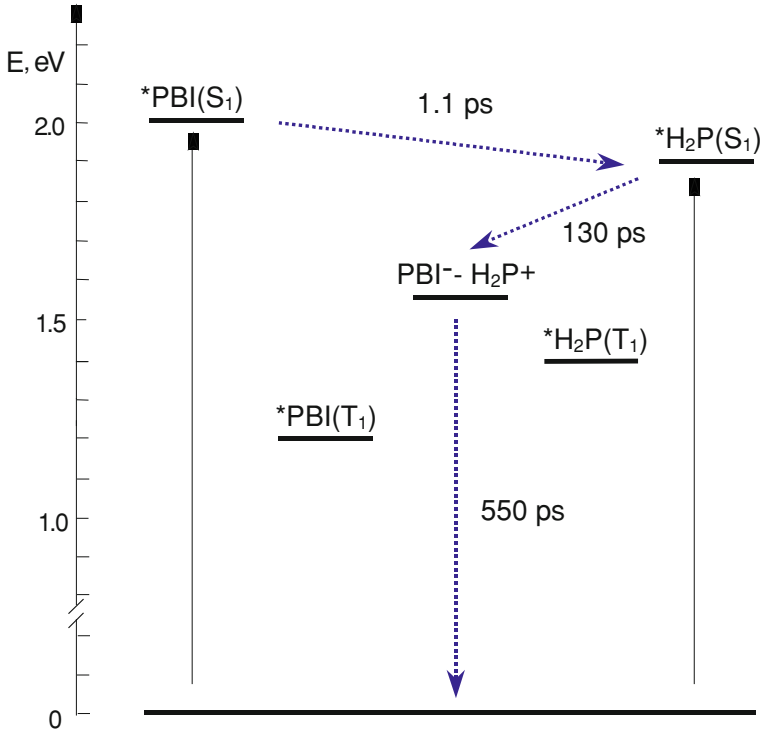

Scheme 8.3 Energy level diagram for $(H_2P)_2PBI$ in dichloromethane. Observed intramolecular photo physical processes are indicated by *dotted arrows*

the ground state, (Scheme 8.3). Kinetic analysis (Fig. 8.16e) gives a time constant for charge recombination of 550 ps.

8.7 Femtosecond Systems, Experimental Suggestions

The first requirement for these measurements is that the laser pulse is stable over time. Key factors for the stability of the laser are the temperature and humidity of the room, which must be kept as constant as possible every day and especially throughout the measurement session, as the thermal stress of the optical parts can compromise stability of the pulses.

Each transient spectrum corresponds to a certain position of the mirrors on the delay line, this position determines the time of arrival of the PROBE beam to the sample and consequently the delay of the probe with respect to the pump beam. This is achieved by the motion, using a stepping motor, of a mechanical device (linear positioning stage), controlled by software. To generate a stable, high-quality white light is needed a stable low power (0.05 mJ) 800 nm laser pulse.

If CaF_2 is used as white light generator, due to a higher continuum generation threshold in CaF_2 and a lower thermal conductivity compared to sapphire, it is necessary to periodically move the substrate while generating the white light continuum. Using sapphire plate movement of the substrate is not required.

The measurement consists of the following steps: (i) determination of the zero line before of the excitation (PROBE before PUMP), (ii) delaying the arrival of the beam on the sample (PROBE after PUMP) and acquisition of the corresponding transient spectrum; (iii) displacement of the PROBE to a further delay and so on. The sequence of delays is set by software by the operator before or during the measurement.

In order to obtain an optimum signal there must be a perfect spatial overlap of the PUMP and PROBE on the sample. The PUMP beam that emerges from the sample should not be detected by optical fibers to prevent damage to them. In contrast, the light of analysis (PROBE) should fit perfectly in the fiber to avoid distortions in the signals.

For substantially photostable samples in solution it is advisable to keep shaking the sample. Commercially available magnetic stirrers are capable of transmitting the torque to a Teflon coated magnetic bar inside of a sample cell. Due to its small size, the stirring bar fits into 2 mm thick cuvettes. Since the rotation of the stirring bar is achieved with a magnetic field the stirrer can be used with hermetically sealed cells.

For photodegradable samples in solution you must use flow cells. When investigating solid samples, due to the inability to stir the sample, one often faces photodegradation of the sample at the surface. To overcome this, a translating sample holder that automatically translates a sample continuously or in steps is required.

References

1. The Nobel Foundation (2006) The nobel prize in chemistry 1967. http://nobelprize.org/chemistry/laureates/1967/index.html
2. Porter G (1967) Nobel Lecture, pp 241–263. http://nobelprize.org/chemistry/laureates/1967/porter-lecture.pdf
3. Lindqvist L (1966) CR Acad Sci Paris—Série C 263:852–854
4. Kaufmann KJ, Rentzepis PM (1975) Acc Chem Res 8:407–412
5. Hubig S, Rodgers MAJ (1989) In: Scaiano JC (ed) Handbook of organic photochemistry vol 1. CRC Press, Boca Raton, pp 315–326
6. Shank CV, Greene BI (1983) J Phys Chem 87:732–734
7. Zewail AH (1993) J Phys Chem 97:12427–12446
8. Bonneau R, Wirz J, Zuberbuhler AD (1997) Pure Appl Chem 69:979–992
9. Tkachenko NV (2006) Optical spectroscopy. Elsevier, Amsterdam Chap. 7
10. Reid GD, Wynne K (eds) (2000) Ultrafast laser technology and spectroscopy in encyclopedia of analytical chemistry Meyers RA. Wiley, Chichester, pp 13644–13670
11. Keene JP, Bell C (1973) Int J Radiat Phys Chem 5:463–477
12. Armaroli N, Diederich F, Dietrich-Buchecker CO, Flamigni L, Marconi G, Nierengarten JF, Sauvage JP (1998) Chem Eur J 4:406–416

13. Clifford J, Gu T, Nierengarten J-F, Armaroli N (2006) Photochem Photobiol Sci 5:1165–1172
14. Monti S, Manet I, Manoli F, Capobianco ML, Marconi G (2008) J Phys Chem B 112:5742–5754
15. de Schryver FC, De Feyter S, Schweitzer G (eds) (2001) Femtochemistry: with the nobel lecture of A. Zewail. Wiley–VCH GmbH, Weinheim
16. Ghirotti M, Chiorboli C, You C-C, Würthner F, Scandola F (2008) J Phys Chem A 112(15):3376–3385

Chapter 9
Spectroelectrochemistry

Margherita Venturi

Abstract The aim of this chapter is to show the importance and utility of coupling electrochemical and spectroscopic techniques as well as the ways to perform such measurements from the operative point of view. In the introduction three paradigmatic examples are illustrated evidencing the potentials of the spectroelectrochemical measurements to characterize species in unusual oxidation states and, in the case of supramolecular systems, to establish the occurrence of conformational rearrangements or mechanical movements. Then, general considerations on the electrochemical methods aimed at obtaining absorption and emission spectra of oxidized and reduces species, like chronoamperometry and chronocoulometry, are discussed. Finally, technical details concerning electrodes to be used and cell design suitable to perform absorption and emission measurements are reported. Problems that can be faced by employing these techniques are also briefly illustrated.

9.1 Introduction

The use of electrochemical techniques coupled with spectrophotometric measurements in the ultraviolet (UV), visible (Vis), and infrared (NIR) region, where the electronic transitions occur, enables to monitor the absorption (see Chap. 3) and/or emission (see Chap. 5) spectrum of oxidized or reduced species [1, 2]. To reach this goal it is necessary to electrolyze all the electroactive species contained

M. Venturi (✉)
Dipartimento di Chimica "G. Ciamician", Alma Mater Studiorum,
Università di Bologna, Via Selmi n. 2, 40126 Bologna, Italy
e-mail: margherita.venturi@unibo.it

P. Ceroni (ed.), *The Exploration of Supramolecular Systems and Nanostructures by Photochemical Techniques*, Lecture Notes in Chemistry 78,
DOI: 10.1007/978-94-007-2042-8_9,

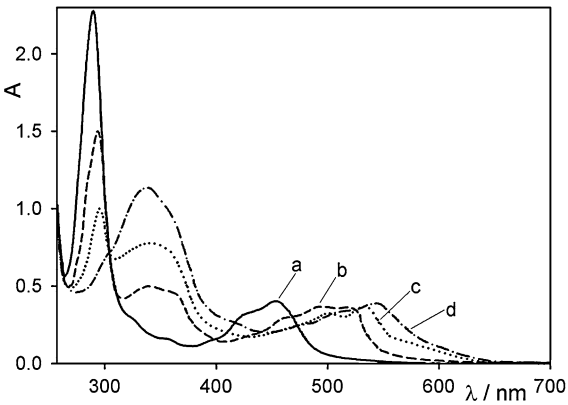

Fig. 9.1 Absorption spectra of **a** 0.9 mM $[Ru(bpy)_3]^{2+}$, and of its three reduced species obtained by electrolysis; **b** $[Ru(bpy)_3]^{+}$ ($E = -1.37$ V); **c** $[Ru(bpy)_3]$ ($E = -1.54$ V); **d** $[Ru(bpy)_3]^{-}$ ($E = -1.78$ V). Dimethylformamide solution, 0.1 M tetrabutyl tetrafuoroborate, at 232 K. Potential values reported versus Ag/AgCl

in the solution layer passed through by the analysing or excitation light. Furthermore, to reduce the electrolysis time thin layer cells are used. The measurements can be performed in situ, and transients or instable redox products can also be monitored by employing low temperatures, controlled atmosphere, and fast data acquisition systems (like diode array spectrophotometers to obtain absorption spectra).

Such a technique is very useful, for example to study the spectroscopic (absorption and emission) properties of metal complexes in unusual oxidation states, non reachable by means of the traditional synthetic routes [3]. In this regard Fig. 9.1 shows the absorption spectra of the $[Ru(bpy)_3]^{2+}$ complex and of its $[Ru(bpy)_3]^{+}$, $[Ru(bpy)_3]$, and $[Ru(bpy)_3]^{-}$ reduced species obtained in dimethylformamide at 232 K by electrolysis at suitable potential values [4].

In the case of supramolecular species [5, 6], spectroelectrochemical measurements are even more important. They, indeed, enable to establish the more stable isomer among the possible ones, and to evidence the occurrence of electrochemically induced molecular movements or conformational rearrangements. In this regard, three studies performed on catenanes (supramolecular systems minimally formed by two interlocked rings) are illustrated in the following.

Catenane $\mathbf{1}^{4+}$ shown in Fig. 9.2 contains the nonsymmetric cyclophane $\mathbf{2}^{4+}$ in which two different electron-acceptors, i.e. a bipyridinium and a bis(pyridinium)ethylene unit, are incorporated. The second ring of this catenane is a symmetric macrocycle with electron donor properties because of the presence of two dioxynaphthalene units [7]. Free $\mathbf{2}^{4+}$ cyclophane exhibits four monoelectronic and reversible reduction processes that, by comparison with suitable model compounds, can be assigned as follows: the first and the fourth processes concern the first and second reduction of the bipyridinium unit, respectively, while the second and the third processes correspond the first and second reduction of the bis(pyridinium)ethylene unit, respectively. In the catenane structure, the four reduction processes concerning the cyclophane are still present; but they are shifted to more negative potential values compared to the free cyclophane.

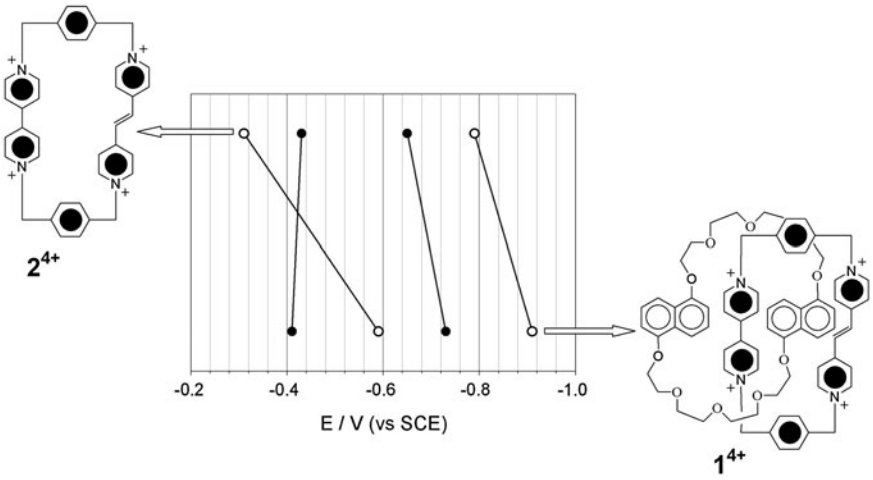

Fig. 9.2 Correlation between the halfwave reduction potentials ($E_{1/2}$) of the bipyridinium (*open circle*) and bis(pyridinium)ethylene (*filled circle*) units in free $\mathbf{2}^{4+}$ cyclophane and in $\mathbf{1}^{4+}$ catenane

This result can be easily rationalized on the basis of the charge transfer interactions that establish with the electron-donor macrocycle. Because of these interactions all the reductions involving the bipyridinium and the bis(pyridinium)ethylene units of the cyclophane become more difficult and, therefore, occur at more negative potentials. However, a simple comparison of the potential values at which the reductions take place in the free cyclophane and in the catenane does not enable to establish if the reduction sequence remains equal when the cyclophane is interlocked in the catenane structure. The unequivocal answer to this point has been given by monitoring the absorption spectrum of the solution electrolyzed at the potential value of the first reduction process. It corresponds indeed to that of the monoreduced bis(pyridinium)ethylene unit. This results shows that in the catenane the bipyridinium unit becomes so difficult to be reduced that its first reduction is shifted at a potential value more negative than that of the bis(pyridinium)ethylene unit. Such a finding is also consistent with a catenane structure in which the bipyridinium unit is located inside the macrocycle where it experiences the interaction with both the electron donor dioxynaphthalene units. As a consequence the bis(pyridinium)ethylene, being located alongside the macrocycle and interacting with only one electron donor unit, shows a smaller displacement of its first reduction that, therefore, occurs before that of the bipyridinium unit.

Catenane [3·Cu^+] illustrated in Fig. 9.3 is an example of metal-based catenanes.

It incorporates a terpyridine ligand in one of its two macrocyclic components and a phenanthroline ligand in both macrocycles [8]. Because of the preference of Cu(I) for a tetracoordinated geometry, in the [3·Cu^+] catenane the metal ion is coordinated tetrahedrally by the two phenathroline ligands, whereas the terpyridine ligand is located far away. Oxidation of Cu(I) to a tetracoordinated Cu(II) ion

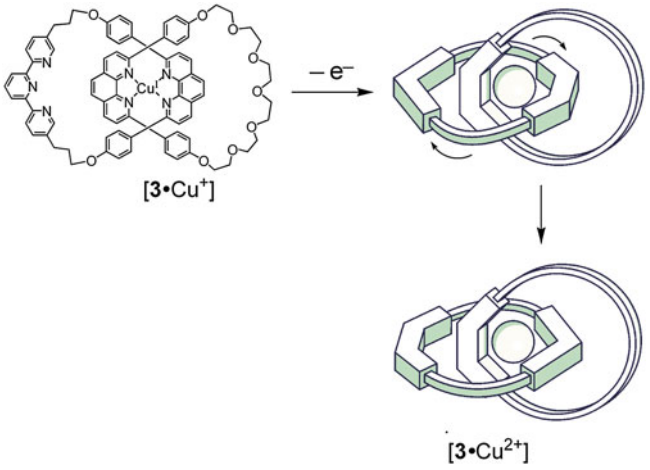

Fig. 9.3 Rotation of one macrocycle with respect to the other induced by Cu(I)/Cu(II) oxidation in catenane [3·Cu^{+}]

has been performed upon electrolysis at +0.8 V versus SCE of the acetonitrile solution of the catenane. In response to the preference of Cu(II) for a pentacoordination geometry, the terpyridine-containing macrocycle circumrotates through the cavity of the other one. In the resulting conformation, the Cu(II) ion adopts a pentacoordination geometry that is significantly more stable than the initial tetracoordination one. The occurrence of the ring circumrotation in [3·Cu^{2+}] has been demonstrated by monitoring the absorption spectrum of the oxidized catenane: in a few days it changes indeed from the spectrum of a tetracoordinated Cu(II) to the one characteristic of a pentacoordinated Cu(II) ion.

The last example is a family of six desymmetrized donor–acceptor catenanes ($\mathbf{4}^{2+}$–$\mathbf{9}^{2+}$ in Fig. 9.4) recently investigated [9].

They are formed by (a) a desymmetrized electron acceptor ring containing two different units, namely a 4,4′-bipyridinium dication (BPY^{2+}) and a neutral naphthalene diimide (NDI) or pyromellitic diimide (PMI) moiety, and (b) an electron donor ring that can be symmetric for the presence of two identical dioxybenzene (DOB) or dioxynaphthalene (DON) units, or desymmetrized by the presence of two different donors, i.e. a tetrathiafulvalene (TTF) and a DON moiety.

Interestingly, the two $\mathbf{6}^{2+}$ and $\mathbf{9}^{2+}$ catenanes, containing four different donor and acceptor units, are fully desymmetrized. In all the catenanes the electron donor ring surrounds the better electron acceptor BPY^{2+} unit, and in the case of catenanes $\mathbf{6}^{2+}$ and $\mathbf{9}^{2+}$ the better electron donor TTF unit is located inside the electron acceptor ring. Such conformations can be switched altering the redox state of the donors and acceptors incorporated in the structure as evidenced by the rich and complex electrochemical patterns exhibited by the catenanes. In this study spectroelectrochemical experiments have been of great importance to assign the

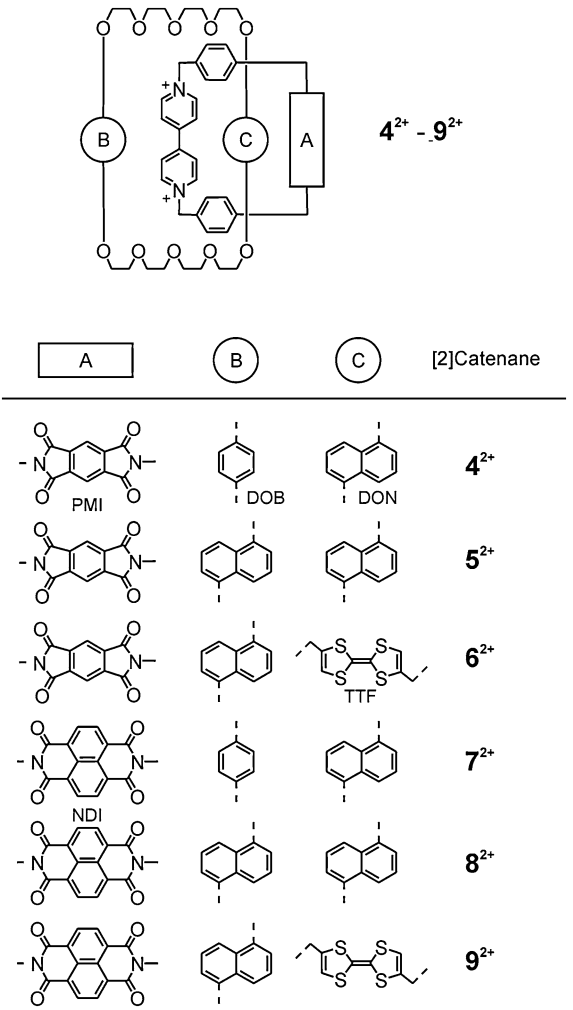

Fig. 9.4 General structure and component units of the desymmetrized catenanes $\mathbf{4}^{2+}$–$\mathbf{9}^{2+}$

redox processes and to establish the mechanical movements that occur upon electrochemical stimulation.

On the reduction side, the cyclic voltammogram of $\mathbf{4}^{2+}$ reveals four reversible monoelectronic processes that, on the basis of spectroelectrochemical experiments and comparison with suitable model compounds [7, 10], have been identified as follows: (i) the first process is consistent with the reduction of a BPY^{2+} unit engaged in CT interactions inside the cavity of the donor ring; (ii) the second reduction concerns the monoreduced BPY^{+} unit, likely still inside the cavity of the donor ring; (iii) the third process corresponds to the reduction of the inside PMI unit (the translocation probably occurs upon reduction of the BPY^{+} unit to its

neutral form); and finally (iv) the fourth reduction involves PMI^{-}, on the position of which relatively to the donor ring there is little information.

In catenanes $\mathbf{5}^{2+}$ and $\mathbf{6}^{2+}$, because of the stronger electron donating power of the crown ethers comprised in the structure, the BPY^{2+} unit becomes more difficult to be reduced than in catenane $\mathbf{4}^{2+}$ so that its second reduction overlaps to the first reduction of the PMI unit. The reduction pattern of $\mathbf{5}^{2+}$ and $\mathbf{6}^{2+}$ (Fig. 9.5a) consists therefore of three reversible waves: (i) the first process, as confirmed by spectroelectrochemical experiments (for $\mathbf{6}^{2+}$ see Fig. 9.5b), concerns the monoelectronic reduction of the BPY^{2+} unit located inside the donor ring; (ii) the second process, which involves the exchange of two electrons, can be unambiguously assigned to the overlapping reduction of the inside BPY^{+} and the alongside PMI [11]; and (iii) the third process, which is monoelectronic, corresponds to the $PMI^{-/2-}$ reduction.

The conformation changes coupled with the four-electron reduction processes for the $\mathbf{4}^{2+}$–$\mathbf{6}^{2+}$ PMI-containing catenanes are summarized in Fig. 9.6.

In the case of the three NDI-based catenanes, $\mathbf{7}^{2+}$–$\mathbf{9}^{2+}$, the reduction pattern comprises four reversible monoelectronic processes regardless of the nature of the donor rings. This behavior can be explained considering that the NDI unit is easier to be reduced than PMI. As a consequence the processes observed can be assigned to $BPY^{2+/+}$, $NDI^{0/-}$, $BPY^{+/0}$, and $NDI^{-/2-}$, respectively, in the order of increasing reduction potential. The proposed conformational changes coupled with these four one-electron reduction processes are as follows (Fig. 9.7): (i) the electron-donor ring remains around the BPY^{+} radical cation after the first reduction; (ii) the second reduction is indicated by spectroelectrochemical experiment to be the $NDI^{0/-}$ process [11], and the potential value, more consistent with the reduction of the NDI moiety in the alongside position, suggests that the donor ring still encircles the monoreduced BPY^{+} unit; (iii) the remarkably negative potential value found for the third process, assigned to the $BPY^{+/0}$ reduction, is in agreement with the assumption that no translocation of the donor component has occurred; and (iv) the fourth process is attributed to the reduction of the NDI^{-} unit, on the position of which relatively to the donor ring there is little information, as noted previously for the PMI-based catenanes.

On the oxidation side, the behavior of the fully desymmetrized catenanes $\mathbf{6}^{2+}$ and $\mathbf{9}^{2+}$ is particularly interesting from the viewpoint of molecular machines and it is the only one here discussed. Their electrochemical patterns are very similar and consist of three oxidative processes (for $\mathbf{6}^{2+}$ see Fig. 9.5a): the first two (Fig. 9.5c) are assigned to the two consecutive monoelectronic TTF oxidations [12], while the third one is ascribed to the oxidation of the DON unit. The first and second TTF oxidations exhibit the same features observed for a previously studied catenane [13, 14] and can be interpreted as follows: after the $TTF^{0/+}$ oxidation, the electron donor ring circumrotates with respect to the electron accepting ring, delivering the DON unit into its cavity.

The present study evidences that upon electrochemical stimulation in a relatively narrow and easily accessible potential window the desymmetrized $\mathbf{4}^{2+}$–$\mathbf{9}^{2+}$ catenanes can be reversibly switched among several (six and seven for $\mathbf{6}^{2+}$ and $\mathbf{9}^{2}$,

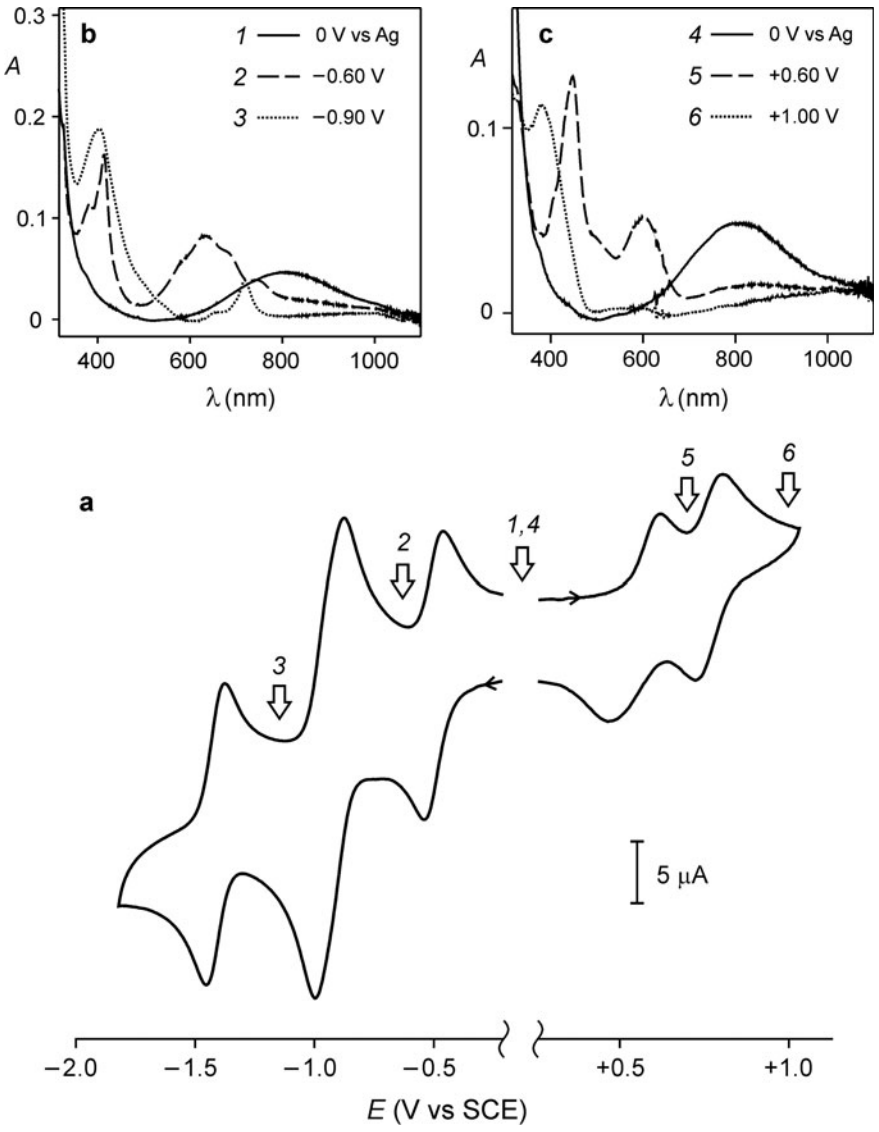

Fig. 9.5 Voltammetric and spectroelectrochemical response of catenane $\mathbf{6}^{2+}$ in CH_3CN at room temperature. **a** Cyclic voltammetric curve (conditions: 0.49 mM, tetraethylammonium hexafluorophosphate 73 mM as supporting electrolyte, 200 mV/s, glassy carbon working electrode). **b** Absorption spectra observed before (*full line*) and after exhaustive reduction at −0.60 V (*dashed line*) and −0.90 V (*dotted line*) versus an Ag quasi-reference electrode. **c** Absorption spectra observed before (*full line*) and after exhaustive oxidation at +0.60 V (*dashed line*) and +1.00 V (*dotted line*) versus an Ag quasi-reference electrode. The numbered arrows in (**a**) mark the potential values at which the corresponding curves in (**b**) and (**c**) were recorded in the spectroelectrochemical experiments

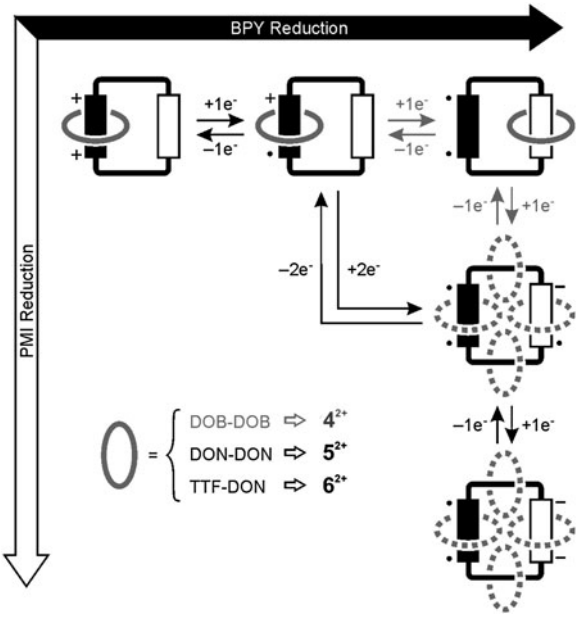

Fig. 9.6 The conformation changes associated with the four reduction processes for catenanes $\mathbf{4}^{2+}$–$\mathbf{6}^{2+}$. Horizontal and vertical processes represent the BPY-centered and PMI-centered reductions, respectively. In the *upper right* part of the scheme, grey arrows refer to the behavior of $\mathbf{4}^{2+}$, while *black arrows* describe the behavior of $\mathbf{5}^{2+}$ and $\mathbf{6}^{2+}$. The *dotted ellipses* indicate that the interactions are turned off and there is little information about the donor ring location

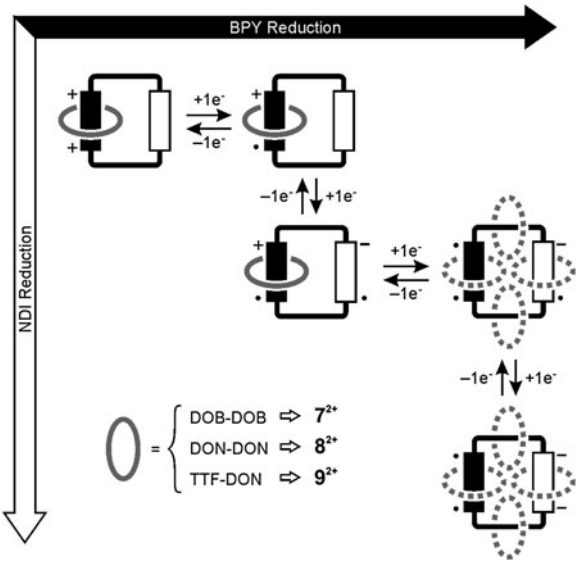

Fig. 9.7 The conformational changes associated with the four reduction processes for catenanes $\mathbf{7}^{2+}$–$\mathbf{9}^{2+}$. Horizontal and vertical processes represent the BPY-centered and NDI-centered reductions, respectively. The *grey ellipses* indicate that the interactions are turned off and there is little information about the donor ring location

respectively) states, all characterized by distinct electronic and optical properties. Such a possibility could open interesting routes for the development of molecular electronic devices that go beyond binary logic.

9.2 General Considerations

From the operative viewpoint, several types of measurements can be performed. In particular, the behaviour of the absorbance or emission intensity can be monitored as a function of:

a. applied potential difference at a fixed wavelength;
b. wavelength (absorption or emission spectrum) at a fixed potential difference;
c. time upon a perturbation of the applied potential difference at a fixed wavelength.

Measurements of types a and c are useful to establish the rate of the reactions following the electron transfer or the number of the exchanged electrons in the redox process [15]. Measurements of type b are more suitable to obtain important spectroscopic information. The absorption and emission spectra enable, indeed, to identify the redox site, i.e. the center involved in the electron transfer process, and to characterize the obtained oxidized or reduced species from the spectroscopic point of view.

Because this volume is mainly focused on the spectroscopic properties, only the electrochemical methods aimed at obtaining the absorption and emission spectra of oxidized and reduced species, i.e. type b measurements, will be described.

Obviously, absorption and in case emission spectra of oxidized and reduced species can be also obtained by addition of suitable chemical reagents. In such a way, however, waste products resulting from the reduction or oxidation of the added reagents accumulate in solution and as a consequence it is often difficult to monitor the species of interest. This inconvenience does not happen when electrochemical techniques are employed. Indeed, these techniques, although they are slightly more complex from the experimental viewpoint, enable to identify with great accuracy a chemical system in all its oxidation states because no waste products are formed.

The electrochemical techniques usually utilized to obtain the spectroscopic properties of redox generated species are those based on potentiometric measurements at potential step, like chronoamperometry and chronocoulometry. Their basic principles are briefly illustrated in the following (for a more detailed discussion see [16]).

A cell with three electrodes is used: the working electrode (WE) at which the electron transfer involving the examined electroactive species occurs, the reference electrode (RE) the potential of which is fixed at a determined value, and the counter electrode (CE). The current flowing between WE and CE is controlled by a potentiostat which maintains the potential difference between WE and RE at the value fixed by the operator by means of a function generator. To minimize the current flow between these electrodes the potential difference is measured through a high impedance circuit.

In the design of the spectroelectrochemical cell it must be assured that the WE–RE distance is small as possible. If this requirement is not fulfilled the measured

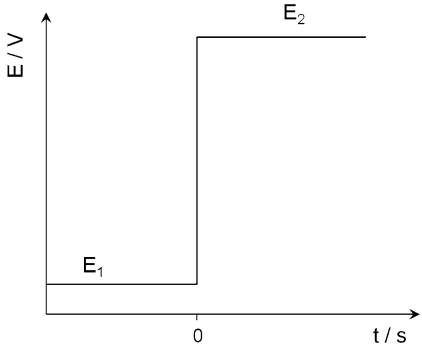

Fig. 9.8 Applied potential difference in a step potential experiment

potential difference contains a non negligible contribution due to the Ohmic drop ($E = i \times R$, according to the Ohm's law) ascribed to the solution that is between the two electrodes. Furthermore, to reduce the effect of the solution resistance a supporting electrolyte with a quite high concentration is used (vide infra), and, if necessary, such effect is compensated by means of a feedback electronic circuit [16].

In the chronoamperometry and chronocoulometry experiments a step potential difference is imposed (Fig. 9.8) from a starting E_1 value, at which no redox process occurs, to a E_2, at which the oxidized or reduced species is mainly present.

The E_2 value is selected on the basis of the $E_{1/2}$ value of the examined species obtained by cyclic voltammetric experiments possibly performed in the same solvent and in the presence of the same supporting electrolyte (vide infra) used in the spectroelectrochemical measurements. Specifically, if $E_{1/2}$ has a negative value, E_2 has to be fixed at a slightly more negative value, whereas if $E_{1/2}$ has a positive value, E_2 has to be fixed at a slightly more positive value. This strategy enables to speed up the oxidation or reduction kinetics so that the concentration of starting electroactive species at the electrode surface becomes practically zero. The current (chronoamperometry) or the charge (chronocoulometry) following this potential perturbation is measured as a function of time.

When the current between WE and CE approaches zero, or the corresponding charge reaches a plateau, electrolysis is completed and the absorption or emission spectrum of the electrogenerated species is recorded. It is also important to verify the reversibility of the process and, therefore, the experiment has to be repeated by applying a potential step opposite of the first one. For a fully reversible process the absorption or emission spectra obtained in the first (forward) and second (reverse) electrolysis have to coincide. If the recorded spectra are different, it means that the electron transfer is followed by a chemical reaction. As a consequence, the obtained spectra could be those of the products of the reaction and not those characteristic of the oxidized or reduced species. The spectroscopic characterization of such redox species with short lifetimes can be obtained by working at low temperatures; under these conditions, indeed, the effect of the unwanted chemical reaction decreases because its rate is slowed down.

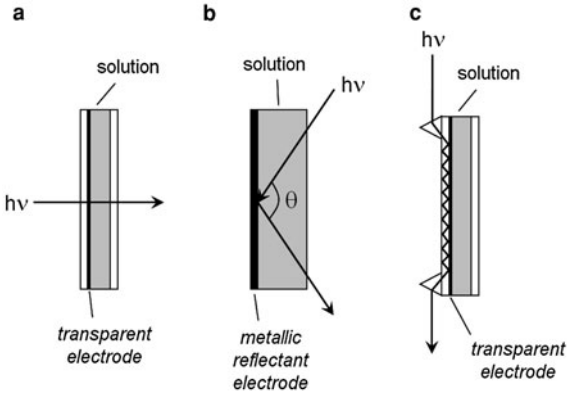

Fig. 9.9 Spectroelectrochemistry techniques based on **a** transmission, **b** specular reflectance, and **c** internal reflection measurements

As already mentioned, the solution to be electrolyzed has to contain an excess (usually a concentration two order of magnitude higher than that of the examined electroactive species) of supporting electrolyte (usually as a salt) to minimize the solution resistance (Ohmic drop, see above). The presence of the supporting electrolyte also enables that the electroactive species transport occurs by diffusion and not by migration under the action of the applied electric field. Furthermore, the solution has to be unstirred to avoid mass transport by convection.

When the spectroelectrochemical experiments are performed to characterize a reduced species, the oxygen dissolved in the solution has to be removed by bubbling a flow of nitrogen or argon through the sample solution and, after that, the cell has to be perfectly sealed.

9.3 Absorption Measurements

The absorption spectra can be obtained working in three different ways. They are based on:

a. *transmission measurements*, in which a light beam comes in the solution through the surface of an optically transparent electrode (OTE) and then it is transmitted (Fig. 9.9a);
b. *specular reflectance meausurements*, in which a light beam is reflected by the metallic surface of the electrode and passes the solution after and before reflection; in such type of measurements the thickness of the solution passed through depends on the incident angle (Fig. 9.9b);

c. *internal reflection measurements,* in which the light beam passes the back side of a transparent electrode with an angle greater than the critical angle so that it is totally reflected; because the reflection occurs at the electrode-solution interface, the light beam is absorbed only by the molecules that are near the electrode, resulting in very low absorbance values; to overcome this inconvenience it is often used a cell shape in which multiple reflections can take place (Fig. 9.9c).

The experiments more suitable to obtain information on the nature of the electrogenerated species are based on transmittance measurements (type a) and therefore they are the only ones discussed herein.

The obvious requirement for this kind of experiments is the use of WEs which are transparent in the examined spectral region. They may be:

1. minigrids made of fine (diameter ca. 50 μm) metallic (Au or Pt) wires; they can contain several hundred wires per centimeter and their transparency is due to the presence of openings (it is, however, necessary to verify that the electrode transparency is not lower than 50%);
2. thin films of a semiconductor (SnO_2 or In_2O_3) deposited on a glass, quartz, or plastic substrate;
3. thin (thickness <100 nm) films of a metal (Au or Pt) deposited on a glass, quartz, or plastic substrate.

The construction design of a spectroelectrochemical apparatus can exhibit various degrees of sophistication; in all cases it involves the integration of an electrolysis cell with a spectrometer. It may be worth discussing a few crucial requirements of cells designed for the most common experiment based on UV-visible absorption spectroelectrochemistry. First of all, as noted above, the working electrode for transmission measurements must be transparent to the employed radiation. Optically transparent electrodes (OTEs) of this type can be made with thin films of semiconductors (e.g., indium tin oxide) or metals (Au, Pt) deposited on conducting glass substrates, or can be minigrids constituted of a fine metal wire mesh. Another important issue is the timescale of the electrolysis, which should be ideally fast enough to permit the spectroscopic detection of electrogenerated species before they become involved in chemical reactions. As discussed in the previous Section, electrolysis times can be shortened using electrodes with large areas and cells with small solution volumes.

The most popular setup employed in this regard is the so-called *optically transparent thin-layer electrode* (OTTLE) cell. The electrodes are sealed into a chamber containing the electroactive species in solution, such that the cell thickness is in the order of hundreds of micrometers (100–500 μm). One important requirement for such kind of measurements is that all the solution in the vicinity of WE (and passed trough by the light beam) is electrolyzed. In this regard, the main advantage of OTTLE cells is that electrolysis is achieved in very short time, thereby decreasing the occurrence of possible side reactions involving the electrogenerated species.

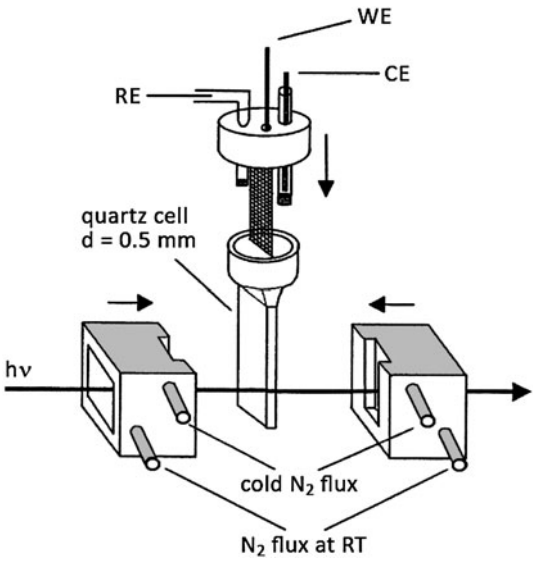

Fig. 9.10 Schematic representation of an OTTLE cell and its housing to perform experiments under temperature control

The concentrations of the electroactive species are in the 5×10^{-4}–2×10^{-3} M range and a concentration of the supporting electrolyte 2 orders of magnitude higher is employed. The concentration of the electroactive species to be used depends not only from the sample availability, but also from its molar absorption coefficient in order to obtain an absorption spectrum with absorbance values in the 0.1–1 range.

Figure 9.10 shows the schematic representation of an OTTLE cell [17]. The cell walls are in quartz and the optical path is 0.5 mm. Its larger, cylindrical shaped top part plays the function of solution reservoir and enables the CE and RE housing. This top part of the cell is sealed with a Teflon plug in which there are four holes: three of them are used to house the electrodes, while the fourth hole enables to fill the cell and to bubble the gas into the cell for oxygen removal.

WE is a metallic minigrid, RE is a Ag/AgCl electrode, and CE, separated by the solution by means of a porous frit, is made of a Pt spiral wire or grid; these requirements are necessary to increase the CE surface and, thereby, to increase the current flowing between WE and CE and to decrease the electrolysis time.

Because the surface area of WE is practically equal to the cell thin layer involved in the electrolysis, no side diffusion occurs. Furthermore, the vertical diffusion from the upper part of the cell can be neglected because the corresponding diffusion layer would be higher than 0.5 cm and, in the case of a diffusion coefficient of 10^{-6} cm^2 s^{-1}, the electrolysis time would be longer than 20 h (the thickness of the diffusion layer is $(\pi Dt)^{1/2}$, where D is the diffusion coefficient and t is the electrolysis time). This means that only the solution layer around WE is electrolyzed: the electrolysis time is decreased without invalidating the absorption measure because only the layer of the solution around WE is electrolyzed.

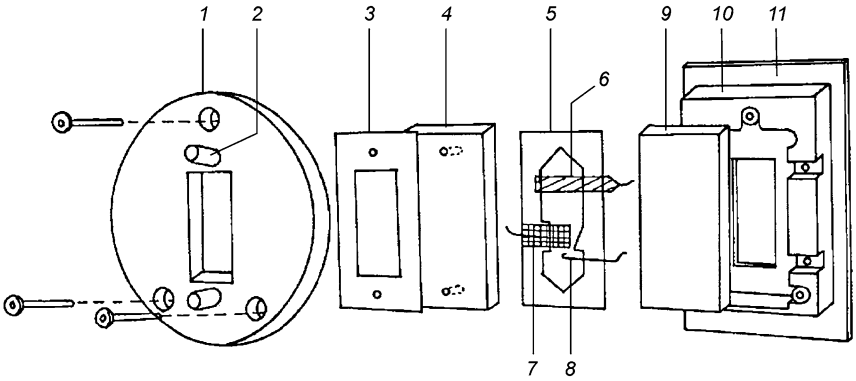

Fig. 9.11 Schematic design of an optically transparent thin-layer electrode (OTTLE) cell for transmission spectroscopic measurements in the UV-visibile-IR regions. Legend: 1, steel plate; 2, solution inlet; 3, Teflon gasket; 4 and 9, front and back quartz windows; 5, polyethylene spacer (ca. 150 μm thick) with melt-sealed electrodes; 6, Pt minigrid counter electrode; 7, Pt or Au minigrid working electrode; 8, Ag wire quasi-reference electrode; 10, Teflon holder; 11, back plate. Reprinted from [18], copyright (1991) with permission from Elsevier

In the cell set-up shown in Fig. 9.10 the WE–RE distance is quite high and therefore it is not easy to control the potential. Indeed, when the current flows in the solution, the different points of WE have different potential values because the Ohmic drops occurring into the cell are different. Nevertheless, if the absorption spectrum is recorded at the steady state, i.e. when the current value is practically zero, or the charge has reached a practically constant value, the Ohmic drop ($E = i \times R$) between WE and RE is very low.

Figure 9.10 also shows the schematic representation of a cell housing that enables to perform measurements under controlled temperatures by means of a gaseous nitrogen flow previously cooled in a liquid nitrogen bath. As already mentioned, measurements at low temperature are important because in this way possible chemical reactions involving the electrogenerated species can be slowed down.

To minimize the problem of the Ohmic drop and to further decrease the solution volume and, thereby, the electrolysis time, sandwich thin layer cell can be used (Fig. 9.11) [18].

The cell is constituted by two metallic holders; both of them have a central hole through which the light beam passes, and two other small holes that are used to fill the cell with the solution. These two holders sandwich two quartz windows and then they are screwed together. By means of suitable spacers it is possible to leave a thin cavity between the quartz windows that is filled with the solution. In this thin cavity a polyethylene spacer (ca. 150 μm thick) with melt-sealed electrodes is also contained. WE and CE are metallic minigrids and a Ag wire plays the role of quasi reference electrode (QRE), the potential of which can be considered constant for a short time interval.

The potential value at which electrolysis has to be performed can be obtained to carry out a cyclic voltammetry at slow scan rate (1–5 mV/s) by using the same cell. From the obtained voltammogram the potential value of interest is easily derived.

The problems usually encountered with this kind of cell are (i) difficult removal of oxygen, because of the impossibility of bubbling an inert gas (gas bubbles could be trapped in the electrodes); (ii) non homogeneous filling of the cell, particularly when solvents with low viscosities and surface tensions are used; (iii) non accurate control of the potential applied to WE because of the presence of a QRE. This latter problem, however, does not represent a substantial inconvenience due to the fact that the electrolysis times are very short (a few seconds).

In the case of diluted solutions (5×10^{-4}–1×10^{-5} M) spectroelectrochemical cells with optical path of 1 cm can be used. It is, however, important to notice that such cells imply noticeable experimental problems the most important of which derives from the use of very low concentrations; electrolysis can, indeed, involve impurities present in the solution, or the supporting electrolyte instead of the electroactive species to be examined.

9.4 Emission Measurements

Compared to absorption the emission measurements have the advantage of a very high sensitivity and, therefore, can be profitably coupled to electrochemical measures. It is, however, important to notice that emission measurements can be applied only in a few cases because luminescent species in the stable redox state or in the oxidized or reduced state are uncommon.

In such kind of experiments the major experimental difficulties derive from the fact that the excitation light must not interfere with the measure of the emission intensity. As already reported in Chap. 5, the luminescence measurements can be performed by following two methodologies: the light beam encounters the cell wall with an incident angle of 45° or 90°. In the first case it is necessary to use a suitably designed electrochemical cell (Fig. 9.12), while in the second case OTTLE cells (like those shown in Fig. 9.10 and 9.11 for absorption measurements) can be employed.

As an alternative approach, optical fibres to send the excitation light and to collect the emission light can be profitably utilized (Fig. 9.13).

Obviously, before measuring the emission spectrum it is useful to record the absorption spectrum; furthermore, to get quantitative information it is necessary to use an excitation wavelength at which the absorbance does not change during electrolysis, or to appropriately correct the obtained results (see Chap. 5).

When OTTLE cells are used, it is important that the cell occupies a fixed and precise position in the spectrofluorimeter to maximize the signal-noise ratio and to obtain reproducible results every time the cell is took away and placed again in the instrument. The cell shown in Fig. 9.12 [19] is constituted by a polyethylene

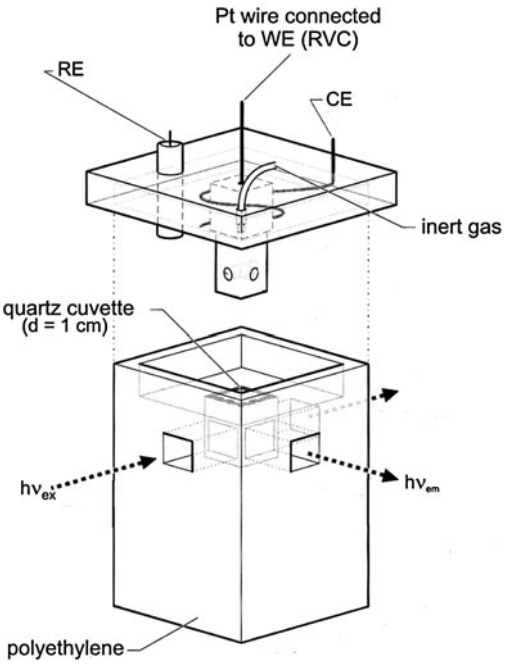

Fig. 9.12 Spectroelectrochemistry cell for emission measurements with an optical path of 1 cm

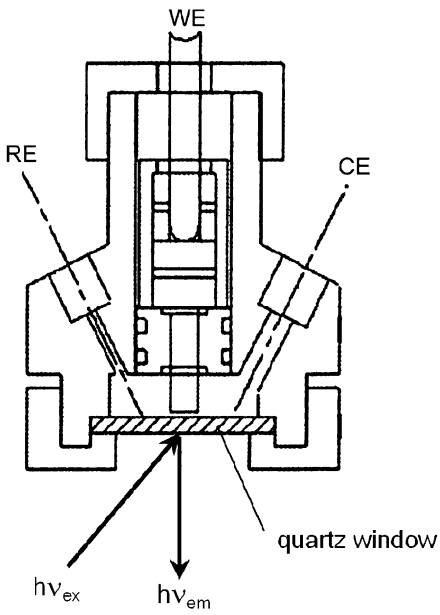

Fig. 9.13 Spectroelectrochemistry cell for emission measurements by using optical fibres

holder that replaces the conventional one: in the upper part of the holder a Pt wire (CE) and a Ag/AgCl electrode (RE) are housed; in the lower part a quartz spectrofluorimetric cuvette with optical path of 1 cm and the WE, constituted by a Reticulated Vitreous Carbon (RVC), are placed. By using such a cell, solutions with concentrations in the range 10^{-4}–10^{-5} M can be electrolyzed quite fast (10–20 min).

In the cell shown in Fig. 9.13 [20] WE is a Pt disk which is placed at a distance of 25–200 μm from the surface of the optical window to speed up electrolysis (1–100 s). The excitation light, sent by means of the optical fibre, encounters the quartz window with an angle of 45°, while the emission light is collected perpendicular to this window by means of another optical fibre. This kind of cell enables to measure the emission in spectroelectrochemical experiments performed on very diluted solutions (5 μM), one order of magnitude lower than the minimum concentration that can be detected in absorption with the same cell and the same electroactive species. This result clearly evidences the higher sensitivity of the emission measurements compared to the absorption ones. Obviously the sensitivity of the spectroelectrochemical experiments coupled to absorption or emission measurements depends on the molar absorption coefficient and the quantum yield, respectively, of the examined species.

References

1. Kaim W, A. Klein A (eds) (2008) Spectroelectrochemistry. RSC Publishing, Cambridge
2. Kaim W, Fiedler J (2009) Chem Soc Rev 38:3373–3382
3. Lee YF, Kirchhoff JR (1994) J Am Chem Soc 116:3599–3600
4. Marcaccio M (1995) Elettrochimica e spettroelettrochimica di specie supramolecolari. Ph.D. Thesis in chemical sciences (VIII cycle), University of Bologna
5. Kaifer AE, Gomez-Kaifer M (1999) Supramolecular electrochemistry. Wiley-VCH, Weinheim
6. Ceroni P, Credi A, Venturi M (eds) (2010) Electrochemistry of functional supramolecular systems. Wiley, Hoboken
7. Ashton PR, Ballardini R et al (1995) J Am Chem Soc 117:11171–11197
8. Livoreil A, Dietrich-Buchecker CO, Sauvage JP (1994) J Am Chem Soc 116:9399–9400
9. Cao D, Amelia M et al (2009) J Am Chem Soc 132:1110–1122
10. Hamilton DG, Davies JE et al (1998) Chem Eur J 4:608–620
11. Gosztola D, Niemczyk MP et al (2000) J Phys Chem A 104:6545–6551
12. Ashton PR, Balzani V et al (1999) J Am Chem Soc 121:3951–3957
13. Asakawa M, Ashton PR et al (1998) Angew Chem Int Ed 37:333–337
14. Balzani V, Credi A et al (2000) J Org Chem 65:1924–1936
15. Lund H, Hammerich O (eds) (2001) Organic electrochemistry, 4th edn. Marcel Dekker, New York, pp 163–167
16. Bard AJ, Faulkner LR (2001) Electrochemical methods, 2nd edn. Wiley, Hoboken
17. Alessio E, Daff S et al (2004) In: Pombiero AJL, Amatore C (eds) Trends in molecular electrochemistry. Marcel Dekker, New York, pp 339–381
18. Krejćik M, Danék M, Hartl F (1991) J Electroanal Chem 317:179–187
19. Lee YF, Kirchhoff JR (1993) Anal Chem 65:3430–3434
20. Dias M, Hudhomme P et al (2004) Electrochem Commun 6:325–330

Index

P. Ceroni (ed.), *The Exploration of Supramolecular Systems and Nanostructures by Photochemical Techniques,* Lecture Notes in Chemistry 78,
DOI: 10.1007/978-94-007-2042-8, © Springer Science+Business Media B.V 2012